

NONLINEAR ANALYSIS TO QUANTIFY  
MOVEMENT VARIABILITY IN  
HUMAN-HUMANOID INTERACTION

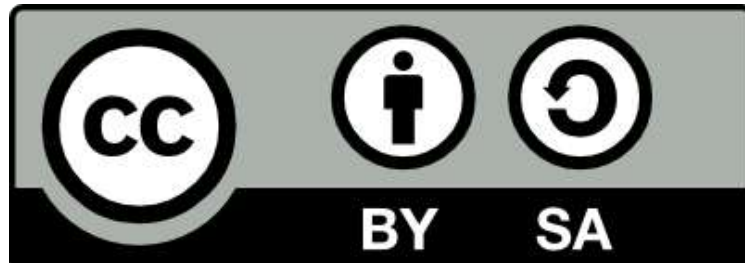
by

MIGUEL XOCHICALE

A thesis submitted to  
The University of Birmingham  
for the degree of  
DOCTOR OF PHILOSOPHY

School of Engineering  
College of Engineering and Physical Sciences  
The University of Birmingham  
20 May 2019

## University of Birmingham Research Archive e-theses repository



This unpublished thesis/dissertation is under a Creative Commons Attribution-ShareAlike 4.0 International (CC BY-SA 4.0) licence.

### You are free to:

**Share** — copy and redistribute the material in any medium or format

**Adapt** — remix, transform, and build upon the material for any purpose, even commercially.

The licensor cannot revoke these freedoms as long as you follow the license terms.

### Under the following terms:



**Attribution** — You must give appropriate credit, provide a link to the license, and indicate if changes were made. You may do so in any reasonable manner, but not in any way that suggests the licensor endorses you or your use.



**ShareAlike** — If you remix, transform, or build upon the material, you must distribute your contributions under the same license as the original.

**No additional restrictions** — You may not apply legal terms or technological measures that legally restrict others from doing anything the license permits.

### Notices:

You do not have to comply with the license for elements of the material in the public domain or where your use is permitted by an applicable exception or limitation.

No warranties are given. The license may not give you all of the permissions necessary for your intended use. For example, other rights such as publicity, privacy, or moral rights may limit how you use the material.

Unless otherwise stated, any material in this thesis/dissertation that is cited to a third party source is not included in the terms of this licence. Please refer to the original source(s) for licencing conditions of any quotes, images or other material cited to a third party.

---

## Abstract

Nonlinear analysis can be applied to investigate the dynamics of time-ordered data. Such dynamics relate to sensorimotor variability in the context of human-humanoid interaction. Hence, this dissertation not only explores questions such as how to quantify movement variability or which methods of nonlinear analysis are appropriate to quantify movement variability but also how methods of nonlinear analysis are affected by real-world time series data (e.g. non-stationary, data length size, sensor sources or noise). Methods are explored to determine embedding parameters, reconstructed state spaces, recurrence plots and recurrence quantification analysis. Additionally, this thesis presents three dimensional surface plots of recurrence quantification analysis with which to consider the variation of embedded parameters and recurrence thresholds. These show that three dimensional surface plots of Shannon entropy might be a suitable approach to understand the dynamics of real-world time series data. This thesis opens new avenues of applications in human-humanoid interaction where humanoid robots can be pre-programmed with nonlinear analysis algorithms to evaluate, for instance, the improvement of movement performances, to quantify and provide feedback of skill learning or to quantify movement adaptations and pathologies.



$$\min_G \max_X F(G, X)$$



## Acknowledgements

I would like to acknowledge to both the Mexican National Council of Science and Technology and the University of Birmingham that funded my curiosity-driven PhD degree. To Professor Chris Baber for supervising my scientific endeavours and who wisely loosed the leash in any of my explorations so as to take me back at the right time to write up this thesis. To Professor Martin J Russell who, in the first year of my PhD, helped with his acute comments and critics to make a better use of the language of mathematics. To Mourad Oussalah who kindly dedicate his time to discuss my research interests and our collaboration with three peer-reiview conference papers. I would also like to thank to Dr. Dolores Columba Perez Flores for her valuable comments that help me to have a better insight on nonlinear analysis, and to Constantino Antonio Garcia Martinez for developing the `nonlinearTseries` R package that was of significant help to accelerate the results of this thesis. Last but not least, many thanks to Patricia Herterich, from Library Services of the University of Birmingham, who helped me to find the first published PhD dissertations in 1901 and e-thesis in 2011 which allow me to state that this thesis is the first Open Access PhD thesis at the University of Birmingham.

**Miguel Xochicale**

**Birmingham, UK**

**May 2019**





# Table of contents

List of figures	xv
<b>1 Introduction</b>	<b>1</b>
1.1 Background . . . . .	1
1.2 Movement variability . . . . .	3
1.2.1 Modelling human movement variability . . . . .	4
1.2.2 Movement variability in human-humanoid interaction . . . . .	9
1.3 Research questions . . . . .	13
1.4 Outline of the thesis . . . . .	15
1.5 Publications . . . . .	17
1.6 Open access PhD thesis . . . . .	18
<b>2 Quantifying Movement Variability</b>	<b>19</b>
2.1 Introduction . . . . .	19
2.2 Fundamentals of time-series analysis . . . . .	19
2.2.1 Linear and non-linear systems . . . . .	20
2.2.2 Stationary and non-stationary signals . . . . .	20
2.2.3 Deterministic and stochastic systems . . . . .	20
2.2.4 Deterministic-chaotic time series . . . . .	21
2.3 Quantifying movement variability with nonlinear analysis . . . . .	21

## Table of contents

---

2.3.1	What to quantify in movement variability? . . . . .	23
2.3.2	Which methods of nonlinear analysis are appropriate to quantify movement variability? . . . . .	24
2.4	Nonlinear analysis with real-world data . . . . .	27
2.4.1	Non-stationarity . . . . .	28
2.4.2	Data length . . . . .	29
2.4.3	Sampling rate . . . . .	30
2.4.4	Noise . . . . .	30
2.5	Final remarks . . . . .	32
<b>3</b>	<b>Nonlinear Analysis</b>	<b>33</b>
3.1	Introduction . . . . .	33
3.2	State Space Reconstruction Theorem . . . . .	34
3.3	Uniform Time-Delay Embedding (UTDE) . . . . .	35
3.4	Estimation of Embedding Parameters . . . . .	37
3.4.1	False Nearest Neighbours (FNN) . . . . .	39
3.4.2	Average Mutual Information (AMI) . . . . .	42
3.4.3	Overall minimum embedding parameters . . . . .	44
3.5	Reconstructed State Space with UTDE . . . . .	45
3.6	Recurrence Plots (RP) . . . . .	45
3.6.1	Structures of Recurrence Plots . . . . .	47
3.7	Recurrence Quantifications Analysis (RQA) . . . . .	49
3.7.1	Measures of RP based on the recurrence density . . . . .	49
3.7.2	Measures of RP based on diagonal lines . . . . .	49
3.7.3	Some weaknesses and strengths of RP and RQA. . . . .	50
3.7.4	3D surface plots of RQA . . . . .	51
3.8	Final remarks . . . . .	54

<b>4</b>	<b>Experiments</b>	<b>55</b>
4.1	Aims . . . . .	55
4.2	Participants . . . . .	56
4.2.1	Human-image imitation activities . . . . .	56
4.2.2	Human-humanoid imitation activities . . . . .	56
4.3	Equipment . . . . .	57
4.4	Ethics . . . . .	57
4.5	Experiments . . . . .	57
4.5.1	Human-image imitation activities . . . . .	57
4.5.2	Human-humanoid imitation activities . . . . .	59
4.6	Processing of time series . . . . .	62
4.6.1	Raw time-series . . . . .	62
4.6.2	Postprocessing time-series . . . . .	64
4.6.3	Window size of time-series . . . . .	64
4.6.4	Normalization of time-series . . . . .	65
4.6.5	Smoothing time-series . . . . .	65
<b>5</b>	<b>Quantifying Human-Image Imitation Activities</b>	<b>67</b>
5.1	Introduction . . . . .	67
5.2	Time series . . . . .	68
5.3	Minimum Embedding Parameters . . . . .	71
5.3.1	Average minimum embedding parameters . . . . .	73
5.4	Reconstructed state spaces with UTDE . . . . .	73
5.5	Recurrences Plots . . . . .	79
5.6	Recurrence Quantification Analysis . . . . .	85
5.7	Weaknesses and strengths of RQA . . . . .	89
5.7.1	Sensors and activities . . . . .	91

## Table of contents

---

5.7.2	Window size . . . . .	97
5.7.3	Smoothness . . . . .	97
5.7.4	Participants . . . . .	100
5.7.5	Final remarks . . . . .	102
<b>6</b>	<b>Quantifying Human-Humanoid Imitation Activities</b>	<b>103</b>
6.1	Introduction . . . . .	103
6.2	Time series . . . . .	104
6.3	Minimum Embedding Parameters . . . . .	107
6.3.1	Average minimum embedding parameters . . . . .	109
6.4	Reconstructed state spaces with UTDE . . . . .	109
6.5	Recurrences Plots . . . . .	113
6.6	Recurrence Quantification Analysis . . . . .	116
6.7	Weaknesses and strengths of RQA . . . . .	119
6.7.1	Sensors and activities . . . . .	121
6.7.2	Window size . . . . .	121
6.7.3	Smoothness . . . . .	125
6.7.4	Participants . . . . .	125
6.7.5	Final remarks . . . . .	128
<b>7</b>	<b>Conclusions and future work</b>	<b>129</b>
7.1	Conclusions . . . . .	129
7.2	Future work . . . . .	132
	<b>Appendix A Open Access Code and Data</b>	<b>139</b>
A.1	Code and data organisation . . . . .	139
A.2	How results can be replicated . . . . .	140

<b>Appendix B Examples of Uniform Time-Delay Embedding</b>	<b>141</b>
B.1 20 sample length vector. . . . .	141
B.2 Time series for horizontal movement of a triaxial accelerometer. . . . .	143
<b>Appendix C Equipment</b>	<b>147</b>
C.1 NeMEMsi IMU sensors . . . . .	147
C.1.1 Issues with IMUs . . . . .	149
C.2 Time-series preprocessing . . . . .	150
C.2.1 Organising Data in Multidimensional Arrays . . . . .	150
C.2.2 Data Synchronisation . . . . .	150
C.2.3 Time Alignment . . . . .	151
C.3 NAO – humanoid robot . . . . .	152
<b>Appendix D Experiment Design</b>	<b>153</b>
D.1 Experiment Check List . . . . .	153
D.2 Information Sheet . . . . .	153
<b>Appendix E Additional Results for HII experiment</b>	<b>159</b>
E.1 Time Series . . . . .	159
E.2 Embedding parameters . . . . .	166
E.2.1 Minimum dimension embedding values . . . . .	166
E.2.2 Minimum delay embedding values . . . . .	171
E.3 RSSs . . . . .	176
E.4 RPs . . . . .	185
E.5 RQAs . . . . .	190
E.5.1 REC values . . . . .	190
E.5.2 DET values . . . . .	193
E.5.3 RATIO values . . . . .	196

## Table of contents

---

E.5.4	ENTR values . . . . .	199
<b>Appendix F Additional results for HHI experiment</b>		<b>203</b>
F.1	Time Series . . . . .	203
F.2	Embedding parameters . . . . .	210
F.2.1	Minimum dimension embedding values . . . . .	210
F.2.2	Minimum delay embedding values . . . . .	213
F.3	RSSs . . . . .	216
F.4	RPs . . . . .	221
F.5	RQAs . . . . .	226
F.5.1	REC values . . . . .	226
F.5.2	DET values . . . . .	227
F.5.3	RATIO values . . . . .	229
F.5.4	ENTR values . . . . .	230
<b>References</b>		<b>233</b>

# List of figures

1.1	Thesis outline . . . . .	16
3.1	State space reconstruction methodology . . . . .	36
3.2	Uniform time-delay embedding . . . . .	38
3.3	Minimum dimension embedding values with Cao's method . . . . .	41
3.4	Minimum delay embedding values with AMI's method . . . . .	43
3.5	Recurrence Plots . . . . .	47
3.6	Patterns in Recurrence Plots . . . . .	48
3.7	3D surface plots . . . . .	53
4.1	Human-image imitation (HII) activities . . . . .	59
4.2	Time series for horizontal and vertical arm movements . . . . .	60
4.3	Human-humanoid imitation activities . . . . .	61
4.4	Time series duration of horizontal and vertical arm movements . . . . .	63
5.1	Time series for horizontal arm movements . . . . .	69
5.2	Time series for vertical arm movements . . . . .	70
5.3	Box plots for minimum embedding dimensions . . . . .	72
5.4	Box plots for 1st minimum AMI . . . . .	72
5.5	RSSs for horizontal arm movements (no beat) . . . . .	75
5.6	RSSs for horizontal arm movements (with beat) . . . . .	76



## List of figures

---

5.7	RSSs for vertical arm movements (no beat) . . . . .	77
5.8	RSSs for vertical arm movements (with beat) . . . . .	78
5.9	RPs for horizontal arm movements (no beat) . . . . .	81
5.10	RPs for horizontal arm movements (with beat) . . . . .	82
5.11	RPs for vertical arm movements (no beat) . . . . .	83
5.12	RPs for vertical arm movements (with beat) . . . . .	84
5.13	Box plots of RQA values for horizontal arm movements . . . . .	87
5.14	Box plots for RQA values for vertical arm movements . . . . .	88
5.15	3D surface plots of RQA metrics . . . . .	90
5.16	3D surface plots of RQA metrics for horizontal arm movements with HS01	93
5.17	3D surface plots of RQA metrics for horizontal arm movements with HS02	94
5.18	3D surface plots of RQA metrics for vertical arm movements with HS01	95
5.19	3D surface plots of RQA metrics for vertical arm movements with HS02	96
5.20	3D surface plots of RQA metrics for different window lengths . . . . .	98
5.21	3D surface plots of RQA metrics with three levels of smoothness . . . . .	99
5.22	3D surface plots of RQA metrics with four participants . . . . .	101
6.1	Time series for horizontal arm movements . . . . .	105
6.2	Time series for vertical arm movements . . . . .	106
6.3	Box plots of minimum embedding parameters . . . . .	108
6.4	RSSs for horizontal arm movements . . . . .	111
6.5	RSSs for vertical arm movements . . . . .	112
6.6	RPs for horizontal arm movements . . . . .	114
6.7	RPs for vertical arm movements . . . . .	115
6.8	Box plots for RQA values . . . . .	118
6.9	3D surface plots for RQA metrics . . . . .	120
6.10	3D surface plots of RQA metrics for HS01 sensor . . . . .	122

6.11 3D surface plots of RQA metrics for RS01 sensor . . . . .	123
6.12 3D surface plots of RQAs metrics with four window lengths . . . . .	124
6.13 3D surface plots of RQA metrics with three levels of smoothness . . . . .	126
6.14 3D surface plots of RQA metrics with three participants . . . . .	127
B.1 Examples of time series with an IMU . . . . .	145
C.1 Inertial Measurement Sensor . . . . .	149
C.2 NAO, humanoid robot from SoftBank . . . . .	152
D.1 Experiment Check List . . . . .	154
D.2 Participant Information Sheet (p. 1/4) . . . . .	155
D.3 Participant Information Sheet (p. 2/4) . . . . .	156
D.4 Participant Information Sheet (p. 3/4) . . . . .	157
D.5 Participant Information Sheet (p. 4/4) . . . . .	158
E.1 Time series for horizontal arm movements (sg0) . . . . .	160
E.2 Time series for horizontal arm movements (sg1) . . . . .	161
E.3 Time series for horizontal arm movements (sg2) . . . . .	162
E.4 Time series for vertical arm movements (sg0) . . . . .	163
E.5 Time series for vertical arm movements (sg1) . . . . .	164
E.6 Time series for vertical arm movements (sg2) . . . . .	165
E.7 Minimum embedding dimensions for horizontal arm movements (no beat)	167
E.8 Minimum embedding dimensions for horizontal arm movements (with beat) . . . . .	168
E.9 Minimum embedding dimensions for vertical arm movements (no beat)	169
E.10 Minimum embedding dimensions for vertical arm movements (with beat)	170
E.11 First minimum AMI values for horizontal arm movements (no beat) . .	172
E.12 First minimum AMI values for horizontal arm movements (with beat) .	173

## List of figures

---

E.13	First minimum AMI values for vertical arm movements (no beat)	174
E.14	First minimum AMI values for vertical arm movements (with beat)	175
E.15	RSSs for horizontal normal arm movements (no beat)	177
E.16	RSSs for horizontal normal arm movements (with beat)	178
E.17	RSSs for horizontal faster arm movements (no beat)	179
E.18	RSSs for horizontal faster arm movements (with beat)	180
E.19	RSSs for vertical normal arm movements (no beat)	181
E.20	RSSs for vertical normal arm movements (with beat)	182
E.21	RSSs for vertical faster arm movements (no beat)	183
E.22	RSSs for vertical faster arm movements (with beat)	184
E.23	RPs for horizontal normal arm movements	186
E.24	RPs for horizontal faster arm movements	187
E.25	RPs for vertical normal arm movements	188
E.26	RPs for vertical faster arm movements	189
E.27	REC values for horizontal arm movements	191
E.28	REC values for vertical arm movements	192
E.29	DET values for horizontal arm movements	194
E.30	DET values for vertical arm movements	195
E.31	RATIO values for horizontal arm movements	197
E.32	RATIO values for vertical arm movements	198
E.33	ENTR values for horizontal arm movements	200
E.34	ENTR values for vertical arm movements	201
F.1	Time series for horizontal arm movements (sg0)	204
F.2	Time series for horizontal arm movements (sg1)	205
F.3	Time series for horizontal arm movements (sg2)	206
F.4	Time series for vertical arm movements (sg0)	207

F.5	Time series for vertical arm movements (sg1) . . . . .	208
F.6	Time series for vertical arm movements (sg2) . . . . .	209
F.7	Minimum embedding dimensions for horizontal arm movements . . . . .	211
F.8	Minimum embedding dimensions for vertical arm movements . . . . .	212
F.9	First minimum AMI values for horizontal arm movements . . . . .	214
F.10	First minimum AMI values for vertical arm movements . . . . .	215
F.11	RSSs for horizontal normal arm movements . . . . .	217
F.12	RSSs for horizontal faster arm movements . . . . .	218
F.13	RSSs for vertical normal arm movements . . . . .	219
F.14	RSSs for vertical faster arm movements . . . . .	220
F.15	RPs for horizontal normal arm movements . . . . .	222
F.16	RPs for horizontal faster arm movements . . . . .	223
F.17	RPs for vertical normal arm movements . . . . .	224
F.18	RPs for vertical faster arm movements . . . . .	225
F.19	REC values for horizontal arm movements . . . . .	226
F.20	REC values for vertical arm movements . . . . .	227
F.21	DET values for horizontal arm movements . . . . .	228
F.22	DET values for vertical arm movements . . . . .	228
F.23	RATIO values for horizontal arm movements . . . . .	229
F.24	RATIO values for vertical arm movement . . . . .	230
F.25	ENTR values for horizontal arm movements . . . . .	231
F.26	ENTR values for vertical arm movements . . . . .	231



# Chapter 1

## Introduction

### 1.1 Background

Human movement involves not only multiple joints and limbs for a specific task in a determined environment but also external information processed through all of our available senses and our prior experiences. Recent studies in human motion recognition have revealed the possibility of estimating features from lower dimension signals to distinguish differences between styles of movement, such as pedalling (Quintana-Duque, 2012, 2016) or walking (Frank et al., 2010; Samà et al., 2013). Similar approaches have been applied to pattern recognition of physiological signals (speech and heart pathologies or epilepsy) (Gómez-García et al., 2014).

Signals of lower dimension are generally time series of one-dimension in  $\mathbb{R}$  which commonly have high nonlinearity, complexity, and non-stationarity (Caballero et al., 2014; Gómez-García et al., 2014; Huffaker et al., 2017). With that in mind, traditional methods in time-domain or frequency-domain generally tend to fail when detecting tiny modulations in frequency or phase (Marwan, 2011). This can mean that subtle signatures of each individual's movement could be missed using traditional methods. However, methods of nonlinear time series analysis can quantify such subtleties in

## Introduction

---

human movement variability (Frank et al., 2010; Gómez-García et al., 2014; Marwan, 2011; Packard et al., 1980; Quintana-Duque, 2012, 2016; Samà et al., 2013; Stergiou and Decker, 2011). Recently, Bradley and Kantz (2015) reviewed methods for nonlinear time series analysis, such as the reconstructed state space (RSS) (Takens, 1981), recurrence plots (RP) (Eckmann et al., 1987) and recurrence quantification analysis (RQA) (Zbilut and Webber, 1992). Such methods are implemented using embedding parameters ( $m$  and  $\tau$ ). However, the computation of embedding parameters is still an open problem since there is no general technique to compute the embedding parameters because time series are system-dependent, meaning that defined parameters may only work for one purpose, e.g., prediction, or may not work well for other purposes e.g., computing dynamical invariants (Bradley and Kantz, 2015).

Additionally, the quality of the time series signals is reflected on the reliability of methods of nonlinear analysis. For instance, methods to compute embedding parameters e.g., autocorrelation, mutual information, and nearest neighbour, require data which are well sampled and with little noise (Garland et al., 2016) or need to be purely deterministic signals (Kantz and Schreiber, 2003). Similarly, methods such as RSS, RP and RQA can break down when datasets have different length, different accuracy and precision (Frank et al., 2010), or when data are contaminated with different sources of noise (Garland et al., 2016). It is surprising that despite these problems, methods of nonlinear analysis have proven to be helpful to understand and to characterise time series in the context of human movement (Bradley and Kantz, 2015; Frank et al., 2010; Gómez-García et al., 2014; Marwan, 2011; Quintana-Duque, 2012, 2016; Samà et al., 2013; Stergiou and Decker, 2011). Another point to consider when analysing time series with methods of nonlinear analysis is the appropriate use of post-processing techniques such as interpolation, normalisation or filtering. However, to my knowledge,

there is little research on the effects and interpretation of post-processing techniques with methods of nonlinear analysis such as RSSs, RPs and RQA.

## 1.2 Movement variability

Variability is inherent within and between all biological systems (Newell and Corcos, 1993). For instance, variability has been studied in electroencephalographic signals in human brains (Klonowski, 2007), in physiological signals like the heart rate variability (Rajendra Acharya et al., 2006; Schumacher, 2004), respiratory patterns of rats (Dhingra et al., 2011), in speech variability where not only the linguistic aspect is investigated but factors like gender, age, social, state of health, emotional state are strongly related to uniqueness of the speaker (Benzeghiba et al., 2007) or even in odor responses based on cultural background and gender (Ferdenzi et al., 2013).

Variability has also been well studied in human body movement, where, for instance, Bernstein (1967) stated that no human movement is repeated exactly with the same trajectory. With that in mind, movement variability has been used as a model of fatigue to prevent chronic musculoskeletal disorders (Mathiassen, 2006; Srinivasan and Mathiassen, 2012). Movement variability has also been considered as an indicator of skilled performance in sport science where, for instance, Wagner et al. (2012) show how movement variability based on statistical analysis varies with skill for three levels of throwing techniques (low-skilled, skilled, and high-skilled). Therefore, Bartlett et al. (2007) concluded that movement variability is ubiquitous across sports (javelin throwing, basketball shooting or running). Another interesting example is that movement variability can be considered as an identifier for personal trait (Sandlund et al., 2017), where many factors of the human body can be considered for identification, such as: age (Krüger et al., 2013; MacDonald et al., 2006; Stergiou et al., 2016; Vaillancourt and Newell, 2003), gender (Svendsen and Madeleine, 2010), pain status (Madeleine et al.,



## Introduction

---

2008; Sandlund et al., 2008), body composition (Chiari et al., 2002), work experience (Madeleine and Madsen, 2009), pace, movement direction or cognitive demands like perception, memory or capacity for introspection (Kanai and Rees, 2011; Srinivasan and Mathiassen, 2012). Additionally, Bartlett et al. (2007) highlighted that movement variability can be interpreted from different theoretical disciplines. For instance, a cognitive control theorist considers variability as undesirable noise and variability is reduced as skill increases, meaning that "becoming dexterous freezes unwanted degrees of freedom in the kinematic chain" (Bartlett et al., 2007, p. 238). In contrast, an ecological motor control specialist considers movement variability either as a functional role in human movement for "coordination change and flexibility to adapt" in different environments (Bartlett et al., 2007, p. 238) or as an exploration and exploitation of body parts in the "perceptual-motor workspace" (Herzfeld and Shadmehr, 2014; Wu et al., 2014).

Stergiou and Decker (2011), in contrast, highlighted that an optimal state of movement variability is associated with healthiness. For instance, motor disabilities may be related to either (i) wide range of behaviours which appear to be random, unfocussed and unpredictable or (ii) narrow range of behaviours which seems to be rigid, inflexible and predictable. Specifically, postural sway variability which is larger for patients with Parkinson disease or the likelihood of falling in elderly individuals which is associated with too little or too much step width variability. This suggest that extremes of movement variability are symptomatic of lower ability to control movement.

### 1.2.1 Modelling human movement variability

Human movement involves a complex system where many sensorimotor variables such as joints, muscles, nervous system, motor unit and cells are the sources for

different types of variability (Newell and Corcos, 1993). Hence, variability encompasses different types, sources and views of variability. For instance, from a biomechanical view, motion variability can be modelled as system of differential equations for the neuro-musculoskeletal control system where motion variations can occur because of "perturbations of initial states of the skeletal system", perturbations of "muscular or neural subsystems ", or "external torques and forces acting on the skeletal system" (Hatze, 1986, p. 13). According to Hatze (1986) motion variability can be caused by (i) direct consequences of adaptive learning process, and (ii) random fluctuations which are the result of stochastic processes in the nervous system. Hence, Hatze (1986) proposed measures of dispersion (e.g. Fourier series and entropy measures) to quantify the deviation of motion from a certain reference. With that, Hatze (1986) pointed out that the combination of deviations from angular coordinates (radians) and linear coordinates (meters) for Fourier series were an unacceptable quantifier as the units are different. Hence, Hatze (1986) proposed the use of entropy as a global quantifier for motion variability and concluded that any movement deviation of a body joint may be the result of deterministic and stochastic causes.

Another approach to model variability has been proposed by Müller and Sternad (2004), who decompose variability into exploration of task tolerance( $T$ ), noise reduction( $N$ ), and covariation( $C$ ). Hence, the quality of performance in goal-oriented tasks, e.g. hitting a target, is defined "by the accuracy and replicability of the results" (deviations from the target) "over repeated attempts of execution" (configuration of joint angles with its velocity, angles and position) (Müller and Sternad, 2004, p. 229). For the experiment, Müller and Sternad (2004) considered table skittles, where participants throw a ball on a string that swings around a center post with the objective of knocking down the skittle at the opposite site. Then, Müller and Sternad (2004) proposed  $D$  as the absolute average of distance to the targets in  $n$  trials and used this as a measure

## Introduction

---

of the collective performance that combines a function for movement based on the execution vector with a function for the minimum distance from the target  $d$ . Therefore, the overall difference in performance  $D$  is decomposed into three unequal contributions of covariation  $C$ , noise reduction  $N$  and task tolerance  $T$ . Considering a 2-D task space that spanned the release angle  $\alpha$  and absolute velocity  $v$ , the components of contributions of variability were calculated from five data sets ( $A$ ,  $A_0$ ,  $A_{shift}$ ,  $B$  and  $B_0$ ): (i) the component of covariation where sets  $A$  and  $A_0$  and  $B$  and  $B_0$  have the same means and variances, (ii) the component of tolerance where sets  $A$  and  $A_{shift}$  differ only on their location in the task space, and (iii) the component of noise where sets  $A_{shift}$  and  $B_0$  have the same means but different variances (see Fig. 6 in Müller and Sternad (2004) for further details). With that in mind, Müller and Sternad (2004) conducted an experiment with forty-two participants for five different locations of the target skittle where for each target a participant performed 320 trials which is a total of 1600 trials and therefore presented statistical confirmation of the contributions of  $T$ ,  $N$  and  $C$  using ANOVA. Hence, Müller and Sternad (2004) concluded that  $T$  and  $N$  contribute more to improvement of a performance of a task than  $C$  for initial practice, meaning that a new combination of angles and velocities explore a large region of solution space (hitting the target). However, for later practice  $T$  diminishes, and  $N$  and  $C$  started to be more relevant. Also, Müller and Sternad (2004) showed in various experiments of throwing actions that variability in the movement results (deviations from the target) is generally smaller than variability in the execution (release angles and velocities) for which it is concluded that covariation between execution variables is another component of variability. With that in mind, Müller and Sternad (2004) concluded that task space exploration is an essential contribution to the improvement of movement performances which is an explanation to the increase of noise in early practice phases.

Seifert et al. (2011) investigated coordination profiles for recreational and competitive breaststroke swimmers and proposed an hourglass model of variability that illustrates the amount of variability as a function of expertise. Hence, Seifert et al. 2011, p. 551 stated recreational swimmers show a considerable amount of intra-variability "as they seek an individually appropriate coordination pattern to accommodate the novel constraints of locomotion in water", whereas experts swimmers, after a considerable practice, will still explore new environments to optimise their technique that create another secondary blooming of variability which is the result of "the environment exploration to optimise their technique with their individual strengths (e.g. physical, anatomical, mental, etc.) and to gain an advantage over competitive swimmers". To test the hourglass model of variability, Seifert et al. (2011) considered the continuous relative phase (CRP) between the elbow phase angle and knee phase angle, therefore CRP is used as an indicator on how swimmers synchronise arm recovery (elbow extension) and leg recovery (knee flexion). Seifert et al. (2011) analysed inter-individual variability of swimmers with the shape of the curves of CRP which provide an indication of the inter-limb coordination, applied statistical measures such as hierarchical clustering using eleven variables of CRP to classify the recreational swimmers into three cluster of coordination (intermediate, most-variable and in-phase) and used Fisher information to test which CRP variables were significantly differentiated the clusters. With that, Seifert et al. (2011) concluded that inter-individual coordination variability for recreational swimmers could be the result of (i) different state of process learning, (ii) environmental constraints (different perception of the aquatic resistance), or (iii) different perception of the task constraints (floating instead of swimming).

Preatoni (2007) and Preatoni et al. (2010, 2013) report that inter-trial variability is defined as combination of functional changes associated with the nonlinear properties of the neuro-musculo-skeletal system ( $V_{nl}$ ) and random fluctuations in the neuro-motor-

## Introduction

---

skeletal system ( $V_e$ ). Additionally, Preatoni et al. 2013, p. 72 stated that the random fluctuations in movement variability can be composed by  $V_e = V_{eb} + V_{ee} + V_{em}$ , where  $V_{eb}$  relates to the behavior and is the "error in the sensory information and in the motor output commands",  $V_{ee}$  is the "changes in the environmental conditions" and  $V_{em}$  is the "changes in measuring and data processing procedures". Therefore, similar as Hatze (1986), Preatoni et al. 2013, p. 77 pointed out that  $V_{nl}$  "may be interpreted as the flexibility of the system to explore different strategies to find the most effective strategy among the many available". Hence, Preatoni et al. 2010, p. 1328 concluded that the total variability represents the changes of contributions for  $V_e$  and  $V_{nl}$  and it is defined as  $V_{tol} = V_e + V_{nl}$ , where  $V_{tol}$  "may reveal the effects of adaptation, pathologies and skills learning". Also, Preatoni et al. (2013) noted that their work only investigated error from biological variability (e.g.  $V_{eb}$ ) which does not consider non-biological noise resulting from measuring instruments or data post-processing techniques, such non-biological noise has high frequency components that are usually removed. Therefore, the work of Preatoni et al. (2010) and Preatoni et al. (2013) does not consider an overall index to quantify movement variability but the combination of both  $V_{eb}$  and  $V_{nl}$ . With that in mind, Preatoni (2007) analysed the influences of  $V_{eb}$  and  $V_{nl}$  for movement repeatability by comparing entropy measures (e.g. ApEn and SampEn) with values of their surrogate counterparts.

Generally, the previous approaches reported different models for movement variability which then are quantified with different tools. For instance, Hatze (1986) and Preatoni et al. (2010, 2013) use entropy measures as the authors consider that the origin of the signals in the human body is the result of deterministic and stochastic processes, whereas Müller and Sternad (2004) and Seifert et al. (2011) reported measures of magnitude that limited the evaluation of the whole trajectories as structures of movement variability in human body activities. Therefore, for this thesis, it is

important to note that even with the proposed models for movement variability (Hatze, 1986; Müller and Sternad, 2004; Preatoni et al., 2010, 2013; Seifert et al., 2011) which have been quantified with statistical or nonlinear tools, little has been investigated with regards to the reliability of the nonlinear tools when using real-world data (Newell and Slifkin, 1998). A further review of nonlinear analysis with real-world data is presented in Chapter 2.

### 1.2.2 Movement variability in human-humanoid interaction

Movement variability in the context of human-humanoid interaction has been investigated for exercising, rehabilitation and dancing purposes in the last six years (Görer et al., 2013; Guneyusu et al., 2015, 2014; Peng et al., 2015; Tsuchida et al., 2013). For instance, Görer et al. (2013) conducted an experiment of a robotic fitness coach where eight elderly participants performed five gestures: three for arm related exercises and two for leg strength exercises. Hence, Görer et al. (2013) with only graphical visualisation of joint angles trajectories extracted from the pose estimation of a kinect sensor, stated that only one subject out of eight fail to imitate the gestures correctly. Additionally, Görer et al. (2013) surveyed participants using a 5-point Likert scale about the positive and negative effect, flow, immersion and challenge of the human-robot interaction activity, concluding that their system is easy to use based on the high scores for immersion and positive effect and low scores for challenge and negative effect. However, the small sample size and somewhat naive analysis of data in the study makes it difficult to generalise these findings.

Another example is the work of Guneyusu et al. (2014) who conducted experiments with children for upper arm rehabilitation using a play-like child robot interaction. Hence, Guneyusu et al. (2014), using a Kinect sensor to get data of join angles of the participants' skeleton, performed an automatic evaluation of three upper body actions

## Introduction

---

(shoulder abduction, shoulder vertical flexion and extension, and elbow flexion) of eight healthy children who mimicked an humanoid robot. To evaluate motion imitation, Guneyusu et al. 2014, p. 202 considered similarity error using Dynamic Time Warping (DTW) that penalise large angle errors over ten percent in the area range of the motion type and applied recall measure as a representation of "how much of angular area of the baseline motion from the humanoid robot is also covered by the child's motion". Then, Guneyusu et al. (2014) presented the evaluation of five physiotherapists using Intraclass correlation coefficient (ICC) which is a metric for reliability of ratings for motion types, and reported that for the first motion, which consists of only one joint, the metric and physiotherapist evaluations showed high agreement, whereas for the second and third motions, which motions were more complex consisting of more joint values, the evaluation between the metrics and physiotherapist ratings differed. Guneyusu et al. 2014, p. 203 stated that during the evaluation of complicated movements, children misperceived the actions for which "therapists compensated such misunderstanding by giving high scores to the children while the proposed system only considered angles". This suggests that it is also possible that the physiotherapist' ratings differed from these data because they were considering aspects which could have been incidental to the movements. With that in mind, it is interesting to note that similarity error and recall measures with the ICC metric are not completely reliable since they did not model movements that involved more than one joint. Then, Guneyusu et al. (2015) analysed movements of more than one joint of four physiotherapists performing five actions: opening a door with a key, touching the opposite shoulder with hand, taking an object from back to neck, taking an object from the back and reaching an object above the head. Guneyusu et al. (2015) applied traditional statistics (e.g. sample mean and sample variance) to characterise the five actions. For instance, the initial positions of arms changed from person to person, specially for the key turning action

which variation were affected by the sample mean, while performances of turning the amplitude of the arm were associated with the standard deviation of the data. However, such statistical differences cannot capture the structure of the time series from each of the participants which performed the movements at different frequencies and therefore with different data length (see Fig. 10 in Guneyasu et al. (2015) for further details).

Movement variability in the context of human-humanoid interaction has also been investigated in robotic dance activities. For example, Tsuchida et al. (2013) explored four dance formations which were performed three times by nine participants who had three years of experience: dancing with a robot, dancing alone, dancing with a self-propelled robot and dancing with a projected video. To visualise dance movements, Tsuchida et al. (2013) presented two participant's movement positions with twelve trajectories each (four dance activities times three trials) of z and x directions obtained with a Kinect sensor. Although, the dance experiment was rich in terms of movement variability for both participants and dance activities, only distance between each of the conditions in the dance formation was considered. With that in mind, Tsuchida et al. (2013) concluded that the sense of dancing with a projected video of a person was the closest to dancing with a real person and the trajectory of dance with a self-propelled robot was the closest to the trajectory of a dancer. Additionally, Tsuchida et al. (2013) only applied traditional statistics (i.e., ANOVA) to characterise dance movements.

Another aspect of movement variability in the context of human-humanoid interaction is the generation of robotic dance. Recently, Peng et al. (2015) reviewed an hierarchical taxonomy of four categories for robotic dance (i.e., cooperative human-robot dance, imitation of human dance motions, synchronisation for music and creation of robotic choreography). Peng et al. (2015) pointed out that the creation of robotic dance is still an open research question because such motions should generally be both interesting and exciting for users. According to Peng et al. (2015), the creation of



## Introduction

---

robotic dances can be accomplished with any of the following methodologies: (i) random generation: where robots can be programmed with series of predefined algorithms that can be chosen randomly, (ii) mapping rule: where robots can react, and therefore dance, to different factors such as colours, sounds, speech, temperature or human activity, (iii) chaotic dynamics: where chaotic systems are sensitive to initial conditions and these systems can create various dance styles from periodic and couple rhythm to jumping styles, resulting in innovative and consistent dance patterns, (iv) interactive reinforcement learning: where the robot can automatically choose motions based on rewards of participants' preferences of graceful motions, (v) evolutionary computation: in which multiple iterations of generations of dance motions can create graceful robotic dance motions, and finally (vi) using a Markov chain model, a discrete time stochastic chain, where each sequence of dance motions is considered as a state in the Markov chain producing dance that synchronise with music and emotions. While the research questions of this thesis are not focused on the creation of good robotic dances (i.e, being innovative or having accordance with human aesthetics) (Peng et al., 2015), it is important to note that sensitivity to initial conditions of chaotic dynamics systems is aligned to the deterministic-chaotic properties of human movement (see Chapter 2 for fundamentals of deterministic-chaotic time series).

Although, movement variability in the context of human-humanoid interaction has not been well investigated in recent years, it can be noted that movement variability is indeed present in activities such as exercise, rehabilitation or dance. Hence, previous works in human-humanoid interaction have analysed gestures, movements or dance activities with the use of traditional statistics, however the following points show some issues in this field of research: (i) it is not clear how Görer et al. (2013) performed the evaluation of synchronisation for gestures between participants and the humanoid nor what were the methods of evaluation of gestures (apart from the visual observations to

classify correct trajectories of gestures), (ii) little has been investigated with regards to the differences in movement variability of physiotherapists in the works of Guneyasu et al. (2014) and Guneyasu et al. (2015), and (iii) in the results of Tsuchida et al. (2013) is not clear why the distribution of trajectories for subject 1 were more uniform than the trajectories of subject 2.

Considering the previous reviewed works in the context of human-humanoid interaction, it can then be suggested that applying nonlinear analysis methods instead of traditional statistics might provide better quantification and understanding of movement variability of persons when interacting with humanoid robots. It is important to note that non-stationary and non-linearity of time-series data from this thesis is assumed (see Chapter 7 for a discussion on the reasoning, as posed by (Schreiber and Schmitz, 2000), of making rather dangerous assumption). That said, the application of nonlinear analysis methods to human-humanoid interaction activities can contribute to the not yet fully explored reliability of nonlinear analysis methods with real-world data (see Chapter 2 for a review of nonlinear analysis methods with real-world data).

### 1.3 Research questions

A number of questions regarding movement variability have been investigated in the last decade: how is variability controlled while learning a new skill? (Bartlett et al., 2007; Seifert et al., 2011; Wagner et al., 2012), is variability associated with disease or health? (Stergiou and Decker, 2011; Stergiou et al., 2006), what are the sources of variability and how do they interact in the production of observed variation of movement? (Preatoni, 2007; Preatoni et al., 2010, 2013). Nonetheless, little has been investigated regarding to the reliability of methods of nonlinear analysis to quantify movement variability (Iwanski and Bradley, 1998; Yao and Lin, 2017) when dealing with real-world data (Bradley and Kantz, 2015; Caballero et al., 2014). Therefore, this thesis explores the

## Introduction

---

effects of three methods of nonlinear analysis (e.g. Reconstructed State Space (RSS), Recurrence Plots (RP) and Recurrence Quantification Analysis (RQA)) with different features of time-series data such as structure, levels of smoothness and window lengths. To perform such exploration, two experiments were conducted with twenty right-handed healthy participants: one for human-image imitation activities and another in the context of human-humanoid imitation activities. For the experiments, participants were asked to imitate simple arm movements and participants and humanoid robot worn inertial sensors to collect time-series data. Hence, the following research questions are investigated in this thesis.

- What are the effects on RSSs, RPs, and RQA metrics of different embedding parameters, different recurrence thresholds and different characteristics of time series (structure, smoothness and window length size)?
- Additionally, what are the weaknesses and strengths of RQA metrics when quantifying movement variability?
- How does the smoothing of raw time series affect methods of nonlinear analysis when quantifying movement variability?

## 1.4 Outline of the thesis

This thesis is organised as shown in Fig. 1.1. Chapter 1 presents a background of quantification of movement variability, state-of-the-art for modelling human movement variability, movement variability in the context of human-humanoid interaction and research questions are stated. Chapter 2 presents an introduction to fundamentals of time series analysis in terms of: (i) what to measure in movement variability? and (ii) which nonlinear tools are appropriate to measure movement variability?, including a review of the state-of-the-art literature of nonlinear analysis with real-world data. In Chapter 3 a review of state space reconstruction method is presented that entails an explanation for uniform time delay embedding (UTDE), a description of the techniques to estimate minimum embedding parameters (e.g. false nearest neighbour and average mutual information), and an introduction to Recurrence Plots (RPs), structures of RPs and different metrics to perform Recurrence Quantification Analysis (RQA) as well as the weakness and strengths of RPs and RQAs. In Chapter 4, the experiments for human-image imitation and human-humanoid imitation are presented describing aims, participants, activities in the experiments, equipment, ethics and preparations of the time series. Chapter 5 and 6 present the results with regards to two experiments (human-image imitation and human-humanoid imitation) for minimum embedding parameters, reconstructed state space using uniform time-delay embedding, recurrence plots, recurrence quantification analysis(RQA) metrics and 3D surfaces of RQA metrics to show the weaknesses and strengths of RQA. Finally, Chapter 7 presents conclusions, the answers for the research questions, the contribution to knowledge and future work after this thesis.

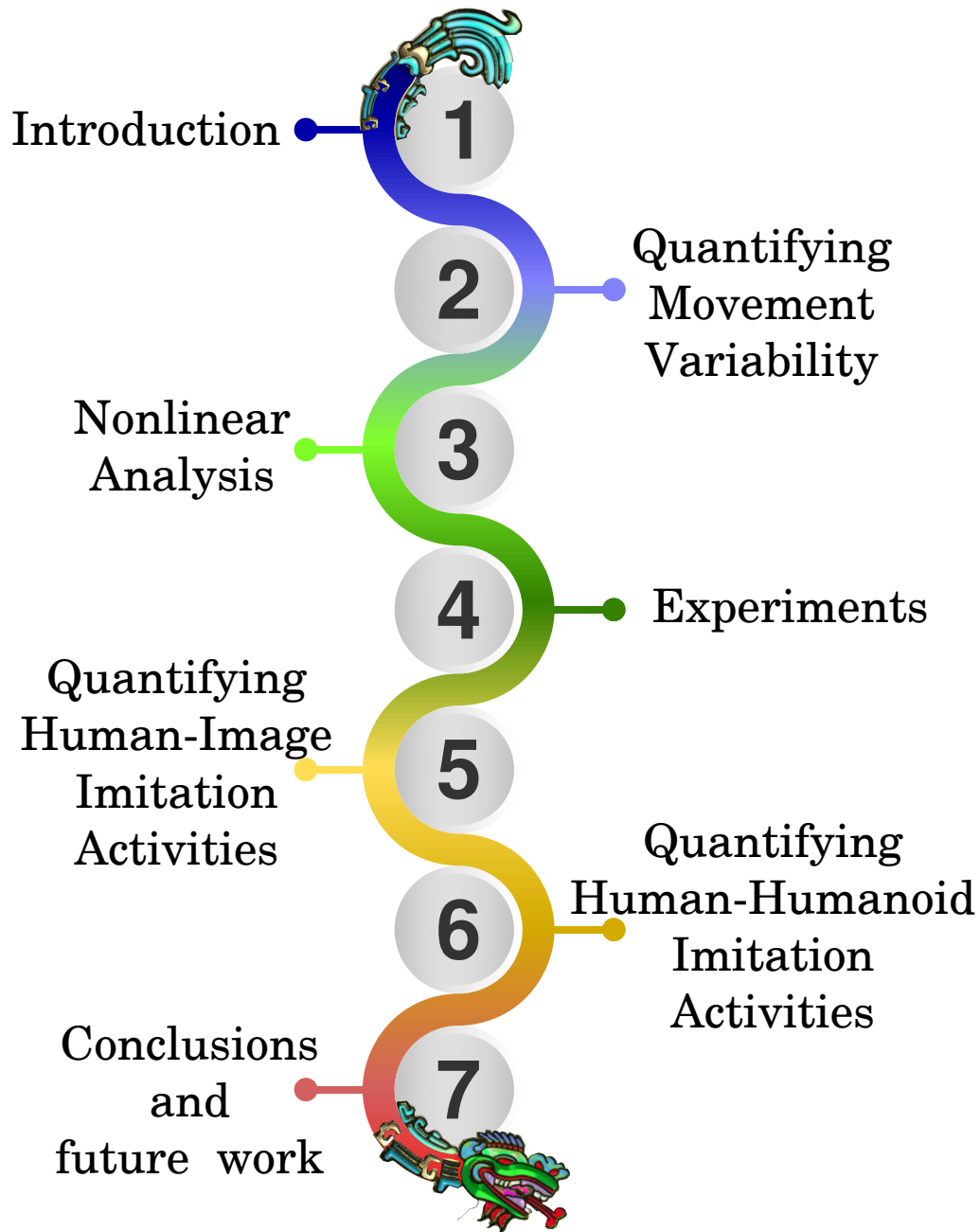


Fig. 1.1 **Thesis outline.** Chapter numbers with its titles. N.B. Quetzalcoatl, a feathered serpent, is flowing between chapters. "To the Aztecs, Quetzalcoatl was both a boundary-maker and a transgressor between earth and sky" (Quetzalcoatl, 2018).

## 1.5 Publications

Partial work of this thesis has been presented in the following four peer-reviewed conferences. Additionally, one preprint has been uploaded to ArXiv which its final version will be submitted to Scientific Reports and a manuscript for the research topic Recurrence Analysis of Complex Systems Dynamics of the journal *Frontiers in Applied Mathematics and Statistics* is in preparation.

Author contributions for the papers of Miguel Xochicale (MX), Chris Baber (CB) and Mourad Oussalah (MO) are as follow: Conceptualisation: MX, CB, MO; Data Curation: MX; Formal Analysis: MX; Funding Acquisition: MX, CB; Investigation: MX; Methodology: MX; Project Administration: MX; Resources: CB; Software: MX; Supervision: CB; Validation: MX; Verification: MX; Writing - Original Draft Preparation: MX; Writing - Review: CB, MO; and Writing - Editing: MX.


- Xochicale M, Baber C, and Oussalah M. Understanding Movement Variability of Simplistic Gestures Using an Inertial Sensor. *in Proceedings of the 5th ACM International Symposium on Pervasive Displays*, Oulu, Finland, June 2016, pages 239–240. <https://github.com/mxochicale/perdis2016>
- Xochicale M, Baber C, and Oussalah M. Analysis of the Movement Variability in Dance Activities Using Wearable Sensors. *in Wearable Robotics: Challenges and Trends*, Segovia, Spain, October 2016, pages 149–154. <https://github.com/mxochicale/werob2016>
- Xochicale M, Baber C, and Oussalah M. Towards the Quantification of Human-Robot Imitation Using Wearable Inertial Sensors. *in Proceedings of the Companion of the 2017 ACM/IEEE International Conference on Human-Robot Interaction*, Vienna, Austria, March 2017, pages 327–328. <https://github.com/mxochicale/hri2017>

## Introduction

---

- Xochicale M, and Baber C. Towards the Analysis of Movement Variability in Human-Humanoid Imitation Activities. *in Proceedings of the 5th International Conference on Human Agent Interaction*, Bielefeld, Germany, October 2017, pages 371–374. <https://github.com/mxochicale/hai2017>.
- Xochicale M, and Baber C. Strengths and Weaknesses of Recurrent Quantification Analysis in the context of Human-Humanoid Interaction, *in ArXiv e-prints*, October 2018. <https://arxiv.org/abs/1810.09249>

## 1.6 Open access PhD thesis

This PhD thesis is open access under the licence of Creative Commons Attribution Share Alike 4.0 International and code and data is available at <https://github.com/mxochicale/phd-thesis/> (Xochicale, 2019). The github repository has been created to make this work reproducible and perhaps help others to advance this field. Throughout the thesis links to R code () are provided in the caption of figures in order to reproduce their results. See Appendix A for details on how code and data is organised and how results can be replicated in this thesis.

# Chapter 2

## Quantifying Movement Variability

### 2.1 Introduction

It has been stated in Chapter 1 that movement variability can be modelled and quantified with methods of nonlinear analysis mainly because (i) the structures of the human physiology (e.g. lungs, neurons, etc.) suggest that many of their dynamics are controlled with nonlinear dynamics (Goldberger et al., 1990) and (ii) data from human movement can be noisy, deterministic, stochastic, non-stationary or deterministic-chaotic (Caballero et al., 2014; Hatze, 1986; Newell and Slifkin, 1998; Preatoni et al., 2010, 2013; Stergiou and Decker, 2011; Stergiou et al., 2006). Therefore, in this chapter fundamentals of time series, methods of nonlinear analysis to quantify movement variability and nonlinear analysis with real-world data are reviewed.

### 2.2 Fundamentals of time-series analysis

Biosignals from living systems can typically be noisy, deterministic, stochastic, non-linear, non-stationary or deterministic-chaotic (Caballero et al., 2014; Gómez-García et al., 2014; Harbourne and Stergiou, 2009; Hatze, 1986; Klonowski, 2007; Newell and



Slifkin, 1998; Stergiou and Decker, 2011; Stergiou et al., 2006; Wijnants et al., 2009). That said, the following sections provide fundamental definitions of time series for this thesis.

### **2.2.1 Linear and non-linear systems**

Linear systems are proportional or additive. For example, the interaction between variables of a linear system are negligible whereas for a nonlinear system such interaction of variables can produce emergent properties arising from the initial conditions of the system (Klonowski, 2007).

### **2.2.2 Stationary and non-stationary signals**

Stationary signals have the same mean and variance as time progress (e.g. a sinusoidal signal), however such stationary signal can also be changeable (e.g. alternative sinusoidal signal). In contrast, when statistics of the time series change with time then such a signal is known as non-stationary signal. Non-stationary signals are therefore characterised by transients and drift over time. Examples of non-stationary signals are the time series of seasonal trends and changes (Kitagawa and Gersch, 1984) or Electroencephalography (EEG) signals which present different and changeable intensity over time (Klonowski, 2007).

### **2.2.3 Deterministic and stochastic systems**

A deterministic system is predictable. Deterministic systems have a small number of variables of importance. Deterministic systems are hence modelled with linear ordinary differential equations and their initial conditions and constants. In contrast, stochastic systems are non-predictable and therefore have more variables of equal importance and are typically modelled with probability theory (Klonowski, 2007).

### 2.2.4 Deterministic-chaotic time series

Deterministic signals can dramatically change with a slight change of initial conditions and then after a long time-scale, the signal can appear to be stochastic (Amato, 1992). Klonowski 2007, p. 11 pointed out that "chaotic systems behave like they were stochastic but they are also deterministic", meaning that chaotic systems are predictable for a short time-scale but nonpredictable in a long time-scale because of the initial conditions of the systems. Preatoni et al. 2013, p. 78, in experiments in sport science, mentioned that "variability is likely to have both deterministic and a stochastic origin". It can then be assumed that time series for human body movement are neither independent nor stochastic but deterministic-chaotic (Harbourne and Stergiou, 2009; Stergiou and Decker, 2011; Stergiou et al., 2006).

## 2.3 Quantifying movement variability with nonlinear analysis

Previous studies have shown that movement variability is not considered as a undesired factor that creates errors but a signature for assessment of healthiness (associated with unhealthy pathological states) or skillfulness (associated with the functionality of movement) (Stergiou and Decker, 2011). That said, movement variability can fundamentally be either quantified based on (i) the magnitude of the variability or (ii) the dynamics of the variability (Caballero et al., 2014). However, finding the appropriate methods to quantify movement variability is still an open problem.

For instance, Preatoni et al. (2010, 2013) point out that conventional statistics (e.g. standard deviation, coefficient of variation, intra-class correlation coefficient) only quantify the overall variability. Also, Stergiou and Decker (2011) stated that statistical tools (e.g. mean, standard deviation and range) are a measure of centrality,

## Quantifying Movement Variability

---

meaning such metrics are compared around a central point. Similarly, Coffey et al. (2011) pointed out that the use of means and standard deviations led to reduction of data and therefore information is discarded.

Additionally, one can apply frequency-domain tools to quantify movement variability. For example, Hatze (1986) proposed a measure of dispersion to quantify the deviation of motion from a certain reference using the Fourier series. However, deviations of motion are from angular coordinates (radians) and linear coordinates (meters) which made them an unacceptable fusion of variables. Vaillancourt et al. (2001) pointed out that it is rare for frequency and amplitude to differ in postural tremor of patients with Parkinson's disease but differences in time-dependent structures are apparent, and associated with a change of regularity of postural tremor. Klonowski (2002, 2007, 2009) stated that frequency-domain tools require stationary data, otherwise using other type of data might create misleading results.

Applying either statistical tools or frequency-domain tools to quantify movement variability might create misleading results, specially when dealing with deterministic-chaotic signals (Amato, 1992; Dingwell and Cusumano, 2000; Dingwell and Kang, 2007; Miller et al., 2006). Hence, the properties of deterministic-chaotic signals are aligned with the subtle changes in the neuro-muscular-skeletal system are caused by influences of environmental changes, training or latent pathologies (Preatoni et al., 2010, 2013) and that movement variability involves evolution of human movement and the exploratory nature of movement (Caballero et al., 2014; Stergiou and Decker, 2011). That said, Caballero et al. (2014); Preatoni et al. (2010); Stergiou and Decker (2011) highlighted that movement variability can be better described and quantified with different methods of nonlinear analysis such as: largest Lyapunov exponent (Bruijn et al., 2009; Donker et al., 2007; Kurz et al., 2010; Yang and Wu, 2011), fractal analysis (Delignères et al., 2003), entropy rate (Cavanaugh et al., 2010), Sample Entropy

## 2.3 Quantifying movement variability with nonlinear analysis

---

(SampEn) (Donker et al., 2007; Liao et al., 2008; Richman and Moorman, 2000; Stins et al., 2009; Vaillancourt et al., 2004), Approximate Entropy (ApEn) (Cavanaugh et al., 2010; Kurz and Hou, 2010; Pincus, 1991; Sosnoff et al., 2006; Sosnoff and Voudrie, 2009), Fuzzy Entropy (FuzzyEn) (Chen et al., 2007), Multiscale Entropy (MSE) (Costa et al., 2002), Permutation Entropy (PE) (Bandt and Pompe, 2002; Vakharia et al., 2015), Quadratic Sample Entropy (QSampEn) (Lake and Moorman, 2011), Amplitude-aware permutation entropy (AAPE) (Azami and Escudero, 2016), Detrended Fluctuation Analysis (DFA) (Gates and Dingwell, 2007, 2008; Hausdorff, 2009) and Recurrence Quantification Analysis (RQA) (Marwan, 2008; Trulla et al., 1996; Zbilut and Webber, 1992).

Having so many nonlinear tools to measure movement variability (MV) led Caballero et al. 2014, p. 67 to raise the following question: "Is there a best tool to measure variability?" which lead me to ask two questions for this thesis: (i) what to quantify in movement variability? and (ii) which tools are appropriate to quantify movement variability?

### 2.3.1 What to quantify in movement variability?

Complexity for this thesis refers to the dynamics of joint biomechanical degrees of freedom of a person performing a task in a certain environment (Davids et al., 2003). That said, Vaillancourt and Newell (2002, 2003) stated that there is no universal increase or decrease in complexity for movement variability as a function of age or disease but a dependency with the task dynamics. For example, in a constant-force task (where the task dynamics is of low dimension), older adults present less complexity due their inability to introduce additional degrees of freedom in the neuromuscular system. However, when the task dynamic is oscillatory, older adults or unhealthy adults (having intrinsic low dimension dynamics of their resting state) present an increase of complexity

because these adults have more difficulty to reduce the dimension output to a lower dimension. In contrast, inspired by Tononi et al. (1998) who modelled complexity with the variables of complexity versus regularity of neural networks, Stergiou et al. (2006) proposed a model for optimal human movement variability with the variables of complexity versus predictability. The model of Stergiou et al. (2006) stated that higher values of complexity are associated with rich behaviour of movements, while lower values of complexity movements are associated with poor behaviours of movements. Hence, higher complexity of movements are characterised by chaotic systems, while lesser complexity of movement is characterised either as noisy systems or periodic systems (having either low or high amounts of predictability) (Stergiou et al., 2006).

Considering the works of Vaillancourt and Newell (2002, 2003), Tononi et al. (1998) and Stergiou et al. (2006), I assume that the quantification of movement variability can be based on the complexity and predictability of human movement.

### **2.3.2 Which methods of nonlinear analysis are appropriate to quantify movement variability?**

Stergiou et al. (2006) proposed a model for movement variability which state that variables of complexity and predictability of a system can be used to characterise and quantify movement variability. With that in mind, this thesis has led me to understand other challenges such as (i) finding, (ii) understanding and (iii) applying the appropriate methods of nonlinear analysis that can measure such variables.

Pincus (1995, 1991) proposed Approximate Entropy (ApEn) to quantify regularity of time series. Then, Richman and Moorman (2000) due to self-matching found that the algorithm of ApEn could evoke the occurrence of  $\ln(0)$  which made ApEn dependant on the available data for which Sample Entropy (SampEn) was proposed as an algorithm that does not consider self-matching. Hence, SampEn values are

### 2.3 Quantifying movement variability with nonlinear analysis

---

independent of the length of time series and its algorithm is simpler than ApEn. Then, instead of using single statistics, Costa et al. (2002) proposed Multiscale Entropy (MSE) which computes SampEn of consecutive coarse-grained time series of the original time series defined by the scale factor. With MSE algorithm, (Costa et al., 2002) noted that pathology dynamics for time series of heartbeat intervals are associated with reduction of complexity. Therefore, Costa et al. 2002, p. 3 concluded that physiological complexity is associated with the adaptive capacity of the organism, disease states and aging which "may be defined by a sustained breakdown of long-term correlations and loss of information". Essentially, entropy measures (AppEn and SampEn), quantify regularity and complexity of time series (Preatoni et al., 2013). However, Goldberger (1996) mentioned that the increase of irregularity in time series is not synonymous of increase with physiological complexity. Similarly, an increase of ApEn or SampEn, "implying increase of irregularity and decrease in predictability" (Goldberger et al., 2002, p. 25), is not synonymous with an increase of dynamical complexity when analysing physiology signals (Costa et al., 2002). Hence, Goldberger et al. (2002) demonstrated that ApEn as a regularity statistic is not a direct index of physiological complexity where, for example, a randomised time series of an healthy heartbeat with multi-scale and complex patterns of variability show a higher value of ApEn even though the time series is less complex. Therefore, Goldberger et al. 2002, p. 24 concluded that the loss of physiological complexity can be "better assessed using other measures which can detect and quantify the presence of long-term correlations in non-stationary series." Hence, Costa et al. (2002); Goldberger et al. (2002); Vaillancourt and Newell (2002) concluded that ApEn and SampEn do not necessary show the right representation of what they intend to measure.

Therefore, considering the previous cons of ApEn, SampEn and MSE, Detrended Fluctuation Analysis (DFA) can tackle the problem of quantifying long-term correlations

## Quantifying Movement Variability

---

of time series (Peng et al., 1995). DFA is based on analysing fractal features and is calculated as the root mean square fluctuation of an integrated and detrended time series and it is represented by a scaling exponent,  $\alpha$ , which is an indicator for roughness of time series, e.g. "the larger the value of  $\alpha$ , the smoother the time series (Peng et al., 1995, p. 83). However, DFA can result in a false conclusion for long-term correlations in the time series (Rangarajan and Ding, 2000, p. 5001), therefore DFA "can falsely classify certain type of time series as fractals" (Wijnants et al., 2009, p. 80). With that in mind, Wijnants et al. (2009) proposed the use of Recurrence Quantification Analysis (RQA) as a technique that does not present constraints with regards to length size, stationary or statistical distribution of the time series. Wijnants et al. (2009) also highlighted that SampEn index is computed over the sequential values of the time series, whereas Shannon entropy with RQA, RQAEn, is computed over the distribution of deterministic lines in the Recurrence Plots (RP) (Marwan, 2008; Trulla et al., 1996; Zbilut and Webber, 1992). Similarly, Rhea et al. (2011) highlighted that algorithms to compute entropy measures are different since ApEn and SampEn are approximations of the Kolmogorov-Sinai Entropy computing the likelihood that a template pattern repeats in the time series while RQAEn is derived from Shannon entropy and is computing number of line segments of varying length in the RP. Even with those differences in the algorithms, smaller values of recurrence percentage of the RQA show the increase on practice of movement dynamics, concluding that such recurrence percentage indicate an increase of system stability (Wijnants et al., 2009).

Another method to measure variability is the largest Lyapunov exponent (LyE) which is used to "quantify the rate at which nearby trajectories converge or diverge" (Stergiou, 2016, p. 85). For instance, "LyE from a stable system with little to no divergence will be zero (e.g. sine wave)" and "LyE for an unstable system that has highest amount of divergence will be positive and relative high in value (e.g. 0.469 for

## 2.4 Nonlinear analysis with real-world data

---

random noise)" and for chaotic systems like the Lorenz system, LyE is in between the two of the previous extremes ( $\text{LyE} \approx 0.1$ ) (Miller et al., 2006, p. 2874).

Measuring human movement variability requires a combination of the pros and cons of the previous methods that analyse either (i) the dynamic complexity or (ii) the degree of regularity, stability or predicability in a system (Goldberger et al., 2002; Harbourne and Stergiou, 2009; Stergiou and Decker, 2011). For instance, Rangarajan and Ding (2000) stated the use of both spectral analysis and random walk analysis, the base of DFA, is a better approach than only using one method because, for instance, using only DFA can lead to false conclusion for long-term correlations in the time series. Similarly, Wijnants et al. (2009) selected different methods (e.g. spectral analysis, standard dispersion analysis, DFA, RQA and SampEn) to quantify movement variability that can complement the strengths of some of them and compensate the weakness of others. Recently, Caballero et al. (2014) proposed the unification of different methods of nonlinear analysis to address every aspect of the dynamics of a systems and the characterisation of movement variability. Although, there is no best method to measure movement variability and an unification of methods to quantify human movement variability is still an open question (Caballero et al., 2014), finding the appropriate method of nonlinear analysis to measure movement variability for a specific problem, and knowing its strengths and weakness of such appropriate method is one of the research questions for this thesis.

## 2.4 Nonlinear analysis with real-world data

Recently, Huffaker et al. (2017) pointed out that one of the caveats when applying methods of nonlinear time series analysis is its unreliability when the estimated metrics come from real-world data which are generally short, noisy and non-stationary. Similarly, Preatoni et al. (2013) mentioned the limitations of methods of nonlinear analysis in



sport activities where data required to be large (e.g. number of trials, duration of the experiment and sampling frequency). Caballero et al. (2014) argued that there are weaknesses of different methods of nonlinear analysis regarding the characteristics of the time series such as non-stationarity, length data size, noise, sampling rate. However, in the work of Huffaker et al. (2017), Preatoni et al. (2013) and Caballero et al. (2014) no further exploration of the metrics of nonlinear analysis with real-world data is presented.

### 2.4.1 Non-stationarity

Non-stationarity of time series signals might create spurious increase or decrease in methods of nonlinear analysis. For instance, Costa et al. (2007) noted that non-stationarity in the signals might alter the increase of irregularity of signals for the shortest scales when applying MSE. Also, Dingwell and Cusumano (2000) reported non-stationarity in time series when using LyE, where LyE requires to be validated using surrogation (Dingwell and Cusumano, 2000; Miller et al., 2006) to ensure the robustness of the metric. Caballero et al. (2014) reported three options when dealing with non-stationary data: (i) remove non-stationary data, (ii) use empirical mode decomposition (EMD), or (iii) apply nonlinear tools, such as DFT and RQA, which are less sensitive to non-stationary data.

To remove non-stationary data, Carroll and Freedman (1993) suggested to remove the trends or to eliminate the initial data (e.g. first 20 seconds of samples) to ignore the trend of time series. For instance, van Dieën et al. (2010), in experiments with center of pressure movements in seated balancing, discarded the first 5 seconds of the time series in the start of the measurement.

Non-stationary time series can also be treated with Empirical Mode Decomposition (EMD) method which decompose nonlinear, non-stationary signals into their intrinsic

## 2.4 Nonlinear analysis with real-world data

---

frequency components (Huang et al., 1998; Wu and Huang, 2004, 2009). Hence, Costa et al. (2007); Flandrin et al. (2004) tested whether EMD is a robust method for detrending and denoising time series and noted that EMD does not require selection of input parameters. However, the reliability of EMD methods is still an open problem. For instance, an extension of EMD called Multivariate Empirical Mode Decomposition (MEMD) has been proposed to analyse multiple time series (Mandic et al., 2013; Rehman and Mandic, 2010). See (Bonnet et al., 2014; Costa et al., 2007; Daubechies et al., 2011; Mert and Akan, 2018; Wu and Hu, 2006) for applications of EMD.

Finally, one can use methods of nonlinear analysis that are unaffected by non-stationarity of time series such as Detrended Fluctuation Analysis (DFA) (Hausdorff et al., 1995) and Recurrence Quantification Analysis (RQA) (Marwan, 2008; Trulla et al., 1996; Zbilut and Webber, 1992). However, Bryce and Sprague (2012) reported negatives of DFA such as the introduction of uncontrolled bias, computational expensiveness and highlighted that DFA cannot provide a generic protection against the non-stationarities of the signals. The implication of this review is that RQA remains a promising approach.

### 2.4.2 Data length

Many of the methods of nonlinear analysis are sensitive to the length of time series (Caballero et al., 2014). For example, given that Multiscale Entropy (MSE) is a statistical measure, the data lengths when using MSE are recommended to be large (e.g. up to the scale of  $6 \times 10^3$  data points) to ensure enough samples for the analysis (Costa et al., 2007). Also, the methods of LyE (Wolf et al., 1985), DFA (Peng et al., 1995), SampEn (Rhea et al., 2011) and ApEn (Richman and Moorman, 2000) require a minimum of data length whereas FuzzyEn (Chen et al., 2007) is more robust for data length. However, the methods of RQA (Riley et al., 1999; Webber and Zbilut, 1994;

Wijnants et al., 2009) and Permutation Entropy (Zunino et al., 2009) are less sensitive to the length of time series.

### 2.4.3 Sampling rate

One possible solution for the sensitivity of nonlinear methods to data length is the increase or decrease of sampling rate (Caballero et al., 2014). However, Duarte and Sternad 2008, p. 267 stated "the increase of sampling rate frequency would only increase artificially the data points without adding information" which raises the problem of oversampling signals. Then, Rhea et al. (2011) investigated the influence of sampling rate in three entropy measures (ApEn, SampEn and RQAEn) concluding that ApEn and RQAEn were robust across to the increase of sampling frequency, while SampEn presented significant difference across all sampling frequencies. Rhea et al. (2011) noted that SampEn is more sensitive to colinearities than ApEn and RQAEn at higher frequencies which lead to a decrease of SampEn. Rhea et al. (2011) then concluded that signals at higher frequencies appear to be more regular due to the increase of data, therefore producing erroneous entropy results. Caballero et al. (2013) stated that for short length time series for SampEn and DFA, the decrease of sampling rate frequency is recommended because it presents less consumption of computational power. Additionally, Caballero et al. (2013) showed the robustness of the methods of SampEn and DFA when using different sampling rate frequencies, stating that frequencies near the dynamics of the activity create a more reliable analysis of the dynamics.

### 2.4.4 Noise

Caballero et al. (2014) reviewed methods of nonlinear analysis that are affected by noise. Rosenstein et al. (1993), for instance, tested the robustness of LyE against three levels of noise (lowest, moderate and highest) in order to note the unreliability of LyE

## 2.4 Nonlinear analysis with real-world data

---

exponents in high-noise environments. However, such case of unreliability of LyE is unreal as the reported values of signal-to-noise ratios are substantially lower than those used at the experiments of Rosenstein et al. (1993). Bandt and Pompe (2002) proposed Permutation Entropy (PeEn) which is an appropriate method for chaotic time series in the presence of observational and dynamical noise. Another example is the work of Chen et al. (2009) who compared the robustness of FuzzEn, ApEn and SampEn metrics against different levels of noise, concluding that for a large value of the parameter  $r$  of ApEn and SampEn, these two metrics can work well with high levels of noise, however when noise increases, ApEn and SampEn fail to distinguish time series with different levels of noise, whereas FuzzEn is robust to such highest levels of noise.

Regardless of the source of noise which can either be mechanical (due to recording equipment) or physiological (due to different neural noise), Rhea et al. (2011) highlighted the importance of the effects on noise in three entropy measures (ApEn, SampEn and RQAEn) which produce different results. Values for AnEn and SampEn, for instance, tended to increase as noise was added to the signals, while RQAEn showed an inverse effect, e.g. RQAEn values decreased as noise in the signal was increased. Similar results for synthetic data were also reported by Pellecchia and Shockley (2015) where RQAEn values decreased from ( $RQAEn \approx 5$ ) for Lorenz system to a ( $RQAEn \approx 2$ ) for a periodic signal with a further decrease ( $RQAEn \approx 0.3$ ) for a sinusoid signal with superimposed noise. Therefore, RQA can be affected by noise (Rhea et al., 2011). However, the effects of noise and non-stationarity can be mitigated with the selection of the right parameters to perform RQA, particularly, using embedding dimensions from 10 to 20 (Webber and Zbilut, 2005).

Another solution for noisy time series is the use of traditional filtering methods. However, the attenuation of all frequencies of the signal along with the noise, given a cutoff frequency, can cut out information that might be useful for nonlinear

time-series. Another option is apply DFA, which additionally to the remove of local trends, it also reduces the noise of the signal (Hausdorff et al., 1995). Alternatively, filtering strategies for nonlinear time-series data can be applied which tailor in a more effective way the properties of nonlinear dynamics (see Bradley and Kantz 2015 and references therein).

## 2.5 Final remarks

In this chapter, literature has been reviewed based on the questions of: (i) what to quantify in movement variability, (ii) which non-linear tools are appropriate to quantify movement variability, and (iii) what are the strengths and weaknesses of nonlinear analysis methods with real-world data. It can then be concluded that little research has been done on the effects with Reconstructed State Spaces (RSSs), Recurrent Plots (RPs), and Recurrence Quantification Analysis (RQA) metrics for different embedding parameters, different recurrence thresholds and different characteristics of time series (window length size, smoothness and structure). That said, nonlinear analysis methods such as estimation of embedding parameters, RSSs, RPs, and RQAs are reviewed in the following chapter.

# Chapter 3

## Nonlinear Analysis

### 3.1 Introduction

Nonlinear analysis investigate the dynamics of observed time-ordered data. Methods of nonlinear analysis, for this thesis, entail determination of embedding parameters, state space reconstruction, uniform time-delay embedding, recurrence plots and recurrence quantification analysis.

The method of state space reconstruction was originally proposed by Packard et al. (1980) and formalised by Takens (1981). Since then, various investigations and disciplines relative to nonlinear time series analysis have benefited from it (Aguirre and Letellier, 2009; Frank et al., 2010; Samà et al., 2013; Stergiou and Decker, 2011). The method of reconstructed state space (RSS) is based on uniform time-delay embedding (UTDE) which is a simple matrix implementation considering the embedding parameters ( $m$  and  $\tau$ ), therefore, matrix represents the reconstruction of an unknown  $d$ -dimensional manifold  $M$  from a scalar time series (e.g. one-dimensional time series in  $\mathbb{R}$ ). A manifold, in this context, is a multidimensional curved surface within a space (e.g. a saddle) (Guastello and Gregson, 2011). Henceforth, the method of state space reconstruction using a scalar time series can preserve dynamic invariants such as correlation dimension,

fractal dimension, Lyapunov exponents or Kolmogorov-Sinai entropy (Bradley and Kantz, 2015; Krakovská et al., 2015; Quintana-Duque and Saupe, 2013; Quintana-Duque, 2012, 2016). However, there are still many challenging research questions to be answered with regards to the selection of appropriate embedding parameters that preserve the dynamics of a system for the computation of methods nonlinear analysis such as RSS, RPs and RQAs. With that in mind, the following methods are described in this chapter: the state space reconstruction theorem (RSSs), uniform time-delay embedding theorem (UTDE), and methods to compute embedding parameters: false nearest neighbours (FNN) and average mutual information (AMI). Additionally, fundamentals of Recurrence plots (RPs), Recurrence quantification analysis (RQA) and the introduction of 3D surface plots of RQA are presented in this chapter.

### 3.2 State Space Reconstruction Theorem

Following the notation employed in Casdagli et al. (1991); Garland et al. (2016); Gibson et al. (1992); Takens (1981); Uzal et al. (2011); Uzal and Verdes (2010), the method of state space reconstruction is defined by:

$$s(t) = f^t[s(0)], \quad (3.1)$$

where  $s, s : A \rightarrow M$  given that  $A \subseteq \mathbb{R}$  and  $M \subseteq \mathbb{R}^d$ , represents a trajectory which evolves in an unknown  $d$ -dimensional manifold  $M$ ,  $f : M \rightarrow M$  is an evolution function and  $f^t$ , with time evolution  $t \in \mathbb{N}$ , is the  $t$ -th iteration of  $f$  that corresponds to an initial position  $s(0) \in M$  (Takens, 1981). Then, a point of a scalar time series  $x(t)$  in  $\mathbb{R}$ , can be obtained with

$$x(t) = h[s(t)], \quad (3.2)$$

### 3.3 Uniform Time-Delay Embedding (UTDE)

---

where  $h$  is a function,  $h : M \rightarrow \mathbb{R}$ , defined on the trajectory  $s(t)$ .

Reconstructed state space can then be described as an  $n$ -dimensional state space defined by  $y(t) = \Psi[\mathbf{X}(t)]$  where  $\mathbf{X}(t) = \{x(t), x(t - \tau), \dots, x(t - (m - 1)\tau)\}$  is the uniform time-delay embedding with a dimension embedding  $m$  and delay embedding  $\tau$  and  $\Psi : \mathbb{R}^m \rightarrow \mathbb{R}^n$  is a further transformation of dimensionality (e.g. Principal Component Analysis, Singular Value Decomposition, etc) being  $n \leq m$ . With that in mind, uniform time-delay embedding,  $\mathbf{X}(t)$ , defines a map  $\Phi : M \rightarrow \mathbb{R}^m$  such that  $\mathbf{X}(t) = \Phi(s(t))$ , where  $\Phi$  is a diffeomorphic map (Takens, 1981) whenever  $\tau > 0$  and  $m > 2d_{box}$  and  $d_{box}$  is the box-counting dimension of  $M$  (Garland et al., 2016). Then, if  $\Phi$  is an embedding of an attractor (i.e. evolving trajectories) in the reconstructed state space, a composition of functions represented with  $F^t$  is induced on the reconstructed state space:

$$\mathbf{X}(t) = F^t[\mathbf{X}(0)] = \Phi \circ f^t \circ \Phi^{-1}[\mathbf{X}(0)]. \quad (3.3)$$

Hence, an embedding is defined as "a smooth one-to-one coordinate transformation with a smooth inverse" (Casdagli et al., 1991, p. 54). Figure 3.1 illustrates the state space reconstruction.

### 3.3 Uniform Time-Delay Embedding (UTDE)

Frank et al. (2010) and Samà et al. (2013) refer to the state space reconstruction outlined in 3.2 as "time-delay embeddings" or "delay coordinates", respectively. However, the term "uniform time-delay embedding" is considered as being more descriptive and appropriate terminology for this thesis.

The uniform time-delay embedding is represented as a matrix of uniform delayed copies of the time series  $\{\mathbf{x}_n\}_{n=1}^N$  where  $N$  is the sample length of  $\{\mathbf{x}_n\}$  and  $n$  is index for the samples of  $\{\mathbf{x}_n\}$ .  $\{\mathbf{x}_n\}_{n=1}^N$  has a sample rate of  $T$ . The delayed copies



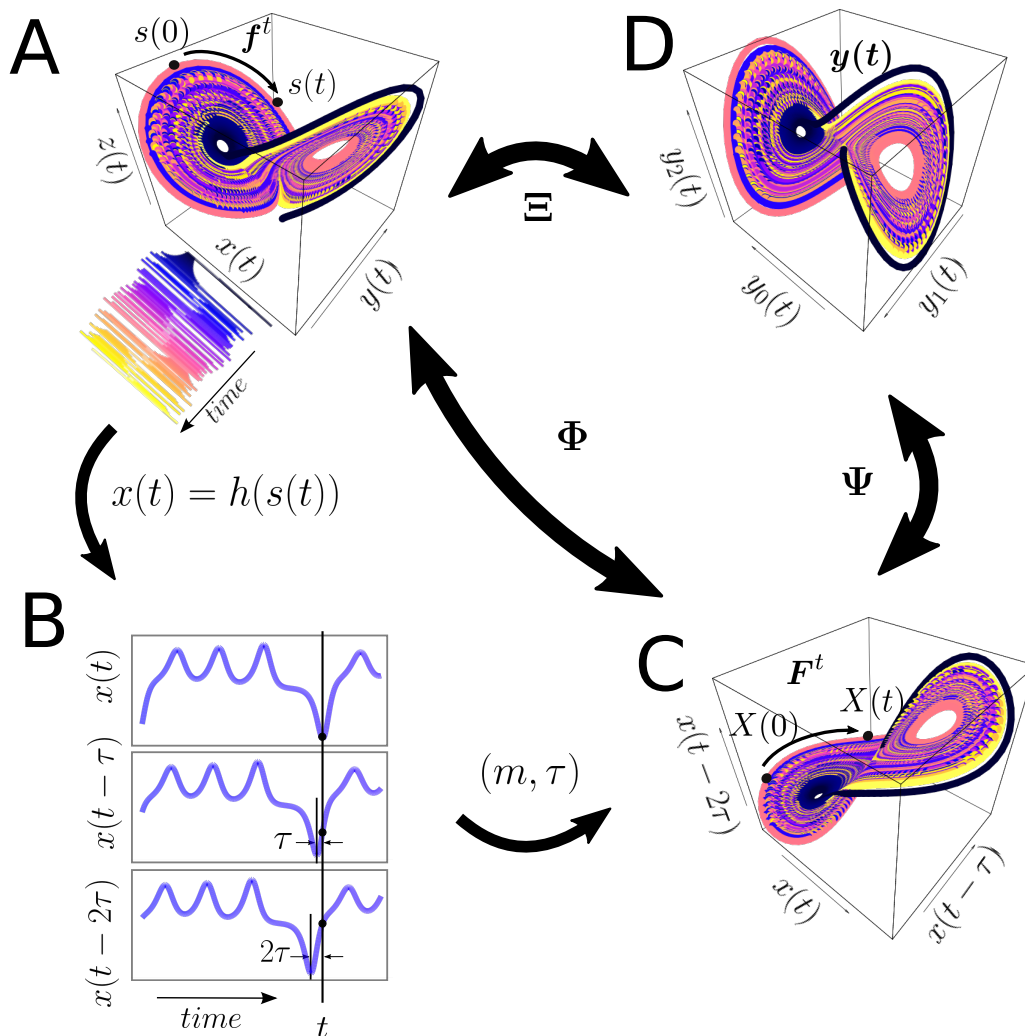


**Fig. 3.1 State space reconstruction methodology.** State space reconstruction is based on  $x(t) = h[s(t)] = h[f^t[s(0)]]$  where  $h[\cdot]$  is a function  $h : M \rightarrow \mathbb{R}$ , defined on the trajectory  $s(t)$ .  $f$  is the true dynamical system,  $f : M \rightarrow M$ , defined as evolution function and  $f^t$ , with time evolution  $t \in \mathbb{N}$  which is the  $t$ -th iteration of  $f$  that corresponds to an initial position  $s(0) \in M$ . The time-delay embedding represented as  $\Phi$ , maps the original  $d$ -dimensional state  $s(t)$  into the  $m$ -dimensional uniform time-delay embedding matrix  $\mathbf{X}(t)$ . The transformation map  $\Psi$  maps  $\mathbf{X}(t)$  into a new state space  $y(t)$  of dimensions  $n < m$ . (A)  $M$ -dimensional state space (e.g. Lorenz system); (B) Delayed copies of 1-dimensional  $x(t)$  from the Lorenz system; (C)  $m$ -dimensional reconstructed state space with  $m$  and  $\tau$ , and (D)  $y(t)$  is the  $n$ -dimensional reconstructed state space. The total reconstruction map is represented as  $\Xi = \Psi \circ \Phi$  where  $\Phi$  is the delay reconstruction map and  $\Psi$  is the coordinate transformation map. This figure is adapted from the work of Casdagli et al. (1991); Quintana-Duque (2012); Uzal et al. (2011). R code to reproduce the figure is available at [github](#).

### 3.4 Estimation of Embedding Parameters

---

of  $\{\mathbf{x}_n\}$  are uniformly separated by  $\tau$  and represented as  $\{\tilde{\mathbf{x}}_{n-i\tau}\}$  where  $i$  goes from  $0, 1, \dots, (m-1)$  (Fig 3.2).  $\{\tilde{\mathbf{x}}_{n-i\tau}\}$  contains information of unobserved state variables and encapsulates the information of the delayed copies of the available time series in the uniform time-delay embedding matrix  $\mathbf{X}_\tau^m, \mathbf{X}_\tau^m \in \mathbb{R}^m$ , defined as

$$\mathbf{X}_\tau^m = \begin{pmatrix} \tilde{\mathbf{x}}_n \\ \tilde{\mathbf{x}}_{n-\tau} \\ \tilde{\mathbf{x}}_{n-2\tau} \\ \vdots \\ \tilde{\mathbf{x}}_{n-(m-1)\tau} \end{pmatrix}^\top, \quad (3.4)$$

where  $m$  is the embedding dimension,  $\tau$  is the embedding delay and  $^\top$  denotes the transpose.  $m$  and  $\tau$  are known as embedding parameters. The matrix dimension of  $\mathbf{X}_\tau^m$  is defined by  $N - (m-1)\tau$  rows and  $m$  columns and  $N - (m-1)\tau$  defines the length of each delayed copy of  $\{\tilde{\mathbf{x}}_n\}$  in  $\mathbf{X}_\tau^m$ . A graphical representation of uniform time-delay embedding is shown in Figure 3.2. See Appendix B for further details and explicit examples of uniform time-delay embedding methodology.

## 3.4 Estimation of Embedding Parameters

The estimation of the embedding parameters ( $m$  and  $\tau$ ) is an essential step for the state space reconstruction in order to apply the method of uniform time-delay embedding (UTDE). Hence, two of the most common algorithms are reviewed, which will be used in this thesis, to compute the embedding parameters: the false nearest neighbour (FNN) and the average mutual information (AMI).

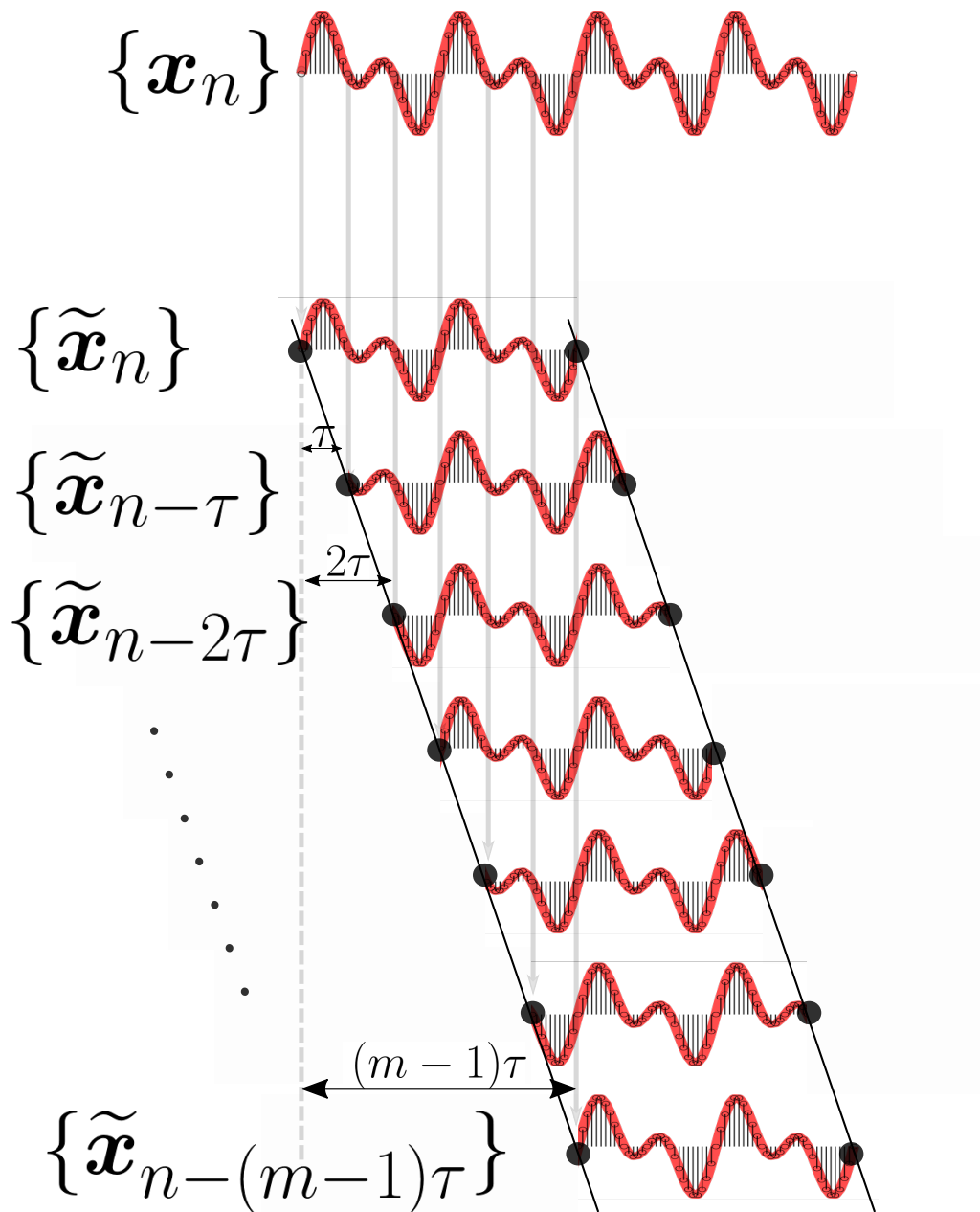


Fig. 3.2 **Uniform time-delay embedding (UTDE)**. UTDE is illustrated as  $m - 1$  delayed copies of  $\{x_n\}$  which is uniformly separated by  $\tau$ . UTDE is represented as  $\{\tilde{x}_n, \dots, \tilde{x}_{n-(m-1)\tau}\}$  (Eq. 3.4). R code to reproduce the figure is available at [\[4\]](#).

### 3.4.1 False Nearest Neighbours (FNN)

To select the minimum embedding dimension  $m_0$ , Kennel et al. (1992) used the method of false neighbours which can be understood as follows: on one hand, when the embedding dimension is too small to unfold the attractor (i.e. evolving trajectories in a state space) "not all points that lie close to each other will be neighbours and some points appear as neighbours as a result of the attractor being projected down into an smaller space", on the other hand, when increasing the embedding dimension "points that are near to each other in the sufficient embedding dimension should remain close as the dimension increase from  $m$  to  $m + 1$ " (Krakovská et al., 2015, p. 3).

From a mathematical point of view, state space reconstruction is done when the attractor is unfolded with either the minimum embedding dimension,  $m_0$ , or any other embedding dimension value where  $m \geq m_0$  (Kennel et al., 1992). In contrast, any large value of  $m_0$  leads to excessive computations (Bradley and Kantz, 2015). Hence, Cao (1997) proposed an algorithm based on the false neighbour method where only the time-series and one delay embedding value are necessary to select the minimum embedding dimension. Cao's algorithm is based on  $E(m)$ , which is the mean value of all  $a(i, m)$ , and defined as:

$$\begin{aligned} E(m) &= \frac{1}{N - m\tau} \sum_{i=1}^{N-m\tau} a(i, m) \\ &= \frac{1}{N - m\tau} \sum_{i=1}^{N-m\tau} \frac{\|\mathbf{X}_i(m+1) - \mathbf{X}_{n(i,m)}(m+1)\|}{\|\mathbf{X}_i(m) - \mathbf{X}_{n(i,m)}(m)\|} \end{aligned} \quad (3.5)$$

where  $\mathbf{X}_i(m)$  and  $\mathbf{X}_{n(i,m)}(m)$  are uniform time-delay embeddings with  $i = 1, 2, \dots, N - (m - 1)\tau$  and  $n(i, m) = 1 \leq n(i, m) \leq N - m\tau$ . From Eq. 3.5  $E(m)$  is only dependent on  $m$  and  $\tau$  for which  $E_1(m)$  is defined as

$$E_1(m) = \frac{E(m+1)}{E(m)}. \quad (3.6)$$

$E_1(m)$  is therefore proposed to describe the variation from  $m$  to  $m + 1$  in order to find the minimum embedding dimension  $m_0$  (Eq. 3.6). As Cao 1997, p. 44 described: " $E_1(m)$  stops changing when  $m$  is greater than some  $m_0$ , if the time series comes from a multidimensional state space then  $m_0 + 1$  is the minimum dimension". Additionally, Cao (1997) proposed  $E_2(m)$  to distinguish deterministic signals from stochastic signals.  $E_2(m)$  is defined as

$$E_2(m) = \frac{E^*(m+1)}{E^*(m)}, \quad (3.7)$$

where

$$E^*(m) = \frac{1}{N - m\tau} \sum_{i=1}^{N-m\tau} \|\mathbf{X}_i(m+1) - \mathbf{X}_{n(i,m)}(m+1)\|. \quad (3.8)$$

For instance, when the signal comes from random noise (values that are independent from each other), all  $E_2(m)$  values are approximately equal to 1 (e.g.  $E_2(m) \approx 1$ ). However, for deterministic data  $E_2(m)$  is not constant for all  $m$  (e.g.  $E_2(m) \neq 1$ ).

Two time series are considered as an example of the use of  $E_1(m)$  and  $E_2(m)$  values, the solution for the  $x$  variable of the chaotic deterministic Lorenz system (Figure 3.3E), and a Gaussian noise time series with zero mean and a variance of one (Figure 3.3F). Then  $E_1(m)$  and  $E_2(m)$  values are computed for each time series. The  $E_1(m)$  values for the chaotic time series appear to be constant after the dimension is equal to six. The determination of six is given that any value of  $m$  can be used as  $E_1(m)$  values are within the threshold of  $1 \pm 0.05$  (Fig 3.3A). Although the  $E_2(m)$  values for the chaotic time series tend to be closer to one as  $m$  increases, these are different to one (Fig 3.3C), for which, it can be concluded that the chaotic time series comes from a chaotic deterministic signal. With regard to the noise time series,  $E_1(m)$  values appeared to be constant when  $m$  is close to thirteen which is defined by the same threshold of  $1 \pm 0.05$  (Figure 3.3B). Then, contrary to the  $E_2(m)$  values for a chaotic Lorenz time series, all values of  $E_2(m)$  for a noise time series are approximately equal to one (Figure 3.3D). Hence,  $E_1(m)$  values then indicate the minimum embedding

### 3.4 Estimation of Embedding Parameters

dimension of the noisy time series is thirteen, however all of the  $E_2(m)$  values are approximately equal to one (Figure 3.3D), for which, it can be concluded that noise time series is a stochastic signal.

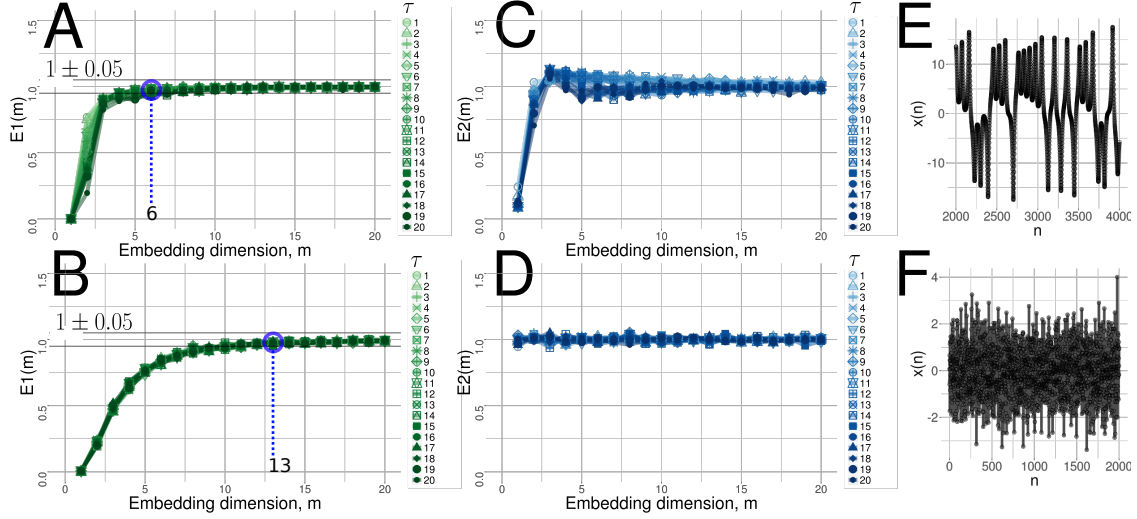


Fig. 3.3 **Minimum dimension embedding values with Cao's method.** (A, B)  $E_1(m)$  values and (C, D)  $E_2(m)$  values with variations of  $\tau$  values from one to twenty for (E) chaotic and (F) random time series. R code to reproduce the figure is available at [\[47\]](#).

It is important to note that for this thesis not only the values for  $E_1(m)$  and  $E_2(m)$  are computed but also a variation of  $\tau$  from 1 to 20 (Figure 3.3 (A,B,C,D)) has been explored. The purpose of using variations for  $\tau$  is to show its independence with regard to the  $E_1(m)$  (Fig. 3.3(A,B)) and  $E_2(m)$  (Fig. 3.3(C,D)). Although Cao (1997) mentioned that no parameters are required to find the minimum embedding dimension, it has been found, in this thesis, that it is necessary to define a threshold for which  $E_1(m)$  values appear to be constant. Hence, for the given examples and the reported results for this thesis, a threshold of 0.05 is defined (see Fig. 3.3(A) with the parallel lines of the threshold near to one  $1 \pm 0.05$ ). Additionally, see optimal embedding parameters on Chapter 7 for further research regarding the selection of such threshold.

### 3.4.2 Average Mutual Information (AMI)

One would experience the following when selecting the delay dimension parameter,  $\tau$ :

- (i) when  $\tau$  is too small, the elements of uniform time-delay embedding will be along the bisectrix of the phase space and the reconstruction is generally not satisfactory,
- (ii) when  $\tau$  is too large the elements of the uniform time-delay embedding will become spread and uncorrelated which makes recovering the underlying attractor (i.e. evolving trajectories in a state space) difficult, if not impossible (Casdagli et al., 1991; Emrani et al., 2014; Garcia and Almeida, 2005).

There are many approaches to compute the embedding parameters (Bradley and Kantz, 2015), for instance, geometry-based methodologies where the amount of space filled in the reconstructed state is the metric to compute the delay embedding (Rosenstein et al., 1994) or theoretical approaches to estimate an optimal parameter for  $\tau$  (Casdagli et al., 1991). However, the autocorrelation function and the average mutual information (AMI) are the two most commonly used algorithms to compute the minimum delay embedding parameter  $\tau_0$ . Emrani et al. (2014) used the autocorrelation function in which the first zero crossing is considered as the minimum delay embedding parameter. However, the autocorrelation function is a linear statistic whereas AMI considers the nonlinear dynamical correlations (Fraser and Swinney, 1986; Krakovská et al., 2015). With that in mind, the AMI algorithm is described below to estimate the minimum delay embedding parameter,  $\tau_0$ .

To compute the AMI, an histogram of  $x(n)$  using  $n$  bins is calculated and then a probability distribution of data is computed (Kantz and Schreiber, 2003). AMI is therefore denoted by  $I(\tau)$  which is the average mutual information between the original time series,  $x(n)$ , and the delayed time series,  $x(n - \tau)$ , delayed by  $\tau$  (Kabiraj et al., 2012). AMI is defined by

$$I(\tau) = \sum_{i,j}^N p_{ij} \log_2 \frac{p_{ij}}{p_i p_j}, \quad (3.9)$$

### 3.4 Estimation of Embedding Parameters

where probabilities are defined as follows:  $p_i$  is the probability that  $x(n)$  has a value inside the  $i$ -th bin of the histogram,  $p_j$  is the probability that  $x(n + \tau)$  has a value inside the  $j$ -th bin of the histogram and  $p_{ij}(\tau)$  is the probability that  $x(n)$  is in bin  $i$  and  $x(n + \tau)$  is in bin  $j$ . The AMI is measured in bits (base 2, also called shannons) (Garcia and Sawitzki, 2016; Kantz and Schreiber, 2003). For small  $\tau$  ( $\tau < 3$ ), AMI will be large ( $I(\tau) > 6$ ) and as  $m$  increase AMI will then decrease rapidly. Hence, as  $\tau$  increase and goes to a large limit,  $x(n)$  and  $x(n + \tau)$  have nothing to do with each other and  $p_{ij}$  is factorised as  $p_i p_j$  for which AMI is close to zero. Then, in order to obtain  $\tau_0$ , "it has to be found in the first minimum of  $I(\tau)$  where  $x(n + \tau)$  adds maximal information to the knowledge from  $x(n)$ " meaning that the redundancy between  $x(n + \tau)$  and  $x(n)$  is the least (Kantz and Schreiber, 2003, p. 151).

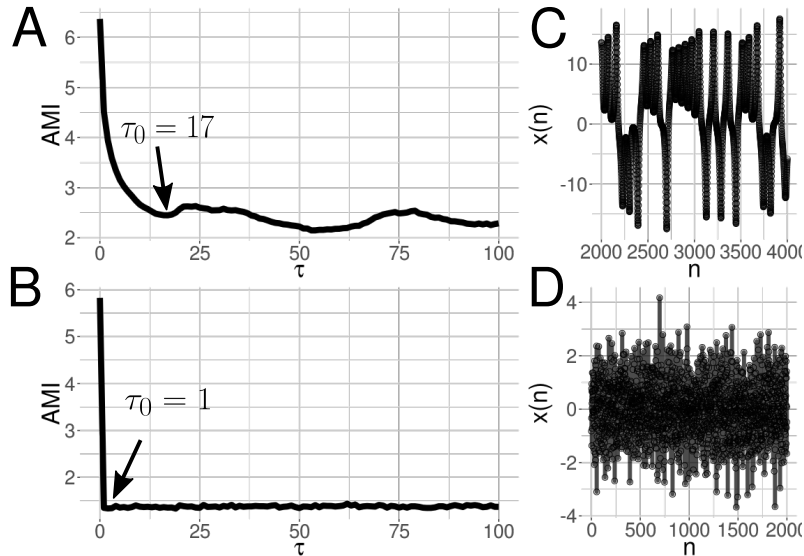


Fig. 3.4 **Minimum delay embedding values with AMI's method.** (A, B) AMI values where its first minimum value in the curve is the minimum time delay embedding ( $\tau_0$ ), for (C) a chaotic and (D) noise time series. R code to reproduce the figure is available at [\[4\]](#).

For example, the AMI is computed for two time series: (i) the  $x$  solution of the deterministic chaotic Lorenz system, and (ii) a noise time series using a normal distribution with mean zero and standard deviation equal to one. The AMI plots are



shown in Figure 3.4, where the minimum delay embedding parameter for the chaotic time series is  $\tau_0 = 17$  and for the noise time series is  $\tau_0 = 1$ . Hence, it can be concluded that the amount of knowledge for any noise time series is zero for which the first minimum embedding parameter is equal to one. On the contrary, the first minimum of the AMI for the chaotic time series is  $\tau_0 = 17$  which is the value that maximize the independence in the reconstructed state space (Bradley and Kantz, 2015).

### 3.4.3 Overall minimum embedding parameters

The method to select minimum embedding parameters ( $m_0$  and  $\tau_0$ ) for this thesis is firstly to compute  $m_0$  with FNN algorithm (considering a threshold of 0.05 for  $E_1(m)$  values) and secondly to compute  $\tau_0$  with AMI (which does not need any extra parameter). From the previous example of the deterministic-chaotic Lorenz system, Fig 3.3(A) is used to determine the minimum dimension embedding ( $m_0 = 6$ ) and Fig 3.4(A) is used to determine the minimum delay embedding ( $\tau_0 = 17$ ). Therefore, with the computation of the minimum embedding parameters, the reconstructed attractor is created in order to ensure with  $\tau_0$  the maximum independence between  $x(t)$  and  $x(t + \tau_0)$  and with  $m_0$  allowing the trajectories in the reconstructed state space to be unfolded.

As time-series data for this thesis are multidimensional (i.e. more than one time series), sample mean of individual minimum values  $m_{0_i}$  and  $\tau_{0_i}$  is used to get an overall value of embedding minimum embedding parameters  $\bar{m}_0$  and  $\bar{\tau}_0$  (Eqs. 3.10 and 3.11):

$$\bar{m}_0 = \frac{1}{N} \sum_{i=1}^N m_{0_i}, \quad (3.10)$$

and

$$\bar{\tau}_0 = \frac{1}{N} \sum_{i=1}^N \tau_{0_i}, \quad (3.11)$$

where  $N$  is the number of time series and  $i = 1, \dots, N$ .

It is also important to mention that a maximum of individual minimum dimension embeddings,  $m_{0,i}$ , can be used instead of the overall sample mean of individual minimum dimension embeddings. The rationale for that is because the maximum value can unfold trajectories in the reconstructed state space that require a lower embedding dimension value. However such statement might be different for the maximum of individual minimum embedding delay as such maximum might not create the maximum independence between  $x(n)$  and  $x(n + \tau)$  for multiple time-series data. See Chapter 7 for future research on optimal embedding parameters.

### 3.5 Reconstructed State Space with UTDE

Given a time series  $x(n)$ , the UTDE matrix is computed with its minimum embedding parameters and then Principal Component Analysis (PCA) is applied in order to select the first three axis of the rotated data to create the reconstructed state spaces (Frank et al., 2010; Samà et al., 2013). See Fig. 3.1 that illustrates and describes the method of reconstructed state space with UTDE.

### 3.6 Recurrence Plots (RP)

Henri Poincaré in 1890 introduced the concept of recurrences in conservative systems, however the discovery was not put into practice until the development of faster computers (Marwan et al., 2007), for which Eckmann et al. (1987) introduced a method where recurrences in the dynamics of a system can be visualised. The intention of Eckmann et al. (1987) was to propose a tool, called Recurrence Plot (RP), that provides insights into high-dimensional dynamical systems where trajectories are very difficult to visualise. Hence, "RP is a tool that helps us to investigate the  $m$ -dimensional phase

space trajectories through a two-dimensional representation of its recurrences" (Marwan and Webber, 2015, p. 7). Similarly, Marwan and Webber (2015) pointed out that in addition to the methodologies of the state space reconstruction and other dynamic invariants (e.g. Lyapunov exponent, Kolmogorov-Sinai entropy), the recurrences of the trajectories in the phase space can provide important clues to characterise the underlying process for periodicities (as Milankovitch cycles) or irregular cycles (as El Niño Southern Oscillation). Such recurrences can not only be visualised using Recurrence Plots (RP) but also be quantified with Recurrence Quantification Analysis (RQA) metrics, which leads to applications of these tools in various areas such as Economics, Physiology, Neuroscience, Earth Science, Astrophysics and Engineering (Marwan et al., 2007).

A recurrence plot based on time series  $\{\mathbf{x}_n\}$  is computed from the state space reconstruction with uniform time-delay embedding method  $X(i) = \{\tilde{\mathbf{x}}_n, \dots, \tilde{\mathbf{x}}_{n-(m-1)\tau}\}$  where  $i = 1, \dots, N$ ,  $N$  is the number of considered states of  $X(i)$  where  $X(i) \in \mathbb{R}^m$  (Eckmann et al., 1987). The recurrence plot is therefore a two-dimensional  $N \times N$  square matrix,  $\mathbf{R}$ , where a black dot is placed at  $(i, j)$  whenever  $X(i)$  is sufficiently close to  $X(j)$ :

$$\mathbf{R}_{i,j}^m(\epsilon) = \Theta(\epsilon_i - \|X(i) - X(j)\|), \quad X(i) \in \mathbb{R}^m, \quad i, j = 1, \dots, N, \quad (3.12)$$

where  $\epsilon$  is a threshold distance,  $\|\cdot\|$  a norm, and  $\Theta(\cdot)$  is the Heaviside function (i.e.  $\Theta(x) = 0$ , if  $x < 0$ , and  $\Theta(x) = 1$  otherwise) (Fig 3.5) (Eckmann et al., 1987; Marwan et al., 2007; Marwan and Webber, 2015). RP is also characterised with a line of identity (LOI) which is a black main diagonal line due to  $R_{i,j} = 1$  for  $i, j = 1, \dots, N$ .

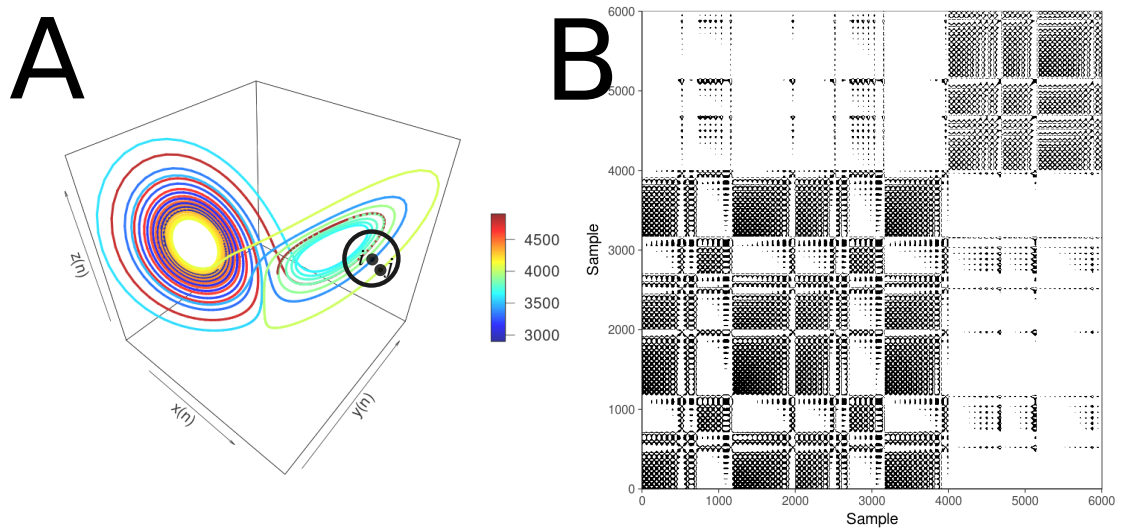
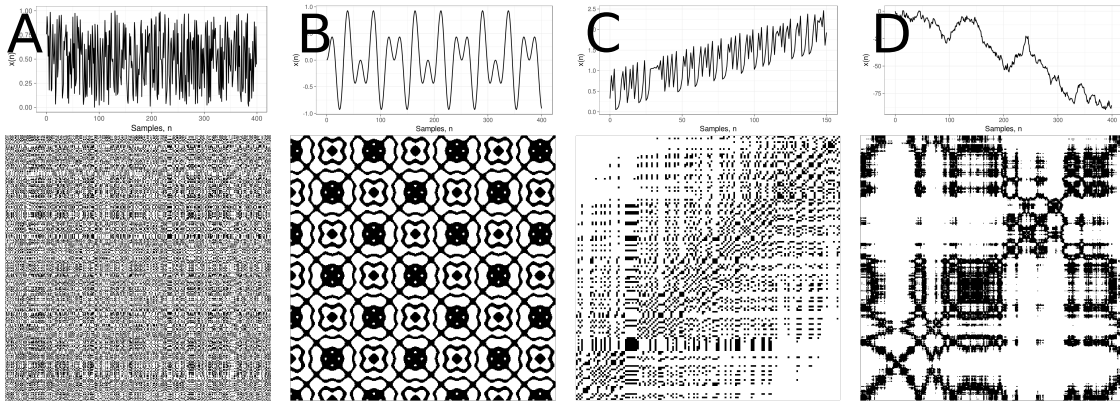


Fig. 3.5 **Recurrence Plots.** (A) State space of the Lorenz system with controlling parameters ( $\rho = 28, \sigma = 10, \beta = 8/3$ ). A point,  $j$ , in trajectory  $X()$  which falls into the neighborhood (black circle) of a given point at  $i$  is a recurrent point and is represented as a black dot in the recurrence plot at location  $(i, j)$  or white otherwise. (B) Recurrence plot using the three components of the Lorenz system and the RP with no embeddings and threshold  $\epsilon = 5$ . This figure is adapted from Marwan and Webber (2015). R code to reproduce the figure is available at [\[45\]](#).

### 3.6.1 Structures of Recurrence Plots

Pattern formations in RPs can be designated either as topology for large-scale patterns or texture for small-scale patterns. In the case of topology, the following pattern formations are presented: (i) homogeneous where uniform recurrence points are spread in the RP e.g., uniformly distributed noise (Figure 3.6A), (ii) periodic and quasi-periodic systems where diagonal lines and checkerboard structures represent oscillating systems, e.g., sinusoidal signals (Figure 3.6B), (iii) drift where paling or darkening recurrence points away from the LOI is caused by drifting systems, e.g., logistic map (Figure 3.6C), and (iv) disrupted where recurrence points are presented white areas or bands that indicate abrupt changes in the dynamics, e.g. Brownian motion (Figure 3.6D) (Eckmann et al., 1987; Marwan and Webber, 2015). Texture, for small-



**Fig. 3.6 Patterns in Recurrence Plots.** Time-series with its respective recurrence plots for: (A) uniformly distributed noise, (B) super-positioned harmonic oscillation ( $\sin \frac{1}{5}t \sin \frac{5}{100}t$ ), (C) drift logistic map ( $x_{i+1} = 4x_i(1 - x_i)$ ) corrupted with a linearly increase term ( $0.01i$ ), and (D) disrupted brownian motion ( $x_{i+1} = x_i + 2rnorm(1)$ ). Figure is adapted from Marwan and Webber (2015). R code to reproduce the figure is available at [\[6\]](#).

scale patterns, can be categorised as: (i) single or isolated recurrence points that represent rare occurring states, do not persist for any time or fluctuate heavily, (ii) dots forming diagonal lines where the length of the small-scale parallel lines in the diagonal are related to the ratio of determinism or predictability in the dynamics of the system, and (iii) dots forming vertical and horizontal lines where the length of the lines represent a time length where a state does not change or change very slowly and the patterns formation represent discontinuities in the signal, and (iv) dots clustering to inscribe rectangular regions which are related to laminar states or singularities (Marwan and Webber, 2015).

Although, the previous pattern descriptions of the structures in the RP offer an idea of the characteristics of dynamical systems from time-series, these descriptions might be misinterpreted and conclusions might tend to be subjective as these require the interpretation of a researcher(s). Because of that, recurrence quantification analysis (RQA) offers objective metrics to quantify the visual characteristics of recurrent pattern structures in the RP (Zbilut and Webber, 1992).

## 3.7 Recurrence Quantifications Analysis (RQA)

Zbilut and Webber (1992) proposed metrics to investigate the density of recurrence points in RPs, then histograms of lengths for diagonal lines in RPs were studied by Trulla et al. (1996), then Marwan (2008) introduced the term Recurrence Quantification Analysis (RQA). There are different RQA metrics such as percentage of recurrence, percentage of determinism, ratio, Shannon entropy of the frequency distributions of the line lengths, maximal line length and divergence, trend and laminarity (Marwan et al., 2007; Marwan and Webber, 2015). For this thesis, I therefore considered only four RQA metrics (i.e. REC, DET, RATIO and ENT) due to their relationship with the variables of complexity and predictability from models of movement variability (Stergiou et al., 2006; Vaillancourt and Newell, 2002, 2003).

### 3.7.1 Measures of RP based on the recurrence density

The percentage of recurrence (REC) or recurrence rate (RR) is defined as

$$REC(\epsilon, N) = \frac{1}{N^2 - N} \sum_{i \neq j=1}^N \mathbf{R}_{i,j}^m(\epsilon), \quad (3.13)$$

which enumerates the black dots in the RP excluding the line of identity. RR is a measure of the relative density of recurrence points in the sparse matrix (Marwan and Webber, 2015).

### 3.7.2 Measures of RP based on diagonal lines

The percent of determinism (DET) is defined as the fraction of recurrence points that form diagonal lines and it is determined by

$$DET = \frac{\sum_{l=d_{min}}^N l H_D l}{\sum_{i,j=1}^N \mathbf{R}_{i,j}(\epsilon)}, \quad (3.14)$$

where

$$H_D(l) = \sum_{i,j=1}^N (1 - \mathbf{R}_{i-1,j-1}(\epsilon))(1 - \mathbf{R}_{i+l,j+l}(\epsilon)) \prod_{k=0}^{l-1} \mathbf{R}_{i+k,j+k}(\epsilon) \quad (3.15)$$

is the histogram of the lengths of the diagonal structures in the RP.

DET can be interpreted as the predictability of the system, for instance, periodic signals have longer diagonal lines, chaotic signals have shorter diagonal lines and absent of diagonal lines results from stochastic signals (Marwan et al., 2007; Marwan and Webber, 2015). Similarly, DET is considered as a measurement for the organisation of points in RPs (Iwanski and Bradley, 1998).

RATIO is defined as the ratio between DET and REC and it is calculated from the frequency distributions of the lengths of the diagonal lines. RATIO is useful to discover dynamic transitions (Marwan and Webber, 2015).

ENT is the Shannon entropy of the frequency distribution of the diagonal line lengths and it is defined as

$$ENT = - \sum_{l=d_{min}}^N p(l) \ln p(l) \quad \text{where} \quad p(l) = \frac{H_D(l)}{\sum_{l=d_{min}}^N H_D(l)}. \quad (3.16)$$

ENT reflects the complexity of the deterministic structure in the system. For instance, for uncorrelated noise or oscillations, the value of ENT is rather small and indicates low complexity of the system, therefore "the higher the ENT is the more complex the dynamics are" (Marwan and Webber, 2015, p. 15).

### 3.7.3 Some weaknesses and strengths of RP and RQA.

One of the main advantages of the use of RP is its capacity to detect small modulations in frequency or phase that are not detectable when using standard methods e.g. spectral or wavelet analysis (Marwan, 2011). Nonetheless, RP is a very young field in nonlinear analysis and many research remains to be done, for instance, RP can create different

### 3.7 Recurrence Quantifications Analysis (RQA)

---

results because of different values for embedding parameters and recurrence thresholds for different size of window length of time-series data (Eckmann et al., 1987; Marwan, 2011). Additionally, the selection of recurrence threshold,  $\epsilon$ , can depend on the system that is under analysis. For instance, when studying dynamical invariants  $\epsilon$  is required to be very small, for trajectory reconstruction  $\epsilon$  is required to have a large threshold or when studying dynamical transition there is little importance about the selection of the threshold (Marwan, 2011). Other criteria for the selection of  $\epsilon$  is that the recurrence threshold should be five times larger than the standard deviation of the observational noise or the use of diagonal structures within the RP is suggested in order to find the optimal recurrence threshold for (quasi-)periodic process (Marwan, 2011).

Iwanski and Bradley (1998) highlighted the importance of choosing appropriate embedding parameters to compute RQA in order to have a better intuition of the nature of the structure of time-series data. In the same investigation, Iwanski and Bradley (1998) pointed out that RQA metrics are quantitatively and qualitatively independent of embedding dimension. However, with an example, Iwanski and Bradley (1998) showed that two dissimilar Recurrence Plots (one from the Rössler system and the other from a varying-period sine wave signal) have got equal values for REC (2.1%) and have got approximately equal values for DET (42.9%, 45.8%, respectively).

#### 3.7.4 3D surface plots of RQA

One approach to tackle some of the previously reviewed weaknesses and strengths of RP and RQA is the method of Zbilut and Webber (1992) in which 3D surface plots are created with an increase of embedding parameters ( $m$  and  $\tau$ ). Zbilut and Webber (1992) explored fluctuations and gradual changes in the 3D surface plots to provide information about the selection of embeddings parameters. Similarly, considering the work of Webber (2018), Marwan and Webber (2015) pointed out that the creation of



3D surface plots are useful for visual selection of recurrence thresholds and embedding parameters (see Fig. 1.16 in Marwan and Webber (2015)).

With that in mind, I propose a similar graphical approach based on the works of Zbilut and Webber (1992), Webber (2018), and Marwan and Webber (2015) in order to visualise fluctuations and changes of 3D surface plots of RQA. Hence, four variables are considered to create 3D surface plots of RQA for this thesis: (i) embedding dimension, (ii) embedding delay, (iii) recurrence threshold, and (iv) metrics of RQA. Figure 3.7(A) illustrates a 3D surface plot of RQA ENTR with unitary increment of embedding parameters ( $m$  and  $\tau$ ) for recurrence threshold  $\epsilon = 2.0$ . Then, Figure 3.7(A), with other variations of recurrence thresholds (i.e.,  $\epsilon = 0.2$ ,  $\epsilon = 1.0$ ,  $\epsilon = 3.0$ ), is used to create Fig 3.7(B) where bands for values of  $\tau$  are concatenated to form a long band that is embedded into Fig 3.7(B) (as illustrated by the arrows). Additionally, five time series with their 3D surface plots of RQA ENTR are shown in Figs 3.7(C to G) to illustrate how 3D surface plots of RQA ENTR differ from each other.

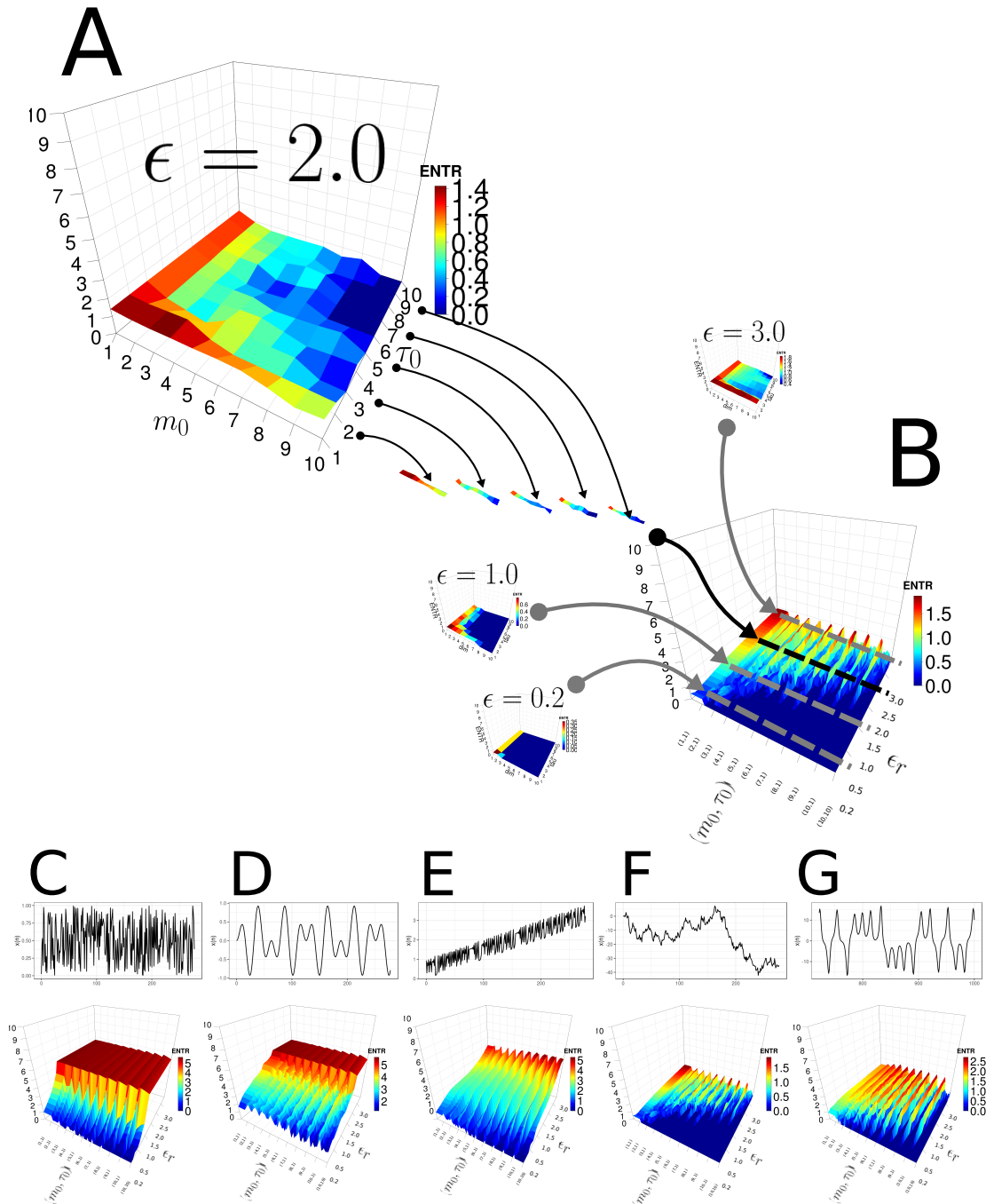


Fig. 3.7 **3D surface plots.** 3D surface plots of RQA ENTR incrementing (A) embedding dimensions ( $m$  and  $\tau$ ), (B) embedding dimensions ( $m$  and  $\tau$ ) and recurrence threshold ( $\epsilon$ ). Four time-series data and their 3D surface plots of RQA Entr for: (C) uniformly distribute noise, (D) super-positioned harmonic oscillation ( $\sin \frac{1}{5}t \sin \frac{5}{100}t$ ), (E) drift logistic map ( $x_{i+1} = 4x_i(1 - x_i)$ ) corrupted with a linearly increase term ( $0.01i$ ), (F) disrupted brownian motion ( $x_{i+1} = x_i + 2rnorm(1)$ ), and (G)  $x(t)$  solution of Lorenz system. R code to reproduce the figure is available at [\[4\]](#).

### 3.8 Final remarks

Fundamentals of nonlinear analysis such as RSS with UTDE, estimation of embedding parameters with FNN and AMI, RP, and four RQA metrics (REC, DET, RATIO, and ENTR) were introduced in this chapter. It is important to note that this thesis is only focused on the application of traditional methods (i.e., FNN and AMI) to compute embedding parameters. See Chapter 7 for future work with optimal embedding parameters estimation. Additionally, some weaknesses and strengths of RP and RQA metrics were presented in this chapter in order to explore issues of real-world time series data. One of the contributions of this thesis is the representation of 3D surface plots of RQAs that exploit the effect of incrementing not only embedding parameters (Iwanski and Bradley, 1998) but also recurrence thresholds. See the following chapters, Chapter 4 for introduction of experiments and Chapters 5 and 6 for results.

# Chapter 4

## Experiments

### 4.1 Aims

Two experiments are designed for this thesis: (i) human-image interaction (HII) and (ii) human-humanoid interaction (HHI), in both experiments participants perform simple arm movements repetitions. Simple arm movements here means, for persons and the humanoid robot, the ideally use of one joint biomechanical degree of freedom moving at normal and faster velocities. Hence, the aims of such experiments is not only to investigate the weaknesses and robustness of RSS, UTDE, embedding parameters, RP and RQA metrics regarding different conditions presented in real-world time series data (noisiness, non-stationarity, smoothness, window size lengths and structures), but also to present experimental scenarios where one can observe how the variables that model movement variability (e.g. complexity, predictability and activity type) affect the results of nonlinear analysis (Stergiou et al., 2006; Vaillancourt and Newell, 2002, 2003).

### 4.2 Participants

Twenty-three participants, from now on defined as  $pN$  where  $N$  is the number of participant, were invited for two experiments to perform simple arm movements. However, it is important to note that although the same number of participants performed the experiments, different number of participants were taken into account for each of the experiments due to either technical problems with the sensors or mistaken instructions of the experiments given to the participants.

#### 4.2.1 Human-image imitation activities

Only six participants ( $p01, p04, p05, p10, p11, p15$ ) were considered for the experiment of Human-image imitation (HII) activities due to problems with the inertial sensors such as bluetooth disconnections and drifting of time synchronisation (Section C.1.1). The six participants for this experiment were male right-handed healthy participants and have a mean and standard deviation (SD) age of mean=19.5 (SD=0.83) years.

#### 4.2.2 Human-humanoid imitation activities

For the experiment of human-humanoid imitation (HHI) activities, data for only twenty participants were analysed since the instructions for  $p01$ , who was the only left-handed, were mistakenly given in a way that movements were differently performed from what had been planned, and for participants  $p13$  and  $p16$  data were corrupted because of bluetooth communications problems with the sensors (Section C.1.1). With that in mind, all of the 20 participants were right-handed healthy participants, being four females and sixteen males, with a mean and standard deviation (SD) age of mean=19.8 (SD=1.39) years.

## 4.3 Equipment

During the experiments, time series were collected with four neMEMSi Inertial Measurement Units (IMUs) with a sampling rate of 50Hz (Comotti et al., 2014). neMEMSi sensors provide tri-axial time series from the accelerometer, gyroscope and magnetometer sensors and quaternions. See Appendix C.1 for further technical information of NeMEMSi IMU sensors. With regard to the human-humanoid imitation activities, NAO, a humanoid robot from Aldebaran (Gouaillier et al., 2009), was programmed with Choregraphe to perform horizontal and vertical arm movements. See Appendix C.3 for further technical information regarding NAO.

## 4.4 Ethics

The experiments of this thesis were conducted in November 2016 and participants confirmed reading and understanding the participant information sheet of the experiments and were able to withdraw from the experiment at any time without giving any reason. The design of the experiments adhered to the University of Birmingham regulations, data were anonymised and videos were stored only on a personal computer in accordance with the Data Protection Act 1998. Refer to Appendix D for further information about the ethics, online participation information sheets and experiment check list.

## 4.5 Experiments

### 4.5.1 Human-image imitation activities

In the experiment of human-image imitation (HHI), four wearable IMUs sensors were used and attached to the right hand of the participant (Figure 4.1 A,D). Then, par-

## Experiments

---

ticipants performed two experiments: (i) an unconstrained arm movement imitation activity where participants only receive instructions and look at images of arm movements, and (ii) a constrained experiment where participants hear a sound beat to synchronise their arm movements.

### **Arm movements following an image while not hearing a beat**

Participants received instructions to perform unconstrained upper arm movements while only looking an image for the following four activities:

- ten repetitions of horizontal arm movement at their comfortable velocity (Fig. 4.1(A, B, C)),
- ten repetitions of vertical arm movement at their comfortable velocity (Fig. 4.1(D, F, E)),
- ten repetitions of horizontal arm movement at a faster velocity than the comfortable velocity but not at their fastest velocity (Fig. 4.1(A, B, C)), and
- ten repetitions of vertical arm movement at a faster velocity than the comfortable velocity but not at their fastest velocity (Fig. 4.1(D, F, E)).

### **Arm movements following an image while hearing a beat**

Participants received instructions to perform constrained upper arm movements while listening a beat for the following four activities:

- ten repetitions of horizontal arm movement at normal velocity (Fig. 4.1(A, B, C)),
- ten repetitions of vertical arm movement at normal velocity (Fig. 4.1(D, F, E)),
- ten repetitions of horizontal arm movement at faster velocity and (Fig. 4.1(A, B, C)), and
- ten repetitions of vertical arm movement at faster velocity (Fig. 4.1(D, F, E)).

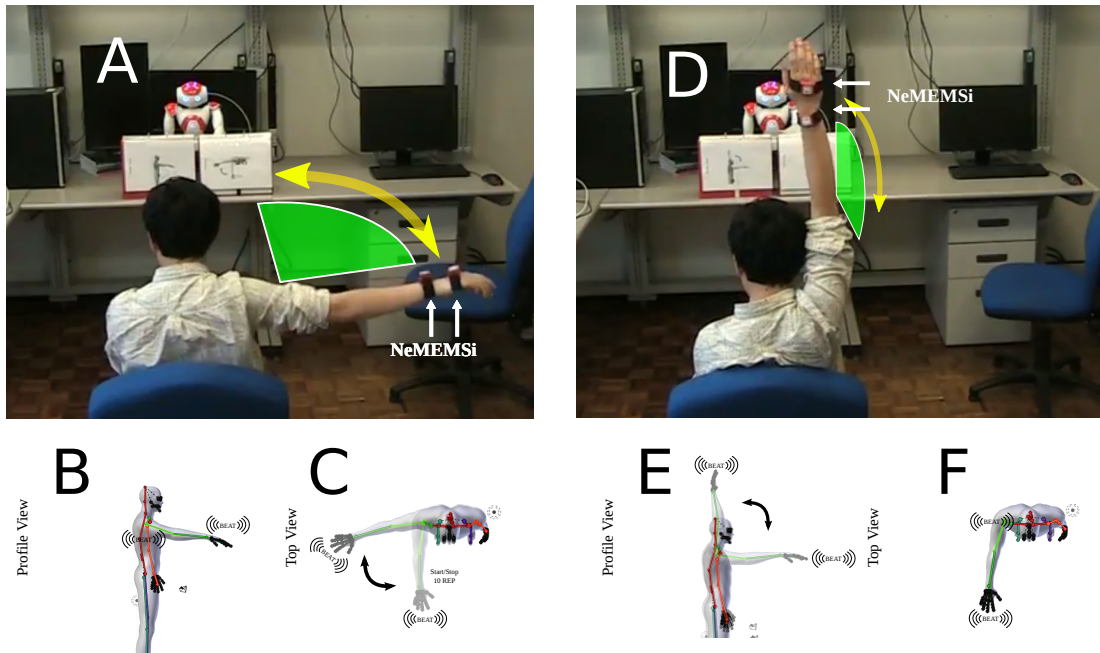


Fig. 4.1 **Human-image imitation (HII) activities.** (A) HII of horizontal arm movement, (B) image of the profile view for horizontal arm movement, (C) image of the top view for horizontal arm movement, (D) HII of vertical arm movement, (E) image of the profile view for vertical arm movement, and (F) image of the top view for horizontal arm movement. (B, C, F and E) show '(((BEAT)))' to indicate the participants arm movements synchronisation when hearing a sound beat.

To visualise the time series of the previous activities, Figs 4.2 show time series using smoothed time series of the gyroscope of Y and Z axis for the sensor HS01 of participant 01. See Appendix E.1 for time series of all participants and activities.

#### 4.5.2 Human-humanoid imitation activities

NAO is commonly used in human-robot interaction activities because its affordability, performance and modularity. However, some of the limitations of NAO are related to (i) its 14 degrees of freedom (DOF) for arms and head, (ii) the range of joint movement and (iii) joint torques and velocities (Gouaillier et al., 2009). With that in mind, four NAO's arm movements were selected, such movements are controlled by the shoulder



## Experiments

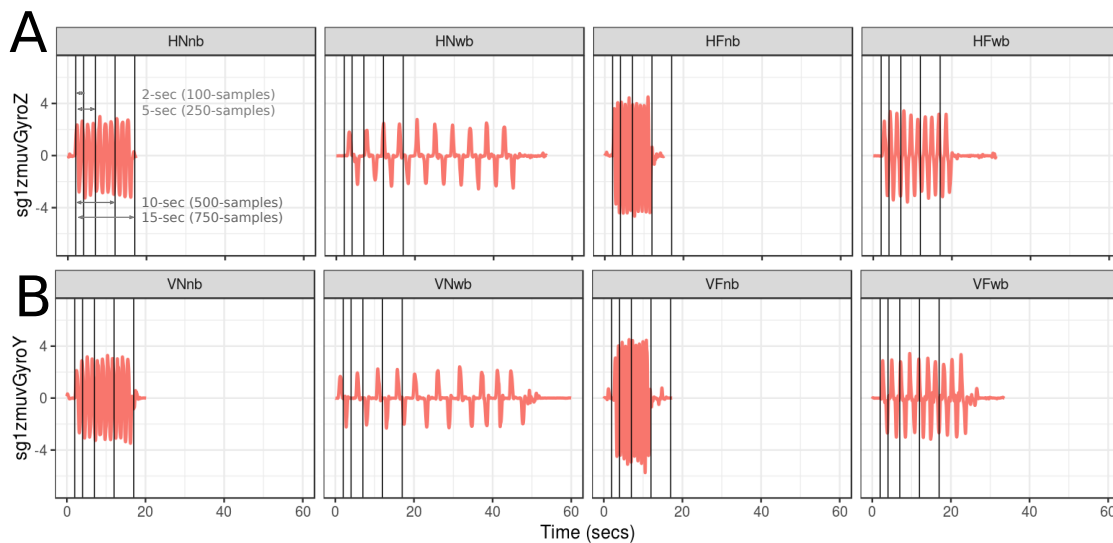


Fig. 4.2 **Time series for horizontal and vertical arm movements.** Time series of smoothed data from gyroscope sensor (sg1zmuvgyroZ and sg1zmuvgyroY) of participant 01 with sensor HS01 for different velocity arm movements: (A) Horizontal Normal with no beat (HNnb), Horizontal Normal with beat (HNwb), Horizontal Faster with no beat (HFnb) and Horizontal Faster with beat (HFwb), and (B) Vertical Normal with no beat (VNnb), Vertical Normal with beat (VNwb), Vertical Faster with no beat (VFnb) and Vertical Faster with beat (VFwb). Additionally, (A) presents vertical lines to show window size lengths for 2-seconds (100 samples), 5-seconds (250 samples), 10-seconds (500 samples) and 15-seconds (750 samples) which are presented in (B), (C) and (D). See Appendix E.1 for time series of all participants and activities. R code to reproduce the figure is available at [\[4\]](#).

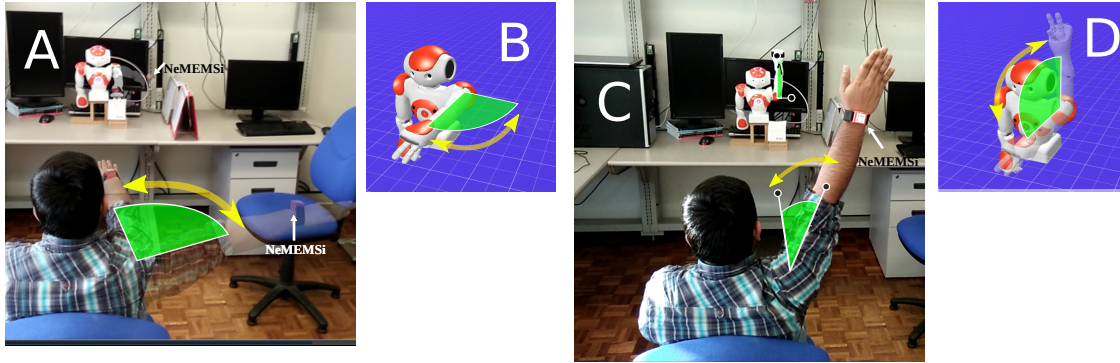


Fig. 4.3 **Human-humanoid imitation activities.** Face-to-face human-humanoid imitation (HHI) activities for (A) HHI of horizontal arm movement, (B) Humanoid performing horizontal arm movement, (C) HHI of vertical arm movement, and (D) Humanoid performing vertical arm movement.

joint for vertical and horizontal movements performed at normal and faster velocity (Figs. 4.3 B,D). See Appendix C.3 for basic information of NAO and see Gouaillier et al. (2009) for detailed information of NAO’s mechanical and dynamic capabilities.

For the human-humanoid imitation (HHI) experiment four wearable IMUs sensors were used in which two sensors were attached to the right hand of the participant and two sensors were attached to the left hand of the humanoid robot (Figure 4.3 A,C). Then, in the face-to-face imitation activity, each participant was asked to imitate repetitions of simple horizontal and vertical arm movements performed by the humanoid robot in the following conditions:

- ten repetitions of horizontal arm movement at normal (HN) and faster (HF) velocity (Fig. 4.3 A), and
- ten repetitions of vertical arm movement at normal (VN) and faster (VF) velocity (Fig. 4.3 C).

The duration of number of samples for NAO’s arm movements were defined by normal and faster velocities of NAO’s shoulder joint (Figs. 4.3 B,D). Hence, the duration for one repetition of the horizontal arm movement at normal velocity, HN,

## Experiments

---

is about 5 seconds considering that each repetition last around 250 samples. For horizontal arm movement at faster velocity, HF, each repetition were performed in around 2 seconds which correspond to 90 samples of data. The vertical arm movement at normal velocity, VN, were performed in 6 seconds which is around 300 samples of data. For vertical arm movement at faster velocity, VF, each repetition lasts about 2.4 seconds which correspond to 120 samples of data. To visualise the distinction between normal and faster velocity for horizontal and vertical arm movements, Fig 4.4 shows smoothed time series for axes Z and Y of the gyroscope sensors with four window lengths: 2-sec (100-samples), 5-sec (250-samples), 10-sec (500-samples) and 15-sec (750-samples). See Appendix F.1 for time series of all participants and activities.

## 4.6 Processing of time series

### 4.6.1 Raw time-series

For this thesis, analysis of time series is only with the accelerometer and gyroscope of the IMU sensors. The justification for that is because Shoaib et al. (2016) provided evidence of an improvement in recognition activities when only combining data from accelerometer and gyroscope. The time-series data for magnetometer and quaternions are left for future investigations as these might create additional variations because of magnetic disturbances.

Time series from the accelerometer are defined by triaxial time series  $A_x(n)$ ,  $A_y(n)$ ,  $A_z(n)$  which forms the matrix  $\mathbf{A}$  (Eq. 4.1), and the same for data from the gyroscope which is defined by triaxial time-series of  $G_x(n)$ ,  $G_y(n)$ ,  $G_z(n)$  representing the matrix  $\mathbf{G}$  (Eq. 4.2). Both triaxial time series of each sensor,  $a$  and  $g$ , are denoted with its respective axes subscripts  $x, y, z$ , where  $n$  is the sample index and  $N$  is the same maximum length of all axes for the time series. Matrices  $\mathbf{A}$  and  $\mathbf{G}$  are represented as

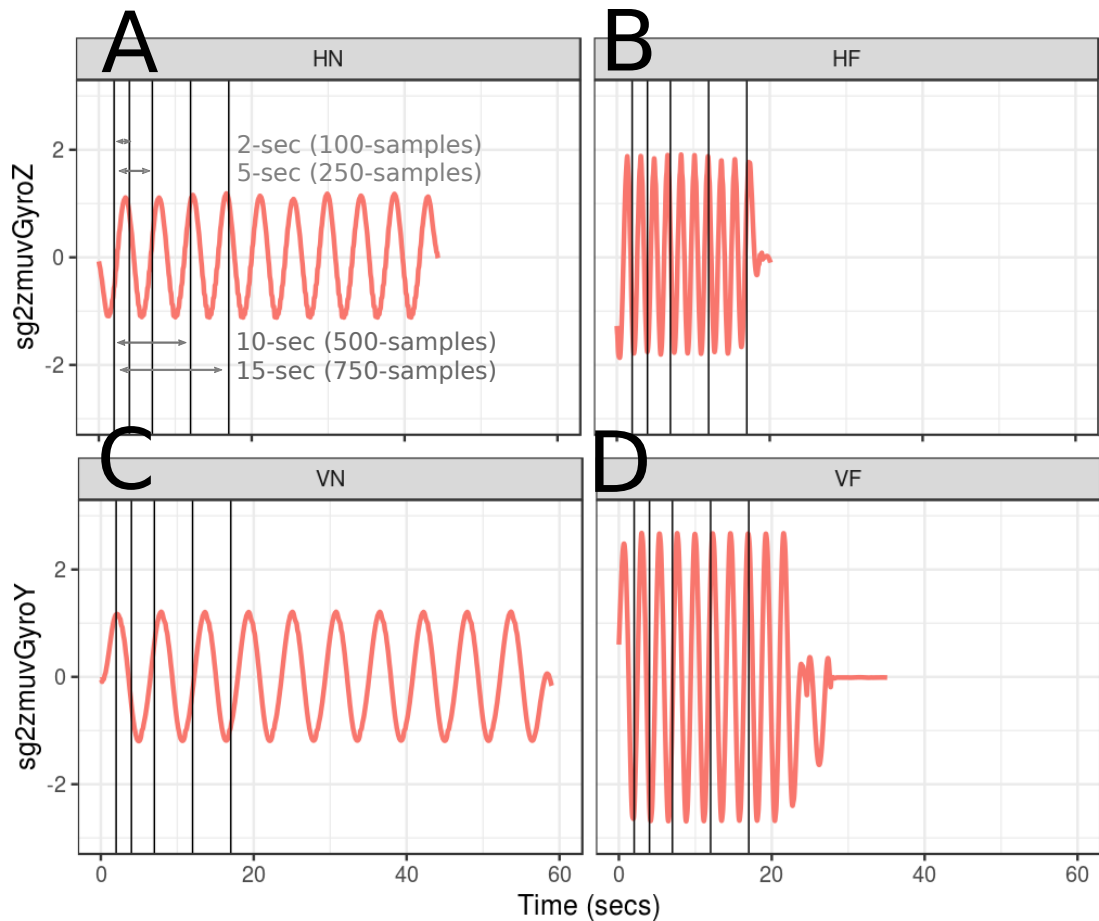


Fig. 4.4 **Time series duration of horizontal and vertical arm movements.** Time series of smoothed data from gyroscope sensor (sg1zmuvgyroZ and sg1zmuvgyroY) of NAO with sensor HS01 for different velocity arm movements: (A) Horizontal Normal arm movement, HN, (B) Horizontal Faster arm movement, HF, (C) Vertical Normal arm movement, VN, and (D) Vertical Faster arm movement, VF. Additionally, (A) presents vertical lines to show window size lengths for 2-seconds (100 samples), 5-seconds (250 samples), 10-seconds (500 samples) and 15-seconds (750 samples) which are presented in (B), (C) and (D). See Appendix F.1 for time series of all participants and activities. R code to reproduce the figure is available at [\[4\]](#).

follow

$$\mathbf{A} = \begin{pmatrix} A_x(n) \\ A_y(n) \\ A_z(n) \end{pmatrix} = \begin{pmatrix} a_x(1), a_x(2), \dots, a_x(N) \\ a_y(1), a_y(2), \dots, a_y(N) \\ a_z(1), a_z(2), \dots, a_z(N) \end{pmatrix}, \quad (4.1)$$

$$\mathbf{G} = \begin{pmatrix} G_x(n) \\ G_y(n) \\ G_z(n) \end{pmatrix} = \begin{pmatrix} g_x(1), g_x(2), \dots, g_x(N) \\ g_y(1), g_y(2), \dots, g_y(N) \\ g_z(1), g_z(2), \dots, g_z(N) \end{pmatrix}, \quad (4.2)$$

where  $n$  is the sample index and  $N$  is the same maximum length of all axes for the time series.

### 4.6.2 Postprocessing time-series

After the collection of raw time-series from four NeMEMsi sensors, time synchronisation alignment and interpolation were performed in order to create time series with same length and synchronised time. See Appendix C.2 for technical information about the IMU sensors and time synchronisation process.

### 4.6.3 Window size of time-series

With regard to the window size, Shoaib et al. (2016) compared seven window lengths (2, 5, 10, 15, 20, 25, 30 seconds) and tested a combination of inertial sensors (accelerometer, gyroscope and linear acceleration sensor) for activity recognition of repetitive activities (walking, jogging and biking) and less repetitive activities (smoking, eating, giving a talk or drinking a coffee). Shoaib et al. (2016) concluded that the increase of window size improved the recognition of complex activities (i.e. less repetitive activities which mainly involve random hand gestures). With that in mind, four window sizes were selected for each of the activities, which are mainly repetitive, in this thesis: 2-s window (100 samples), 5-s window (250 samples), 10-s (500 samples) and 15-s window (750

samples). Figures 4.2 and 4.4 illustrate vertical lines to show four window lengths which were chosen in order to cover a total time of 15 seconds (750 samples) for either (i) eight activities in human-image imitation or (ii) four activities in human-humanoid imitation. Figures 4.2 and 4.4 also show the starting point of time-series data from 2 seconds (100 samples) in order to avoid picking time-series data that do not correspond to the experiment (i.e., any movements before the experiment). The latter statement is important for the application of nonlinear analysis methods as picking dynamics of time-series data that do not correspond to the activity will therefore produce different results to the ones that only consider the duration of the activity.

#### 4.6.4 Normalization of time-series

Time series are normalised to have zero mean and unit variance using sample mean and sample standard deviation (Ioffe and Szegedy, 2015). The sample mean and sample standard deviation using  $x(n)$  is given by

$$\mu_{x(n)} = \frac{1}{N} \left( \sum_{i=1}^N x(i) \right), \quad \sigma_{x(n)} = \sqrt{\frac{\sum_{i=1}^N (x(i) - \mu_{x(n)})^2}{N - 1}}, \quad (4.3)$$

then the normalised data,  $\hat{x}(n)$ , is computed as follows

$$\hat{x}(n) = \frac{x(n) - \mu_{x(n)}}{\sigma_{x(n)}}. \quad (4.4)$$

#### 4.6.5 Smoothing time-series

Applying low-pass filters is a common way to either capture low frequencies (below 15 Hz) that represent 99% of the human body energy or to get the gravitational and body motion components of accelerations (below 0.3 Hz) (Anguita et al., 2013). However, filtering such information can cut-off frequencies that are important for the

## Experiments

---

conservation of (i) the original properties of raw time-series data and (ii) the structure of the time-series data in terms of width and heights. In addition to that, arm movements of NAO can sometimes produce jerky movements due to: (i) the control of dynamic response (fast acceleration/deceleration), (ii) the stiffness of the gear mechanism, or (iii) the high frequencies of oscillations because of resonances (see Gouaillier et al. (2009) for NAO's mechanical and dynamic capabilities). Hence, instead of cutting out frequencies with a low-pass filter for the experiments in the context of human-robot interaction, this thesis considers the application of Savitzky-Golay filter to smooth time series data. The latter statement might give insight into the effect of smoothness of real-world time series data for nonlinear analysis methods.

Savitzky-Golay filter is based on the principle of moving window average which preserves the area under the curve (the zeroth moment) and its mean position in time (the first moment) but the line width (the second moment) is violated and that results, for example, in the case of spectrometric data where a narrow spectral line is presented with reduced height and width (Press et al., 1992). The aim of Savitzky-Golay filtering is hence to find the filter coefficients  $c_n$  that preserve higher momentums which are based on local least-square polynomial approximations (Press et al., 1992; Savitzky and Golay, 1964; Schafer, 2011). Therefore, Savitzky-Golay coefficients are computed using an R function `sgolay(p,n,m)` where `p` is the filter order, `n` is the filter length (must be odd) and `m` is the  $m$ -th derivative of the filter coefficients (signal R developers, 2014). Smoothed signal is represented with a tilde over the original signal:  $\tilde{x}(n)$ .

# Chapter 5

## Quantifying Human-Image Imitation Activities

### 5.1 Introduction

In this chapter, results for experiments of human-image imitation activities, described in Section 4.5.1, are presented by including time series, minimum embedding parameters, the reconstructed state spaces (RSS) using uniform time-delay embedding technique (UTDE), recurrence plots (RP), recurrent quantification analysis (RQA), and weaknesses and strengths of RQA with three dimensional surface plots of RQA.

Time series data for this experiment are described as follows:

- Six participants defined as  $pN$  where  $N$  is the number of participant.
- Three levels of smoothness for the normalised data (`sg0zmu`, `sg1zmu` and `sg2zmu`), computed from two different filter lengths (29 and 159) with the same polynomial degree of 5 using the function `sgolay(p,n,m)` (signal R developers, 2014),



## Quantifying Human-Image Imitation Activities

---

- Four window lengths: 2-sec (100 samples), 5-sec (250 samples), 10-sec (500 samples) and 15-sec (750 samples), and
- Eight velocities of arm movement activity: horizontal movements in normal and faster velocity with no beat (HNnb, HFnb) and with beat (HNwb, HFwb), and vertical movements in normal and faster velocity with no beat (VNnb, VFnb) and with beat (VNwb, VFwb).

To make the visual comparison easier, time series for only three participants (*p04*, *p05*, *p10*) with a window length of 10 seconds are considered for the following results. See Appendix E for further results.

### 5.2 Time series

Figures 5.1 and 5.2 show time series for horizontal and vertical arm movements of participants following an image while not hearing a beat (nb) and hearing a beat (wb). Also, three levels of smoothness of normalised time series are presented (sg0, sg1 and sg2). The remaining time series are presented in Appendix E.1.

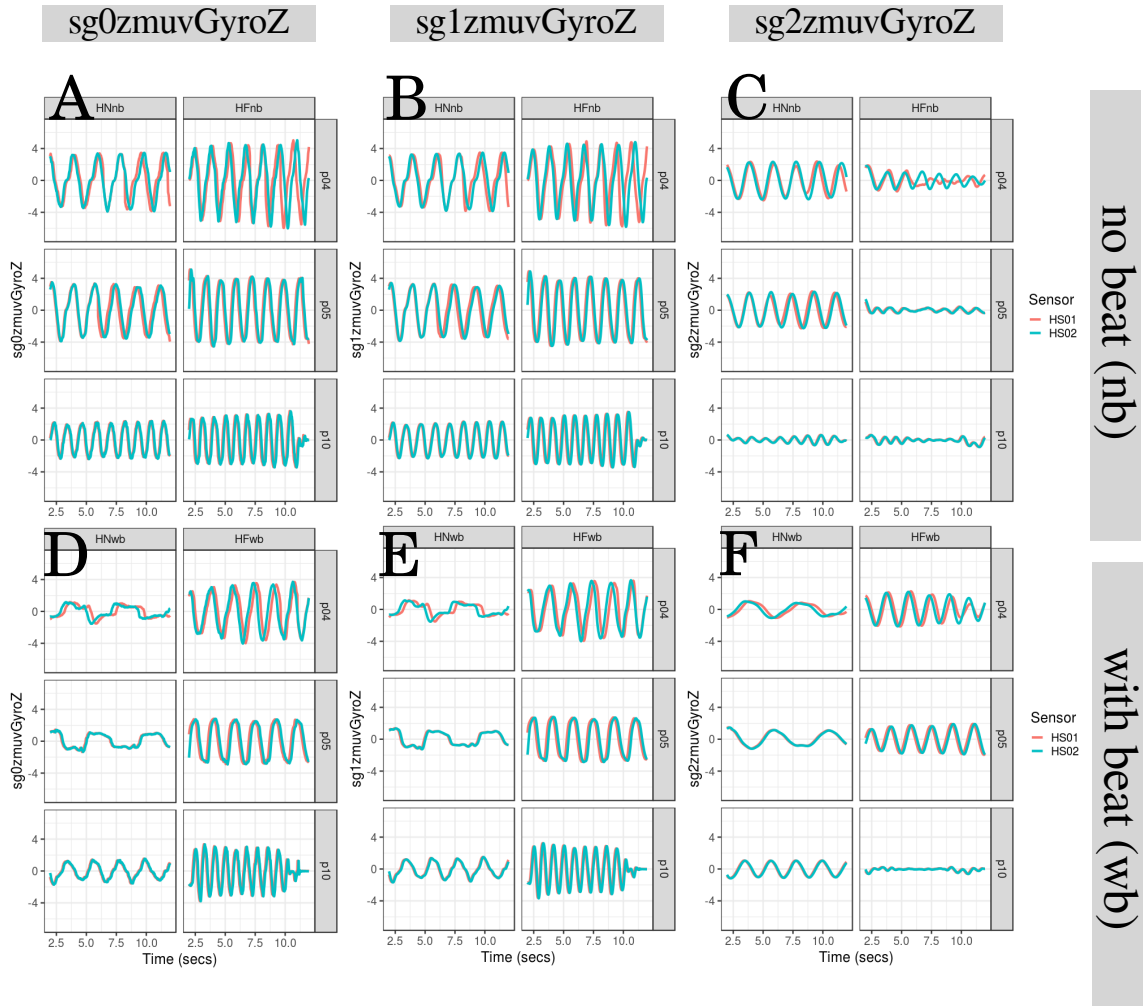


Fig. 5.1 **Time series for horizontal arm movements.** Time series for (A,D) raw-normalised ( $sg0zmuVgyroZ$ ), (B,E) normalised-smoothed 1 ( $sg1zmuVgyroZ$ ), and (C,F) normalised-smoothed 2 ( $sg2zmuVgyroZ$ ). Time series are for three participants ( $p04$ ,  $p05$ , and  $p10$ ) for horizontal movements in normal and faster velocity with no beat (HNnb, HFnb) and with beat (HNwb, HFwb) using the normalised GyroZ axis ( $zmuVgyroZ$ ) and two sensors attached to the participant wrist (HS01, HS02). R code to reproduce the figure is available at [\[45\]](#).

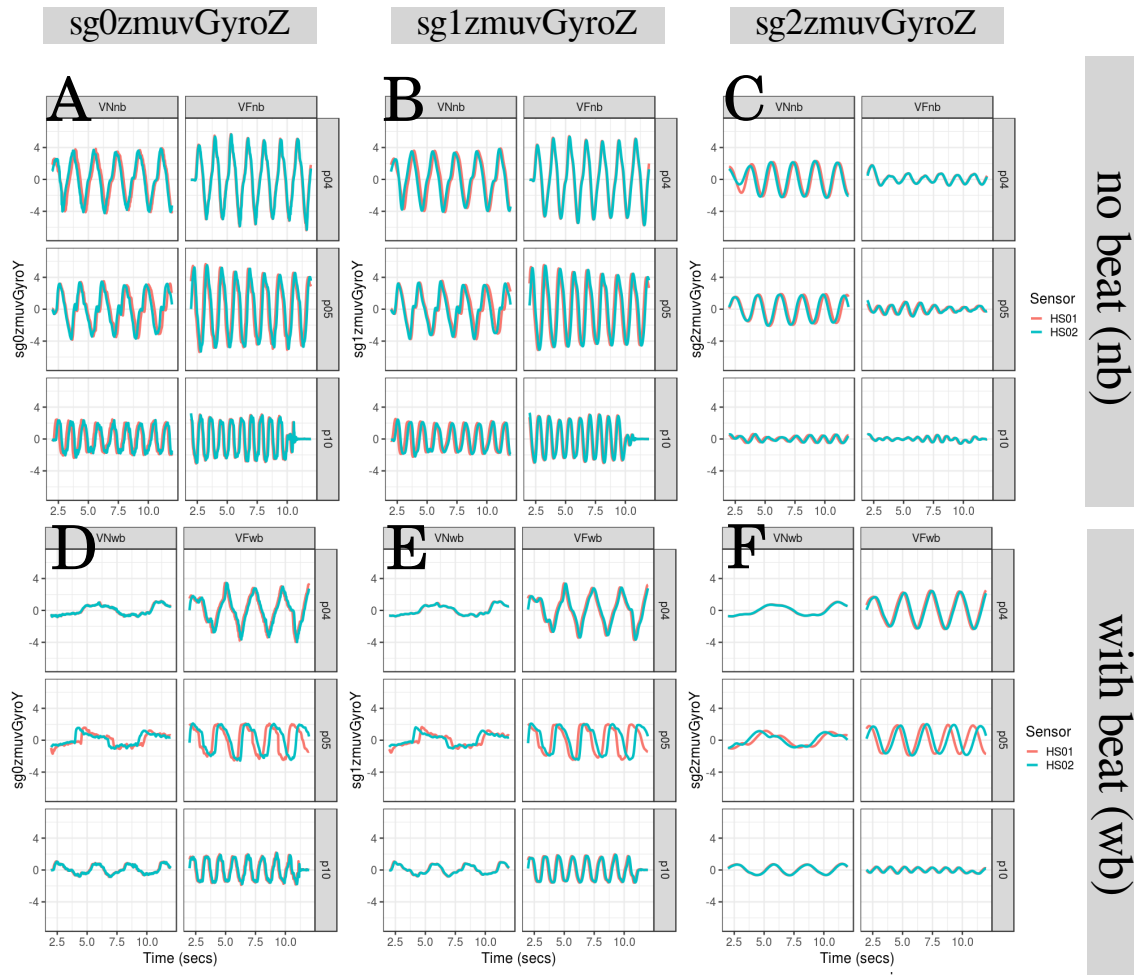


Fig. 5.2 **Time series for vertical arm movements.** Time series for (A,D) raw-normalised ( $sg0zmvGyroY$ ), (B,E) normalised-smoothed 1 ( $sg1zmvGyroY$ ), and (C,F) normalised-smoothed 2 ( $sg2zmvGyroY$ ). Time series are for three participants ( $p04$ ,  $p05$ , and  $p10$ ) for vertical movements in normal and faster velocity with no beat (VNnb, VFnb) and with beat (VNwb, VFwb) using the normalised GyroY axis (zmvGyroY) and two sensors attached to the participant wrist (HS01, HS02). R code to reproduce the figure is available at [\[4\]](#).

## 5.3 Minimum Embedding Parameters

The first step to create Reconstructed State Spaces (RSSs) with the use of Uniform Time-Delay Embedding (UTDE) is to compute the average minimum embedding parameters for all participants, sensors and activities using False Nearest Neighbour (FNN) and Average Mutual Information (AMI) algorithms.

Hence, Figs. 5.3 illustrate the box plots for minimum embedding dimensions. For horizontal arm movements (Figs. 5.3(A)), one can notice how the interquartile range appear to be near to one independently of the activity or sensor. With regards to the level of smoothness, there is a decrease of sample mean (gray rhombus) as the smoothness increase. Similarly, for vertical arm movements (Figs. 5.3(B)) the interquartile range of activities and sensors appears to be near to one. In addition to that, the increase of smoothness is affected by a decrease in sample means (gray rhombus) meaning that there is a decrease of dimensionality of the dynamics of the time series data. For further details of the minimum dimension values see Figures in Appendix E.2.

Figs. 5.4 illustrate the box plots for first minimum AMI. Box plots for horizontal arm movements (Figs. 5.4(A)) for HNwb appear more spread (interquartile range between 10 to 20) while other activities there is a slight variation of values (interquartile range between 5 to 10). Little can be said regardless the sample mean of each axis (gray rhombus) which is not proportionally affected as the smoothed of the time series increase. Box plots for vertical arm movements (Figs. 5.4(B)) show that the interquartile range of each activity is constant except for the activity VFwb. Additionally, the increase of smoothness of time series (sg0 to sg2) made the sample mean (gray rhombus) to increase which means that the maximal information to knowledge from  $x(n)$  to  $x(t + \tau_0)$  also increase. For further details of the minimum dimension values see Figures in Appendix E.2.

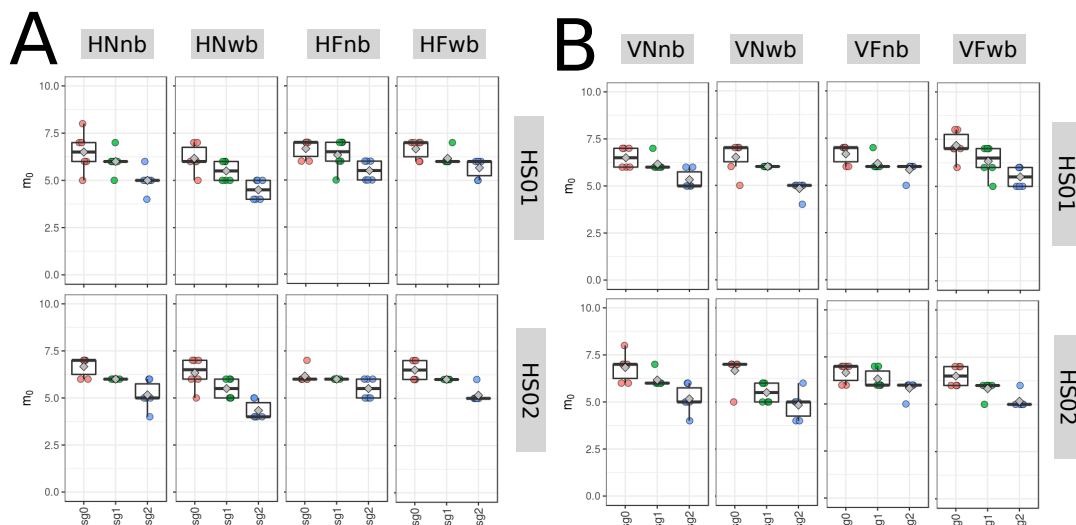


Fig. 5.3 **Box plots for minimum embedding dimensions.** Box plots of minimum embedding dimensions for (A) horizontal and (B) vertical arm movements for normal and faster velocity (N/F) with no beat (nb) and with beat (wb) movements using sensors 01 and 02 attached to the wrist of the participant (HS01, HS02). Minimum embedding dimensions are for six participants ( $p01$ ,  $p04$ ,  $p05$ ,  $p10$ ,  $p11$ ,  $p15$ ) with three smoothed signals ( $sg0$ ,  $sg1$  and  $sg2$ ) and window length of 10 seconds. R code to reproduce the figure is available at [\[4\]](#).

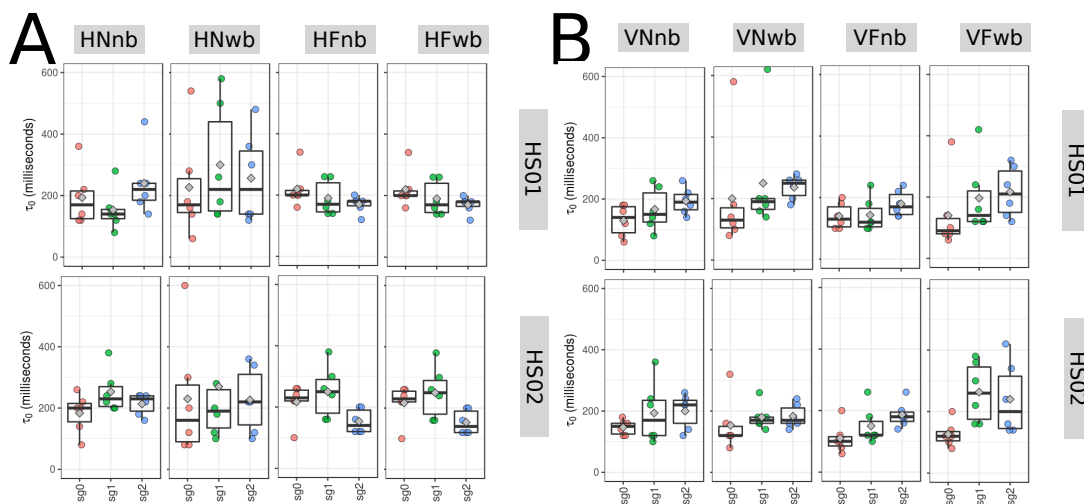


Fig. 5.4 **Box plots for 1st minimum AMI.** Box plots of the 1st minimum AMI values for (A) horizontal and (B) vertical arm movements for normal and faster velocity (N/F) with no beat (nb) and with beat (wb) movements using sensors 01 and 02 attached to the wrist of the participant (HS01, HS02). First minimum AMI values in milliseconds are for six participants ( $p01$ ,  $p04$ ,  $p05$ ,  $p10$ ,  $p11$ ,  $p15$ ) with three smoothed signals ( $sg0$ ,  $sg1$  and  $sg2$ ) and window length of 10 seconds. R code to reproduce the figure is available at [\[4\]](#).

### 5.3.1 Average minimum embedding parameters

Although the implementation of Uniform Time-Delay Embedding (UTDE) is simple, the main challenge is the selection of appropriate embedding parameters to reconstruct the state spaces of each time series as these are unique in terms of its structure (modulation of amplitude, frequency and phase) (Bradley and Kantz, 2015; Frank et al., 2010; Samà et al., 2013). With that in mind, one problem that this thesis has faced is the selection of embedded parameters that can represent all time series. The solution to that problem was to compute a sample mean over all values for all participants, activities and sensors (Section 3.4.3). Hence, the average minimum embedding parameters is computed with a sample mean of  $\bar{m}_0 = 6$  from the minimum values of  $E_1(m)$  in Figs 5.3 and a sample mean of  $\bar{\tau}_0 = 10$  from minimum values of AMIs in Figs 5.4. Hence, Reconstructed State Spaces (RSSs), Recurrence Plots (RPs) and Recurrence Quantification Analysis (RQA) metrics are computed with the average minimum embedding parameters ( $\bar{m}_0 = 6, \bar{\tau}_0 = 10$ ).

## 5.4 Reconstructed state spaces with UTDE

Reconstructed state spaces for horizontal normal and horizontal faster arm movements with no beat are shown in Fig 5.5. The smoothness of the time series show a slightly change of smoothed trajectories in the RSSs for sg0zmuvGyroZ and sg1zmuvGyroZ, while the RSSs trajectories for sg2zmuvGyroZ appear to be distorted (Fig 5.5). One can see slightly differences in the RSSs trajectories when comparing sensors HS01 and HS02 for horizontal normal arm movement with no beat (Fig 5.5(A, B)) and horizontal faster arm movements with no beat (Fig 5.5(C, D)). With regards to the type of movement, the RSSs trajectories appear to change little when comparing horizontal normal with faster arm movements (Fig 5.5).

Fig 5.6 shows trajectories of the reconstructed state space for horizontal normal and horizontal faster arm movements while beat sounds. Hence, as in Fig 5.5, it can also be noted in Fig 5.6 that the smoothness of  $sg0zmuvGyroZ$  and  $sg1zmuvGyroZ$  appear to affect little the RSSs trajectories, while RSSs trajectories for  $sg2zmuvGyroZ$  substantially change so as to show different patterns. However, the trajectories in the RSS appear to change little when comparing the differences between the type of sensors HS01 and HS02 (Fig 5.6). For the type of movements, trajectories show differences for horizontal normal and horizontal faster arm movements (Fig 5.6).

Fig 5.7 show trajectories for reconstructed state spaces of vertical normal and vertical faster arm movements with no beat. Smoothness of the RSSs trajectories is slightly noticed for  $sg0zmuvGyroY$  and  $sg1zmuvGyroY$ , whereas RSSs trajectories for  $sg2zmuvGyroY$  are evidently different (Fig 5.7). When comparing the RSSs trajectories from sensors HS01 and HS02, it can be noted little change, whereas the comparison from type of movement, the trajectories difference is more notable (Fig 5.7).

Fig 5.8 show trajectories for reconstructed state space of vertical normal and vertical faster arm movements for participants hearing a beat. Smoothness of RSSs trajectories appear to show slightly differences between  $sg0zmuvGyroY$  and  $sg1zmuvGyroY$ , however RSSs trajectories for  $sg2zmuvGyroY$  are different (Fig 5.8). With regards to the type of sensor HS01 and HS02, RSSs trajectories appear to change little, whereas for type of activity of normal and faster arm movements, RSSs trajectories show evidently differences (Fig 5.8).

## 5.4 Reconstructed state spaces with UTDE

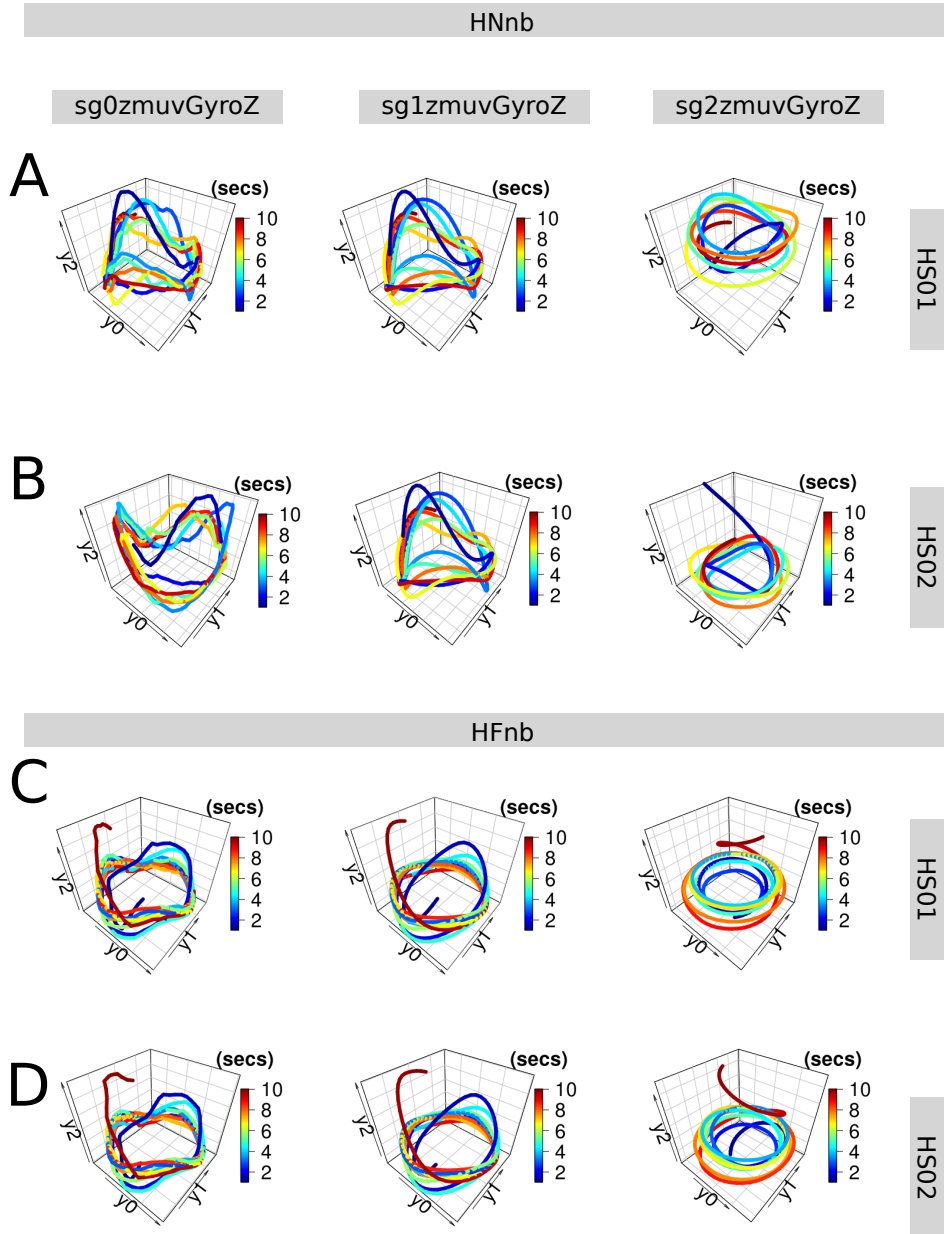


Fig. 5.5 **RSSs for horizontal arm movements (no beat)**. Reconstructed state spaces of participant p01 for (A, B) horizontal normal movements with no beat (HNnb) and (C, D) horizontal faster velocity with no beat (HFnb). Time series for raw-normalised (sg0zmvGyroZ), normalised-smoothed 1 (sg1zmvGyroZ) and normalised-smoothed 2 (sg2zmvGyroZ) with (A, C) sensor attached to the participant (HS01), and (B, D) sensor attached to the participant (HS02). Reconstructed state spaces were computed with embedding parameters  $\overline{m}_0 = 6$ ,  $\overline{\tau}_0 = 10$ . R code to reproduce the figure is available at [\[47\]](#).



## Quantifying Human-Image Imitation Activities

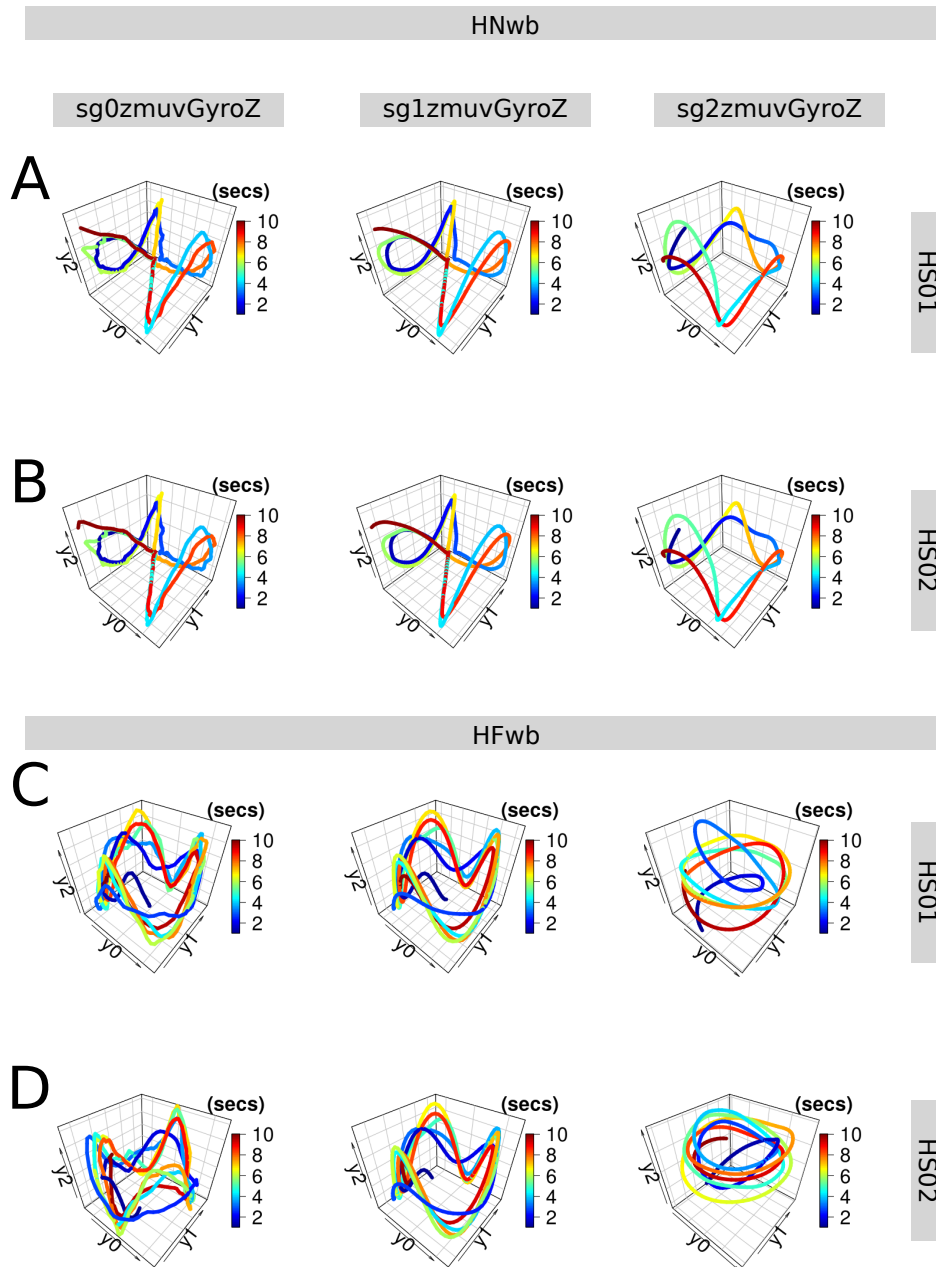


Fig. 5.6 **RSSs for horizontal arm movements (with beat)**. Reconstructed state spaces of participant p01 for (A, B) horizontal normal movements with beat (HNwb) and (C, D) horizontal faster velocity with beat (HFwb). Time series for raw-normalised (sg0zmvGyroZ), normalised-smoothed 1 (sg1zmvGyroZ) and normalised-smoothed 2 (sg2zmvGyroZ) with (A, C) sensor attached to the participant (HS01), and (B, D) sensor attached to the participant (HS02). Reconstructed state spaces were computed with embedding parameters  $\overline{m}_0 = 6$ ,  $\overline{\tau}_0 = 10$ . R code to reproduce the figure is available at [\[1\]](#).

## 5.4 Reconstructed state spaces with UTDE

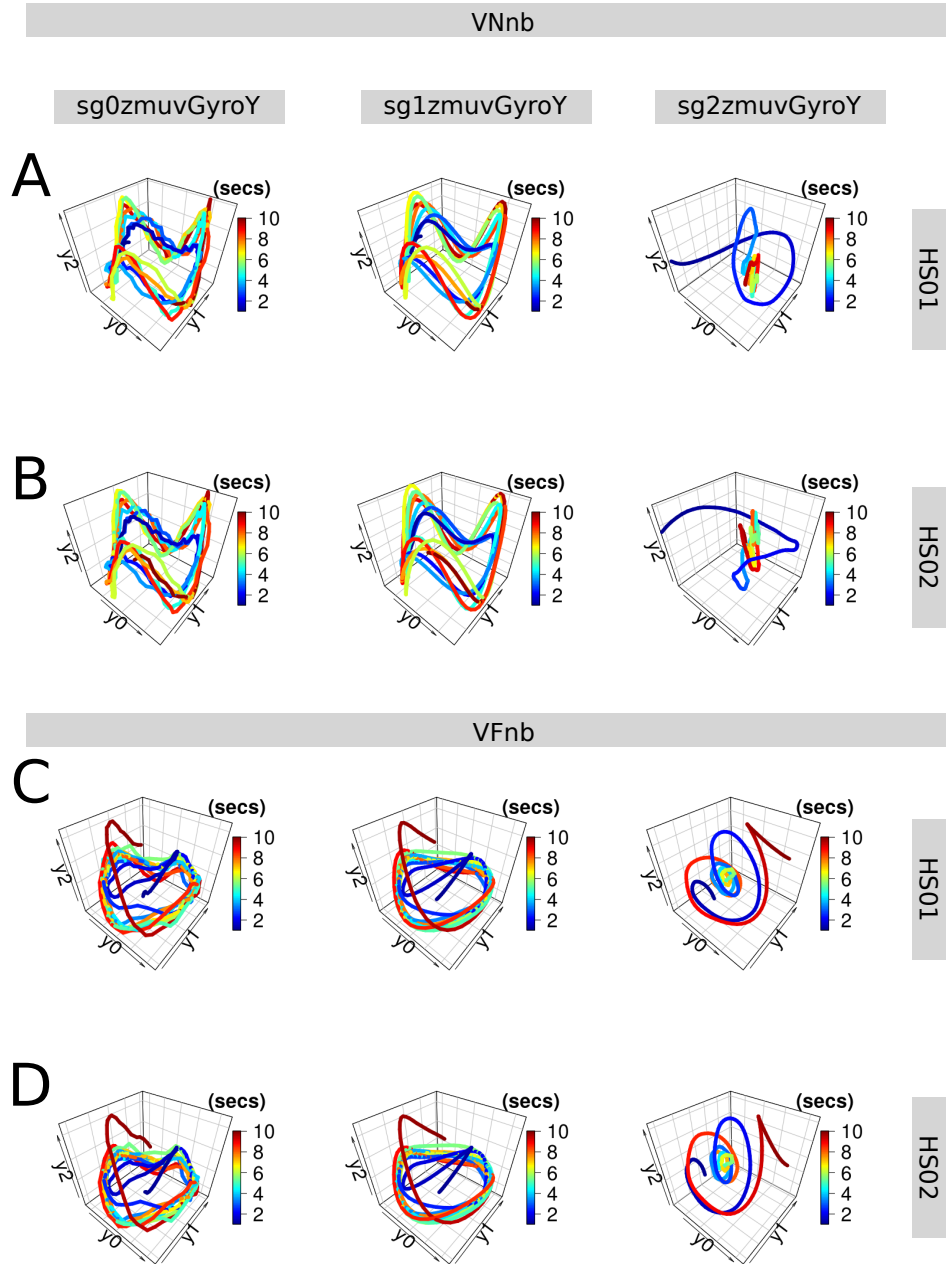


Fig. 5.7 RSSs for vertical arm movements (no beat). Reconstructed state spaces of participant p01 for (A, B) vertical normal movements with no beat (VnNb) and (C, D) vertical faster velocity with no beat (VFnb). Time series for raw-normalised (sg0zmuvGyroY), normalised-smoothed 1 (sg1zmuvGyroY) and normalised-smoothed 2 (sg2zmuvGyroY) with (A, C) sensor attached to the participant (HS01), and (B, D) sensor attached to the participant (HS02). Reconstructed state spaces were computed with embedding parameters  $\overline{m}_0 = 6$ ,  $\overline{\tau}_0 = 10$ . R code to reproduce the figure is available at [\[47\]](#).

## Quantifying Human-Image Imitation Activities

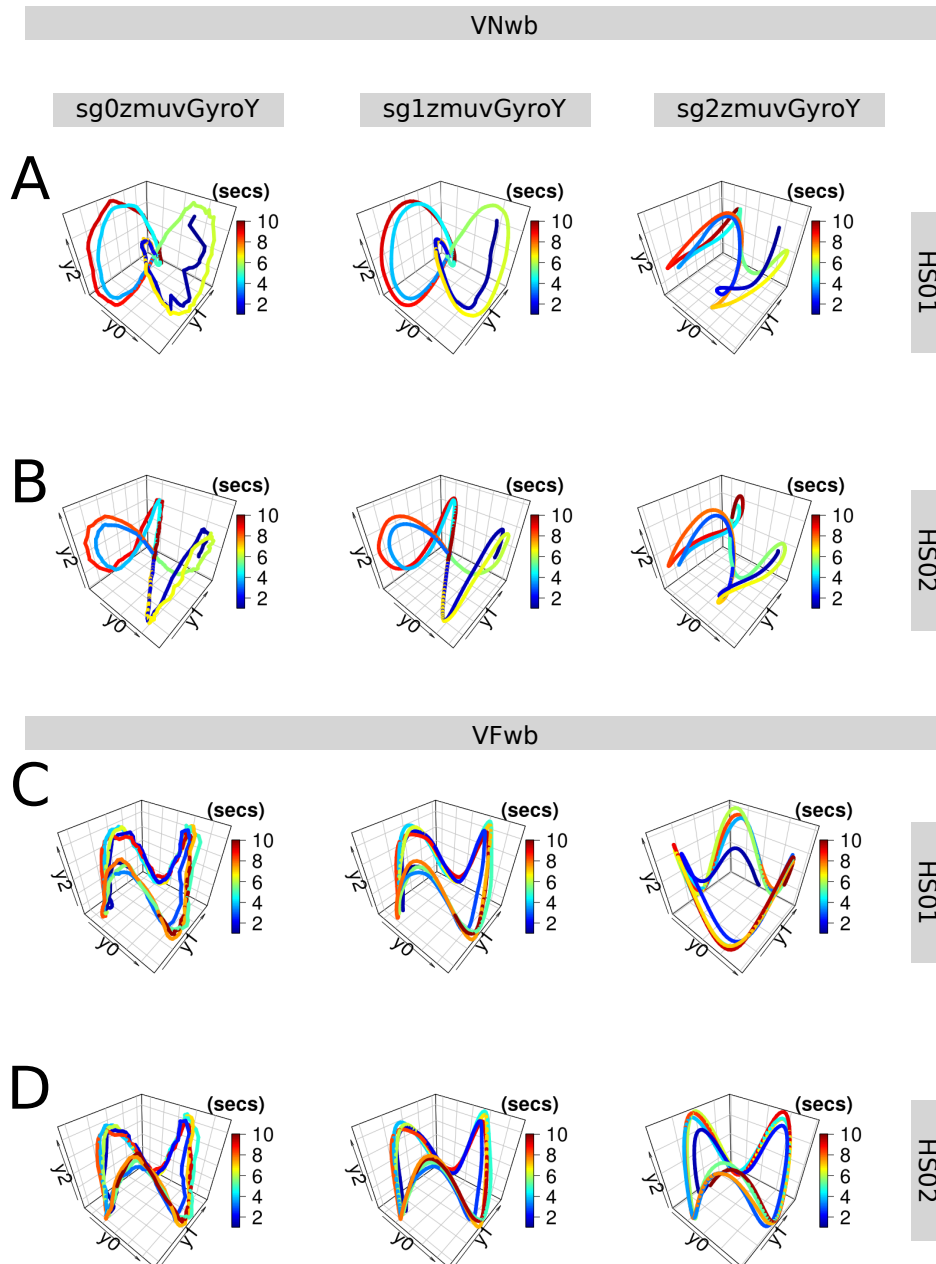


Fig. 5.8 RSSs for vertical arm movements (with beat). Reconstructed state spaces of participant p01 for (A, B) vertical normal movements with beat (VNwb) and (C, D) vertical faster velocity with beat (VFwb). Time series for raw-normalised (sg0zmvGyroY), normalised-smoothed 1 (sg1zmvGyroY) and normalised-smoothed 2 (sg2zmvGyroY) with (A, C) sensor attached to the participant (HS01), and (B, D) sensor attached to the participant (HS02). Reconstructed state spaces were computed with embedding parameters  $\overline{m}_0 = 6$ ,  $\overline{\tau}_0 = 10$ . R code to reproduce the figure is available at [\[1\]](#).

## 5.5 Recurrences Plots

Patterns of recurrence plots (RPs) are described in this section. Recurrence plots are computed with embedding parameters  $\overline{m}_0 = 6$ ,  $\overline{\tau}_0 = 10$  and a recurrence threshold  $\epsilon = 1$  for participant *p01* performing horizontal and vertical arm movements in normal and faster velocity with beat and no beat sound (Figs 5.9, 5.10, 5.11 and 5.12).

Figs 5.9 show recurrence plots for horizontal normal and horizontal faster arm movements with no beat sound. For horizontal normal arm movements with no beat, patterns in RPs for *sg0zmuvGyroZ* and *sg1zmuvGyroZ* look similar, however patterns in RPs for *sg2zmuvGyroZ* are different, such behavior of RPs patterns is similar with regards to the smoothness presented in horizontal and faster arm movements with beat (Fig 5.10). With regards to the type of sensor, there is little visual differences in RPs patters, while patterns of RPs for different activities present diagonal lines that appear to be closer and more dense for horizontal faster arm movement than horizontal normal arm movements (Fig 5.9).

Figs 5.10 show patterns of RPs for horizontal normal and faster arm movements while participants listen to a beat. For these patterns in the RPs, the type activities for normal and faster arm movements can be easily noticed in the patterns, as well as the change of smoothness between *sg0zmuvGyroZ* and *sg1zmuvGyroZ* with the patterns for *sg2zmuvGyroZ*. It can also noted that there is little visual differences between the RP patters for sensor HS01 and HS02.

Figs 5.11 show patterns of RPs for vertical normal and faster arm movements while no hearing a beat. One can note the evidently differences of patterns between the levels of smoothness where, for instance, patterns of RPs from *sg0zmuvGyroY* and *sg1zmuvGyroY* looks similar while RPs for *sg2zmuvGyroY* are completely black. Similarly, one can see little visual changes when comparing RPs patterns between

## Quantifying Human-Image Imitation Activities

---

sensors HS01 and HS02. However, the RPs patterns create a more dense presence of diagonal lines for faster arm movements than for normal arm movements.

Figs 5.12 show RPs patterns for vertical normal and faster arm movements for participants hearing a beat. Patterns of RP for vertical normal and vertical faster arm movements are visually noticeable as well as RPs patterns for changes in the increase of smoothness between `sg0zmuvGyroY` and `sg1zmuvGyroY` and with `sg2zmuvGyroY`. Once can also note that there is little visual changes of RPs patterns from different sensors.

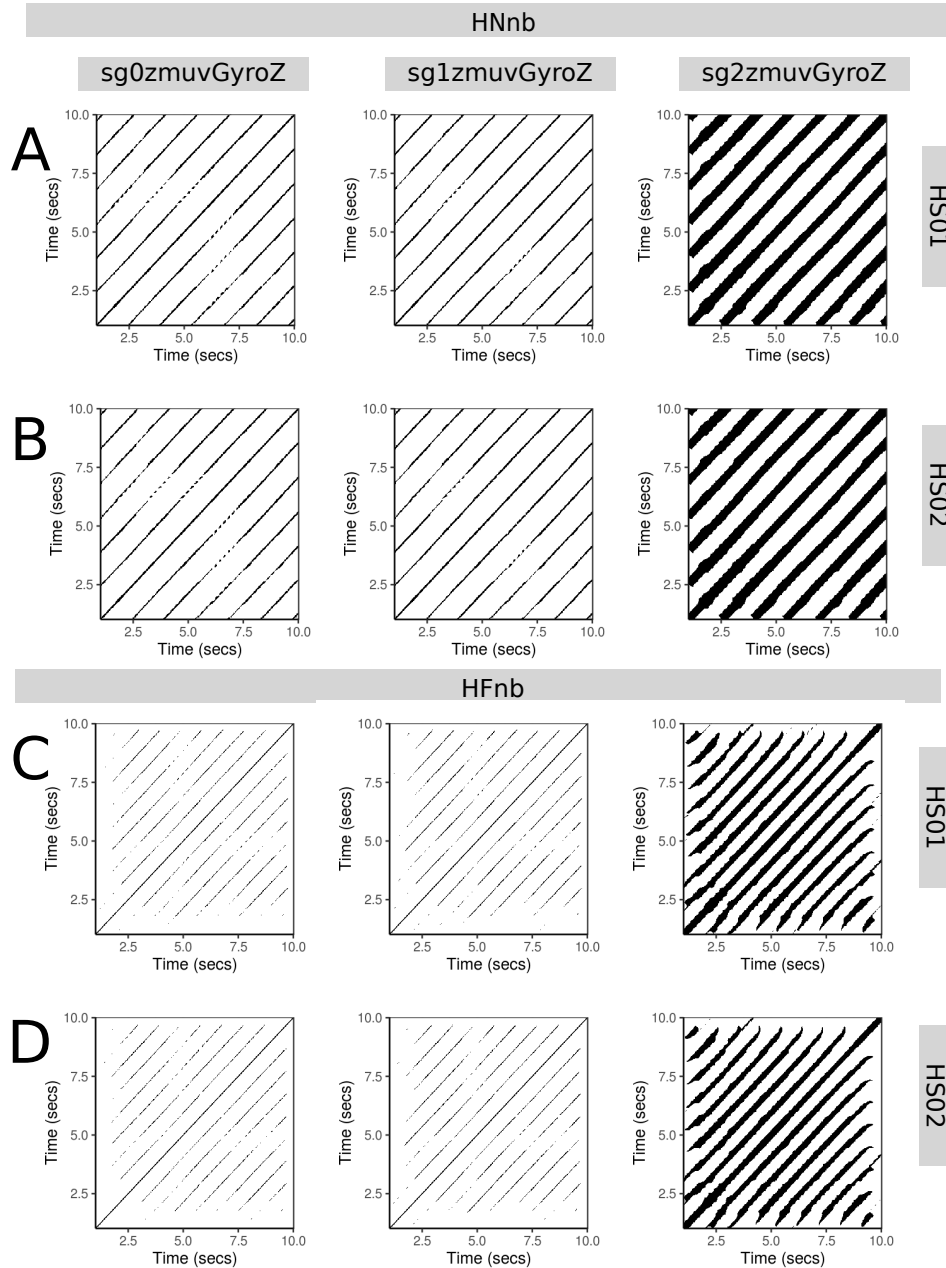


Fig. 5.9 **RPs for horizontal arm movements (no beat)**. Recurrence plots of participant p01 for (A, B) horizontal normal movements with no beat (HNnb) and (C, D) horizontal faster movements with no beat (HFnb). Time series for raw-normalised (sg0zmvGyroZ), normalised-smoothed 1 (sg1zmvGyroZ) and normalised-smoothed 2 (sg2zmvGyroZ) with (A, C) sensor 01 attached to the participant (HS01), and (B, D) sensor 02 attached to the participant (HS02). Recurrence plots were computed with embedding parameters  $\overline{m}_0 = 6$ ,  $\overline{\tau}_0 = 10$  and recurrence threshold  $\epsilon = 1$ . R code to reproduce the figure is available at [\[4\]](#).

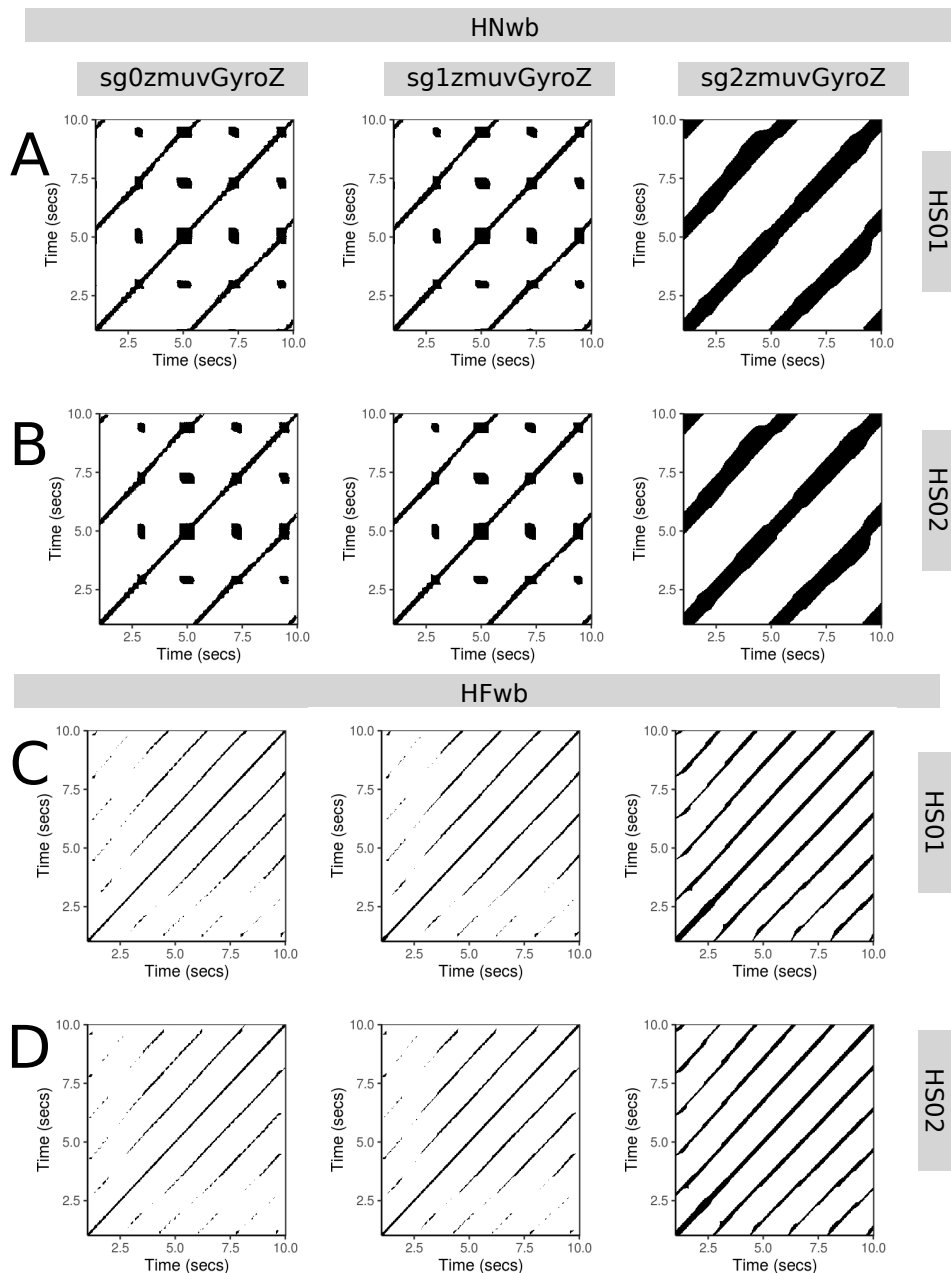


Fig. 5.10 **RPs for horizontal arm movements (with beat)**. Recurrence plots of participant p01 for (A, B) horizontal normal movements with beat (HNwb) and (C, D) horizontal faster movements with beat (HFwb). Time series for raw-normalised (sg0zmovGyroZ), normalised-smoothed 1 (sg1zmovGyroZ) and normalised-smoothed 2 (sg2zmovGyroZ) with (A, C) sensor 01 attached to the participant (HS01), and (B, D) sensor 02 attached to the participant (HS02). Recurrence plots were computed with embedding parameters  $\overline{m}_0 = 6$ ,  $\overline{\tau}_0 = 10$  and recurrence threshold  $\epsilon = 1$ . R code to reproduce the figure is available at [\[4\]](#).

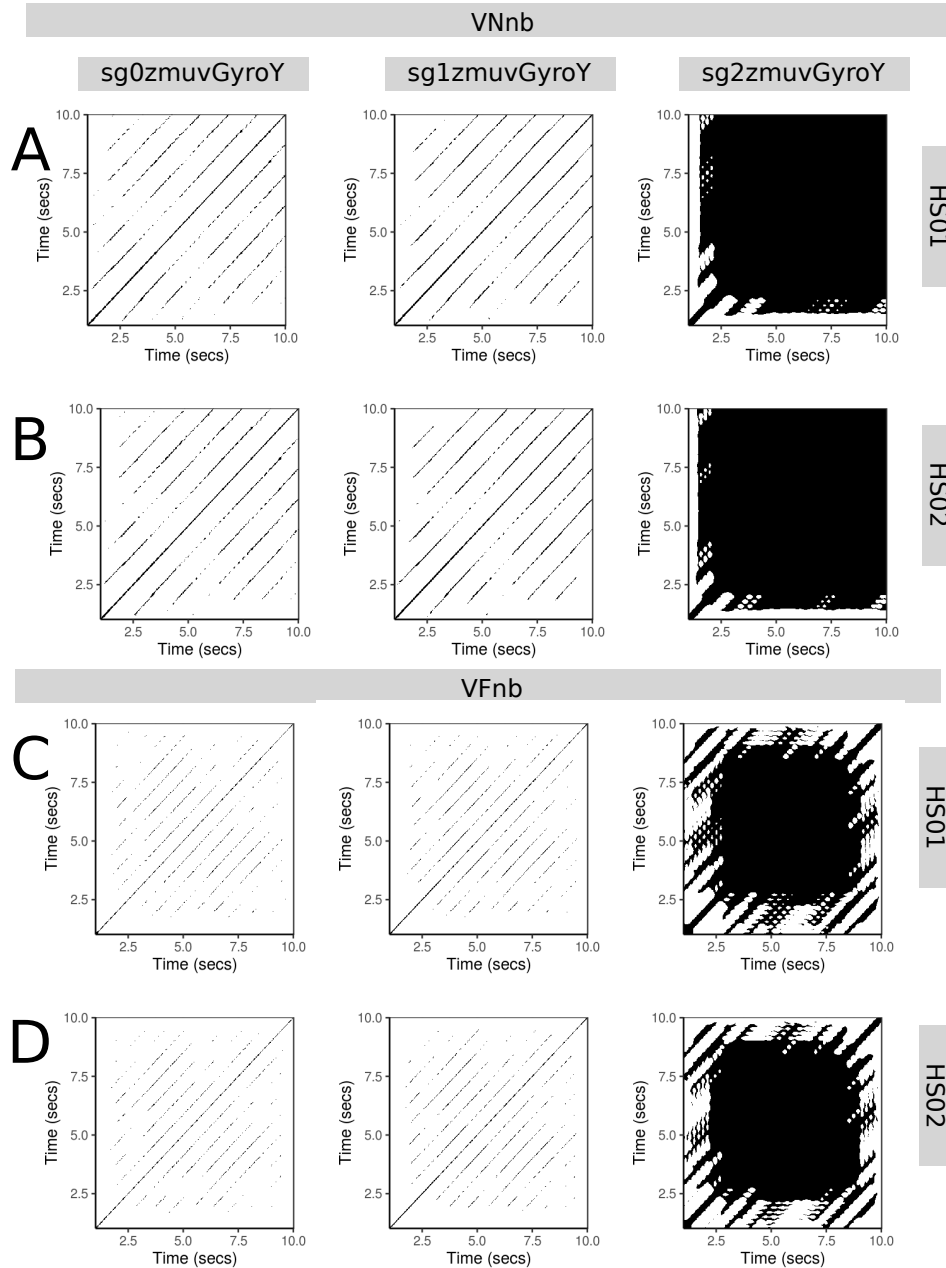


Fig. 5.11 RPs for vertical arm movements (no beat). Recurrence plots of participant p01 for (A, B) vertical normal movements with no beat (VNnb) and (C, D) vertical faster movements with no beat (VFnb). Time series for raw-normalised (sg0zmvGyroY), normalised-smoothed 1 (sg1zmvGyroY) and normalised-smoothed 2 (sg2zmvGyroY) with (A, C) sensor 01 attached to the participant (HS01), and (B, D) sensor 02 attached to the participant (HS02). Recurrence plots were computed with embedding parameters  $\overline{m}_0 = 6$ ,  $\overline{\tau}_0 = 10$  and recurrence threshold  $\epsilon = 1$ . R code to reproduce the figure is available at [\[4\]](#).



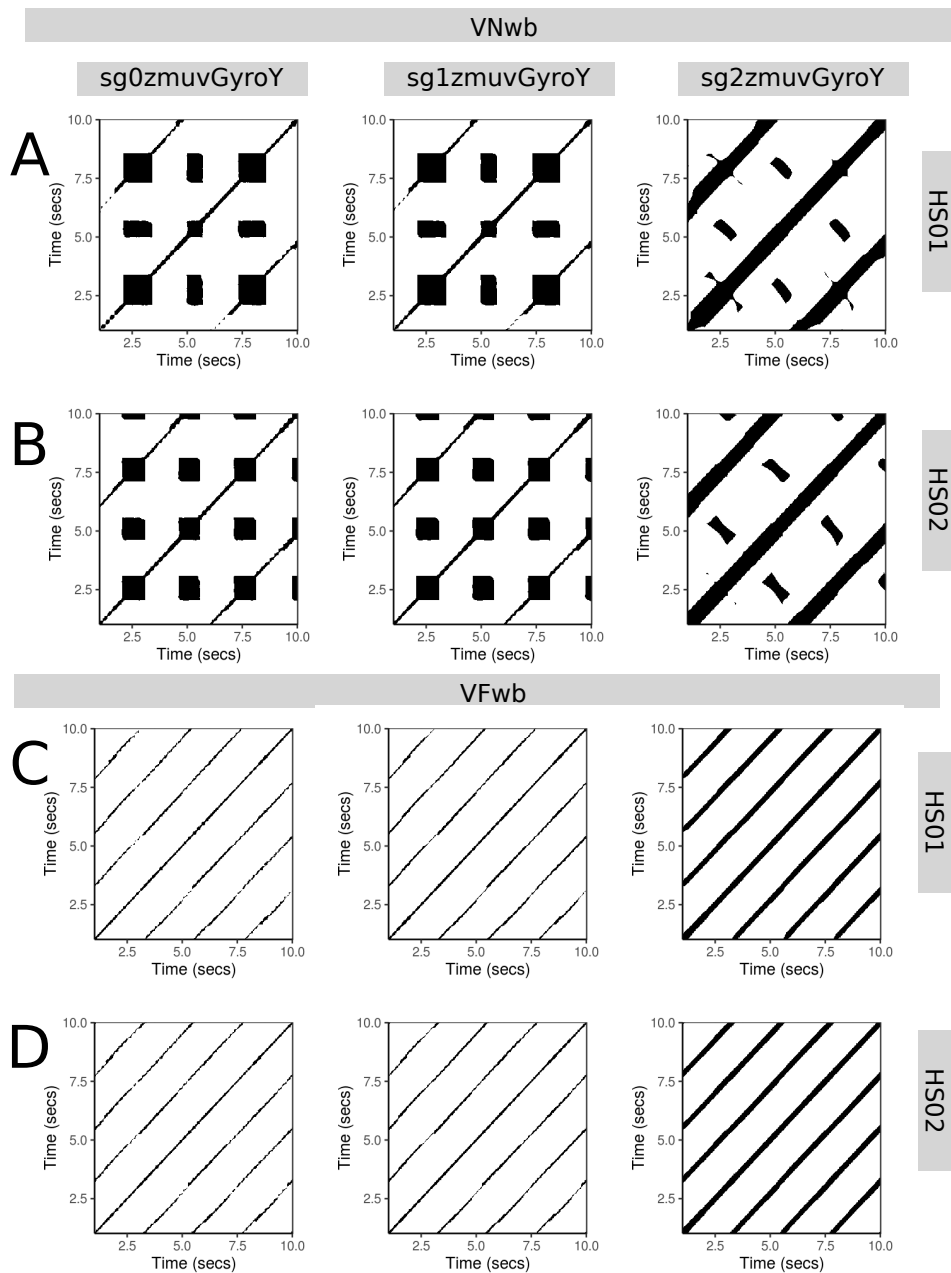


Fig. 5.12 RPs for vertical arm movements (with beat). Recurrence plots of participant p01 for (A, B) vertical normal movements with beat (VNwb) and (C, D) vertical faster movements with beat (VFwb). Time series for raw-normalised (sg0zmovGyroY), normalised-smoothed 1 (sg1zmovGyroY) and normalised-smoothed 2 (sg2zmovGyroY) with (A, C) sensor 01 attached to the participant (HS01), and (B, D) sensor 02 attached to the participant (HS02). Recurrence plots were computed with embedding parameters  $\overline{m}_0 = 6$ ,  $\overline{\tau}_0 = 10$  and recurrence threshold  $\epsilon = 1$ . R code to reproduce the figure is available at [\[4\]](#).

## 5.6 Recurrence Quantification Analysis

In this section is shown Recurrence Quantification Analysis (RQA) metrics (REC, DET, RATIO and ENTR) of six participants ( $p01, p04, p05, p10, p11, p15$ ) for horizontal arm movements (HNnb, HNwb, HFnb, HFwb) and vertical arm movements (VNnb, VNwb, VFnb, VFwb) with sensors HS01 and HS02, and three smoothed time series (sg0zmuvgyro, sg1zmuvgyro and sg2zmuvgyro). I hence compute four metrics of RQA metrics (REC, DET, RATIO and ENTR) with embedding parameters  $\overline{m}_0 = 6$ ,  $\overline{\tau}_0 = 10$  and recurrence threshold  $\epsilon = 1$ .

### REC values

Figs 5.13(A) and 5.14(A) show box plots of REC values, representing % of black dots in the RPs, for horizontal arm movements and vertical arm movements. In figs 5.13(A) can be noted that the interquartile range for sg2 is greater than the sg0 and sg1 for activities HNnb and HFnb, while REC values for activities HNwb and HFwb appear to increase its sample mean (gray rhombus) as the smoothness increase. Similarly, in figs 5.14(A) can be seen that there is a large interquartile range for sg2 in activities with no beat (VNnb, VFnb), while activities with beat (VNwb and VFwb) appear to be increase its sample mean (gray rhombus) as the smoothness of the time series increase. REC values from sensors HS01 and HS01 appear to differ little for both horizontal and vertical arm movements. For further details of individual REC values of participants, see Figs E.27 and E.28 in Section E.5.

### DET values

DET values, representing predictability and organisation of the RPs, appear to be constant irregardless of the source of time series (Figs 5.13(B) and 5.14(B) ). However,

## Quantifying Human-Image Imitation Activities

---

it can be noted a slight increase of DET values as the smoothness increase. For further details of individual DET values of participants, see Figs E.29, E.30 in Section E.5.

### **RATIO values**

RATIO values, representing dynamics transitions, for horizontal and vertical arm movements are shown in Figs 5.13(C) and 5.14(C). In Figs 5.13(C), for vertical arm movements, can be noted that HNwb activity present the less interquartile range while other seem to have similar interquartile range. Also, the increase of smoothness makes RATIO values to decrease (see gray rhombus). Similarly, in Figs 5.14(C), for vertical arm movements, is shown that VNwb has the less interquartile range as well as sg2 for VFnb and VFwb activities. The increase of smoothness of time series affect in the way that the sample mean values of RATIO values (gray rhombus) decrease. For further details of individual DET values of participants, see Figs E.31, E.32 in Section E.5.

### **ENTR values**

Figs 5.13(D) and 5.14(D) show ENTR values, representing the complexity of the structure of time series, for horizontal and vertical arm movements. Generally, figs 5.13(D) and 5.14(D) illustrate that the increase of smoothness causes an increase of sample mean (gray rhombus) of ENTR values in each of the activities and sensors. For both vertical and horizontal ENTR values for Nwb seems to be a bit higher than Nnb, while Fnb and Fwb appear to be have similar values. Also, there is little change between HS01 and HS02 sensors. For further details of individual ENTR values of participants, see Figs E.33, E.34 in Section E.5.

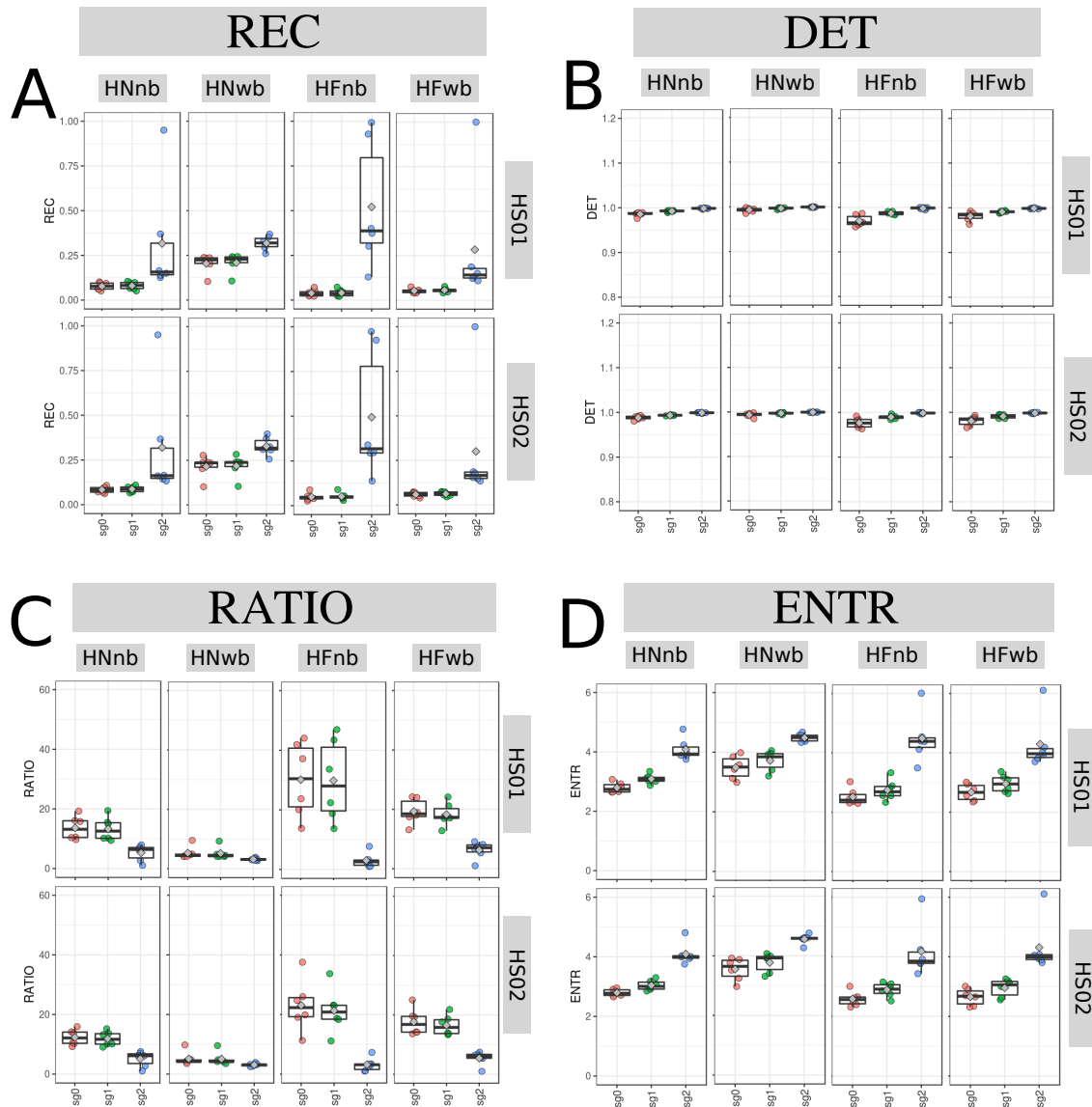


Fig. 5.13 **Box plots of RQA values for horizontal arm movements.** Box plots of (A) REC, (B) DET, (C) RATIO, and (D) ENTR values for 6 participants performing HNnb, HNwb, HFnb and HFwb movements with sensors HS01, HS02 and three smoothed-normalised time series (sg0, sg1 and sg2). RQA values were computed with embedding parameters  $\overline{m}_0 = 6$ ,  $\overline{\tau}_0 = 10$  and recurrence threshold  $\epsilon = 1$ . R code to reproduce the figure is available at [\[47\]](#).

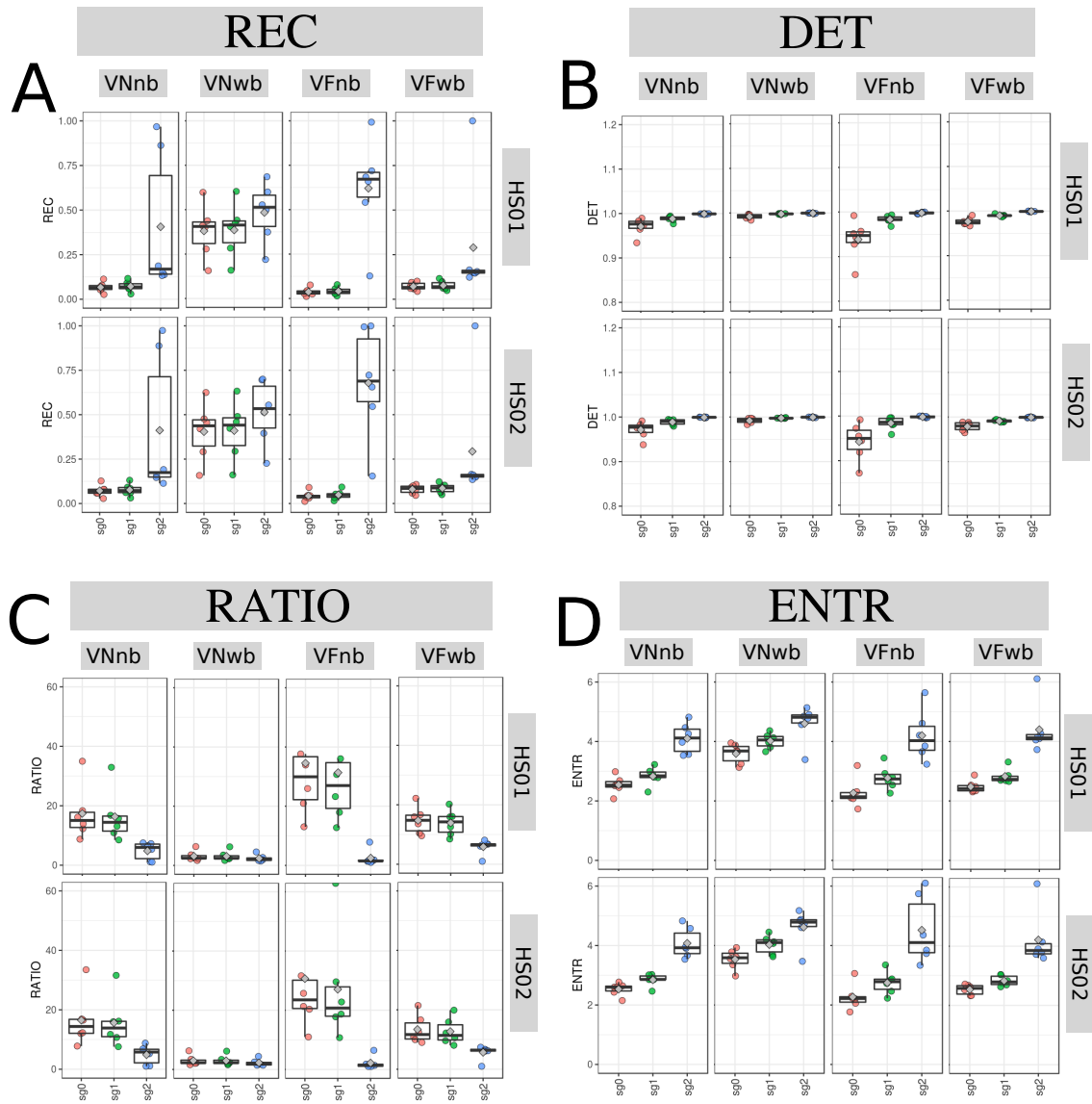


Fig. 5.14 **Box plots for RQA values for vertical arm movements.** Box plots of (A) REC, (B) DET, (C) RATIO, and (D) ENTR values for 6 participants performing V Nnb, V Nwb, V Fnb and V Fwb movements with sensors HS01, HS02 and three smoothed-normalised time series (sg0, sg1 and sg2). RQA values were computed with embedding parameters  $\overline{m}_0 = 6$ ,  $\overline{\tau}_0 = 10$  and recurrence threshold  $\epsilon = 1$ . R code to reproduce the figure is available at [\[47\]](#).

## 5.7 Weaknesses and strengths of RQA

Surfaces for RQA metrics (REC, DET, RATIO, ENTR) are computed with the variation of embedding values by an increase of one ( $0 \leq m \leq 10$ ,  $0 \leq \tau \leq 10$ ) and recurrence thresholds by an increase of 0.1 ( $0.2 \leq \epsilon \leq 3$ ). Hence, different characteristics of 3D surface plots of RQA are shown by considering different activities, sensors, window lengths and level of smoothness and participants.

Figs 5.15 show the 3D surface plots for RQA metrics (REC, DET, RATIO, ENTR) using time series of participant *p01*, sensor HS01, activity HNnb, sg0zmuVgyroZ axis and a 10 seconds window length. The 3D surface plot of REC values, representing the % of recurrence dots in the RP, show highest values of REC when embedding values are near to 1 and the recurrence threshold is at the maximum ( $\epsilon = 3$  for this surface plot). Similarly, it can be seen a decrease of REC values as the embedding dimension and embedding delay values increase, however there is an increase of REC values as the recurrence threshold is increasing (Fig 5.15(A)). Regarding the 3D surface plots of DET values, representing predictability and organisation of the RPs, Fig 5.15(B) show slightly uniform values when varying both embedding parameters and recurrence threshold with the exception of embedding parameters near to 1 and recurrence thresholds near to 0.2 where the DET values are smaller. 3D surface for RATIO values, representing dynamic transitions, show a plateau with low values recurrence threshold values greater than 1.0. However, there is a fluctuated increase of RATIO values as the embedding values increase given that the recurrence threshold is lower than 1 (Fig 5.15(C)). For ENTR values, representing the complexity of the structure of the time series, Fig 5.15(D) show a maximum value of ENTR when embedding parameters are near to 1 and recurrence threshold values are near to 3.0. It can also be noted fluctuations in the 3D surface when ENTR values are greater than 2.5 (red surface) for embedding dimensions between 3 to 9 and a decrease of ENTR values per each embedding dimension for

## Quantifying Human-Image Imitation Activities

delay embedding values (yellow surface). Additionally, ENTR values decrease as the embedding dimension and delay embedding decrease.

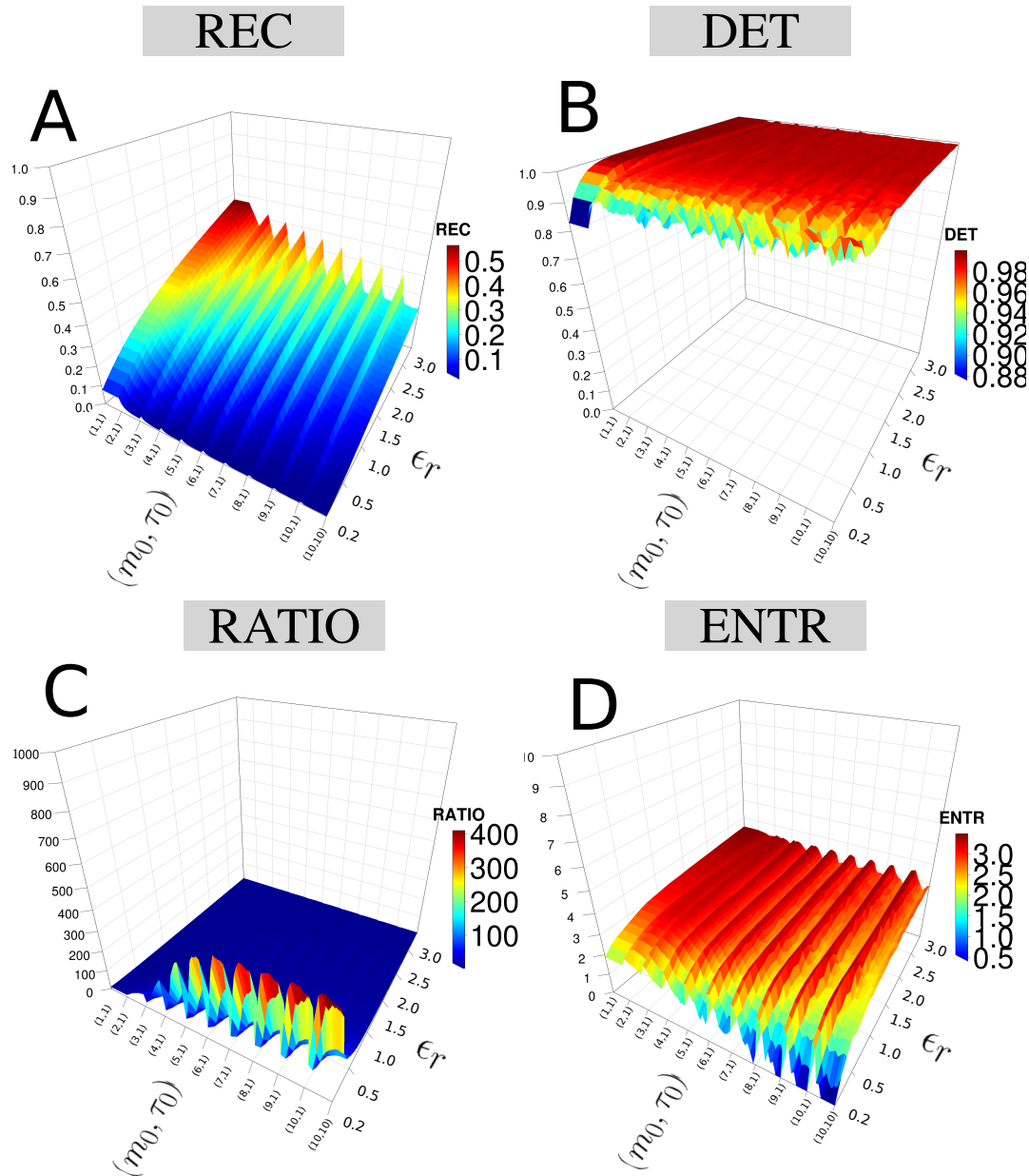


Fig. 5.15 **3D surface plots of RQA metrics.** 3D surface plots of RQA metrics (A) REC, (B) DET, (C) RATIO and (D) ENTR with an increasing pair of embedding parameters ( $0 \leq m_0 \leq 10$ ,  $0 \leq \tau_0 \leq 10$ ) and recurrence thresholds ( $0.2 \leq \epsilon_r \leq 3$ ). RQA metrics are computed with the time series of participant *p01* using HS01 sensor, HNNb activity, sg0zmvGyroZ axis and 10 seconds for window length. R code to reproduce the figure is available at [GitHub](#).

### 5.7.1 Sensors and activities

Figs 5.16 and 5.17 show 3D surface plots of RQA metrics (REC, DET, RATIO, ENTR) for horizontal arm movements (HNnb, HNwb, HFnb, HFwb) using sensor HS01 and HS02 for participant *p01* with *sg0zmvGyroZ* axis and 10 seconds window length. Hence, Figs 5.16 present 3D surface plots of RQA metrics for HS01, where 3D surface plots of REC values (Fig 5.16(A)) appear to be similar across the activities (HNnb, HFnb, HFwb) with the exception of HNwb which decrease of REC values is mainly affected by the increase of recurrence threshold and slightly affected to the increase of embedding dimension parameters. For DET values, 3D surface plots in Figs 5.16(B) appear to show values near to 1.0 (red colour surface), however HNwb shown fluctuations of DET values as the embedding dimension increase, it can also be noted a decrease of DET values for certain values of recurrence threshold (2.6 for HNwb, 0.3 for HFnb, and 0.3 for HFwb). For Fig 5.16(C)), 3D surface plots of RATIO values appear to be similar, showing a plateau for values between 0 to 50 (blue surface) and the increase of peaks is different for each of the activities. For Fig 5.16(D), ENTR values present different surface formations, for instance, HNnb show fluctuated higher values of ENTR (red colour surface), whereas for activity HNwb the ENTR values are higher (red colour surface) for recurrence threshold near to 3.0, ENTR values for HFnb appear to be higher when embedding dimension is near to 10, while higher values for ENTR values for HFwb appear to be when the recurrence threshold is near to 0.2.

Then, looking and comparing visually one by one of the 3D surface plots for sensors HS01 and HS02 in Figs 5.16 and 5.17, one can notice little differences in the shape of the surface plots. Similarly, there is little variations in the surface plots for vertical arm movements with the sensors HS01 and HS02 (Figs 5.18 and 5.19).

With regards to horizontal and vertical movements, 3D surface plots appear to be similar for REC, DET and RATIO values with sensor HS01 (Figs 5.16 and 5.18) and



## Quantifying Human-Image Imitation Activities

---

sensor HS02 (Figs 5.17 and 5.19), however 3D surface plots of ENTR values in each of the arm movements presents distinguishable variations in the surface plots, see Figs 5.16(D) and 5.18(D) for horizontal and vertical arm movements with sensor HS01 and Figs 5.17(D) and 5.19(D) for horizontal and vertical arm movements with sensor HS02.

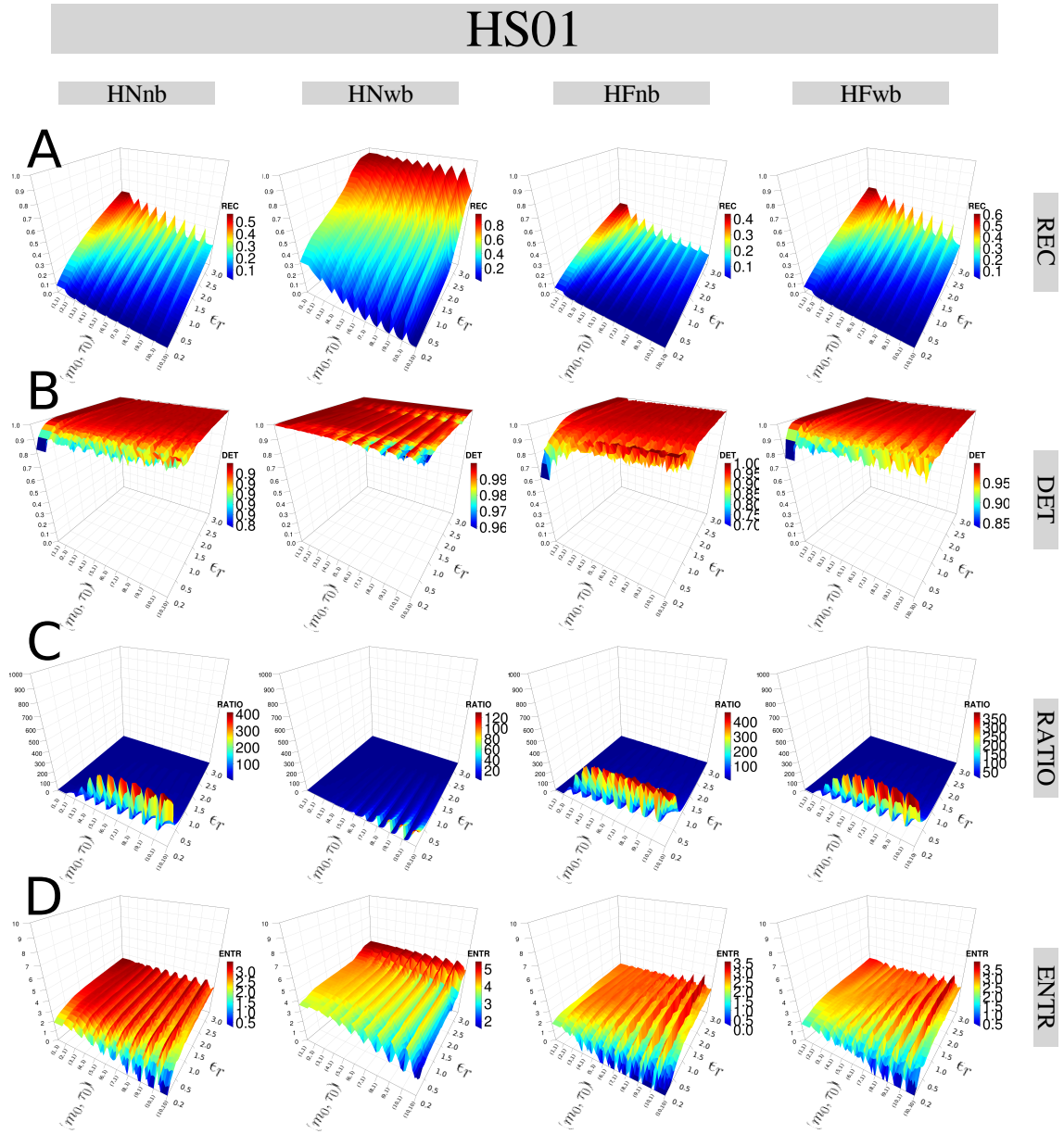


Fig. 5.16 **3D surface plots of RQA metrics for horizontal arm movements with HS01.** 3D surface plots for (A) REC, (B) DET, (C) RATIO and (D) ENTR values with increasing pair of embedding parameters ( $0 \leq m \leq 10$ ,  $0 \leq \tau \leq 10$ ) and recurrence thresholds ( $0.2 \leq \epsilon \leq 3$ ). RQA metrics are computed with the time series of participant *p01* for sensors HS01, horizontal arm movement activities (HNnb, HNwb, HFnb, HFwb) and *sg0zmvGyroZ* axis with 10 seconds window length. R code to reproduce the figure is available at [\[4\]](#).

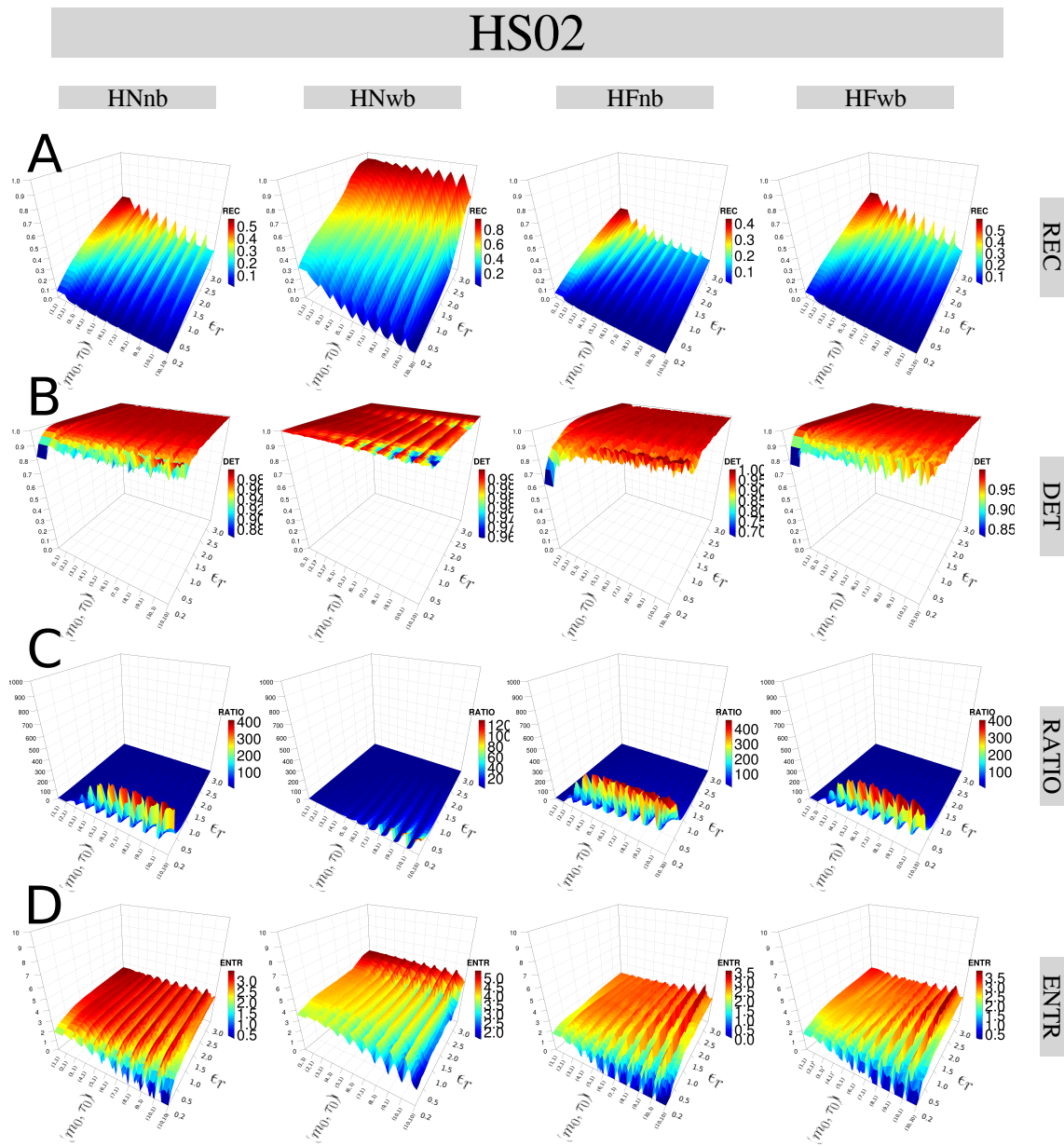


Fig. 5.17 3D surface plots of RQA metrics for horizontal arm movements with HS02. 3D surface plots for (A) REC, (B) DET, (C) RATIO and (D) ENTR values with increasing pair of embedding parameters ( $0 \leq m \leq 10$ ,  $0 \leq \tau \leq 10$ ) and recurrence thresholds ( $0.2 \leq \epsilon \leq 3$ ). RQA metrics are computed with the time series of participant  $p01$  for sensors HS02, horizontal arm movement activities (HNnb, HNwb, HFnb, HFwb) and sg0zmvGyroZ axis with 10 seconds window length. R code to reproduce the figure is available at [\[4\]](#).

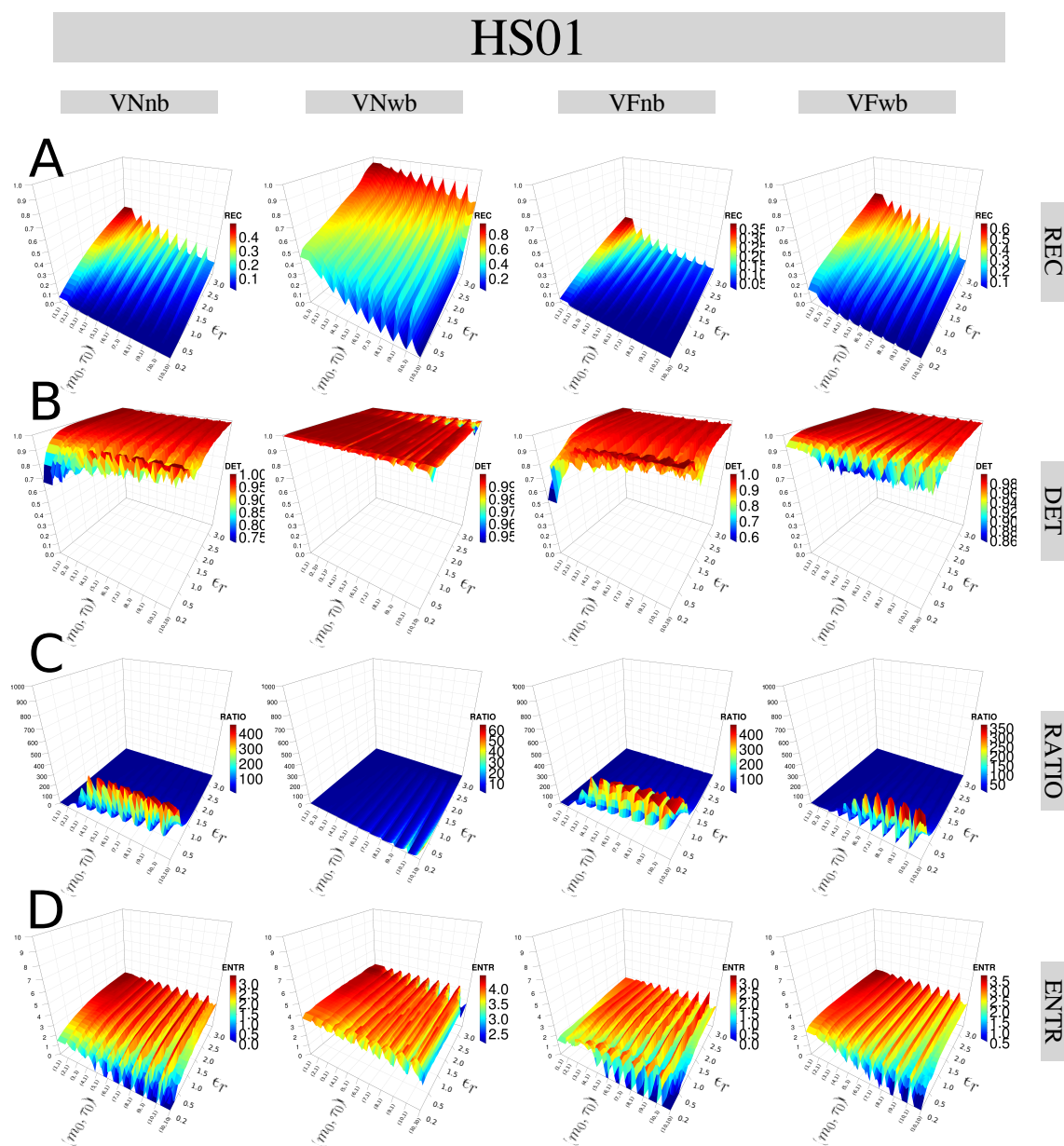


Fig. 5.18 **3D surface plots of RQA metrics for vertical arm movements with HS01.** 3D surface plots for (A) REC, (B) DET, (C) RATIO and (D) ENTR values with increasing pair of embedding parameters ( $0 \leq m \leq 10$ ,  $0 \leq \tau \leq 10$ ) and recurrence thresholds ( $0.2 \leq \epsilon \leq 3$ ). RQA metrics are computed with the time series of participant *p01* for sensors HS01, vertical arm movements activities (VNnb, VNwb, VFnb, VFwb) and sg0zmuvGyroY axis with 10 seconds window length. R code to reproduce the figure is available at [GitHub](#).

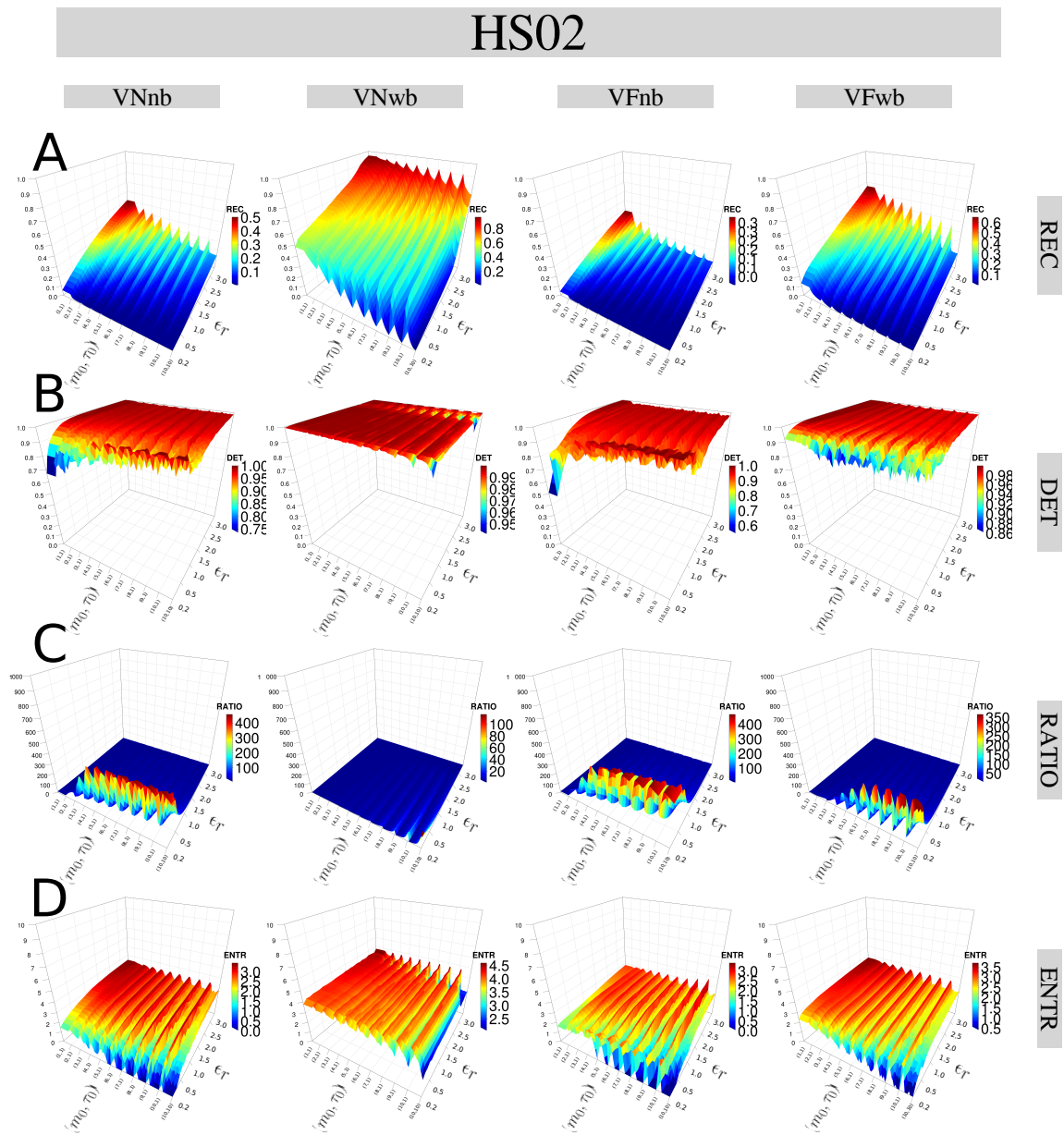


Fig. 5.19 **3D surface plots of RQA metrics for vertical arm movements with HS02.** 3D surface plots for (A) REC, (B) DET, (C) RATIO and (D) ENTR values with increasing pair of embedding parameters ( $0 \leq m \leq 10$ ,  $0 \leq \tau \leq 10$ ) and recurrence thresholds ( $0.2 \leq \epsilon \leq 3$ ). RQA metrics are computed with the time series of participant *p01* for sensors HS02, vertical arm movements activities (VNnb, VNwb, VFnb, VFwb) and sg0zmuvGyroY axis with 10 seconds window length. R code to reproduce the figure is available at [\[4\]](#).

### 5.7.2 Window size

3D surface plots of REC values with a short window length (2-secs) can affect the shape of 3D surface, however for window size of 5-sec, 10-sec and 15-sec, the 3D surface plots appear to show little changes (Figs 5.20(A)). For instance, one can see 3D surface plots of DET values with a window of 2 seconds window length is slightly different to other surface plots but keeping the plateau (red surface) in each of the surface plots (Figs 5.20(B)). Similarly, the 3D surface plots of RATIO values preserve the same plateau (blue surface) with little variations in the surface plots as window length is incrementing (Figs 5.20(C)). 3D surface plots of ENTR values appear to have similar aspects as the fluctuations of the curves keeps the same values (red and yellow colours). It can also be noted that the smoothness of 3D surface plots decrease as the embedding dimension parameters increase and such smoothness is also affected by the window length (see Figs 5.20(D)).

### 5.7.3 Smoothness

Figs 5.21 show the effects of three levels of smoothness (sg0zmvGyroZ, sg1zmvGyroZ and sg2zmvGyroZ) in the RQA metrics. Generally, 3D surface plots from sg2zmvGyroZ are affected by the smoothness. It can also be noted that REC values and ENTR values present a slightly different surface plots (see Figs 5.21(A, D)), while DET and RATIO values appear to be similar which is mainly reflected in the colour of the curves (see Figs 5.21(B, C)). In Figs 5.21(A), 3D surface plots for REC values tend to be smoothed as the smoothness of the time series increase to the point where the increase of recurrence threshold affects the shape of the surface plots. Similarly, in Figs 5.21(D), 3D surface for ENTR values is affected by the smoothness of the time series to the point that the fluctuations in the surface does change drastically the shape by showing only an increase of ENTR values as the recurrence threshold increase.

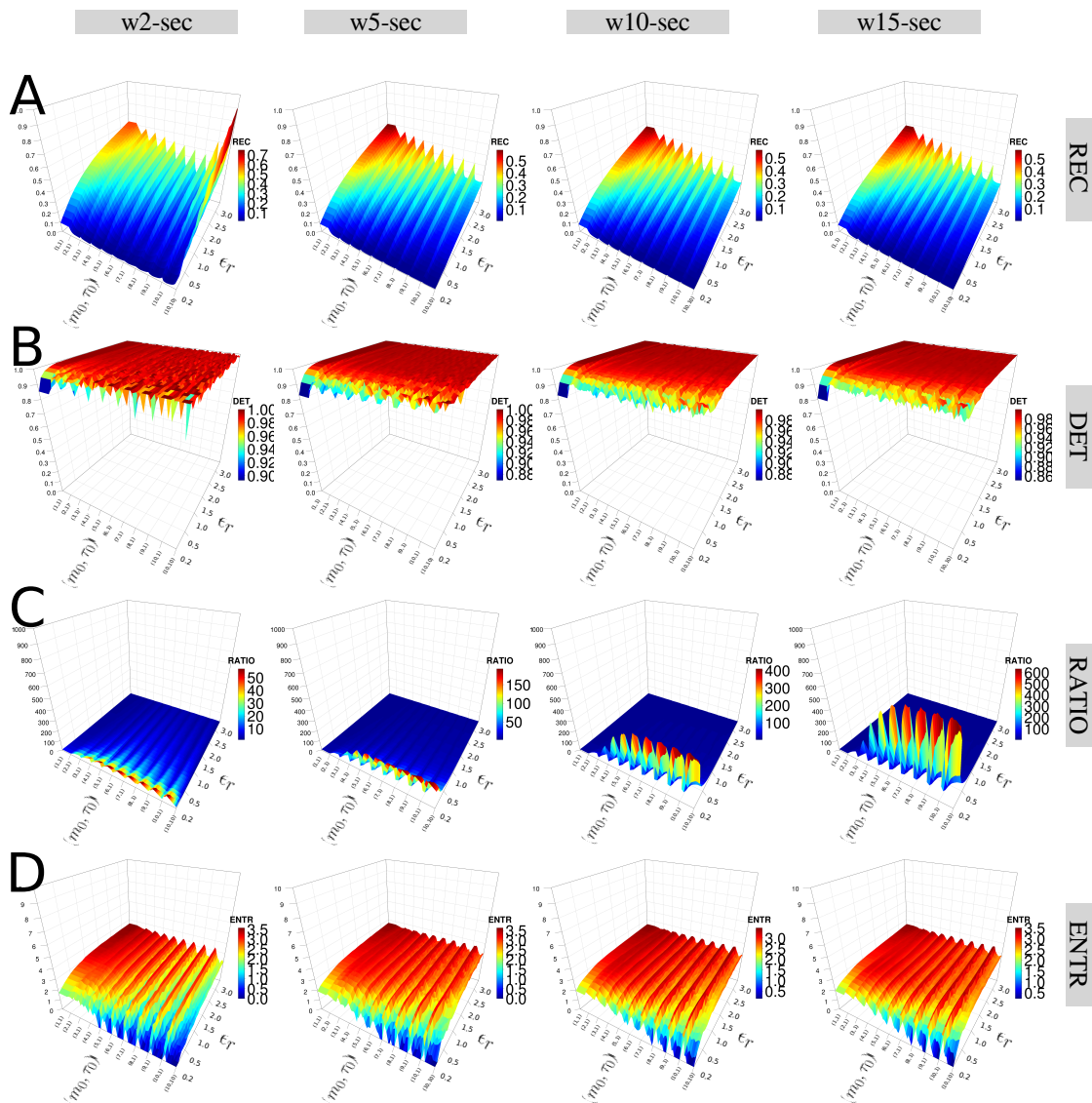


Fig. 5.20 3D surface plots of RQA metrics for different window lengths. 3D surface plots for four window lengths (w2-sec, w5-sec, w10-sec and w15-sec) and for (A) REC, (B) DET, (C) RATIO, and (D) ENTR values with increasing pair of embedding parameters ( $0 \leq m \leq 10$ ,  $0 \leq \tau \leq 10$ ) and recurrence thresholds ( $0.2 \leq \epsilon \leq 3$ ). RQA metrics are computed with the time series of participant  $p01$  using HS01 sensor, HNNb activity and sg0zmuV GyroZ axis. R code to reproduce the figure is available at [\[45\]](#).

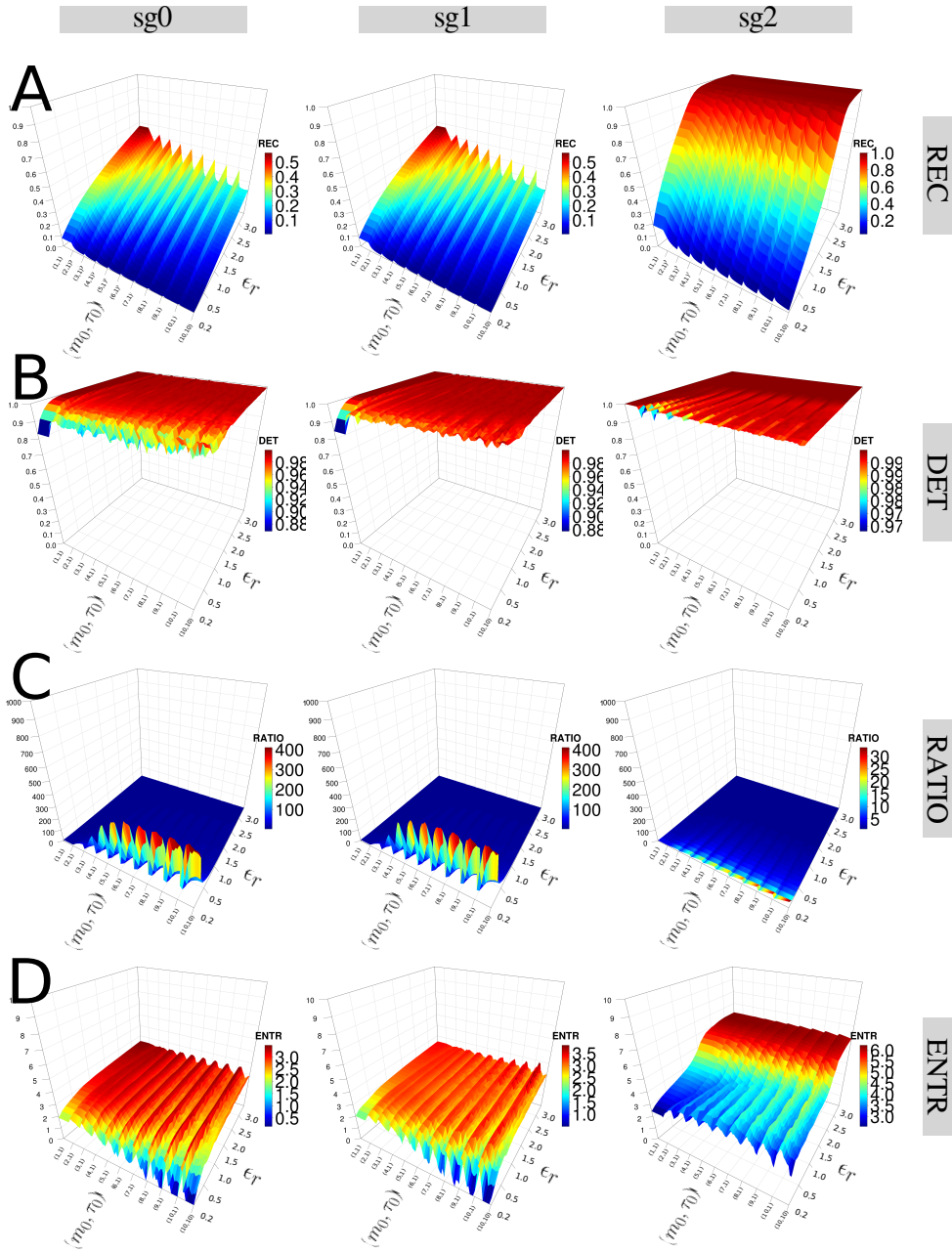


Fig. 5.21 3D surface plots of RQA metrics with three levels of smoothness. 3D surface plots for three levels of smoothness (sg0zmvGyroZ, sg1zmvGyroZ, and sg2zmvGyroZ) and for (A) REC, (B) DET, (C) RATIO, and (D) ENTR values with increasing pair of embedding parameters ( $0 \leq m \leq 10$ ,  $0 \leq \tau \leq 10$ ) and recurrence thresholds ( $0.2 \leq \epsilon \leq 3$ ). RQA metrics are computed with the time series of participant  $p01$  with HS01 sensor, HNNb activity and 10 seconds window length. R code to reproduce the figure is available at [\[4\]](#).



### 5.7.4 Participants

The shape of 3D surface plots of RQA metrics is also affected when using time series from different participants (Figs 5.22). For instance, 3D surface of DET values show slightly but noticeable differences in the fluctuations when embedding dimension and recurrence threshold increase (Figs 5.22(B)) which is similar for ENTR values where the fluctuations of the 3D surface plots changes for each of the participants (Figs 5.22(D)). However, the shape of 3D surface plots for RET values and RATIO values is little affected by the change of participants (Figs 5.22(A, C)).

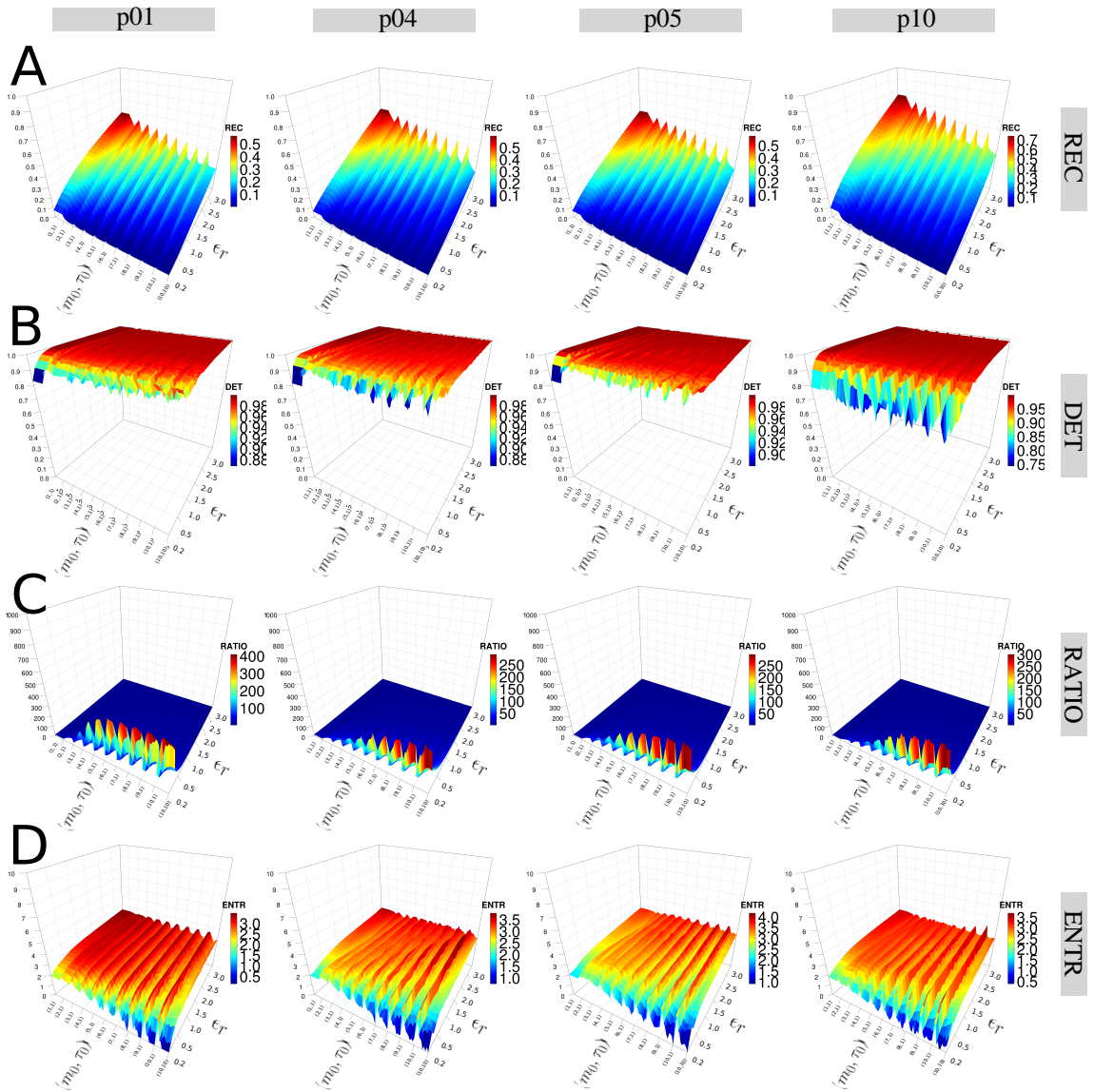


Fig. 5.22 **3D surface plots of RQA metrics with four participants.** 3D surface plots for participants  $p01$ ,  $p04$ ,  $p05$  and  $p10$  and for (A) REC, (B) DET, (C) RATIO, and (D) ENTR with increasing pair of embedding parameters ( $0 \leq m \leq 10$ ,  $0 \leq \tau \leq 10$ ) and recurrence thresholds ( $0.2 \leq \epsilon \leq 3$ ). RQA metrics are computed with the time series of sg0zmuVgyroZ axis, HS01 sensor, HNnb activity and 10 seconds window length. R code to reproduce the figure is available at [\[6\]](#).

### 5.7.5 Final remarks

Different sources of time series (participants, sensors, activities, window length or level of smoothness) produce different results in nonlinear analysis methods (e.g. FNN, AMI, RSSs with UTDE, RPs and RQAs) and these results are sensitive to different parameters of nonlinear analysis methods (e.g., minimum dimension threshold, embedding parameters or recurrence thresholds). That said, 3D surface plots of RQA metrics with the variation of embedding parameters and recurrence thresholds appear to be helpful to understand the dynamics of any type of time series data. That is the case of 3D surface plots of ENTR values which with only the selection of variation of range of parameters (e.g., embedding parameters or recurrence thresholds), the 3D surface plots show clearly differences in the shape of 3D surface plots irregardless of the source of the time series. Hence, computing 3D surface plots of ENTR values with little parametrisation might be of help to understand the dynamics of human movement variability from different sources of time series data.

# Chapter 6

## Quantifying Human-Humanoid Imitation Activities

### 6.1 Introduction

Similarly as in Chapter 5, in this Chapter, results for experiments of human-humanoid imitation activities, described in Section 4.5.2, are presented by including time series, minimum embedding parameters, the reconstructed state spaces (RSS) using uniform time-delay embedding technique (UTDE), recurrence plots (RP), recurrent quantification analysis (RQA), and weaknesses and strengths of RQA with three dimensional surface plots of RQA.

Time series data for this experiment are described as follows:

- Twenty participants defined as  $pN$  where  $N$  is the number of participant.
- Three levels of smoothness for the normalised data (`sg0zmu`, `sg1zmu` and `sg2zmu`), computed from two different filter lengths (29 and 159) with the same polynomial degree of 5 using the function `sgolay(p,n,m)` (signal R developers, 2014),

## Quantifying Human-Humanoid Imitation Activities

---

- Four window length size: 2-sec (100 samples), 5-sec (250 samples), 10-sec (500 samples) and 15-sec (750 samples), and
- Four velocities of arm movement activity: horizontal normal (HN), horizontal faster (HF), vertical normal (VN) and vertical faster (VF)

To make the visual comparison easier, time series for only three participants ( $p01$ ,  $p02$ ,  $p03$ ) with a window length of 10 seconds (500 samples) are considered for the following results. See Appendix F for further results.

### 6.2 Time series

Figures 6.1 and 6.2 show time series of horizontal arm movements using axis GyroZ and vertical arm movements using axis GyroY. The remaining time series are presented in Appendix F.1.

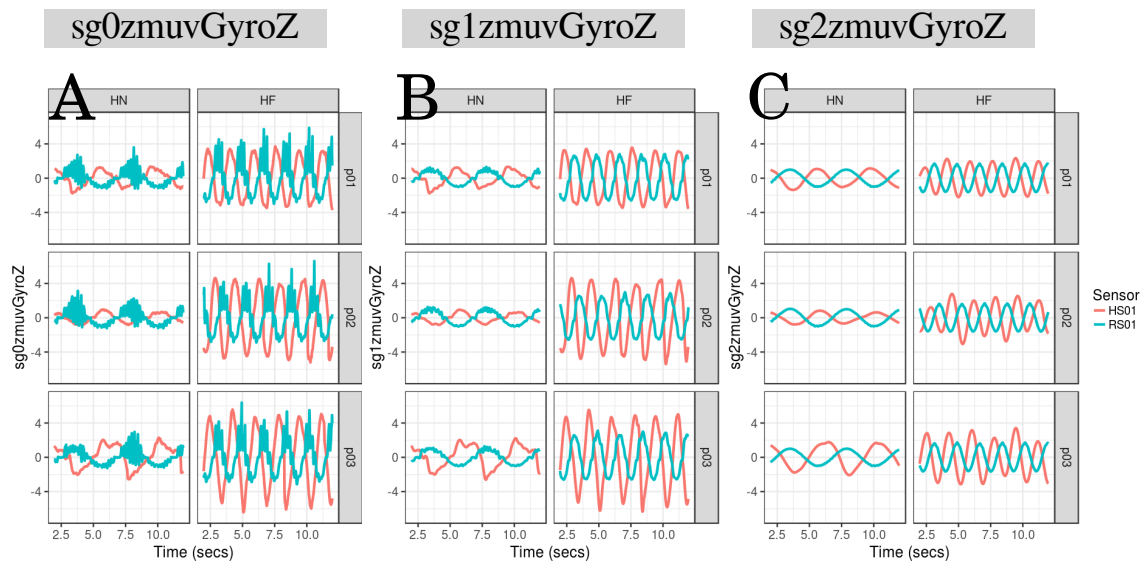


Fig. 6.1 **Time series for horizontal arm movements.** (A) raw-normalised ( $sg0zmuVgyroZ$ ), (B) normalised-smoothed 1 ( $sg1zmuVgyroZ$ ) and (C) normalised-smoothed 2 ( $sg2zmuVgyroZ$ ). Time series are only for three participants ( $p01$ ,  $p02$ , and  $p03$ ) for horizontal movements in normal and faster velocity (HN, HF) with the normalised GyroZ axis ( $zmuVgyroZ$ ) and with one sensor attached to the participant (HS01) and other sensor attached to the robot (RS01). R code to reproduce the figure is available at [\[4\]](#).

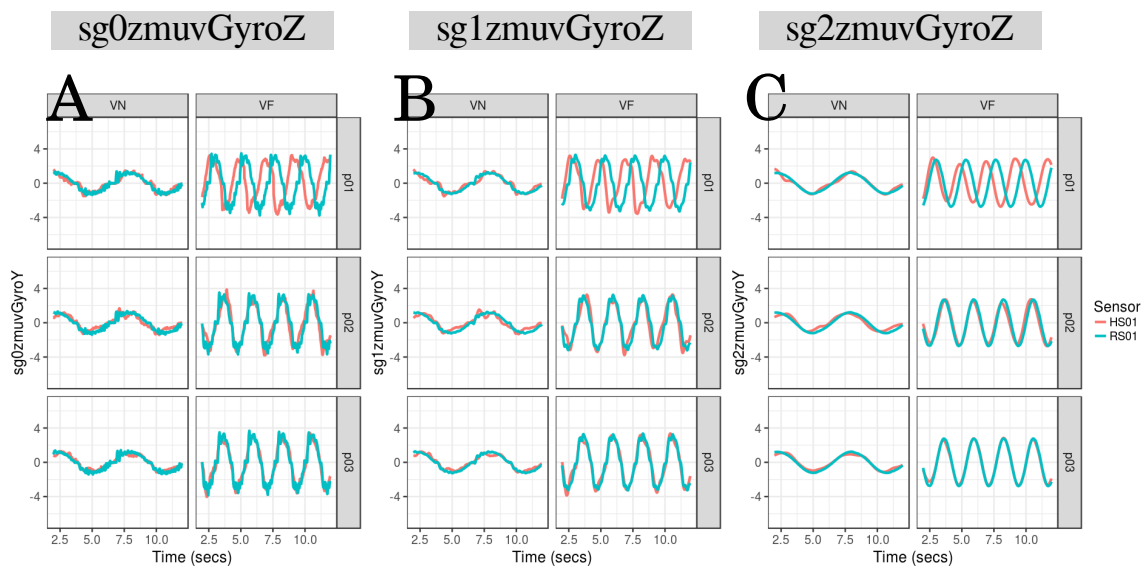


Fig. 6.2 **Time series for vertical arm movements.** (A) raw-normalised (sg0zmuvgyroY), (B) normalised-smoothed 1 (sg1zmuvgyroY) and (C) normalised-smoothed 2 (sg2zmuvgyroY). Time series are only for three participants ( $p01$ ,  $p02$ , and  $p03$ ) for vertical movements in normal and faster velocity (VN, VF) with the normalised GyroY axis (zmuvgyroY) and with one sensor attached to the participant (HS01) and other sensor attached to the robot (RS01). R code to reproduce the figure is available at [\[17\]](#).

## 6.3 Minimum Embedding Parameters

As mentioned in Section 5.3 in Chapter 5, minimum embedding parameters using FNN and AMI algorithms are computed for time series of this section. Hence, Figs 6.3(A) show box plots of the minimum embedding dimensions of twenty participants performing horizontal and vertical arm movements at normal and faster velocities (HN, HF, VN and VF) with attached sensors to participants (HS01) and to the robot (RS01). Generally, Figs 6.3(A) show that minimum embedding values appear to be constant for sensor RS01 as their interquartile range in the box plots are near to 0.1 with the exception of two axis. Minimum embedding values for sensor HS01 appear to show more variations as their interquartile range of the box plots are near to 1 with four exceptions. Additionally, it can be seen in Figs 6.3(A) that there is a decrease of mean values (rhombus) in the box plots as smoothness of time series increase. See Figs. F.7 and F.8 in Appendix F.2 for detailed values of embedding dimensions for each participant.

Similarly, the first minimum values of AMI values for participants ( $p01$  to  $p20$ ), activities (HN, HF, VN, and VF) and sensors (HS01, RS01) are shown in the box plots of Figs 6.3(B). It can be seen that values for HS01 tend to be more spread as the smoothness of the time series is increasing (see the increase of both mean (rhombus) and interquartile range). However, AMI values for RS01 do not show such a similar increase in relation with the increase of smoothness excepting for HF and VF (see the increase of both mean (rhombus) and interquartile range) (Figs 6.3(B)). Similarly to the minimum parameters in Chapter 5 (see 5.3), there is a decrease of minimum embedding dimension as the smoothness is increasing, meaning that there is a decrease of the dynamics of the time series data. Also, the sample mean (gray rhombus) of first minimum AMI increase as the smoothness increase, meaning that the maximal



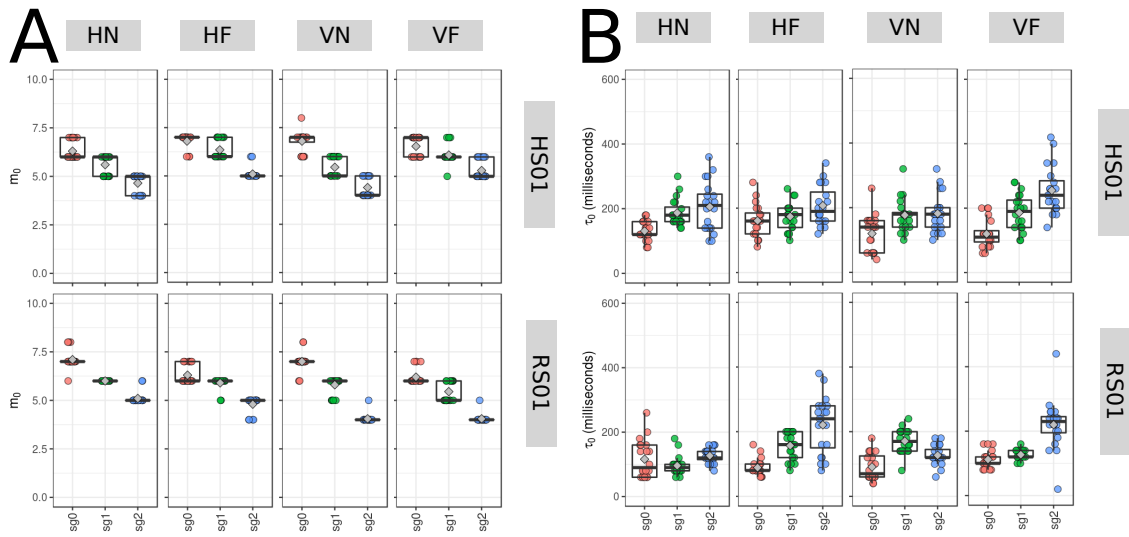


Fig. 6.3 **Box plots of minimum embedding parameters.** Box plots of (A) minimum embedding dimensions and (B) first minimum AMI values for Horizontal Normal (HN), Horizontal Faster (HF), Vertical Normal (VN) and Vertical Faster (VF) with sensors attached to participants (HS01) and sensor attached to robot (RS01). Minimum embedding dimensions ( $m_0$  and  $\tau_0$ ) are for twenty participants ( $p01$  to  $p20$ ) with three smoothed signals (sg0zmvGyroZ (sg0) , sg1zmvGyroZ (sg1) and sg2zmvGyroZ (sg2)) and window length of 10-sec (500 samples). R code to reproduce the figure is available at [\[17\]](#).

information to knowledge at  $\tau_0$  also increase. See Figs. F.9 and F.10 in Appendix F.2 for more details about AMI values for each participant.

### 6.3.1 Average minimum embedding parameters

Following the Section 3.4.3 to compute the overall average of minimum embedding parameters, the sample mean for the minimum values of  $E_1(m)$  from Figs 6.3(A) is  $\bar{m}_0 = 6$  and the sample mean for minimum values of AMIs from Figs 6.3(B) is  $\bar{\tau}_0 = 8$ , for which the overall average minimum embedding parameters is ( $\bar{m}_0 = 6$ ,  $\bar{\tau}_0 = 8$ ). Hence, the average minimum embedding parameters ( $\bar{m}_0 = 6$ ,  $\bar{\tau}_0 = 8$ ) has been considered to compute Reconstructed State Spaces (RSSs), Recurrence Plots (RPs) and Recurrence Quantification Analysis (RQA) metrics for human-humanoid activities.

## 6.4 Reconstructed state spaces with UTDE

Considering Section 3.5 and time series for participant *p01* (Figs 6.1, 6.2) the reconstructed state spaces for horizontal arm movements (Figs 6.4) and vertical arm movements (Figs 6.5) are computed with  $\bar{m}_0 = 6$  and  $\bar{\tau}_0 = 8$

The trajectories of the RSSs for horizontal normal and faster from HS01 and RS01 are slightly smoothed as the time-series smoothness increase (Figs 6.4). Although the frequency of the movement increase from normal to faster velocity activities, the trajectories RSSs in Figs 6.4(B) show higher oscillations specially for a maximum values of smoothness (sg2zmvGyroZ), while the trajectories in the RSS for HF in Figs 6.4(D) show a lower and smoothed oscillations as the smoothness increase. In contrast, the time series for vertical movements are less noisy and well structured (Figs 6.2) for which the trajectories in the RSSs seem to be less organised, specially for Fig 6.5(A,C), while time series for vertical faster movements (VF) which have more periods (Figs 6.2) present trajectories in the RSS with well defined patterns (6.5(C,D)). It is important to note that the smoothness of time series also create an effect on

## Quantifying Human-Humanoid Imitation Activities

---

smoothness in the trajectories of the RSS, being the RS01 more organised and more persistent while trajectories for HS01 are more changeable (Figs. 6.4, 6.5).

Therefore, one can observe by eye the differences in each of the trajectories in the reconstructed state spaces (Figs 6.4, 6.5), however one might be not objective when quantifying those differences since such observations might vary from person to person. With that in mind, in early experiments of this thesis, it had been tried to objectively quantify those differences using euclidean distances between the origin to each of the points in the trajectories in the trajectories of the RSSs, however these created suspicious metrics, specially for trajectories which looked very messy. Hence, it has been proposed the application of Recurrence Quantification Analyses (RQA) in order to have a more objective quantification of the differences in each of the cases of the time series.

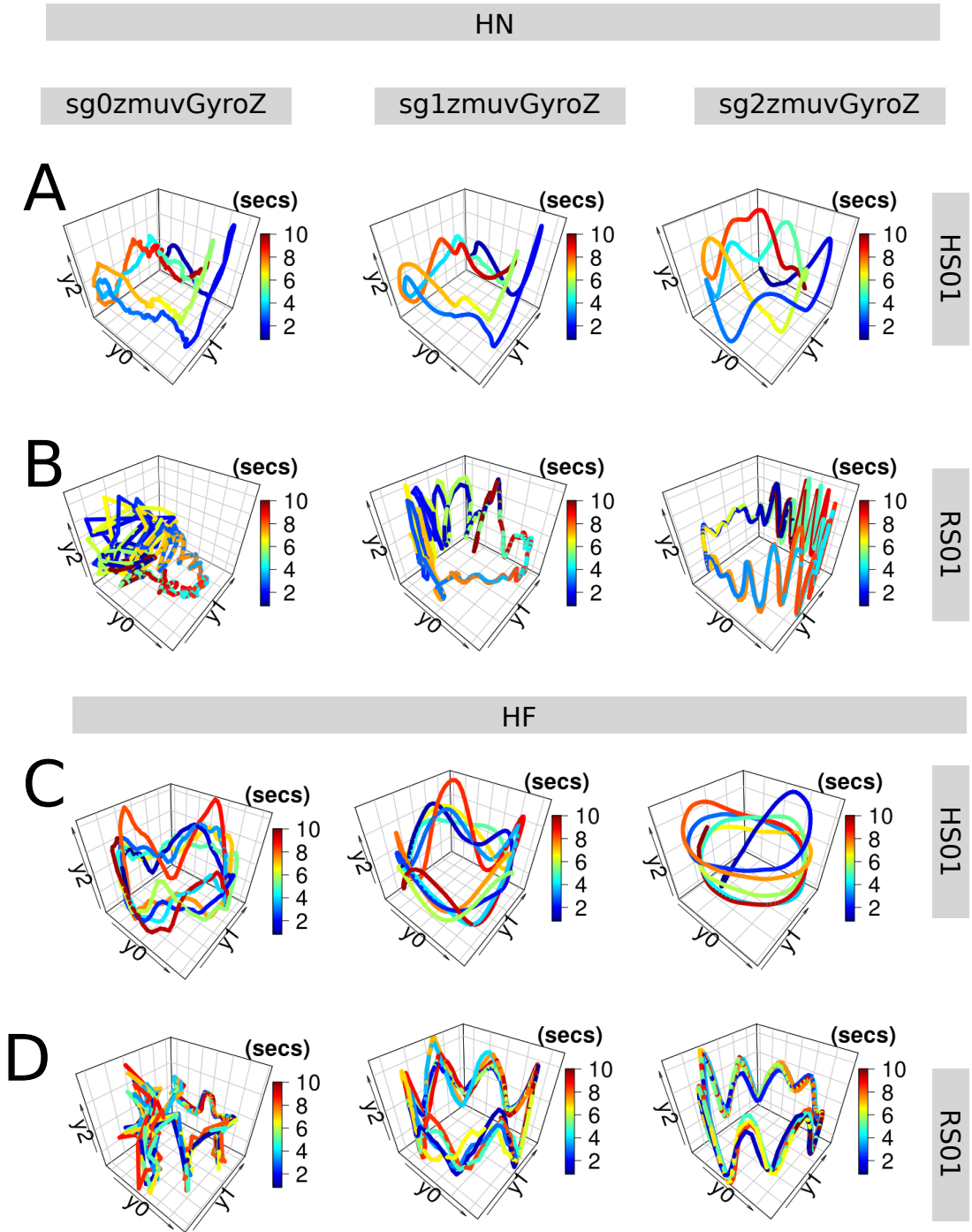


Fig. 6.4 **RSSs for horizontal arm movements.** Reconstructed state spaces of participant p01 for horizontal movements in normal and faster velocity (HN, HF) with raw-normalised (sg0zmuvgyroZ), normalised-smoothed 1 (sg1zmuvgyroZ) and normalised-smoothed 2 (sg2zmuvgyroZ) time series of the sensors attached to the participant (HS01) and other sensor attached to the robot (RS01). Reconstructed state spaces were computed with embedding parameters  $\bar{m}_0 = 6$ ,  $\bar{\tau}_0 = 8$ . R code to reproduce the figure is available at [\[47\]](#).

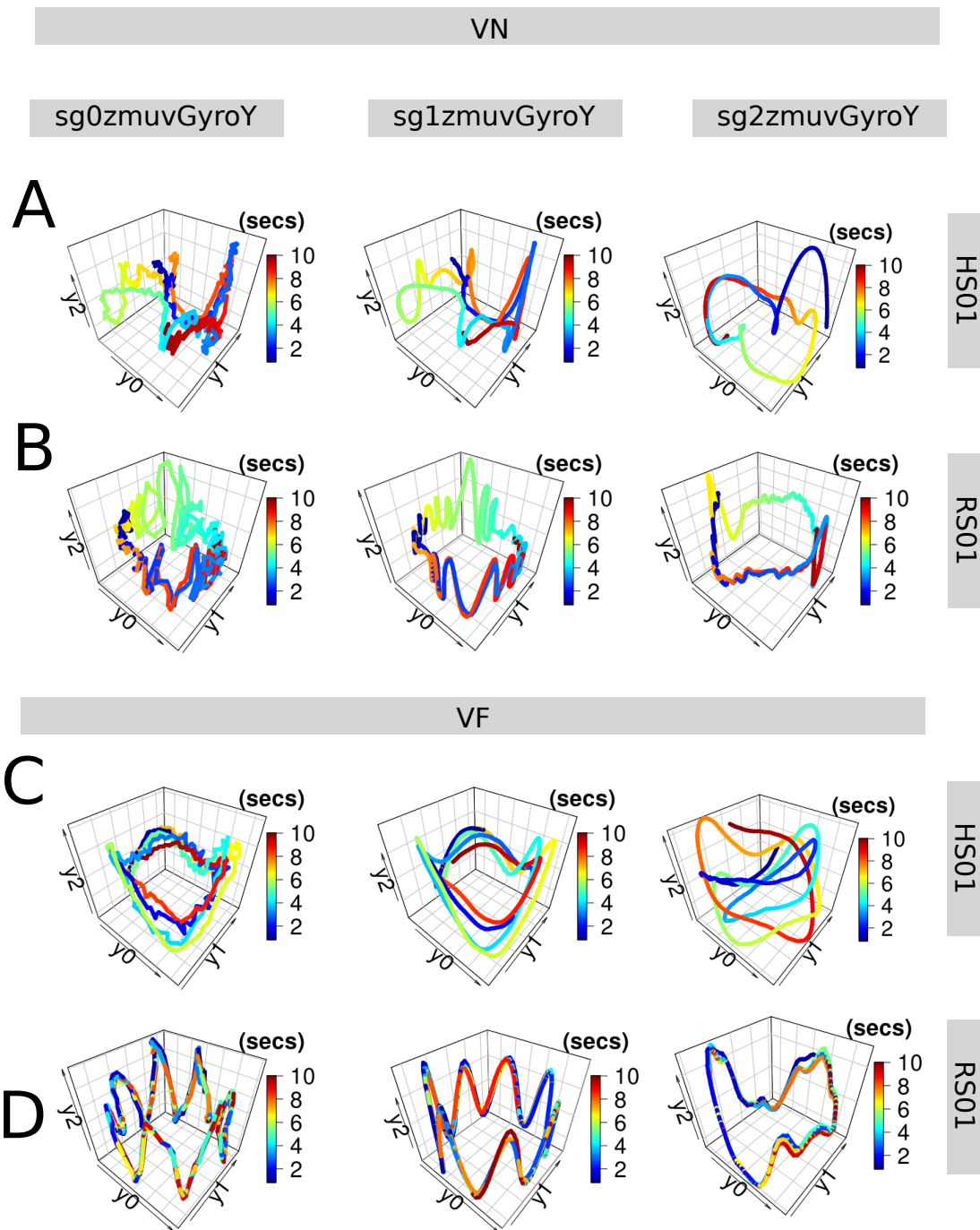


Fig. 6.5 **RSSs for vertical arm movements.** Reconstructed state spaces of participant p01 for vertical arm movements in normal and faster velocity (VN, VF) with raw-normalised (sg0zmuvgyroZ), normalised-smoothed 1 (sg1zmuvgyroZ) and normalised-smoothed 2 (sg2zmuvgyroZ) time series of the sensors attached to the participant (HS01) and other sensor attached to the robot (RS01). Reconstructed state spaces were computed with embedding parameters  $\bar{m}_0 = 6$ ,  $\bar{\tau}_0 = 8$ . R code to reproduce the figure is available at [\[43\]](#).

## 6.5 Recurrences Plots

Considering the time series of Figs 6.1 and 6.2, Recurrence Plots are computed for horizontal arm movements (Fig 6.6) and vertical arm movements (Fig 6.7) using the average embedding parameters ( $\overline{m}_0 = 6$ ,  $\overline{\tau}_0 = 8$ ) and a recurrence threshold of  $\epsilon = 1$ . For the selection of the recurrence threshold, Marwan (2011) pointed out that choosing an appropriate recurrence threshold is crucial to get meaningful representations in the RPs, however, for this thesis where quantifying movement variability is our aim, little importance has been given to the selection of the recurrence threshold for the RPs as long as it is able to represent the dynamical transitions in each of the time series.

In general, the increase of smoothness in time series results in thicker and better defined diagonal lines in the RPs (Figs 6.6, 6.7). Additionally, due to the changes in velocities of the movements the patterns in the RPs present an increase of diagonal lines and a decrease of line thickness. Although, the patterns of RPs show consistency with the movements type and velocities changes, it can be noticed that patterns of the RPs for HS01 are not well defined while patterns of the RPs for RS01 shown a more consistent pattern (Fig 6.6, 6.7).

It is important to note that only RPs for participant 01 are presented in (Fig 6.7, 6.6), however other RPs for all participants are presented in Appendix F.4. With that in mind, it can be highlighted that, as similar as, the Reconstructed State Spaces (Figs 6.4, 6.5), the patterns in the RPs can be easily noticed by eye for different conditions of the time series (Figs 6.6, Fig 6.7), however these characteristics in the patterns of the RPs are subjective for the person who analysed them and might vary from person to person. That lead us to apply Recurrence Quantification Analysis (RQA) in order to have an objective quantification metric for the movement variability for each of the conditions of the time series.

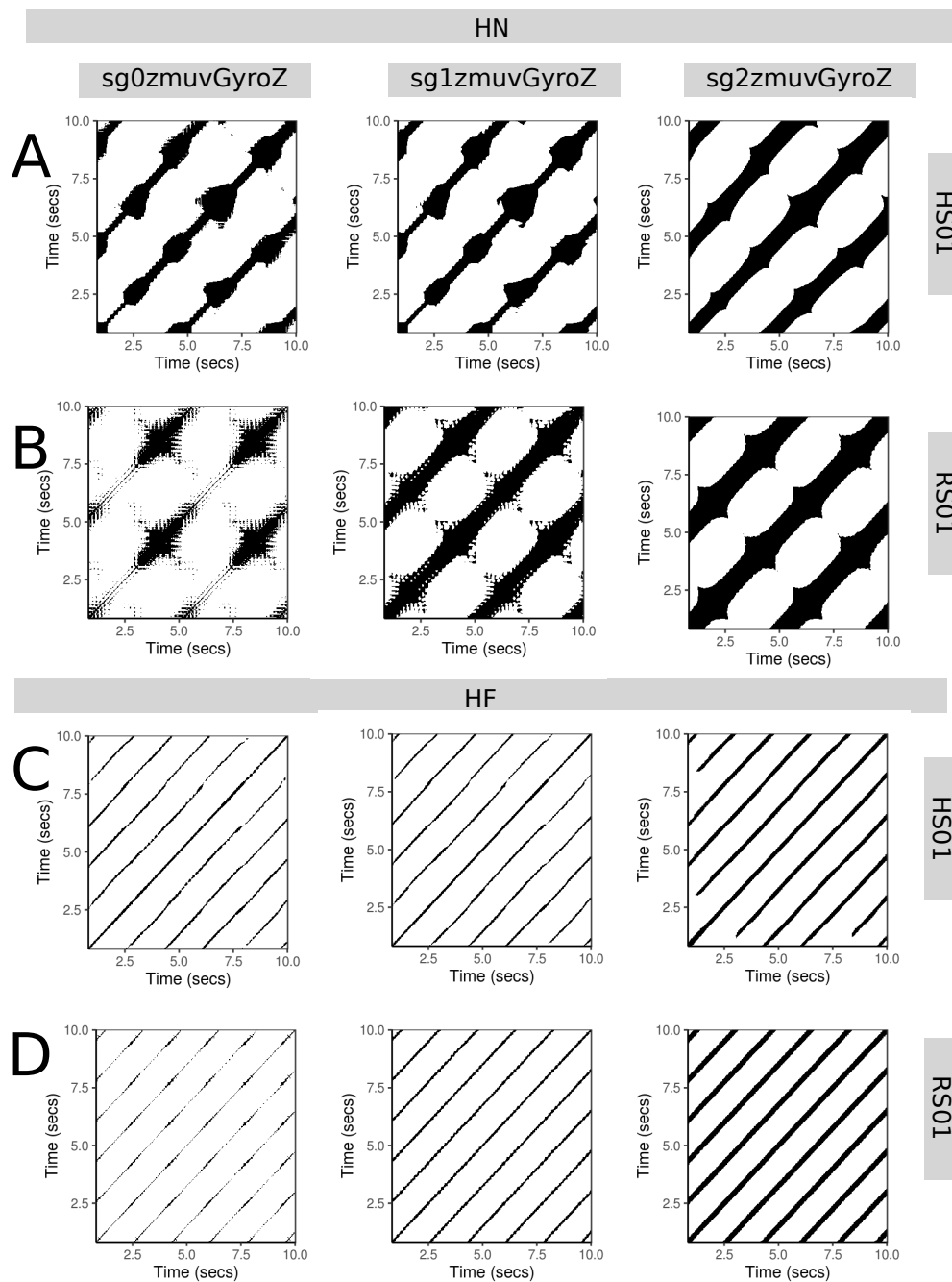


Fig. 6.6 **RPs for horizontal arm movements.** Recurrence plots of participant *p01* for horizontal movements in normal and faster velocity (HN, HF) with time series of raw-normalised (`sg0zmvGyroZ`), normalised-smoothed 1 (`sg1zmvGyroZ`) and normalised-smoothed 2 (`sg2zmvGyroZ`), and sensors attached to the participant (HS01) and to the robot (RS01). Recurrence plots were computed with embedding parameters  $\overline{m}_0 = 6$ ,  $\overline{\tau}_0 = 8$  and recurrence threshold  $\epsilon = 1$ . R code to reproduce the figure is available at [\[48\]](#).

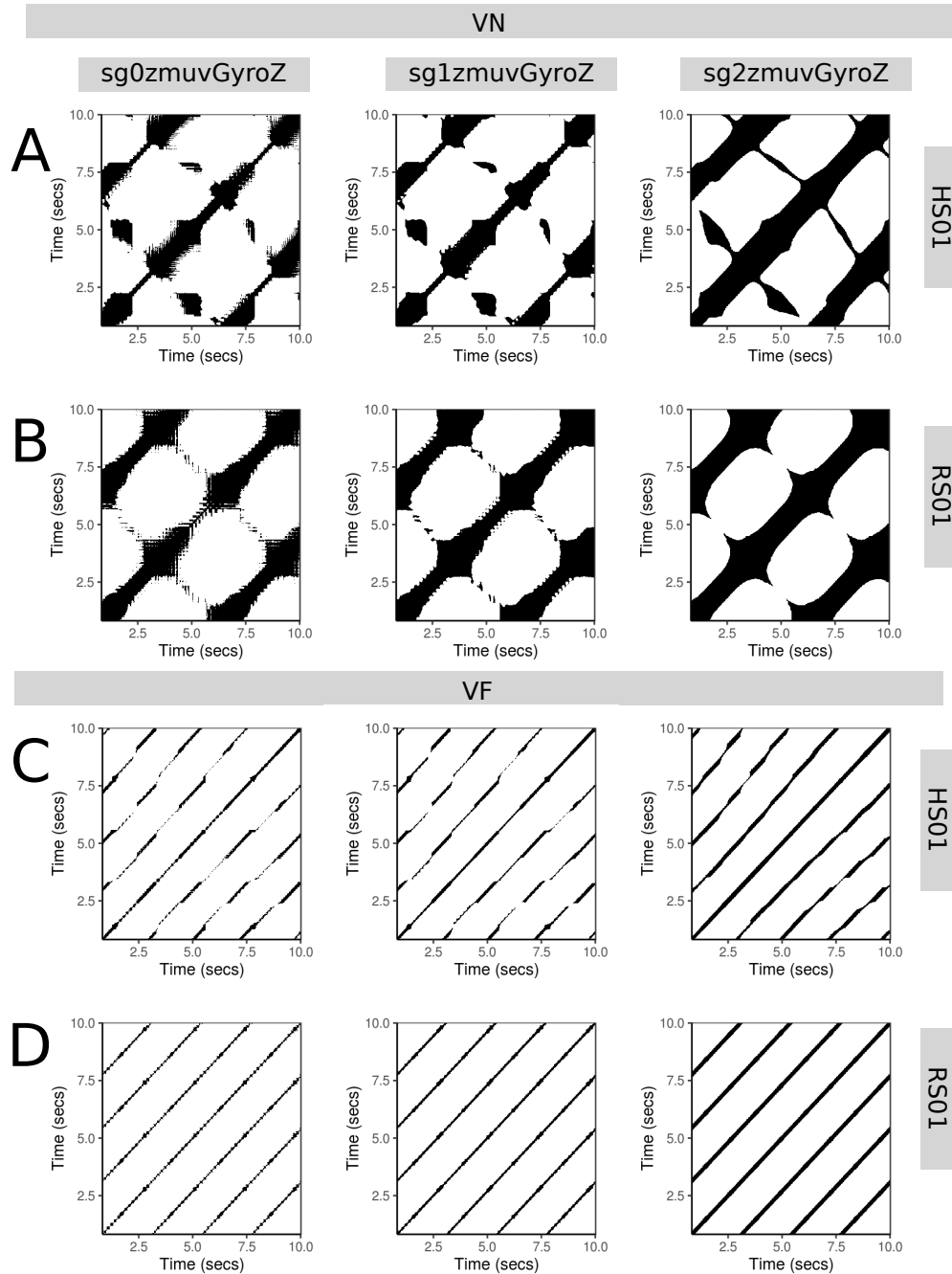


Fig. 6.7 **RPs for vertical arm movements.** Recurrence plots of participant  $p01$  for vertical movements in normal and faster velocity (VN, VF) with time series of raw-normalised (sg0zmvGyroZ), normalised-smoothed 1 (sg1zmvGyroZ) and normalised-smoothed 2 (sg2zmvGyroZ), and sensors attached to the participant (HS01) and to the robot (RS01). Recurrence plots were computed with embedding parameters  $\bar{m}_0 = 6$ ,  $\bar{\tau}_0 = 8$  and recurrence threshold  $\epsilon = 1$ . R code to reproduce the figure is available at [\[42\]](#).



## 6.6 Recurrence Quantification Analysis

Considering the RPs for 20 participants performing four activities (HN, HF, VN and VF) with sensors attached to the human (HS01) and to the humanoid robot (RS01) and with the increase of smoothness of time series (sg0zmvGyroZ, sg1zmvGyroZ and sg2zmvGyroZ), I hence compute four metrics of RQA metrics (REC, DET, RATIO and ENTR) with embedding parameters  $\overline{m}_0 = 6$ ,  $\overline{\tau}_0 = 8$  and recurrence threshold  $\epsilon = 1$ .

### REC values

It can be seen in the box plots of Figs 6.8(A) that REC values, representing the % of black dots in the RPs, are more spread for HN and VN movements (higher interquartile range) than HF and VF movements (lower interquartile range) for HS01 sensor. In contrast, REC values for RS01 sensor present little variation (interquartile range of 0.01). With regard to the increase of smoothness of time series (sg0, sg1 and sg2), REC values present little variation as the smoothness is increasing for time series from HS01 (changes of mean values (rhombus)) while REC values are more affected with the smoothness for data from RS01 (see the incremental changes of mean values (rhombus)). See Figs F.19 and F.20 in Appendix F.5 for more details about individual REC values for each participant.

### DET values

Figs 6.8(B) illustrate DET values, representing predictability and organisation of the RPs, which change very little (interquartile range is around 0.1) for type of movement, level of smoothness or type of sensor. See Figs F.21 and F.22 in Appendix F.5 for more details about individual DET values for each participant.

### **RATIO values**

Figs 6.8(C) present RATIO values, representing dynamic transitions, for horizontal and vertical movements. It can be seen that RATIO values for HS01 sensor vary less for HN movements (interquartile range around 2) than HF movements (interquartile range around 5). It can also be noticed a decrease of variation in RATIO values as the smoothness of the time series is increasing (grey rhombus). See Figs F.23 and F.24 in Appendix F.5 for more details about individual RATIO values for each participant.

### **ENTR values**

Fig. 6.8(D) show ENTR values, representing the complexity of the structure the time series, for both horizontal and vertical movements. ENTR values for HS01 sensor show more variation (interquartile range around 0.5) than ENTR values for RS01 sensor which appear to be more constant (interquartile range 0.1). It can also be said that the smoothness of time series affects each of the axis by an increase of mean values (see gray rhombos). See Figs F.25 and F.26 in Appendix F.5 for more details about individual ENTR values for each participant.

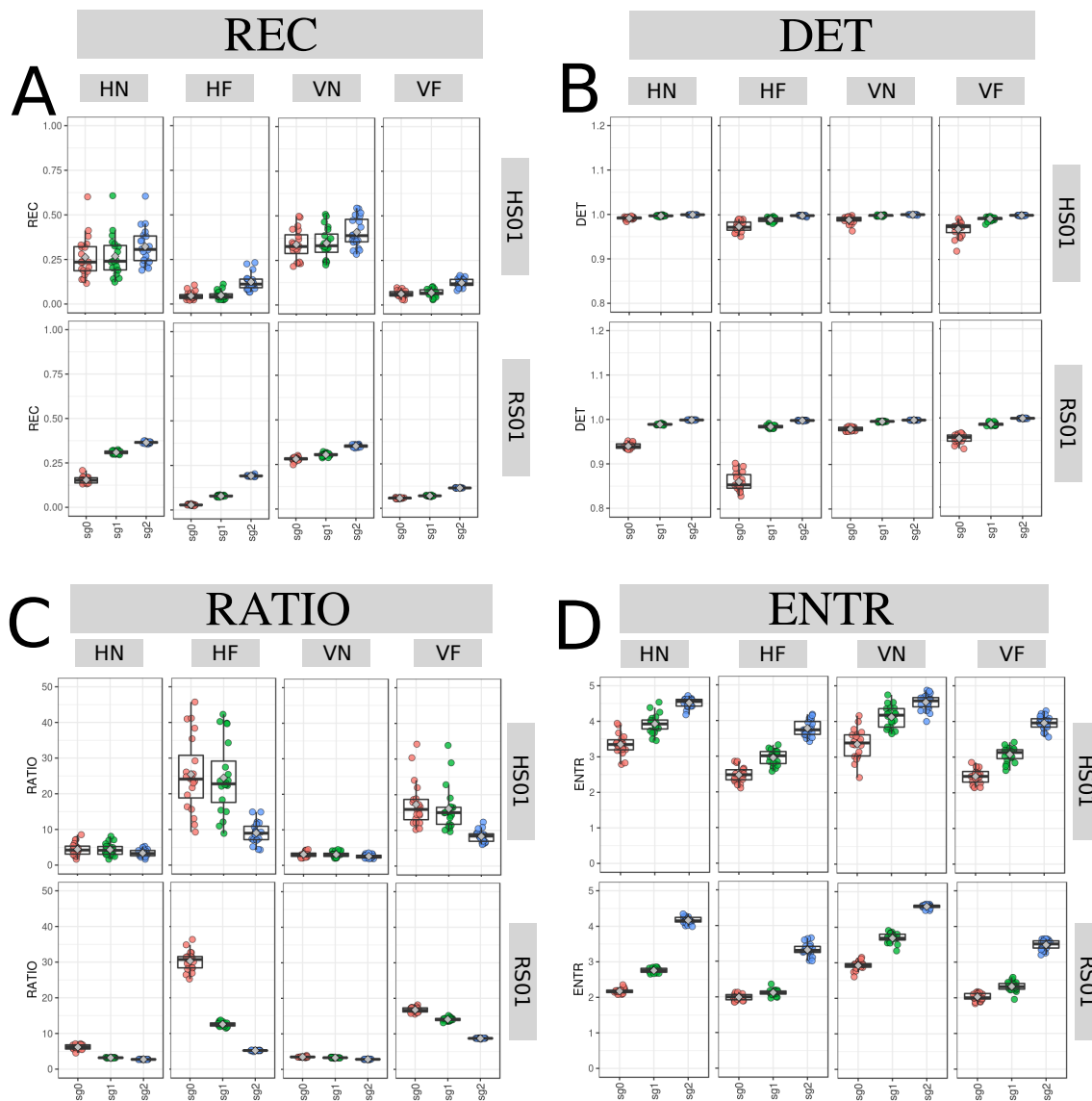


Fig. 6.8 **Box plots for RQA values.** Box plots of (A) REC, (B) DET, (C) RATIO, and (D) ENTR values for 20 participants performing HN, HF, VN and VF movements with sensors HS01, RS01 and three smoothed-normalised time series (sg0, sg1 and sg2). RQA values were computed with embedding parameters  $\overline{m}_0 = 6$ ,  $\overline{\tau}_0 = 8$  and recurrence threshold  $\epsilon = 1$ . R code to reproduce the figure is available at [\[47\]](#).

## 6.7 Weaknesses and strengths of RQA

Considering the Section 3.7.3 regarding the weaknesses and strengths of RQA, RQA metrics (i.e., REC, DET, RATIO and ENTR) are computed and plotted 3D surface plots using an unitary increase of pair embedding parameters ( $0 > m \leq 10$ ,  $0 > \tau \leq 10$ ) and a decimal increase of 0.1 for recurrence thresholds ( $0.2 \geq \epsilon \leq 3$ ) (Fig. 6.9). Hence, Fig. 6.9(A) shows an increase for REC values, the percentage of black dots in the RP, as the recurrence threshold increases, while the variation for embedding parameters creates little decrease of REC values as the embedding dimensions increase and even slighter decrements of REC values for the increase of  $\tau$ . For the 3D surface plots of DET values (Fig. 6.9(B)), representing predictability and organisation of the RPs, one can note a plateau for DET values near to 1 for embedding dimension parameters of less than 5 and recurrence threshold values of greater than 2 (red surface). It can also be observed that the increases of delay embedding made the DET values increase so as to make an cascade effect in the surface along with the increase of dimension embedding  $m$ . For RATIO values, representing dynamic transitions, Fig. 6.9 shows that the 3D surface plots present a plateau (blue surface) of RATIO values near to zero for recurrence thresholds greater than 1.0, while fluctuations are more evident for recurrence thresholds of less than 1.0, particularly it can also be noted an increase in the fluctuations of RATIO values as the embedding dimension is increasing. For ENTR values in Fig. 6.9(D), representing the complexity of the structures in time series, one can note that the increase of recurrence threshold is, not strictly proportional to the increase of ENTR values. It can also be observed in Fig. 6.9(D) that the increase of delay embeddings hardly affects the ENTR values for embedding dimensions of 1, while for higher values of embedding dimensions there is a decrease of ENTR values, and there is a decrease of ENTR values as delay dimension value is increasing.

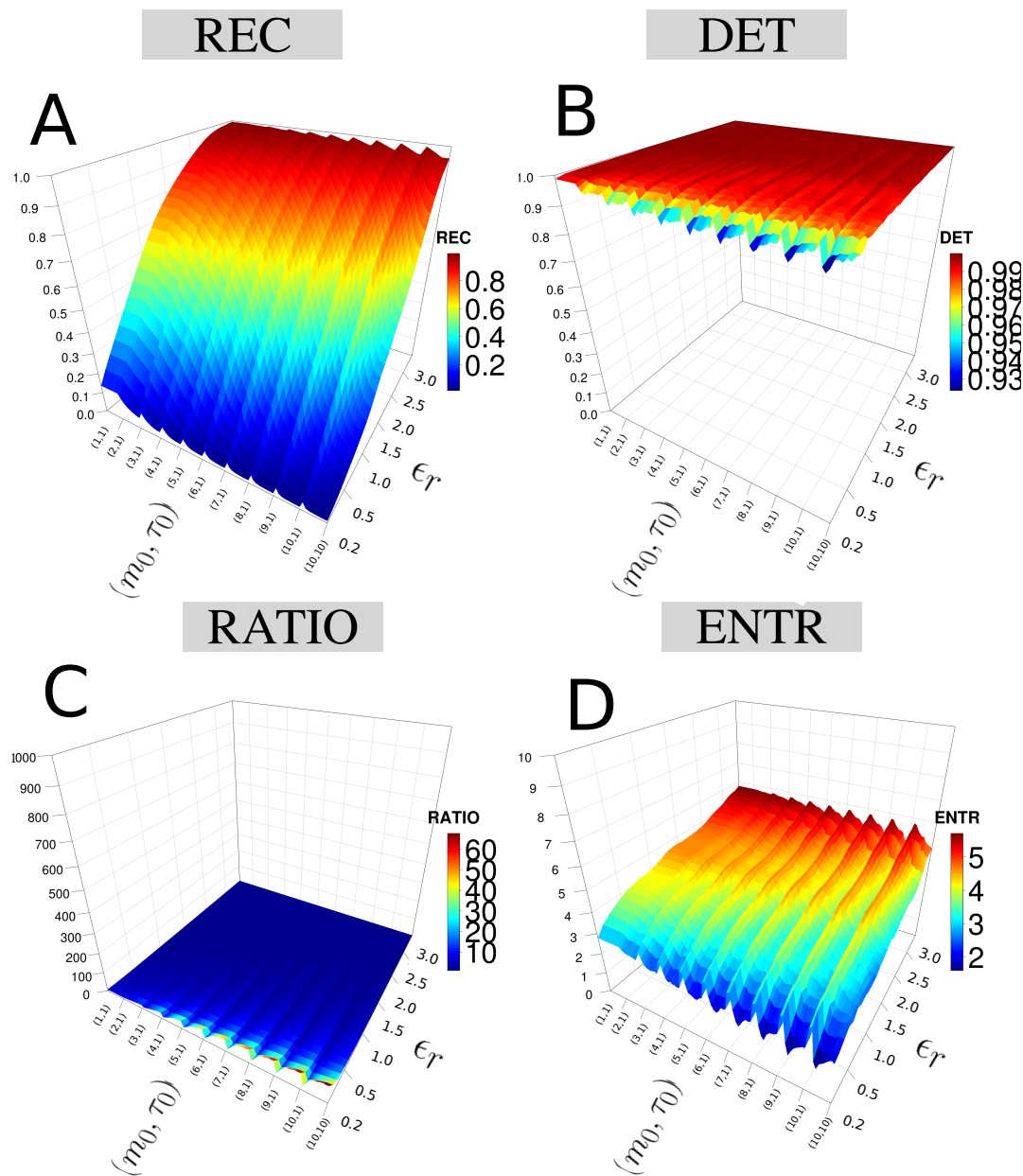


Fig. 6.9 **3D surface plots for RQA metrics.** 3D surface plots for (A) REC, (B) DET, (C) RATIO and (D) ENTR values with increasing pair of embedding parameters ( $0 \leq m \leq 10$ ,  $0 \leq \tau \leq 10$ ) and recurrence thresholds ( $0.2 \leq \epsilon \leq 3$ ). RQA metrics are computed with the time series of participant *p01* using HS01 sensor, HN activity, sg0zmuV GyroZ axis and 10 seconds for window length. R code to reproduce the figure is available at [\[45\]](#).

### 6.7.1 Sensors and activities

We also computed 3D surface plots of RQA metrics for different sensors and different activities (Figs. 6.10, 6.11), where it can generally be noted similar 3D surface plots patterns for RQA metrics as the ones in Fig. 6.9.

The 3D surface plots for REC values (Fig. 6.10(A)) show slightly differences with regard to vertical or horizontal activities however there are notable differences for normal and faster velocities, specially for the faster movements where the 3D surface plots shows a maximum REC value for embedding dimension values near to 1 and for recurrence thresholds near to 3. The 3D surface plots of DET values (Fig. 6.10(B)) and RATIO values (Fig. 6.10(C)) show slightly notable variations across the type of activities. For 3D surface plots of ENTR values it can be noted a slightly variation for surface plots of normal and faster velocities (Fig 6.10(D)).

As similar as Fig 6.10, the 3D surface plots patters for RS01 in Fig 6.11 show the differences between the activities performed at normal and faster velocities specially for REC and ENTR values (Fig 6.10(A, D)), while 3D surface plots for DET and RATIO values show slightly variations (Fig 6.10(B, C)).

### 6.7.2 Window size

Figs. 6.12 illustrate 3D surface plots for RQA metrics with four window lengths of 2-sec, 5-sec, 10-sec, and 15-sec. In general, it can be said that the increase of window length of the time series creates 3D surface plots patterns with better resolution.

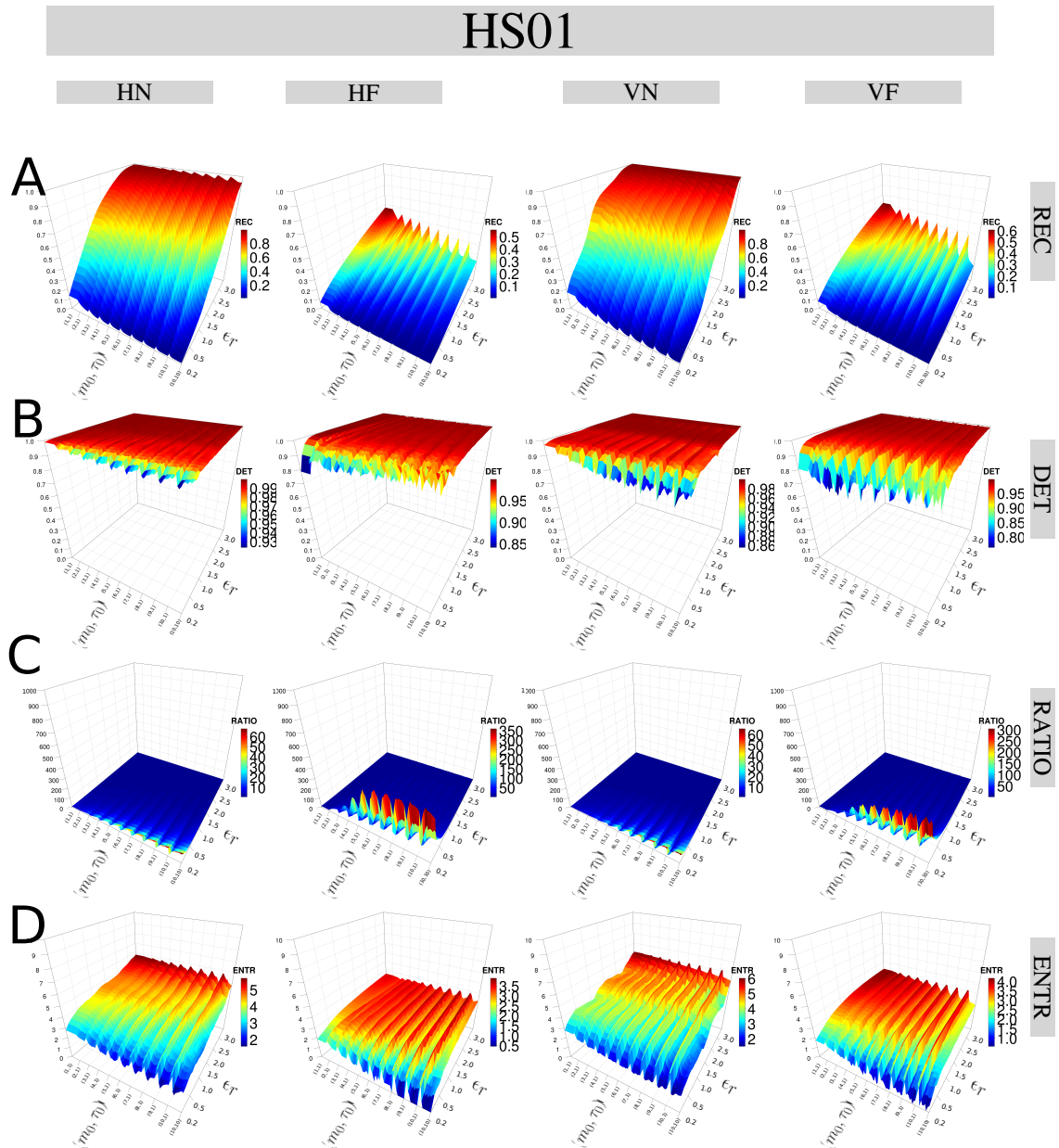


Fig. 6.10 3D surface plots of RQA metrics for HS01 sensor. 3D surface plots of RQA metrics ((A) REC, (B) DET, (C) RATIO, and (D) ENTR) with increasing embedding parameters and recurrence thresholds are for time series of participant  $p01$  for sensors HS01, activities (HN, HF, VN and VF) and sg0zmuVgyroZ axis with 10 seconds window length. R code to reproduce the figure is available at [\[1\]](#).

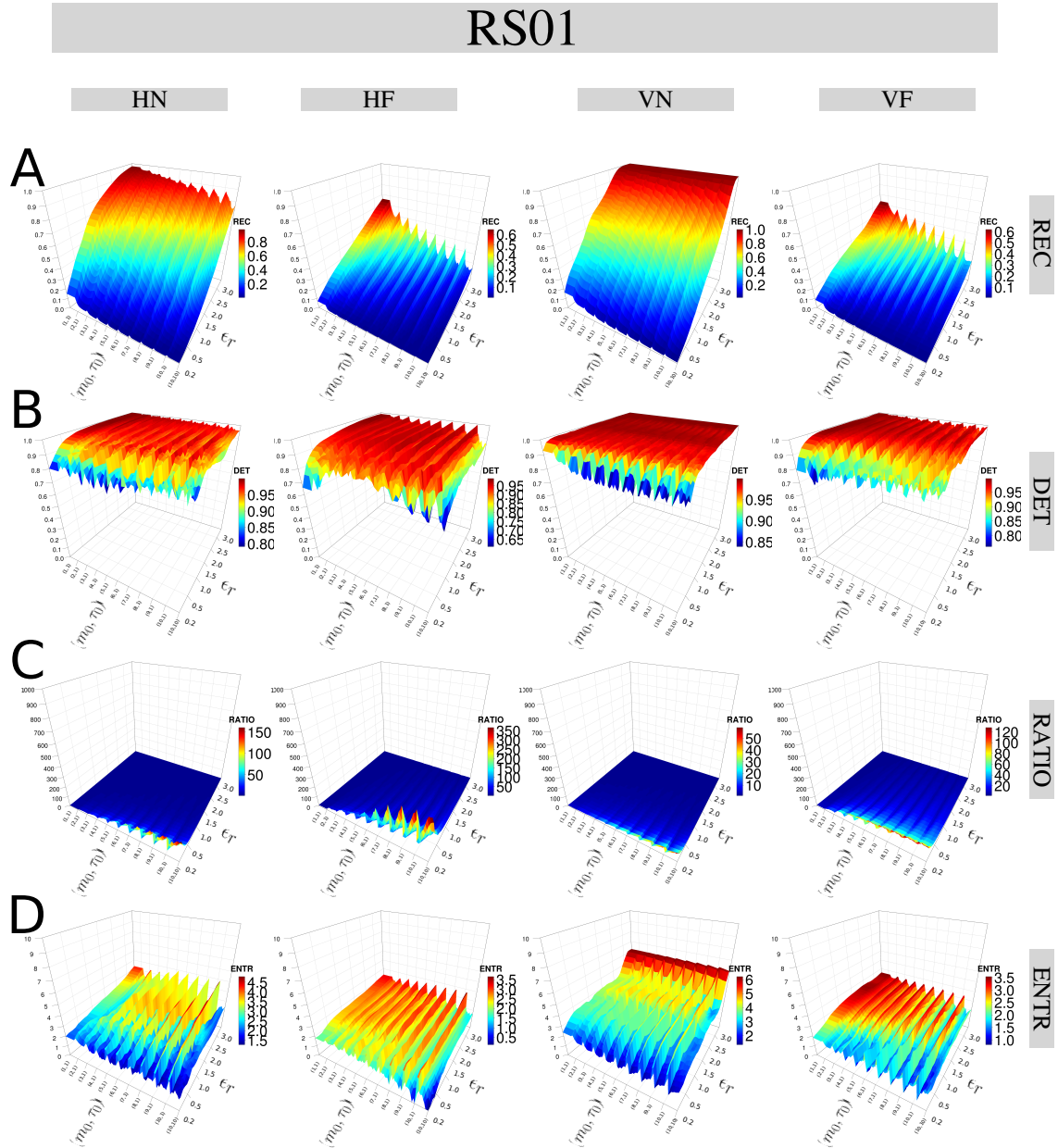


Fig. 6.11 3D surface plots of RQA metrics for RS01 sensor. 3D surface plots of RQA metrics ((A) REC, (B) DET, (C) RATIO and (D) ENTR) with increasing embedding parameters and recurrence thresholds are for time series of humanoid robot for sensors RS01, activities (HN, HF, VN and VF) and sg0zmvGyroZ axis with 10 seconds window length. R code to reproduce the figure is available at [\[4\]](#).



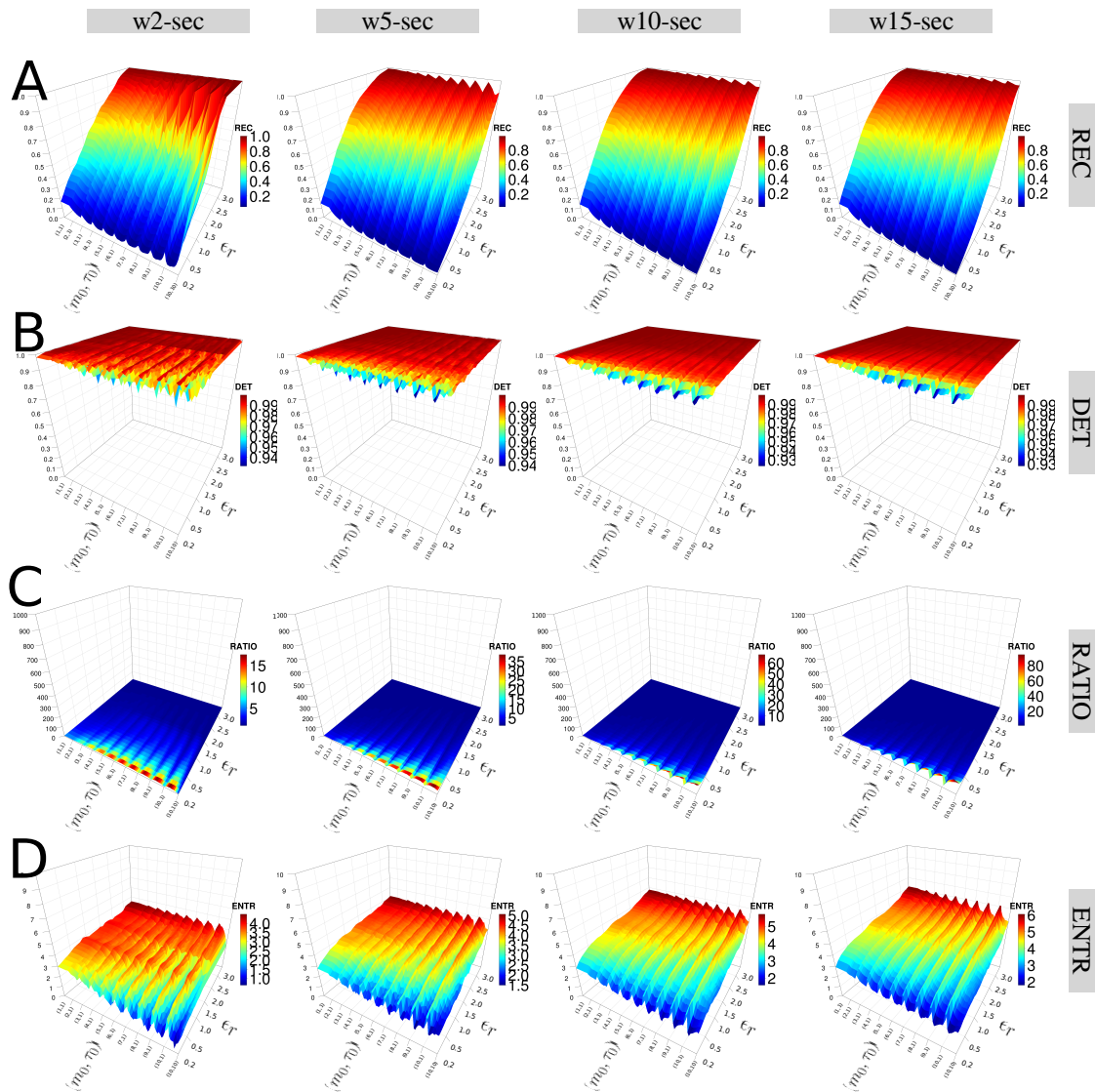


Fig. 6.12 **3D surface plots of RQAs metrics with four window lengths.** 3D surface plots of RQA metrics ((A) REC, (B) DET, (C) RATIO, and (D) ENTR) with increasing embedding parameters and recurrence thresholds for four window lengths (w2-sec, w5-sec, w10-sec and w15-sec). RQA metrics values are for time series of participant  $p01$  using HS01 sensor, HN activity and sg0zmvGyroZ axis. R code to reproduce the figure is available at [\[45\]](#).

### 6.7.3 Smoothness

Figs 6.13 present 3D surface plots of the RQA metrics considering three levels of smoothness of the time series (sg0, sg1, sg2). It can then be noted that such smoothness have a direct effect on the smoothness of the 3D surface plots. Especially for dimension embeddings lower than 2 with in REC and ENTR values (Fig. 6.13(A, D)). The 3D surface plots of DET values are smoothed to a degree that the plateau (red surface) is increase, while RATIO values appear to be less affected to the level of smoothness (Fig. 6.13(C)).

### 6.7.4 Participants

Figs 6.14 illustrate 3D surface plots of RQA metrics for four participants. It can be noted that differences of the 3D surface plots across participants are more notable with REC (Fig. 6.14(A)) and ENTR values (Fig. 6.14(D)), while minor differences of 3D surface plots across participants are presented in DET (Fig. 6.14(B)) and RATIO vales (Fig. 6.14(C)).

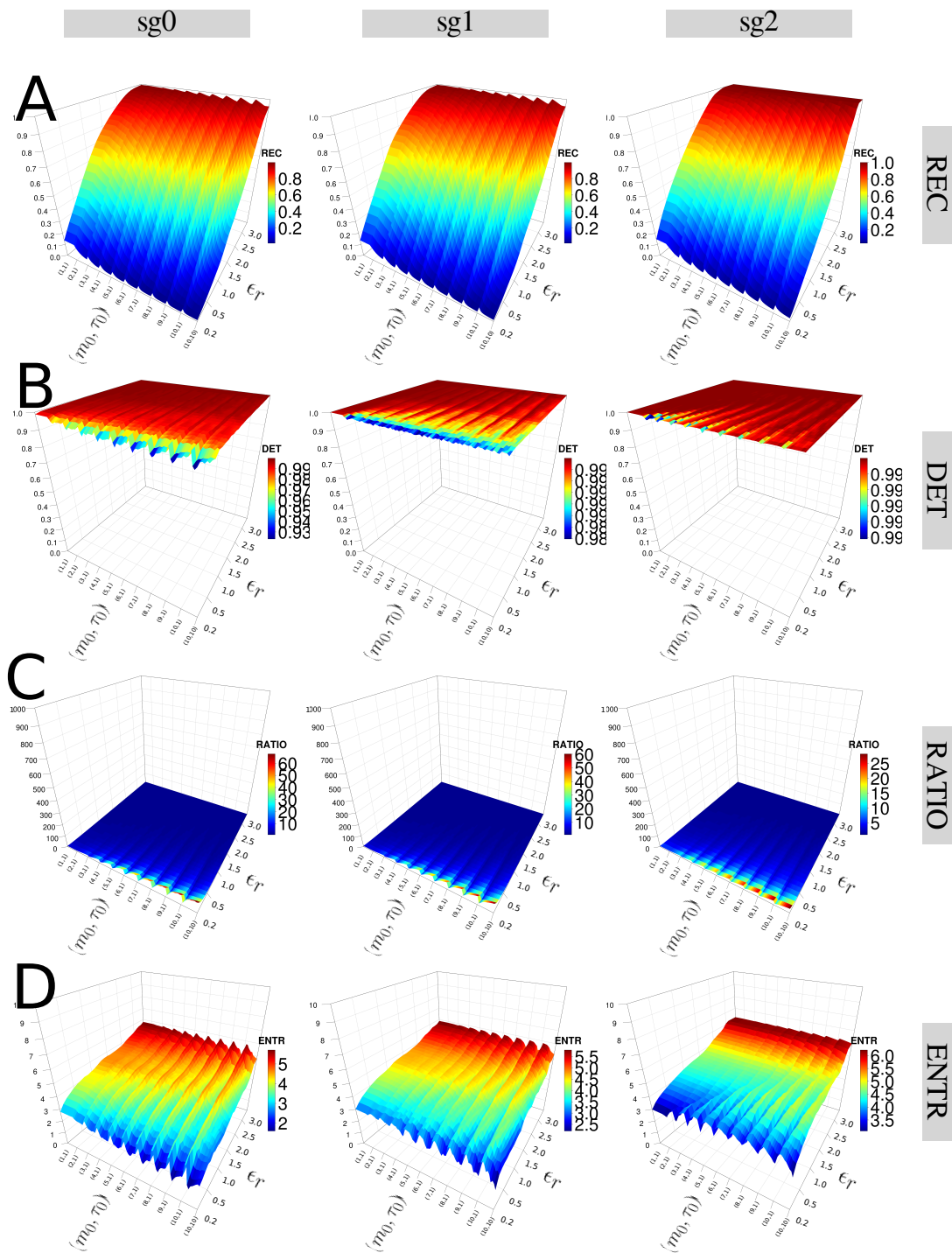


Fig. 6.13 3D surface plots of RQA metrics with three levels of smoothness. 3D surface plots of RQA metrics ((A) REC, (B) DET, (C) RATIO, and (D) ENTR) with increasing embedding parameters and recurrence thresholds for three levels of smoothness (sg0zmuvgyroZ, sg1zmuvgyroZ and sg1zmuvgyroZ). RQA metrics are computed from time series of participant  $p01$  using HS01 sensor, HN activity and 10 seconds window length. R code to reproduce the figure is available at [\[4\]](#).

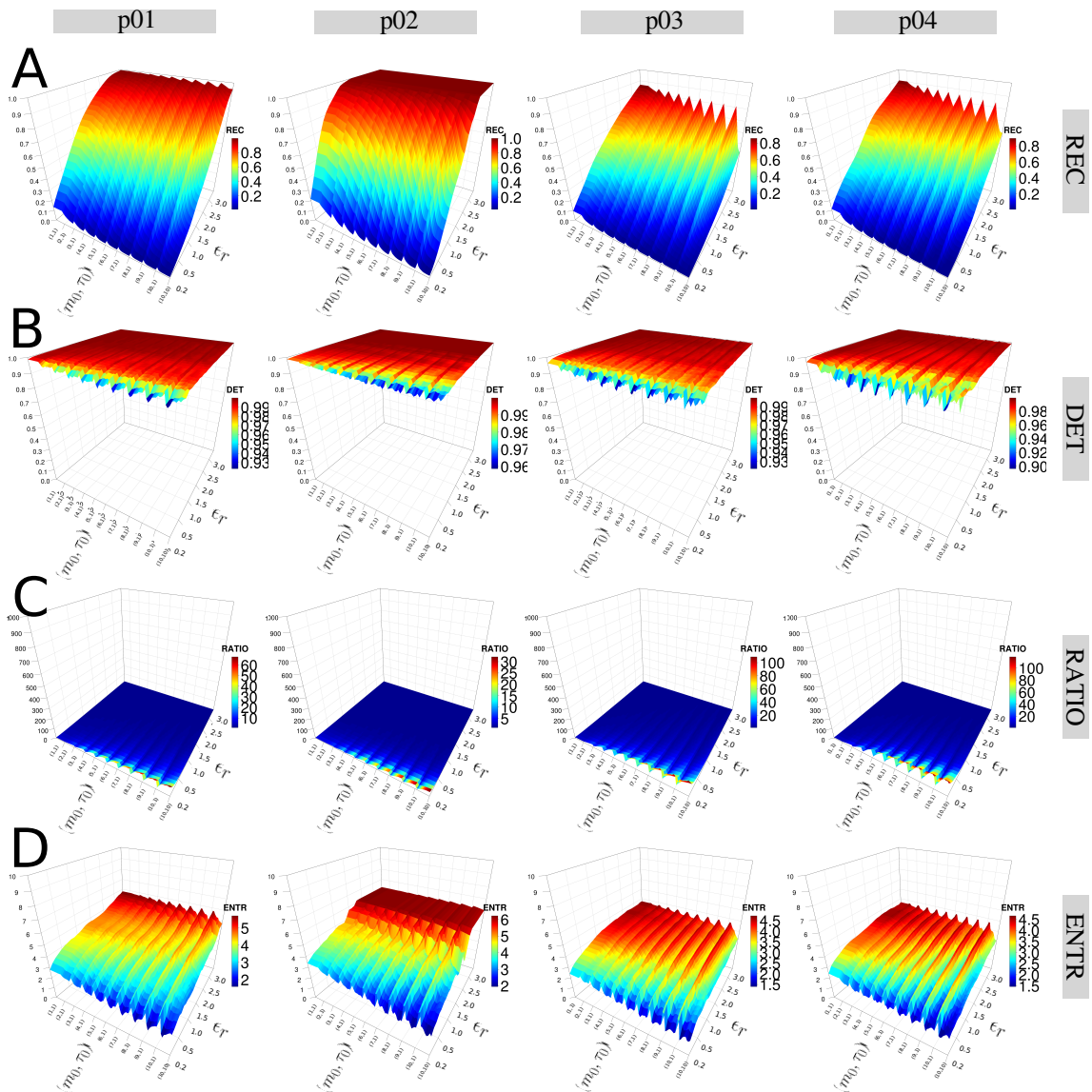


Fig. 6.14 **3D surface plots of RQA metrics with three participants.** 3D surface plots of RQA metrics ((A) REC, (B) DET, (C) RATIO, and (D) ENTR) for participants  $p01$ ,  $p02$ ,  $p03$  and  $p04$  with increasing embedding parameters and recurrence thresholds. RQA metrics values are for time series of HS01 sensor, HN activity and 10 seconds window length. R code to reproduce the figure is available at [\[4\]](#).

### 6.7.5 Final remarks

It can be noted that the changes of RQA metrics are evident with both the increase of embedding dimension parameters and the recurrence threshold for different structures, window size, levels of smoothness of the time series. For instance, RATIO values present a plateau (blue colour surface) which is independently to the source of time series, however there are peaks that change differently based on the source of time series. For DET values, 3D surface plots present a fluctuated surface (red colour) which slightly differs with the source of time series. With regards to REC values, 3D surface plots are affected by the velocity of movements. For example, surface plots for normal velocity presents an increase of REC values as recurrence threshold increases and keeping slightly uniform surface plot changes for the increase of embedding parameters. However for faster velocity arm movements, 3D surface plot fluctuations decrease as the embedding dimension increases and recurrence thresholds increases. Similarly as the results of human-image activities (see Section 5.7 in Chapter 5), 3D surface plots of ENTR values for human-humanoid interaction present changes to any of the types of time series which might be of help to understand the dynamics of movement variability in human-humanoid activities from different time series.

# Chapter 7

## Conclusions and future work

### 7.1 Conclusions

In this thesis, nonlinear analysis methods have been explored from reconstructed state spaces (RSS) with uniform time-delay embedding (UTDE) to recurrence quantification analysis (RQA) with recurrence plots (RP). However, it is necessary to compute and then select appropriate embedding parameters before using any of the tools for nonlinear analysis (see Chapter 3). Iwanski and Bradley (1998) stated that patterns in recurrence plots and metrics for recurrence quantification analysis are independent of embedding dimension parameters. However, that is not the case for different recurrence thresholds. Hence, embedded parameters and recurrence thresholds were considered to create three dimensional surface plots of recurrence quantification analysis which was hypothesised to be a better approach to understand the impact of different characteristic of real-world time series data such as window size length, participants, sensors and levels of smoothness.

No scientific work has been reported regarding the use of nonlinear analysis (e.g. RSS with UTDE, RP and RQA) to quantify movement variability in the context of human-humanoid interaction. This thesis has explored the weaknesses and strengths

of RQA using 3D surfaces of the variation of embedding parameters and recurrence thresholds which lead me to conclude that this approach requires less parametrization than others used in this thesis (e.g. RSS with UTDE, RP and RQA). Additionally, it was found that the 3D surface plots for RQA ENTR metric can be used to model any of the effects of movement variability for different activities or different participants as well as the post processing of real-world time series data with different window size length, smoothness and structures (shape, amplitude and phase) of time series (see Sections of weaknesses and strengths of RQA in Chapters 5 and 6).

In the following sections, positives and negatives of this thesis are pointed out by answering the raised research questions posed in Chapter 1.

**What are the effects on RSSs, RPs, and RQA metrics of different embedding parameters, different recurrence thresholds and different characteristics of time series (structure, smoothness and window length size)?**

It is evident that time series from different sources of time series (e.g. participants, movements, axis type, window size lengths or levels of smoothness) present differences for not only embedding parameters but also for the patterns in RSS, RP, RQA and 3D surfaces of RQA metrics. With that in mind, it can be concluded that the selection of appropriate embedding parameters and recurrence threshold is crucial to get meaningful results from nonlinear analysis tools. However, in this thesis it has been found that the creation of 3D surface plots of RQA metrics is a new approach that is independent of the type of time series and the selection of embedding parameters. Specifically, it was found that 3D RQA ENTR is robust against different sources of time series data, which can lead to insight into the quantification of movement variability.

### **What are the weaknesses and strengths of RQA metrics when quantifying movement variability?**

From the reported results in chapters 5 and 6, it can be stated that the weaknesses of RQA, investigated in this thesis, are three: (i) the requirement of an expert(s) to interpret and compute embedding parameters and recurrence thresholds, (ii) the implementation and computation of methods of nonlinear analysis is laborious and computation of the parameters for such methods is still an open problem, and (iii) the selection of particular parameters to apply methods of nonlinear analysis does not necessarily give the best representation of the dynamics of the time series.

Hence, by proposing a variation of embedded parameters and recurrence thresholds to create 3D surfaces of RQA, it can be stated two strengths of RQA metrics: (i) little set up of parametrisation for 3D RQA metrics is required and (ii) 3D RQA ENTR might be a suitable approach to give insight to the understanding of the dynamics of different characteristic of time series.

### **How does the smoothing of raw time series affect methods of nonlinear analysis when quantifying movement variability?**

The answer to this question depends on (i) what to quantify in movement variability and also (ii) which hardware is involved in the collection of time-series data. For instance, to avoid erratic changes in the metrics of nonlinear analysis, smoothing raw signals can both help to obtain well defined trajectories in RSS and patterns in RP as well as constant values in RQA's metrics. However, on one hand, it has been observed that the increase of smoothness of time-series data created more complex trajectories (i.e. not well defined) in the Reconstructed State Spaces and also added more black dots in Recurrence Plots (see RSSs and RPs sections in Chapters 5 and 6). On the



## Conclusions and future work

---

other hand, two metrics of RQA (e.g. DET and ENTR) are more robust against the effect of smoothness of time series.

Additionally, smoothing time-series data can preserve the structure of the dynamics of NAO's arm movements when applying nonlinear analysis, as sometimes NAO produces jerky arm movements due to (i) its 14 degrees of freedom (DOF) for arms and head, (ii) the range of joint movement, (iii) joint torques and velocities, (iv) control of dynamic response (fast acceleration/deceleration), (v) stiffness of gear mechanics, or (vi) the number of degrees of freedom (see Gouaillier et al. (2009) for more references on NAO's mechanical and dynamic capabilities).

## 7.2 Future work

### Inertial sensors

To have fundamental understating of the nature of signals collected through inertial sensor in the context of human-robot interaction, future experiments can be conducted considering the application of derivates of the accelerometer data. With that in mind, the following points can be explored (i) both the jerkiness of movements and the nature of arm movements which typically have minimum jerk (Flash and Hogan, 1985), (ii) the relationship of movement between different body parts, for instance, how rapidly or slowly a person performs arm and leg movements (de Vries et al., 1982; Mori and Kuniyoshi, 2012) or (iii) the application, to real-world time series data, of higher derivatives of displacement with respect time such as jounce, snap, crackle and pop (Eager et al., 2016).

### Smoothing time-series data

It has been hypothesised that one might create a closer representation of the nature of movement variability when using raw data from sensors. However, the quality of raw time-series data from inertial sensors can be affected by changes in sample rate, drift effect of long time-series data or changes of external variables such as temperature and magnetic fields to inertial sensors. Additionally, humanoid robots can sometimes produce jerky movements due its mechanical and dynamic capabilities. That said, further investigation is required to be done regarding the search of the appropriate balance between and the raw data and the degree of smoothness that can get closer to the quantification of the nature of movement variability in the context of human-humanoid interaction.

### Surrogate data analysis

Non-stationarity and non-linearity of experimental time-series data were assumed in this thesis (see Chapter 1). Such assumption was made based on the ambiguity of nonlinear analysis methods to quantify movement variability and the not yet fully explored area of application of nonlinear analysis methods in human-humanoid interaction (see Chapters 1 and 2). From the examiners of the PhD viva, one recommendation to avoid such prejudice of the type of data is to test the non-linearity and non-stationarity of the experimental time series data before nonlinear analysis methods are applied. Hence, a possible avenue to tackle such caveat is to apply surrogate data analysis to test that data have not been generated by "a stationary Gaussian linear stochastic process that is observed through an invertible, static, but possible linear stochastic function" (Schreiber and Schmitz, 2000, p. 2). However, applying surrogate data analysis to time series data that show strong periodicity or quasi-periodicity might create misleading results and perhaps provide unfair conclusion (see [\[4\]](#) on how different realisations

## Conclusions and future work

---

of the same periodic sinusoidal signal show to be sometimes stationarity and others non-stationarity). Hence, further research require to be done, perhaps consider the works of Stam et al. (1998) and Small and Tse (2002) to test weak non-stationarity of periodic and quasi-periodic time series data. Also, for future work, it can be considered other time series data from activities that involve more than one joint in order to test the robustness of not only nonlinear analysis methods but also surrogate data analysis.

## Nonlinear analysis

### Optimal embedding parameters

The method of False Nearest Neighbour (Cao, 1997) states that values of  $E_1(m)$  become insensitive to the increase of dimension, for which, in this thesis, a threshold has been defined in order to obtain the minimum embedding dimension  $m_0$ . However, a further investigation is required to be done for the selection of the threshold in the  $E_1(m)$  plots, as there were no particular method but visual inspection of the  $E_1(m)$  curves to set such a threshold (see Section 3.4.1 in Chapter 3). Similarly, further research is required to be done with regards to the selection of the minimum delay embedding because it is not clear: (i) why the choice of the first minimum of the AMI is the minimum delay embedding parameter (Kantz and Schreiber, 2003) or (ii) why the probability distribution of the AMI function is computed with the use of histograms which depend on a heuristic selection of number of bins for the AMI partitioning (Garcia and Almeida, 2005). Additionally, "the AMI method is proposed for two dimensional reconstructions and extended to be used in a multidimensional case which is not necessarily held in higher dimensions" (Gómez-García et al., 2014, p. 156).

**Other methodologies for state space reconstruction.**

In addition to the method of Uniform Time-Delay Embedding to reconstruct state spaces, other methods have been stated a better dynamic representations of time series in the reconstructed state spaces such as: (i) the nonuniform time-delay embedding methodology where the consecutive delayed copies of  $\{\mathbf{x}_n\}$  are not equidistant (Pecora et al., 2007; Quintana-Duque and Saupe, 2013; Quintana-Duque, 2012, 2016; Uzal et al., 2011), or (ii) the uniform 2 time-delay embedding method which takes advantage of finding an embedding window instead of the traditional method of finding the embedding parameters separately (Gómez-García et al., 2014). As a future work, it might be worthwhile to apply (i) and (ii) methods to the current problem.

**RP and RQA parameters**

There are different avenues that can be investigated with regard to the computation of RP and RQA parameters. However from this thesis, it is suggested that the work of Marwan et al. (2007) and Marwan and Webber (2015) can be the starting point for further research with regards to different criteria for (i) neighbours, (ii) different norms ( $L_1$ -norm,  $L_2$ -norm, or  $L_\infty$ -norm ) or (iii) different methods to select the recurrence thresholds such as: using only certain percentage of the signal ( $\sqrt{m_0} \times 10\%$  of the fluctuations of the time series) (Letellier, 2006), and selecting a determined amount of noise, and using a factor based on the standard deviation of the observational noise (Marwan et al., 2007).

**Robustness of Entropy measures with RQA**

Further investigation is required to be done with regards to the application of Shannon entropy with recurrence plots. Letellier (2006), for example, investigated the robustest of the Shannon entropy based on line segments distributions of recurrence plots  $S_{RP}$

## Conclusions and future work

---

against the Shannon entropy based on system dynamics  $S_{SD}$ . With that, Letellier (2006) pointed out that Shannon entropy based on recurrence plots has strong dependency with the choice of observable (i.e. variable of the dynamical system) while Shannon entropy based on system dynamics is more robust to noise-contaminated signals. Recently, with the introduction of the use of microstates, Corso et al. (2017) tackled the problem of Shannon entropy with RQA where ENTR values decrease despite the increase of non-linearity in a logistic map (Marwan et al., 2007). Additionally, Corso et al. (2017) presented the robustness of their method with changes to recurrence thresholds.

### Advanced RQA quantifications

In addition to the application of RQA metrics (REC, RATIO, DET and ENTR) for recurrence quantification, advanced RQA metrics can be applied to the context of human-humanoid interaction. For example, RP based on complex networks statics, calculation of dynamic invariants, study of the intermittency in the systems, application of different windowing techniques, or the study of bivariate recurrence analysis for correlations, coupling directions or synchronisation between dynamical systems (Marwan et al., 2007; Marwan and Webber, 2015).

### Variability in perception of velocity

While conducting the experiments where participants performed arm movements with different velocities (e.g. normal and faster), it has been noted that participants perceive velocity differently. Particularly, some participants considered a normal velocity movement as being performed in slow velocity and others participants considered a slow velocity movement as being performed in normal velocity. With that in mind, it has been hypothesised that the differences in perception of velocities are related to different factors of a person such as (i) the background, (ii) personality traits or

(iii) even their movement experience (in music or sports) that make them more aware of their body movements. That said, further research require to be done to have better understanding on why each participant perceive the velocity of body movement differently, how such variability of perception of movement can be quantified, and what impact such differences might have for the control of movement or for the ability to recognise decrease in control ability.

### **A richer dataset of real-world time series**

It should be highlighted that the experiments for this thesis are limited to twenty three healthy right-handed participants of a range age of mean 19.8 and SD=1.39. Hence, participants of different ages, state of health and anthropomorphic features would create a richer dataset of real-world time series data to apply nonlinear analysis tools in the context of human-humanoid interaction.

### **Applications**

The application of the literature in human movement variability in the context of human-humanoid interaction can present different avenues. For instance, implement nonlinear analysis algorithms in humanoid robots in order to (i) evaluate the improvement of movement performances (Müller and Sternad, 2004), (ii) quantify and provide feedback of level skillfulness as a function of movement variability (Seifert et al., 2011) or (iii) quantify movement adaptations, pathologies and skill learning (Preatoni, 2007; Preatoni et al., 2010, 2013). Also applications in human-humanoid rehabilitation (Görer et al., 2013; Guneyusu et al., 2015), where the use of nonlinear analysis can provide adequate metrics to quantify and provide feedback for movement variability.



# Appendix A

## Open Access Code and Data

### A.1 Code and data organisation

Code path has ten directories with a descriptive name of their content as shown below:

```
0_machineinfo/  
1_dependencies/  
2_libraries_functions/  
3_anthropometrics/  
4_figs_ch3/  
5_creation_of_curated_timeseries/  
6_figs_ch4/  
7_figs_ch5/  
8_figs_ch6/  
x_surrogate/
```

Code path is available at [\[42\]](#). Data is organised in paths for raw data time series and preprocessed datasets [\[42\]](#).



## A.2 How results can be replicated

This thesis has been written in GNU Linux Operating System. Therefore, for the replication of this thesis, it is suggested that users install Ubuntu 14.04.5 LTS or Ubuntu 16.04.2 LTS on their machines (other GNU Linux distributions can also work). Additionally, it is suggested installing the latest version of R with all its dependencies and GNU Octave, version 4.0.2 (follow the alphabetic order of the scripts to install all dependencies [\[4\]](#)).

For figure replication, the paths are organised with three paths: `code/` contains R scripts that create figures in `scr/`, and `vector/` contains the vector files.

# Appendix B

## Examples of Uniform Time-Delay Embedding

Two examples regarding the methodology of uniform time-delay embedding are presented: (A.1) using a 20 sample length vector, and (A.2) using a time series from horizontal movement of a triaxial accelerometer.

### B.1 20 sample length vector.

For this example, it has been proposed to work with a vector  $\{\mathbf{x}_n\}_{n=1}^{20}$  with a sample length  $N = 20$  in order to implement an uniform time-delay embedding matrix,  $\mathbf{X}_\tau^m$ , with embedding dimension of  $m = 5$  and delay dimension of  $\tau = 3$  (Eq. (3.4)). The

## Examples of Uniform Time-Delay Embedding

---

representation of the uniform time-delay embedding matrix  $\mathbf{X}_3^5$  is as follows

$$\mathbf{X}_3^5 = \begin{pmatrix} \tilde{\mathbf{x}}_n \\ \tilde{\mathbf{x}}_{n-3} \\ \tilde{\mathbf{x}}_{n-6} \\ \tilde{\mathbf{x}}_{n-9} \\ \tilde{\mathbf{x}}_{n-12} \end{pmatrix}^\top \quad (\text{B.1})$$

The dimension of the uniform time-delay embedding matrix is defined by  $N - (m - 1)\tau$  rows and  $m$  columns.  $N - (m - 1)\tau$  is also the sample length of the delayed copies of  $\mathbf{x}_n$  which is equal to eight ( $20 - ((5 - 1) * 3) = 8$ ). Therefore,  $\mathbf{X}_3^5$  can be explicitly represented as

$$\mathbf{X}_3^5 = \begin{pmatrix} x_1 & x_2 & x_3 & x_4 & x_5 & x_6 & x_7 & x_8 \\ x_4 & x_5 & x_6 & x_7 & x_8 & x_9 & x_{10} & x_{11} \\ x_7 & x_8 & x_9 & x_{10} & x_{11} & x_{12} & x_{13} & x_{14} \\ x_{10} & x_{11} & x_{12} & x_{13} & x_{14} & x_{15} & x_{16} & x_{17} \\ x_{13} & x_{14} & x_{15} & x_{16} & x_{17} & x_{18} & x_{19} & x_{20} \end{pmatrix}^\top \quad (\text{B.2})$$

After transposing  $\mathbf{X}_3^5$ , one can see that the ranges of values of the uniform time-delay embedded matrix are between  $((m - 1)\tau) + 1$  to  $N$  (for this example from 13 to 20):

---

## B.2 Time series for horizontal movement of a triaxial accelerometer.

$$\mathbf{X}_3^5 = \begin{pmatrix} x_1 & x_4 & x_7 & x_{10} & x_{13} \\ x_2 & x_5 & x_8 & x_{11} & x_{14} \\ x_3 & x_6 & x_9 & x_{12} & x_{15} \\ x_4 & x_7 & x_{10} & x_{13} & x_{16} \\ x_5 & x_8 & x_{11} & x_{14} & x_{17} \\ x_6 & x_9 & x_{12} & x_{15} & x_{18} \\ x_7 & x_{10} & x_{13} & x_{16} & x_{19} \\ x_8 & x_{11} & x_{14} & x_{17} & x_{20} \end{pmatrix} = \begin{pmatrix} \mathbf{X}[13] \\ \mathbf{X}[14] \\ \mathbf{X}[15] \\ \mathbf{X}[16] \\ \mathbf{X}[17] \\ \mathbf{X}[18] \\ \mathbf{X}[19] \\ \mathbf{X}[20] \end{pmatrix}. \quad (\text{B.3})$$

## B.2 Time series for horizontal movement of a tri-axial accelerometer.

In this example, it is considered a time series of a triaxial accelerometer (Figure B.1(C)), captured from repetitions of a horizontal trajectory (Figure B.1(A)) performed by user (Figure B.1(B)). From Figure B.1(C)) is evidently that the  $A_y(n)$  is the most affected axis of the accelerometer due to the movement's characteristics in the horizontal trajectory. With that in mind,  $A_y(n)$  is selected as the input time series for the uniform time-delay embedding theorem.

Considering that the sample rate of the data is 50 Hz, it has been proposed to work with a vector of sample length of  $N = 1000$  which corresponds to 20 seconds of data. Then, with minimum embedding parameters  $m = 7$  and  $\tau = 11$ , the dimensions of the uniform time-delay embedding matrix,  $\mathbf{A}_{y_{11}}^7$ , are 934 (  $N - (m - 1)\tau$  ) rows and 7 (  $m$  )

## Examples of Uniform Time-Delay Embedding

---

columns.  $\mathbf{A}_{y_{11}}^7$  is therefore represented as follows:

$$\mathbf{A}_{y_{11}}^7 = \begin{pmatrix} A_y(n) \\ A_y(n-11) \\ A_y(n-22) \\ A_y(n-33) \\ A_y(n-44) \\ A_y(n-55) \\ A_y(n-66) \end{pmatrix}^\top = \begin{pmatrix} a_y(1) & \dots & a_y(934) \\ a_y(12) & \dots & a_y(945) \\ a_y(23) & \dots & a_y(956) \\ a_y(34) & \dots & a_y(967) \\ a_y(45) & \dots & a_y(978) \\ a_y(56) & \dots & a_y(989) \\ a_y(67) & \dots & a_y(1000) \end{pmatrix}^\top \quad (\text{B.4})$$

$$\mathbf{A}_{y_{11}}^7 = \begin{pmatrix} a_y(1) & a_y(12) & a_y(23) & a_y(34) & a_y(45) & a_y(56) & a_y(67) \\ \vdots & \vdots & \vdots & \vdots & \vdots & \vdots & \vdots \\ a_y(934) & a_y(945) & a_y(956) & a_y(967) & a_y(978) & a_y(989) & a_y(1000) \end{pmatrix} \quad (\text{B.5})$$

$$\mathbf{A}_{y_{11}}^7 = \begin{pmatrix} \mathbf{A}_{y_{11}}^7[67] \\ \vdots \\ \mathbf{A}_{y_{11}}^7[1000] \end{pmatrix}. \quad (\text{B.6})$$

## B.2 Time series for horizontal movement of a triaxial accelerometer.

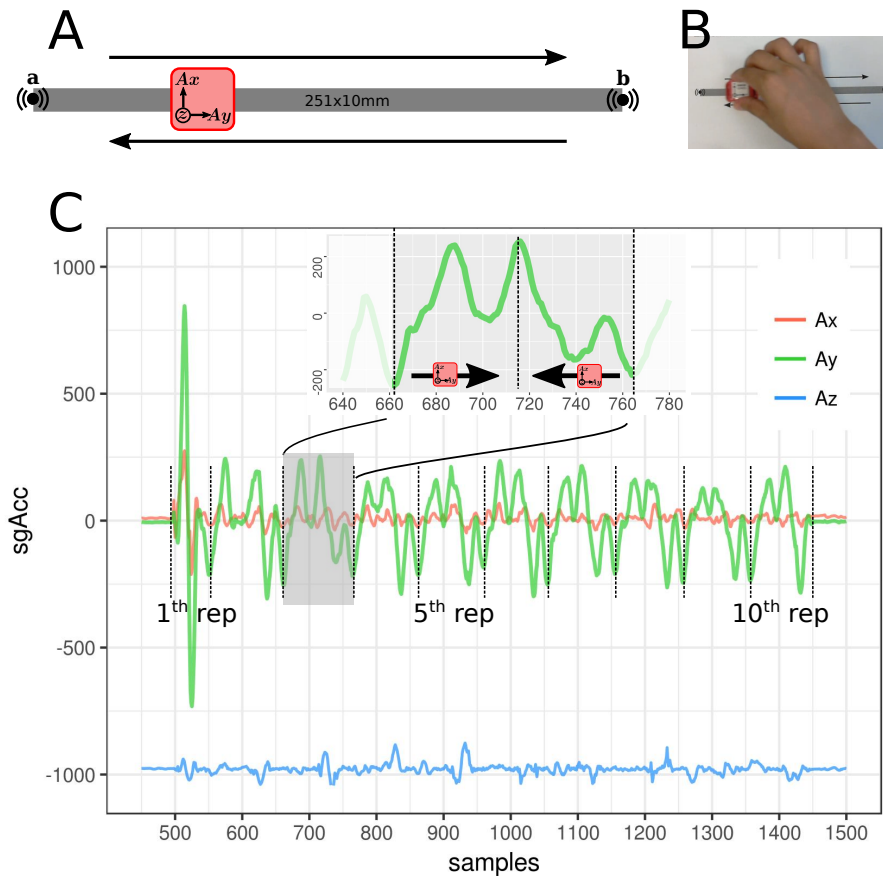


Fig. B.1 **Example of time series with an IMU** (A). Triaxial accelerometer (in red) is moved repetitively across a line of 251 mm from point **a** to **b** and then from **b** to **a**. The points **a** and **b** indicate when a click sound is produced. (B). Person's hand holding and moving the sensor horizontally across the line. (C). Time series for the triaxial accelerometer ( $A_x(n)$ ,  $A_y(n)$ ,  $A_z(n)$ ) for ten repetitive horizontal movements across a line. The top time series only shows  $A_y$  axis which corresponds to one cycle of the horizontal movement and the black arrows represent the movement's direction of the accelerometer with respect to the produced time series.



# Appendix C

## Equipment

### C.1 NeMEMsi IMU sensors

For this thesis, data were collected using NeMEMsi sensors that provide 3D accelerometer, 3D magnetometer, 3D gyroscope and quaternions (Comotti et al., 2014). Figure C.1 shows NeMEMsi sensor. It is important to note that NeMEMsi sensors were tested against the state-of-the-art device MTi-30 IMU from xsense. The comparison values between NeMEMsi and MTi-30 in terms of standard deviation of the noise of each component of the Euler angles at a stated state are lower than 0.1 degrees. Additionally, the NeMEMsi provide not only to have a lower-power consumption but also the smaller dimensions against other state-of-the-art brands of IMUs. In the following sections, some features of the NeMEMsi IMU are presented. See Comotti et al. (2014) for further details.



## Equipment

---

### Sample rate and power consumption

Data streaming can be set up to be streamed at 25 Hz, 50 Hz and 100Hz which affects the power consumption from 29mAh, 32mAh and 35mAh, respectively. For this thesis, the sample rate were set up to 50 Hz.

### Sensors

The outputs of the NeMEMsi sensor includes:

#### Orientation

- \* Euler angles (Yaw, Pitch and Roll).
- \* Quaternions.

#### Accelerometer (Linear acceleration)

- \* Raw and calibrated XYZ measurement from  $\pm 2$  /  $\pm 4$  /  $\pm 6$  /  $\pm 8$  /  $\pm 16$

#### Gyroscope (Rate of turn)

- \* Raw and calibrated XYZ measurement from  $\pm 245$  /  $\pm 500$  /  $\pm 2000$  degrees per second.

#### Magnetometer (Magnetic field)

- \* Raw and calibrated XYZ measurement from  $\pm 4$  /  $\pm 8$  /  $\pm 12$  /  $\pm 16$  gauss.

### Microprocessor

- \* Architecture: ARM 32-bit Cortex M4 CPU with FPU and DSP instructions
- \* Max.frequency: 100MHz

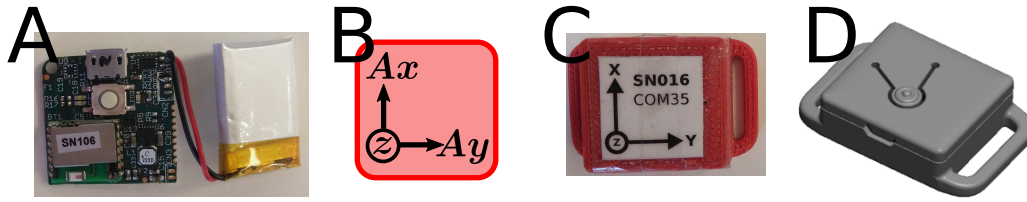


Fig. C.1 **Inertial Measurement Sensor** (A) Printed Circuit Board (PCB) with 165mAh battery, (B) axis orientation, (C) real case, and (D) 3D model for the case.

\* Memory Size: 512 Kbytes

\* RAM: 128 Kbytes SRAM

## Connectivity

\* Bluetooth: Class 2, bluetooth 3.0

\* Range: 10 m

\* Transmission rate: Up to 560 kbps with Service Port to Port

\* Multipoint: Up to 7 slaves

## Form factor

\* Electronics physical dimension: 25L x 25W x 4H (mm)

\* Electronics Weight: 3.3 gr

\* Dimension with battery and casing: 42L x 28W x 11.5 (mm)

\* Weight with batter and casing: 15 gr

### C.1.1 Issues with IMUs

For the experiment of human-image imitation activities where eight activities were performed per participant, it has been observed that time synchronisation had issues because of the drift in time for time series data (2 minutes of data collection). Additionally, these experiments had problems with disconnections to bluetooth module. In

contrast, for the human-humanoid imitation activities where only four activities were performed per participant (1 minutes of data collection), data collection of time series had fewer issues with regard to the drift in time and bluetooth data streaming.

## C.2 Time-series preprocessing

The following sections explain how the organising data in multidimensional arrays, data synchronisation, data Synchronisation, and time alignment are computed. Code and data for the following sections is available at [\[4\]](#).

### C.2.1 Organising Data in Multidimensional Arrays

Scripts in MATLAB were created to synchronise the data using the clock drift and clock offset values which were provided for each of the NeMEMSi sensors. Then the data from each sensor is aligned in time using using `finddelay()` and `alignsignals()`.

### C.2.2 Data Synchronisation

To find the delay between two two sensors that were attached to the same place of the body parts, a function called `finddelayMX()` was created. Such function computes the autocorrelation between two signals using `(xcorr())` then the maximum value of the autocorrleation function is extracted to create a delay between the values of maximum index in the autocorrelation function and the length of the first signal.

The function `alignsignalsMX()` was used to align two signals based on `finddelayMX()`. The function `alignsignalsMX()` use six inputs of which `sA` and `sB` are for the sensors, `windowframe` for the information of the signal is extracted from another activities, the `MainAxis` of which the signal are going to be extracted, the `truncate delay` that is created to synchronise the signals adding an extra delay that is based on the length of

previous signals and tuning delay that can be useful to tune the delay in the case of the delay is not appropriate when the signals are too noisy. Then, `aligntwosignals()` is applied to align only two signals. The inputs of `aligntwosignals()` are X and Y for the input vectors, truncate delay for the previous delay of two signals and tuning delay in case that signals are too noisy and the `xcorr` fail to find an appropriate delay.

### C.2.3 Time Alignment

Given four vectors of time  $t_1, t_2, t_3, t_4$ , the minimum and maximum values were extracted for the start time of the four sequence of time, it was also extracted the minimum and maximum values to the end of each of the four sequences of time. However, after aligning the vectors it has then been noticed that there were different values of length across vectors i.e., 1880, 1986, 1987, 1988. Therefore the length for the second vector was used as the primary length because is the one that presents the minimum value of the three maximum lengths. Then `interp1(x,v,vq,'pchip')` was used to interpolate the length of each of the vectors, for example: 1986, 1986, 1986, 1986. It has been chosen `pchip` function since the interpolation present values for each of the points as oppose to `linear` function which create NA values.

### C.3 NAO – humanoid robot

A NAO humanoid robot version 04 from SoftBank (Fig. C.2) was used for the experiments of human-humanoid interaction. NAO were programmed for simple horizontal and vertical arm movements using Choregraphe, an API to program NAO, and then interpolated values of the animation were exported to a python script.

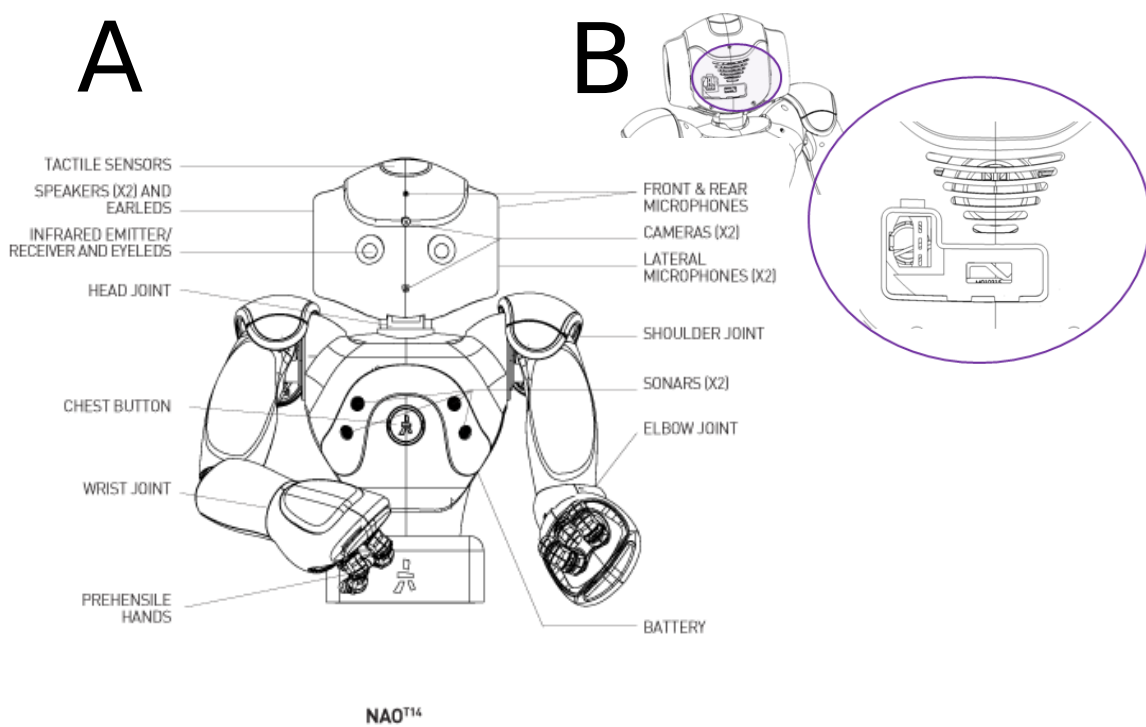


Fig. C.2 NAO, humanoid robot from SoftBank. (A) NAO body type T4 with its parts, and (B) back design of NAO version 04.

# Appendix D

## Experiment Design

### D.1 Experiment Check List

Figure D.1 shows the experiment check list for the experiments which consist of: 1. Participant Information, 2. Setting up sensors, 3. Experiments, 4. Stop sensors, and 5. Extra notes.

### D.2 Information Sheet

Figures D.2, D.3, D.4 and D.5 show a google form for the Online Participation Sheet.

# Experiment Design

---

## Experiment Check List. Participant: p\_---

### Human-Humanoid Imitation Activities

#### 1. Information

- 1.1 Participant Information Sheet
- 1.2 Anthropometric Data
- 1.3 Sitting the participant on the Chair
- 1.4 Start Recording Video
- 1.5 Show participant p\_-- to the camera

#### 2. Setting Up Sensors

Status HII	Description	Status HRI
<input type="checkbox"/>	Create Data Path	<input type="checkbox"/>
<input type="checkbox"/>	Open Muse Applications	<input type="checkbox"/>
<input type="checkbox"/>	Turn ON the sensors	<input type="checkbox"/>
<input type="checkbox"/>	Pair the sensor [sensor number and port number]	<input type="checkbox"/>
<input type="checkbox"/>	Set the sampling rate to 50 Hz	<input type="checkbox"/>
<input type="checkbox"/>	Open settings for Time Sync parameters	<input type="checkbox"/>
<input type="checkbox"/>	Compute the Time Sync parameters	<input type="checkbox"/>
<input type="checkbox"/>	PrintScreen the Time Sync parameters and Save Capture	<input type="checkbox"/>
<input type="checkbox"/>	Close settings and set parameters	<input type="checkbox"/>
<input type="checkbox"/>	Start Recording data	<input type="checkbox"/>
<input type="checkbox"/>	Shake all sensors	<input type="checkbox"/>

- 2.1.a Attach Sensors to the Participant (check sensor orientation)
- 2.1.b Attach Sensors to the Robot (check sensor orientation)
- 2.1.a Attach Sensors to the Participant (check sensor orientation)
- 2.2.b Attach Sensors to the Participant (check sensor orientation)

#### 3. Experiment

- 3.1.a Human-Image Int [NO BEAT]
- 3.2.b Human-Robot Int [BEAT]

Status	Description
<input type="checkbox"/>	Hor Normal
<input type="checkbox"/>	Ver Normal
<input type="checkbox"/>	Hor Fast
<input type="checkbox"/>	Ver Fast

Status	Description
<input type="checkbox"/>	./HN.sh p_--
<input type="checkbox"/>	./VN.sh p_--
<input type="checkbox"/>	./HF.sh p_--
<input type="checkbox"/>	./VF.sh p_--

- 3.2.a Human-Image Int [BEAT]

Status	Description
<input type="checkbox"/>	aplay HN_beat.wav
<input type="checkbox"/>	aplay VN_beat.wav
<input type="checkbox"/>	aplay HF_beat.wav
<input type="checkbox"/>	aplay VF_beat.wav

#### 4. Stop

- 4.1.a Stop Sensor Recording
- 4.1.b Stop Sensor Recording
- 4.2.a Save Data
- 4.2.b Save Data
- 4.3.a Disconnect Sensors
- 4.3.b Disconnect Sensors
- 4.4 Stop Video Recording

#### 5. Notes

Fig. D.1 Experiment Check List.

25/10/2018

A Study of Movement Variability in Human-Humanoid Interaction Activities

### A Study of Movement Variability in Human-Humanoid Interaction Activities

\*Required

#### Introduction

---

The aim of this study is to explore how participant's performance of simple movements affects the movement variability in the following conditions: a) following an image while not hearing a beat and while hearing a beat; and b) following a humanoid-robot while not hearing a beat and while hearing a beat.

The estimated time for the study is between 40 to 45 minutes.

---

Miguel P. Xochicale [<http://mxochicale.github.io/>]  
Doctoral Researcher in Human-Robot Interaction  
School of Electronic, Electrical and System Engineering  
University of Birmingham, UK

#### 1. Online Participant Information Sheet

##### Who will conduct the research?

---

The study is conducted by Miguel P. Xochicale as part of his PhD degree in Electronic, Electrical and System Engineering at the University of Birmingham. The research is supervised by Professor Chirs Baber and Professor Martin Russell in the Electronic, Electrical and System Engineering department at the University of Birmingham.

##### What is the purpose of the research?

---

The aim of this study is to explore how participant's performance of simple movements affects the movement variability in the following conditions: a) following an image while not hearing a beat and while hearing a beat; and b) following a humanoid-robot while not hearing a beat and while hearing a beat.

##### What will happen during the experiment?

---

During the experiment you will be asked to wear two inertial sensors in your right hand and you will perform 10 repetitions for horizontal and vertical arm movements in six conditions:

Condition 1. Following an image while NOT hearing a beat  
Condition 2. Following an image while hearing a slow beat rate  
Condition 3. Following an image while hearing a fast beat rate

(a 5 minutes break will be given at this point)

Condition 4. Following a humanoid-robot while NOT hearing a beat  
Condition 5. Following a humanoid-robot while hearing a slow beat rate  
Condition 6. Following an image while hearing a fast beat rate.

[https://docs.google.com/forms/d/1dPN6D\\_S3CRg4pkDYplfDg6f5nh6FaQ4Z7M0xl\\_11Fq4/edit](https://docs.google.com/forms/d/1dPN6D_S3CRg4pkDYplfDg6f5nh6FaQ4Z7M0xl_11Fq4/edit)

1/4

Fig. D.2 Participant Information Sheet (p. 1/4)



## **What type of data will be collected during the experiment?**

Three types of data will be collected:

- i) Data from inertial sensors will be collected. Each inertial sensor has an accelerometer, magnetometer, gyroscope.
- ii) Audio from a microphone to record the movements of the humanoid-robot.
- iii) A video will be recorded for visualisation and demonstration purposes (let me know if you are uncomfortable with the video recording).

## **What happens to the data collected?**

The data will be analysed in order to explore how participant's performance of simple movements affects the movement variability in the previous six conditions of movement.

## **How Is Confidentiality Maintained in the experiment?**

The law called the Data Protection Act (1998) tells us how to keep your information secure.

Your data will be treated as confidential and you will be assigned a unique identifying code which will be used to identify your data. If you have decided to provide your name and email address, it will remain confidential and we will not give your details to anyone else. No other personal data will be recorded about participants (no ethnicity, address, telephone number, etc. )

## **What is the duration of the experiment?**

The estimated time for the study is between 40 to 45 minutes.

## **Where the experiment will be conducted?**

The experiment will be conducted in room N310 which is in third floor at Gisbert Kapp Building (G8), University of Birmingham.

## **Will the results of this research be published?**

Data collected will be used for conference and journal publications and the PhD thesis results.

## **Will be compensation for participating?**

You are invited to participate in this study but will receive no compensation.

## **Can I withdrawal from the experiment after given my consent?**

Yes, you can withdrawal from the experiment at any time after given your consent which might be either before the start of your experiment session, during the session, or after finishing the session. In case of withdrawal, all your data will be discarded and will not be used anywhere in the study.

25/10/2018

A Study of Movement Variability in Human-Humanoid Interaction Activities

### Contact Details

---

If you have any questions about the project, you can contact Miguel by e-mail or telephone, using the details provided below:

Doctoral Researcher: Miguel P. Xochicale [[map479@bham.ac.uk](mailto:map479@bham.ac.uk)].  
Department: School of Electronic Electrical and Systems Engineering

Primary Supervisor: Professor Chirs Baber [[c.baber@bham.ac.uk](mailto:c.baber@bham.ac.uk)]  
Department: School of Electronic Electrical and Systems Engineering

Secondary Supervisor: Professor Martin Russell [[m.j.russell@bham.ac.uk](mailto:m.j.russell@bham.ac.uk)]  
Department: School of Electronic Electrical and Systems Engineering

#### 1. Statement of understanding/consent \*

*Tick all that apply.*

- I confirm that I have read and understand the participant information online sheet for this study. I have had the opportunity to aks questions if necessary and have had these answered satisfactorily.
- I understand that I am able to withdraw from the experiment at any time without giving any reason. If I withdraw my data will be removed from the study and will be destroyed.
- I understand that my personal data will be processed for the purposes detailed above, in accordance with the Data Protection Act 1998.
- Based upon the above, I agree to take part in this study.

#### 2. Your Name \*

\_\_\_\_\_

#### 3. Email \*

\_\_\_\_\_

### 2. Antropometric Data

#### 4. Participant Number (e.g. p11) \*

\_\_\_\_\_

#### 5. What is your gender? \*

*Mark only one oval.*

- Male
- Female

#### 6. What is your age in years? \*

\_\_\_\_\_

#### 7. What is your handedness? \*

*Mark only one oval.*

- Left
- Right

[https://docs.google.com/forms/d/1dPN6D\\_S3CRg4pkDYplfDg6f5nh6FaQ4Z7M0xl\\_11Fq4/edit](https://docs.google.com/forms/d/1dPN6D_S3CRg4pkDYplfDg6f5nh6FaQ4Z7M0xl_11Fq4/edit)

3/4

Fig. D.4 Participant Information Sheet (p. 3/4)

# Experiment Design

---

25/10/2018

A Study of Movement Variability in Human-Humanoid Interaction Activities

8. **Have you received formal music training? \***

*Mark only one oval.*

- No
- Yes (less than 5 years)
- Yes (more than 5 years)

9. **What is your arm length in centimetres? \***

*Mark only one oval.*

- Less than 45
- 45
- 46
- 47
- 48
- 49
- 50
- 51
- 52
- 53
- 54
- 55
- 56
- 57
- 58
- 59
- 60
- More than 60

10. **What is your height in centimeters? \***

\_\_\_\_\_

11. **What is your weight in kilograms? \***

\_\_\_\_\_

---

Powered by  
 Google Forms

[https://docs.google.com/forms/d/1dPN6D\\_S3CRg4pkDYplfDg6fSnh6FaQ4Z7M0xl\\_11Fq4/edit](https://docs.google.com/forms/d/1dPN6D_S3CRg4pkDYplfDg6fSnh6FaQ4Z7M0xl_11Fq4/edit)

4/4

Fig. D.5 Participant Information Sheet (p. 4/4)

# Appendix E

## Additional Results for HII experiment

### E.1 Time Series

Figures E.1 E.2, and E.3 show time series for horizontal arm movements and figures E.4, E.5, E.6 show time series for vertical arm movements. Time series are only for a window size of 10 seconds window length. For the remained window lengths, the reader is welcome to download the data and code at Xochicale (2019). See Appendix A for details on how code and data is organised and how results can be replicated.

## Additional Results for HII experiment

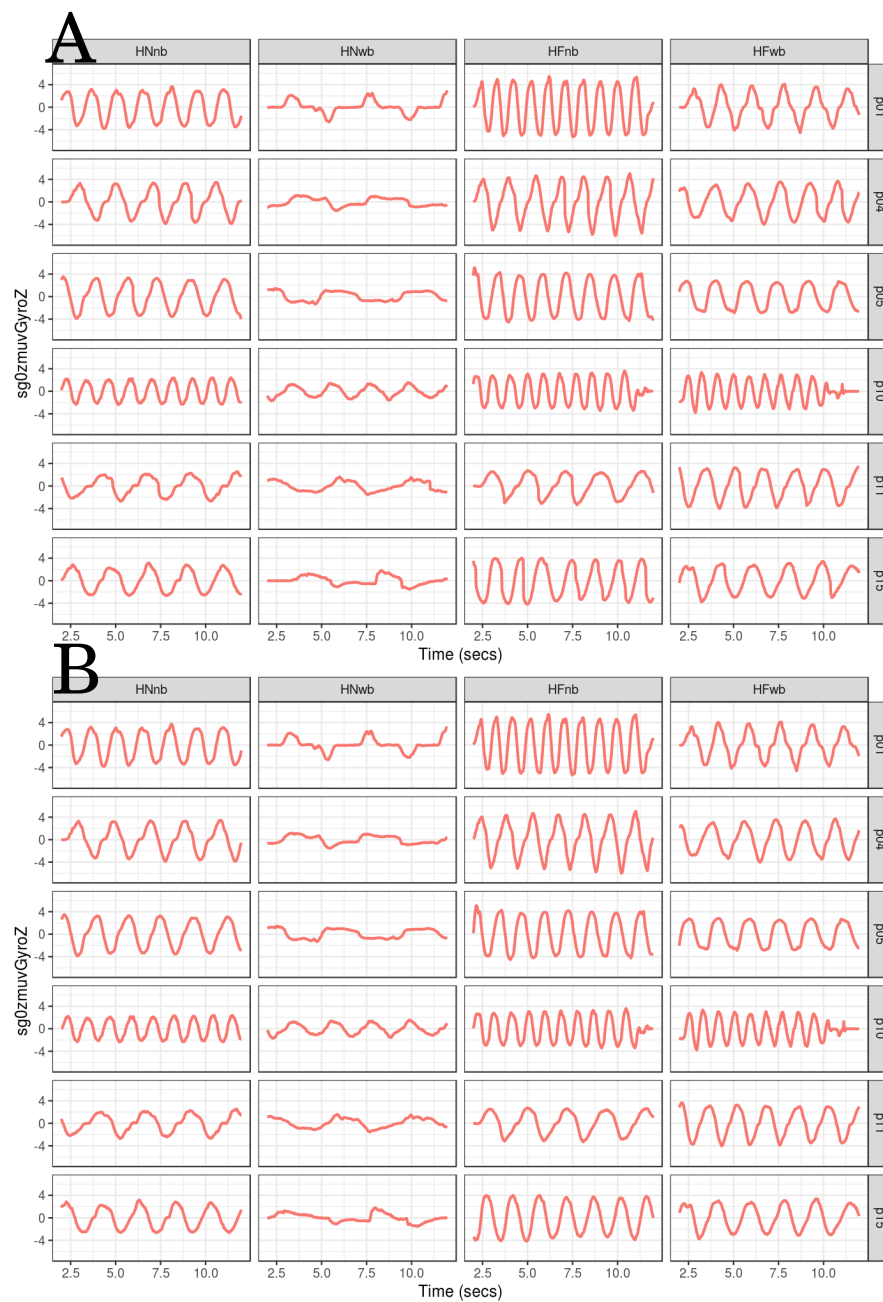


Fig. E.1 **Time series for horizontal arm movements (sg0)** Time series for sg0GyroZ are for six participants (*p01*, *p04*, *p05*, *p10*, *p11*, *p15*) for horizontal movements in normal and faster velocity with no beat (HNnb, HFnb) and with beat (HNwb, HFwb) using the normalised GyroZ axis (zmuV GyroZ). Two sensors were attached to the wrist of the participants (HS01, HS02), where plots in (A) are from human sensor HS01 and plots in (B) are from human sensor HS02. R code to reproduce the figure is available at [\[6\]](#).

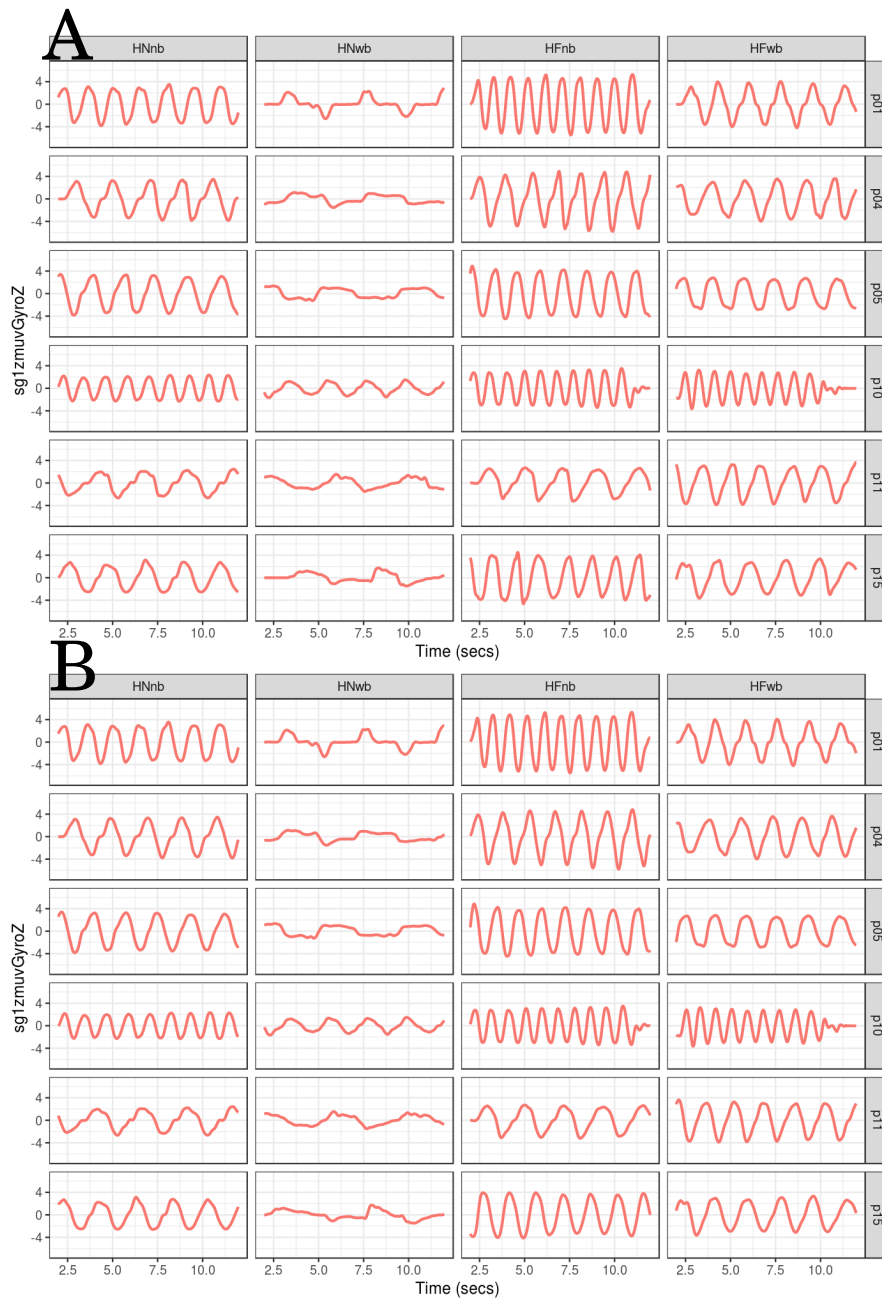


Fig. E.2 **Time series for horizontal arm movements (sg1)** Time series for  $sg1GyroZ$  for six participants ( $p01$ ,  $p04$ ,  $p05$ ,  $p10$ ,  $p11$ ,  $p15$ ) for horizontal movements in normal and faster velocity with no beat (HNnb, HFnb) and with beat (HNwb, HFwb) using the normalised  $GyroZ$  axis ( $zmuvGyroZ$ ). Two sensors were attached to the wrist of the participants (HS01, HS02), where plots in (A) are from human sensor HS01 and plots in (B) are from human sensor HS02. R code to reproduce the figure is available at [\[45\]](#).

## Additional Results for HII experiment

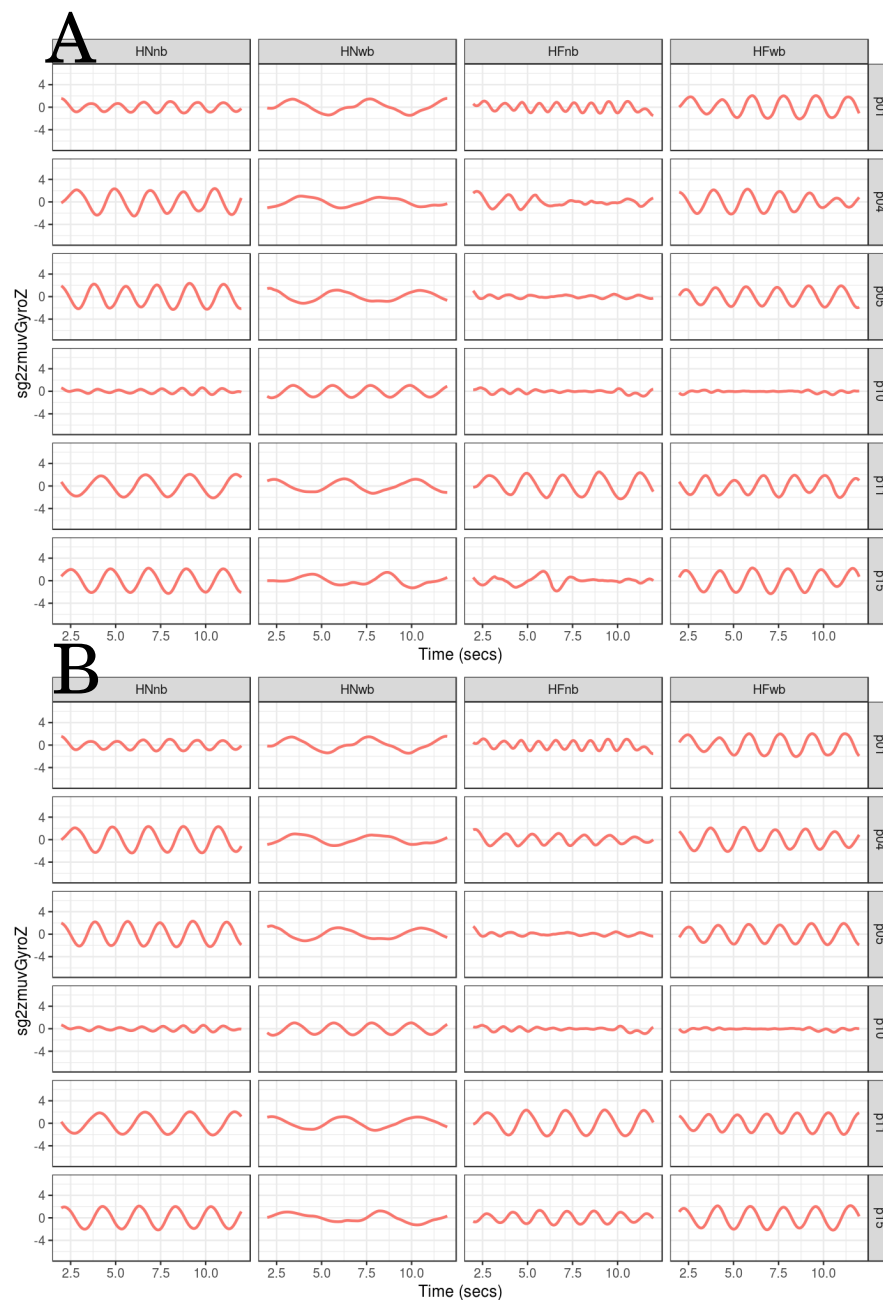


Fig. E.3 **Time series for horizontal arm movements (sg2)** Time series for sg2GyroZ for six participants (*p01*, *p04*, *p05*, *p10*, *p11*, *p15*) for horizontal movements in normal and faster velocity with no beat (HNnb, HFnb) and with beat (HNwb, HFwb) using the normalised GyroZ axis (zmuvGyroZ). Two sensors were attached to the wrist of the participants (HS01, HS02), where plots in (A) are from human sensor HS01 and plots in (B) are from human sensor HS02. R code to reproduce the figure is available at [\[4\]](#).

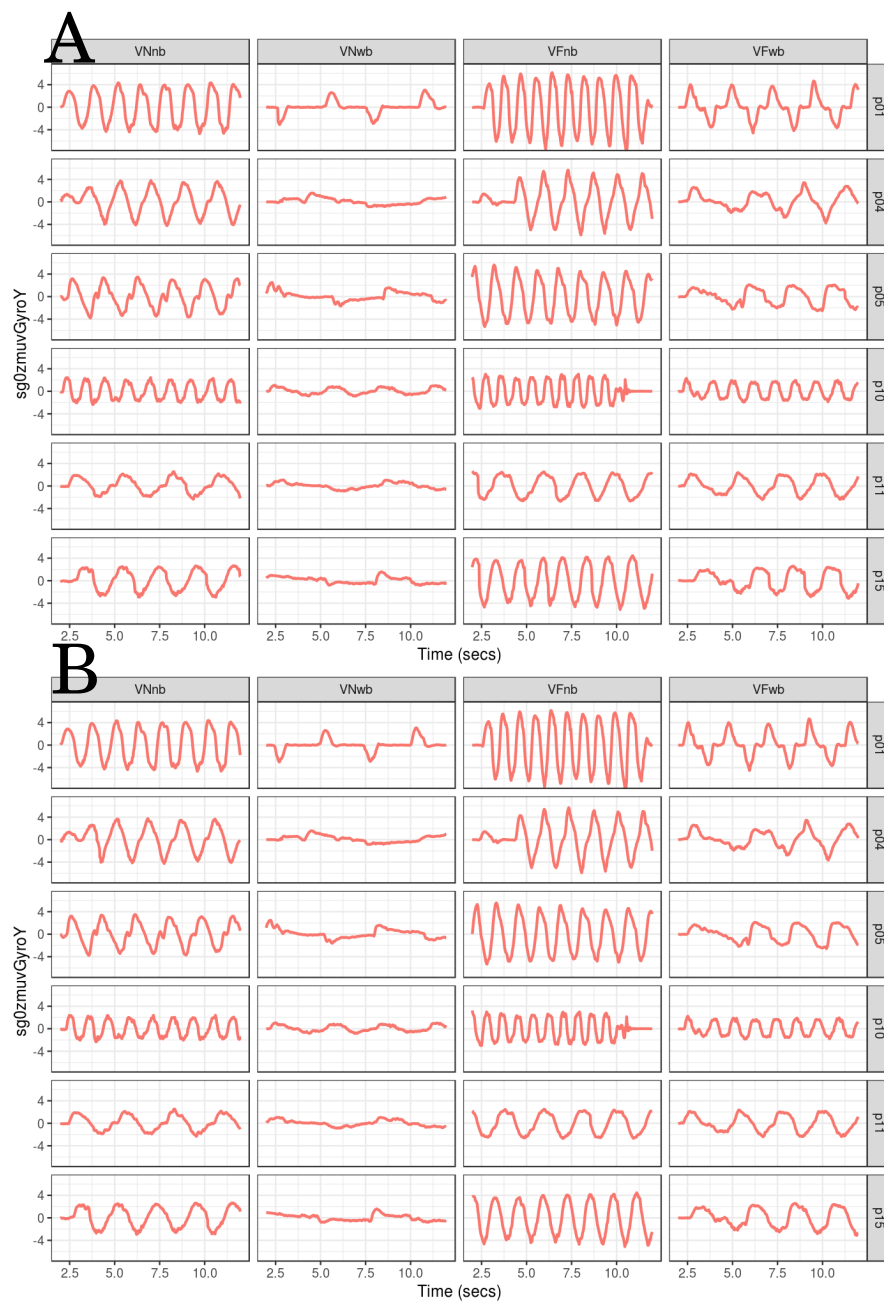


Fig. E.4 **Time series for vertical arm movements (sg0)** Time series for sg0GyroY are for six participants ( $p01$ ,  $p04$ ,  $p05$ ,  $p10$ ,  $p11$ ,  $p15$ ) for vertical movements in normal and faster velocity with no beat (VNnb, VFnb) and with beat (VNwb, VFwb) using the normalised GyroZ axis (zmuvgyroY). Two sensors were attached to the wrist of the participants (HS01, HS02), where plots in (A) are from human sensor HS01 and plots in (B) are from human sensor HS02. R code to reproduce the figure is available at [\[4\]](#).



## Additional Results for HII experiment

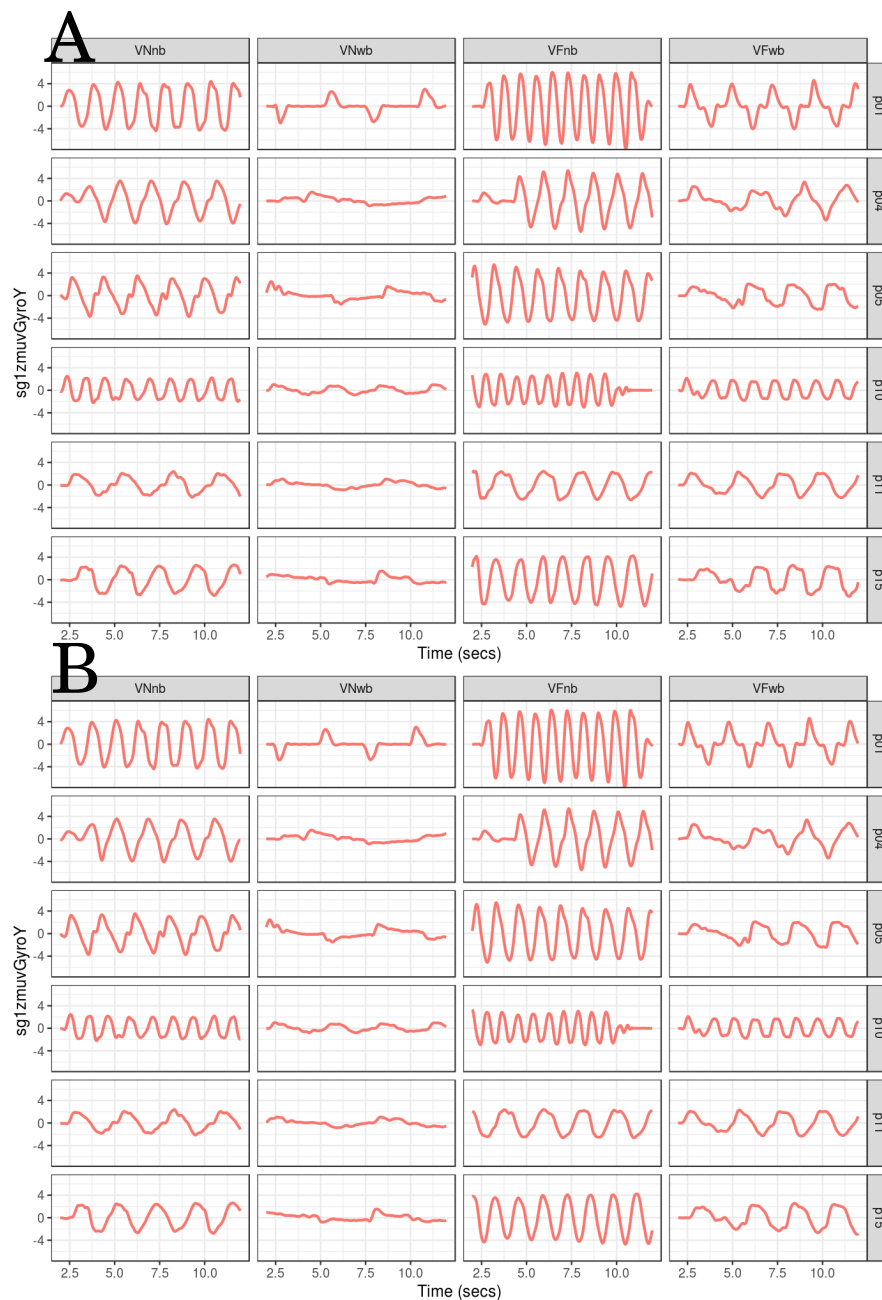


Fig. E.5 **Time series for vertical arm movements (sg1)** Time series for sg1GyroY for six participants (*p01*, *p04*, *p05*, *p10*, *p11*, *p15*) for vertical movements in normal and faster velocity with no beat (VNnb, VFnb) and with beat (VNwb, VFwb) using the normalised GyroZ axis (zmuvGyroY). Two sensors were attached to the wrist of the participants (HS01, HS02), where plots in (A) are from human sensor HS01 and plots in (B) are from human sensor HS02. R code to reproduce the figure is available at [\[48\]](#).

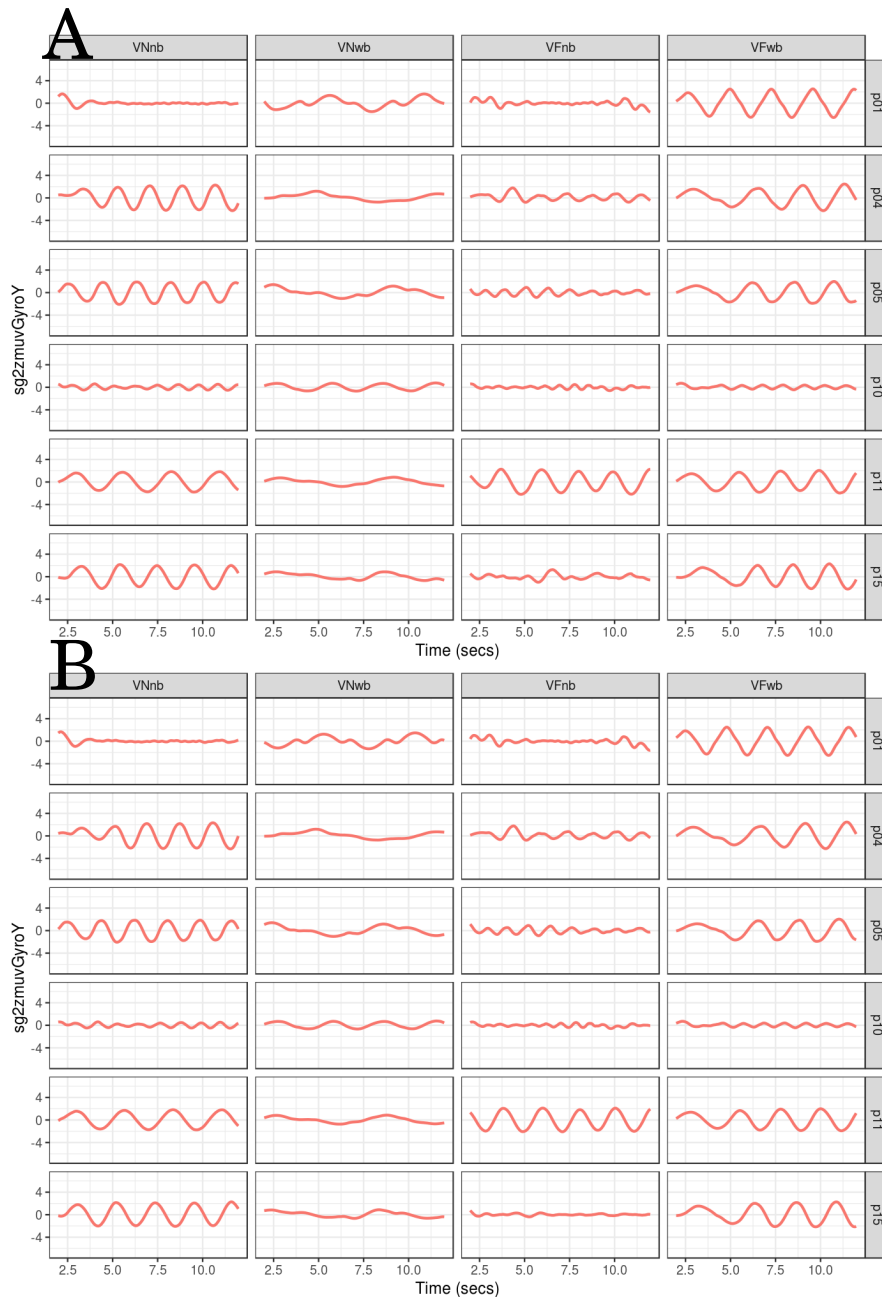


Fig. E.6 **Time series for vertical arm movements (sg2)** Time series for sg2GyroY for six participants (*p01*, *p04*, *p05*, *p10*, *p11*, *p15*) for vertical movements in normal and faster velocity with no beat (VNnb, VFnb) and with beat (VNwb, VFwb) using the normalised GyroY axis (zmuvGyroY). Two sensors were attached to the wrist of the participants (HS01, HS02), where plots in (A) are from human sensor HS01 and plots in (B) are from human sensor HS02. R code to reproduce the figure is available at [\[4\]](#).

## E.2 Embedding parameters

### E.2.1 Minimum dimension embedding values

Values of minimum embedding dimensions for horizontal normal arm movements with no beat (HNnb) and horizontal faster arm movements with no beat (HFnb) are shown in Fig E.7 which values of minimum embedding dimensions present a fluctuation of values between four and seven over six participants. It can also be noted a slightly variation of minimum embedding dimension values over participants when comparing HS01 and HS02 (Fig E.7(A, B)). With regards to the smoothness of the time series, the minimum embedding values are also smoothed showing less variations of values over six participants (Fig E.7).

Values of minimum embedding dimension for horizontal normal arm movements with beat (HNwb) and horizontal faster arm movements with beat (HFwb) are shown in Fig E.8 where is shown a fluctuations of values for minimum embedding dimension between five and seven. Similarly as in Fig E.7, Fig E.8 show changes of minimum embedding dimension between participants and the smoothness of the time series also affects the smoothness of minimum embedding dimension values.

Values of minimum embedding dimension for vertical arm movements with no beat are shown in Figs E.9(A, B) where the smoothness of the time series have little effect on the minimum embedding dimension values, whereas smoothness of time series affects the smoothness of the minimum embedding values for vertical faster arm movements with no beats (Fig E.9(C, D)).

Fig E.10 shows the variation of minimum embedding values for vertical arm movements with beat where the smoothness of the time series affects both vertical normal and vertical faster movements with a slight decrease on each of the values as the smoothness increase.

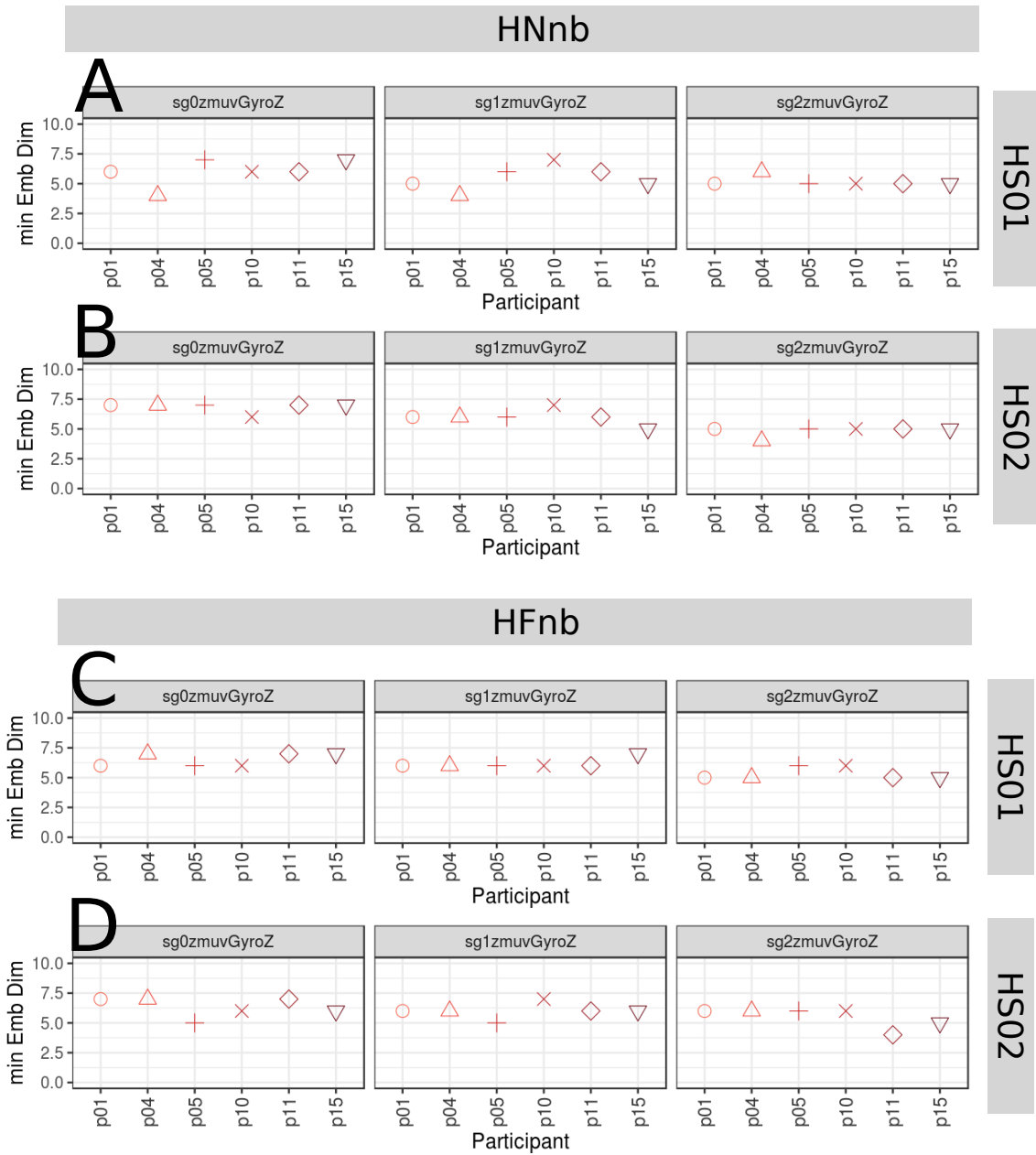


Fig. E.7 **Minimum embedding dimensions for horizontal arm movements (no beat)**. (A, B) Horizontal Normal with no beat (HNnb), and (C, D) Horizontal Faster with no beat (HFnb) movements. (A, C) Sensor 01 attached to the participant (HS01), and (B, D) sensor 02 attached to the participant (HS02). Minimum embedding dimensions are for six participants (p01, p04, p05, p10, p11, p15) with three smoothed signals (sg0zmuvGyroZ, sg1zmuvGyroZ and sg2zmuvGyroZ) and window length of 10-sec (500 samples). R code to reproduce the figure is available at [\[4\]](#).

## Additional Results for HII experiment

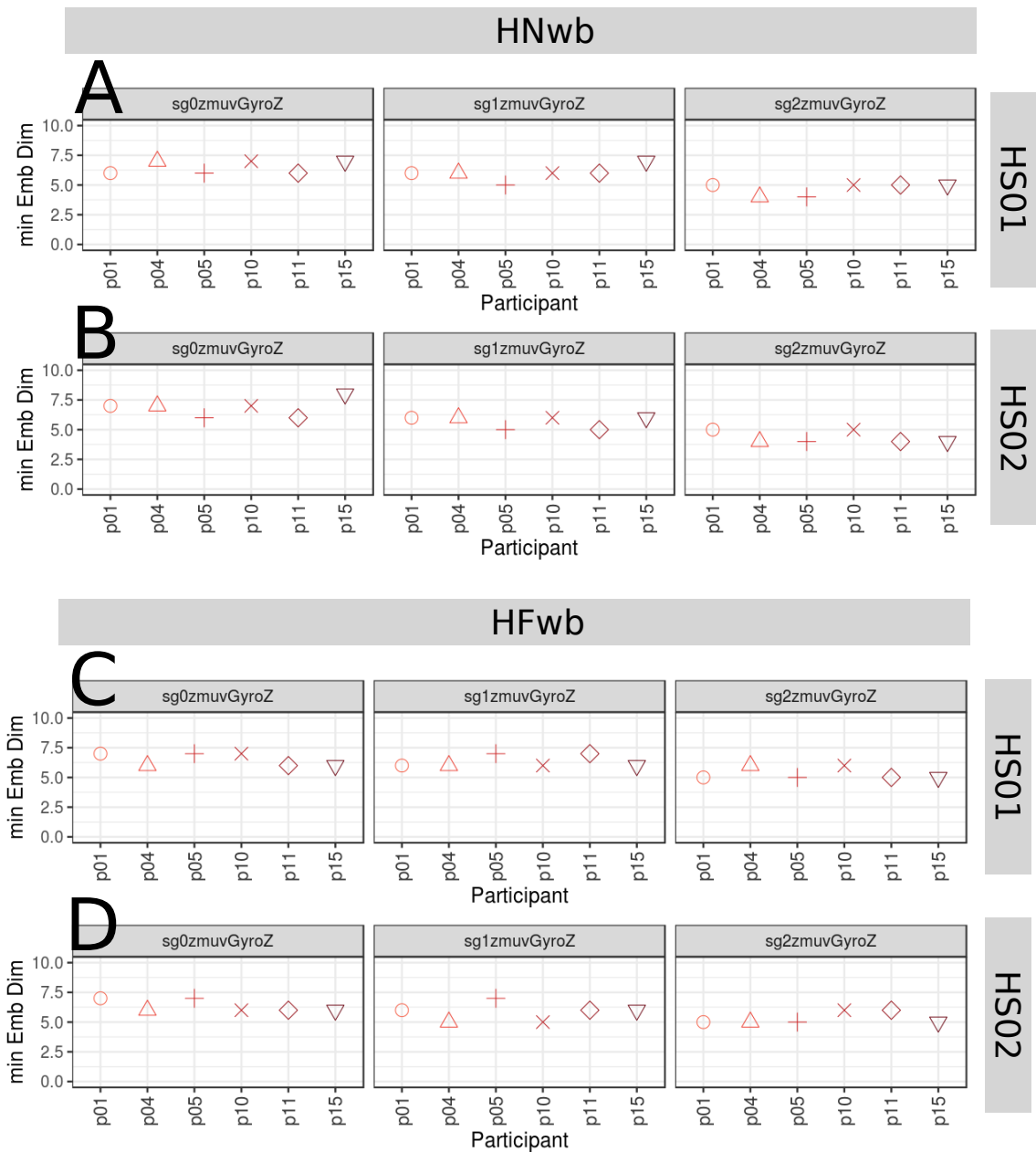


Fig. E.8 **Minimum embedding dimensions for horizontal arm movements (with beat)**. (A, B) Horizontal Normal with beat (HNwb), and (C, D) Horizontal Faster with beat (HFwb) movements. (A, C) Sensor 01 attached to the participant (HS01), and (B, D) sensor 02 attached to the participant (HS02). Minimum embedding dimensions are for six participants (p01, p04, p05, p10, p11, p15) with three smoothed signals (sg0zmvGyroZ, sg1zmvGyroZ and sg2zmvGyroZ) and window length of 10-sec (500 samples). R code to reproduce the figure is available at [GitHub](#).

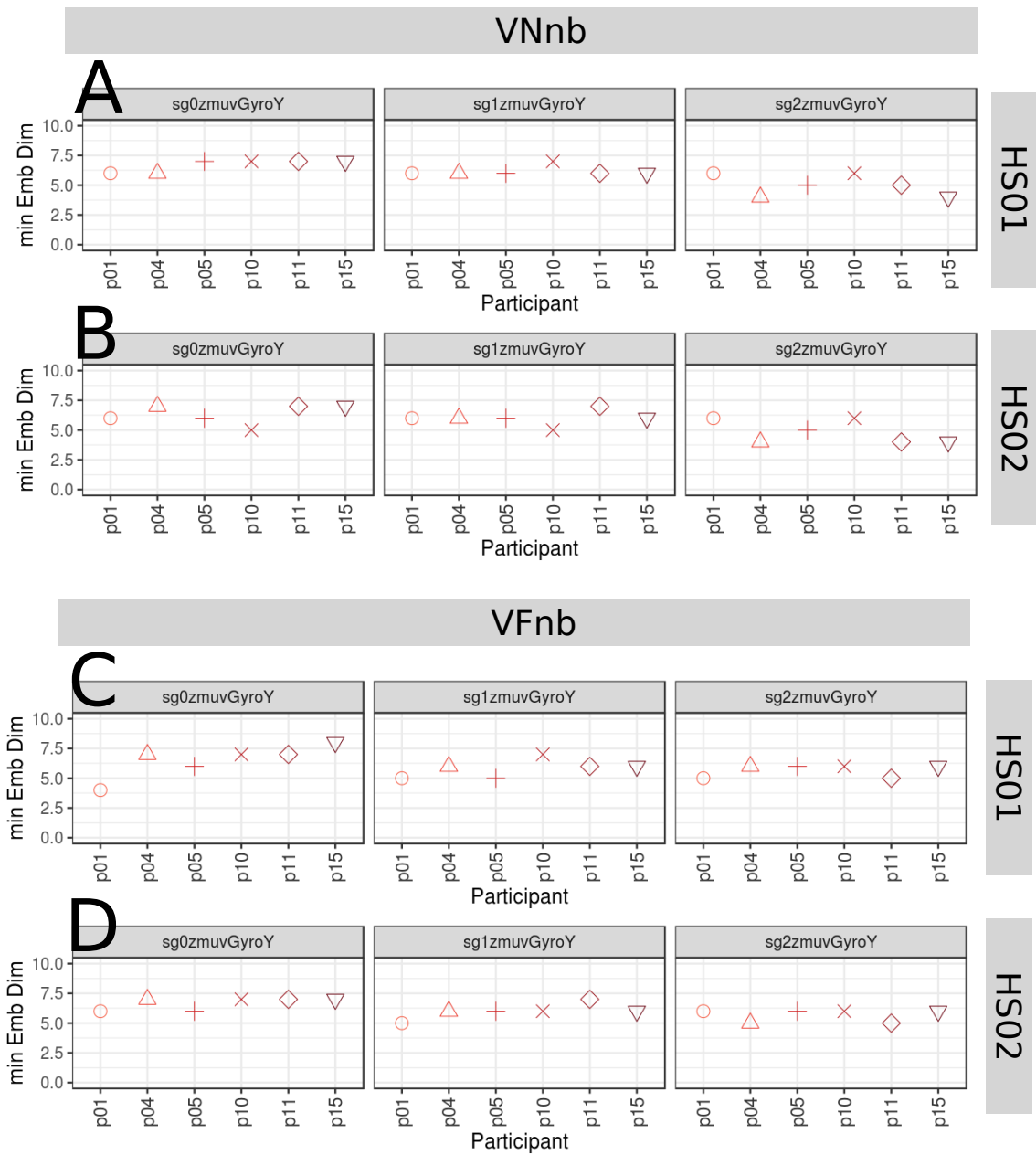


Fig. E.9 **Minimum embedding dimensions for vertical arm movements (no beat)**. (A, B) Vertical Normal with no beat (VNnb), and (C, D) Vertical Faster with no beat (VFnb) movements. (A, C) Sensor 01 attached to the participant (HS01), and (B, D) sensor 02 attached to the participant (HS02). Minimum embedding dimensions are for six participants (p01, p04, p05, p10, p11, p15) with three smoothed signals (sg0zmvGyroZ, sg1zmvGyroZ and sg2zmvGyroZ) and window length of 10-sec (500 samples). R code to reproduce the figure is available at [GitHub](#).

## Additional Results for HII experiment

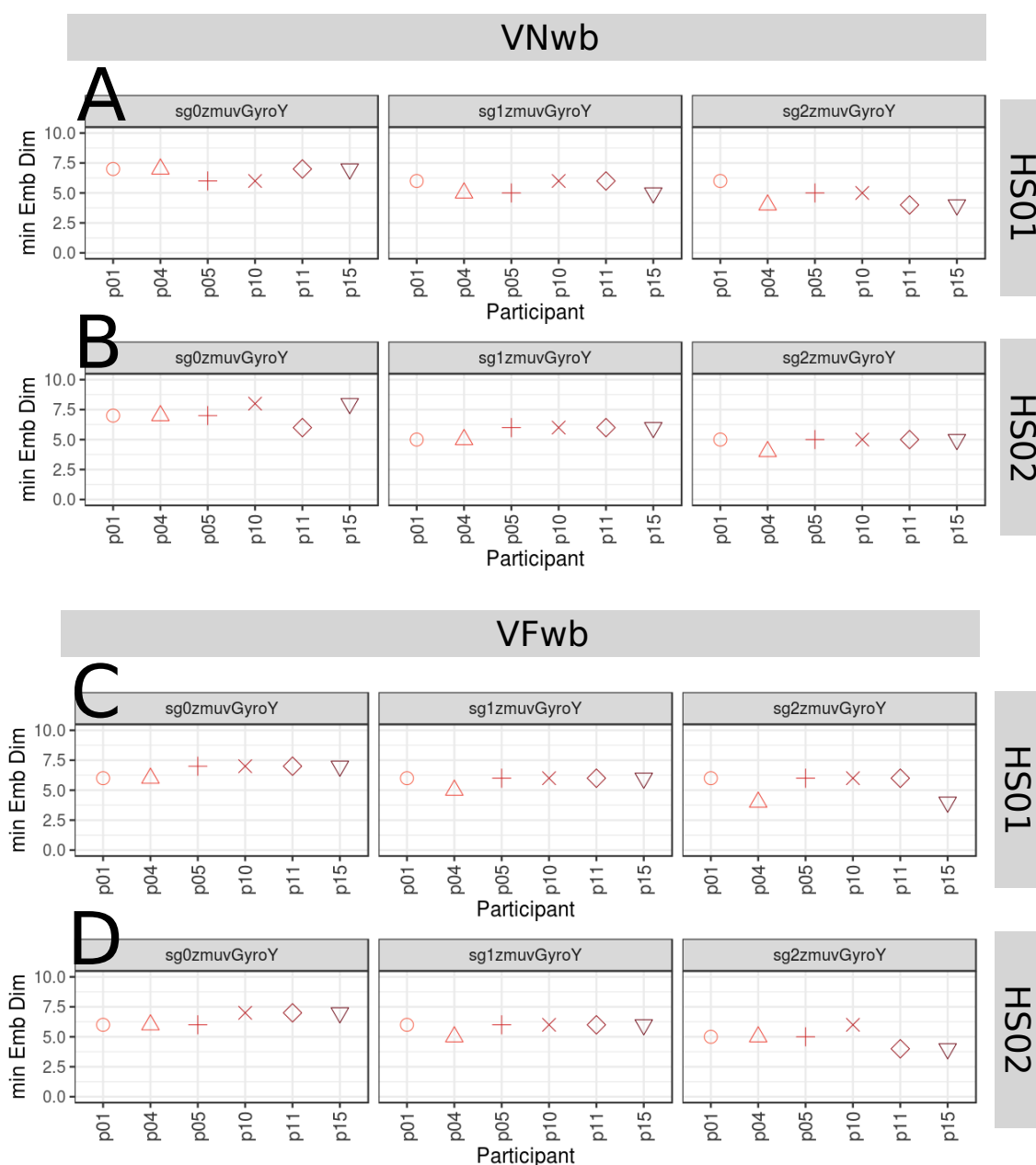


Fig. E.10 **Minimum embedding dimensions for vertical arm movements (with beat)**. (A, B) Vertical Normal with beat (VNwb), and (C, D) Vertical Faster with beat (VFwb) movements. (A, C) Sensor 01 attached to the participant (HS01), and (B, D) sensor 02 attached to the participant (HS02). Minimum embedding dimensions are for six participants (p01, p04, p05, p10, p11, p15) with three smoothed signals (sg0zmvGyroZ, sg1zmvGyroZ and sg2zmvGyroZ) and window length of 10-sec (500 samples). R code to reproduce the figure is available at [GitHub](#).

### E.2.2 Minimum delay embedding values

The general behavior for horizontal and vertical arm movements with regards to the smoothness of the time series is that the first minimum AMI values increase as the increase of the smoothness which is due to smoothed AMI curves (Figs E.11, E.12, E.13 and E.14).

Fluctuations of minimum AMI values from sensor HS01 are more evident than for sensor HS02 for horizontal normal arm movements with no beat (Fig E.11(A, B)), whereas fluctuations of minimum AMI values from sensors HS01 and HS02 for horizontal faster arm movements with no beat appear to be similar (Fig E.11(C, D)). Similarly, fluctuations of minimum AMI values are more evidently for horizontal normal arm movements with beat (Fig E.12(A, B)) than horizontal faster arm movements with beat (Fig E.12(C, D)).

As smoothness increase, minimum AMI values for vertical normal arm movements with no beat appear to fluctuate more (Figs E.13(A, B)) than vertical faster arm movements with no beat (Figs E.13(C, D)), whereas for vertical normal and vertical faster arm movements with beat the fluctuation of minimum AMI values is more evidently, specially when comparing vertical normal arm movements (Figs E.14(A, B)) with vertical faster arm movements (Figs E.14(C, D)).



## Additional Results for HII experiment

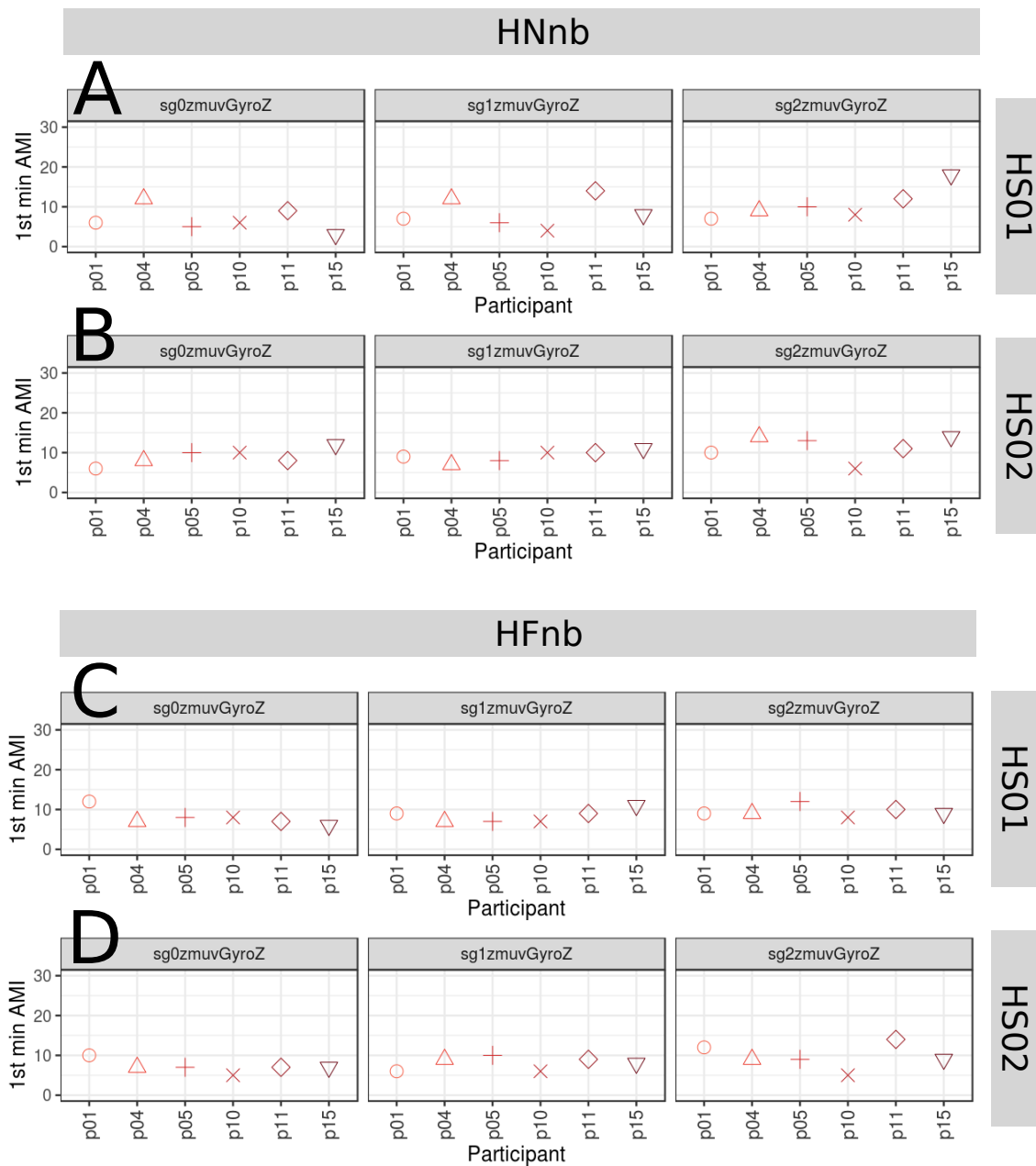


Fig. E.11 **First minimum AMI values for horizontal arm movements (no beat)**. (A, B) Horizontal Normal with no beat (HNnb), and (C, D) Horizontal Faster with no beat (HFnb) movements. (A, C) Sensor attached to the participant (HS01), and (B, D) sensor attached to the participant (HS02). First minimum AMI values are for six participants (p01, p04, p05, p10, p11, p15) with three smoothed signals (sg0zmuVgyroZ, sg1zmuVgyroZ and sg2zmuVgyroZ) and window length of 10-sec (500 samples). R code to reproduce the figure is available at [GitHub](#).

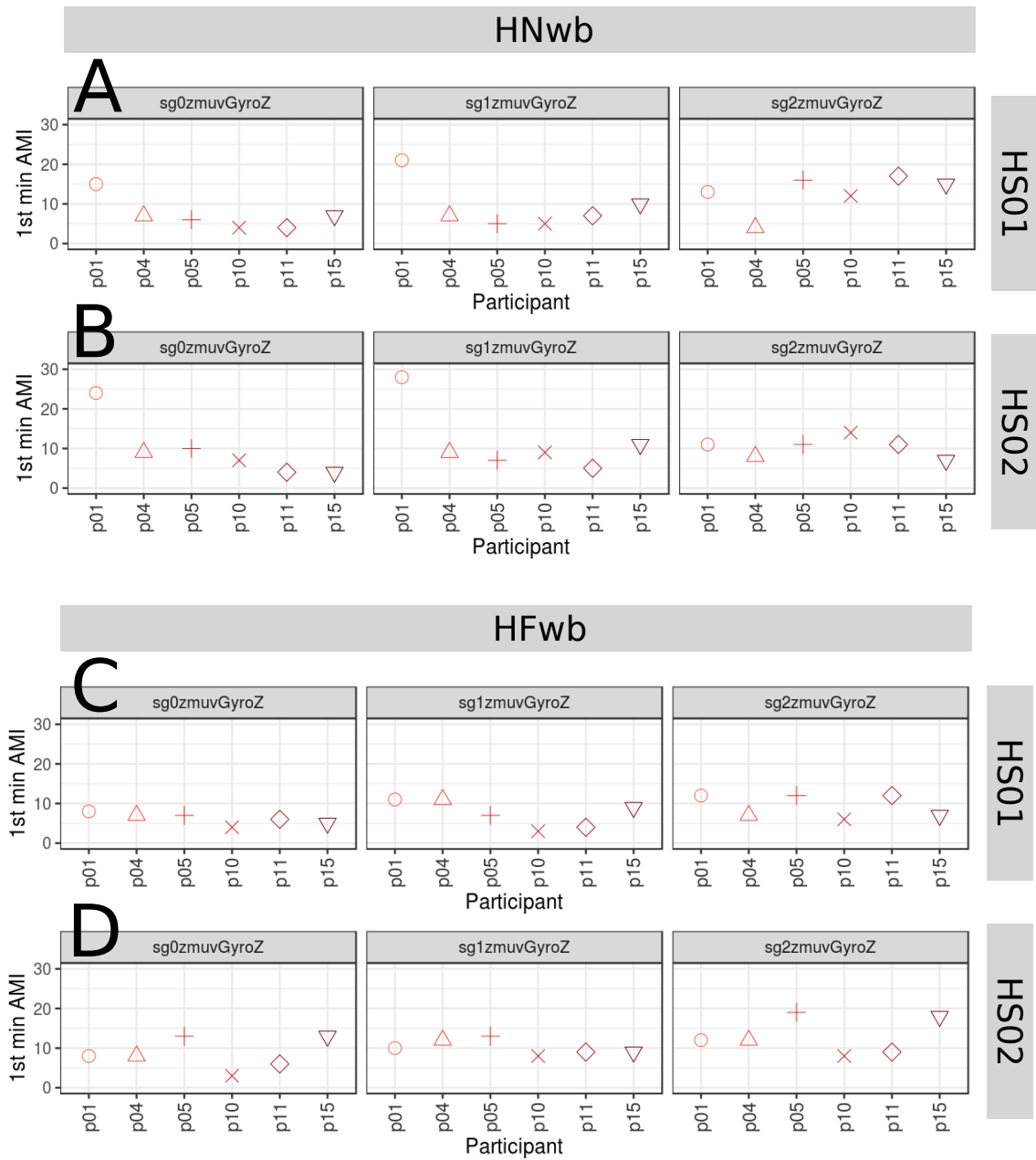


Fig. E.12 **First minimum AMI values for horizontal arm movements (with beat)**. (A, B) Horizontal Normal with beat (HNwb), and (C, D) Horizontal Faster with beat (HFwb) movements. (A, C) Sensor attached to the participant (HS01), and (B, D) sensor attached to the participant (HS02). First minimum AMI values are for six participants (p01, p04, p05, p10, p11, p15) with three smoothed signals (sg0zmvGyroZ, sg1zmvGyroZ and sg2zmvGyroZ) and window length of 10-sec (500 samples). R code to reproduce the figure is available at [GitHub](#).

## Additional Results for HII experiment

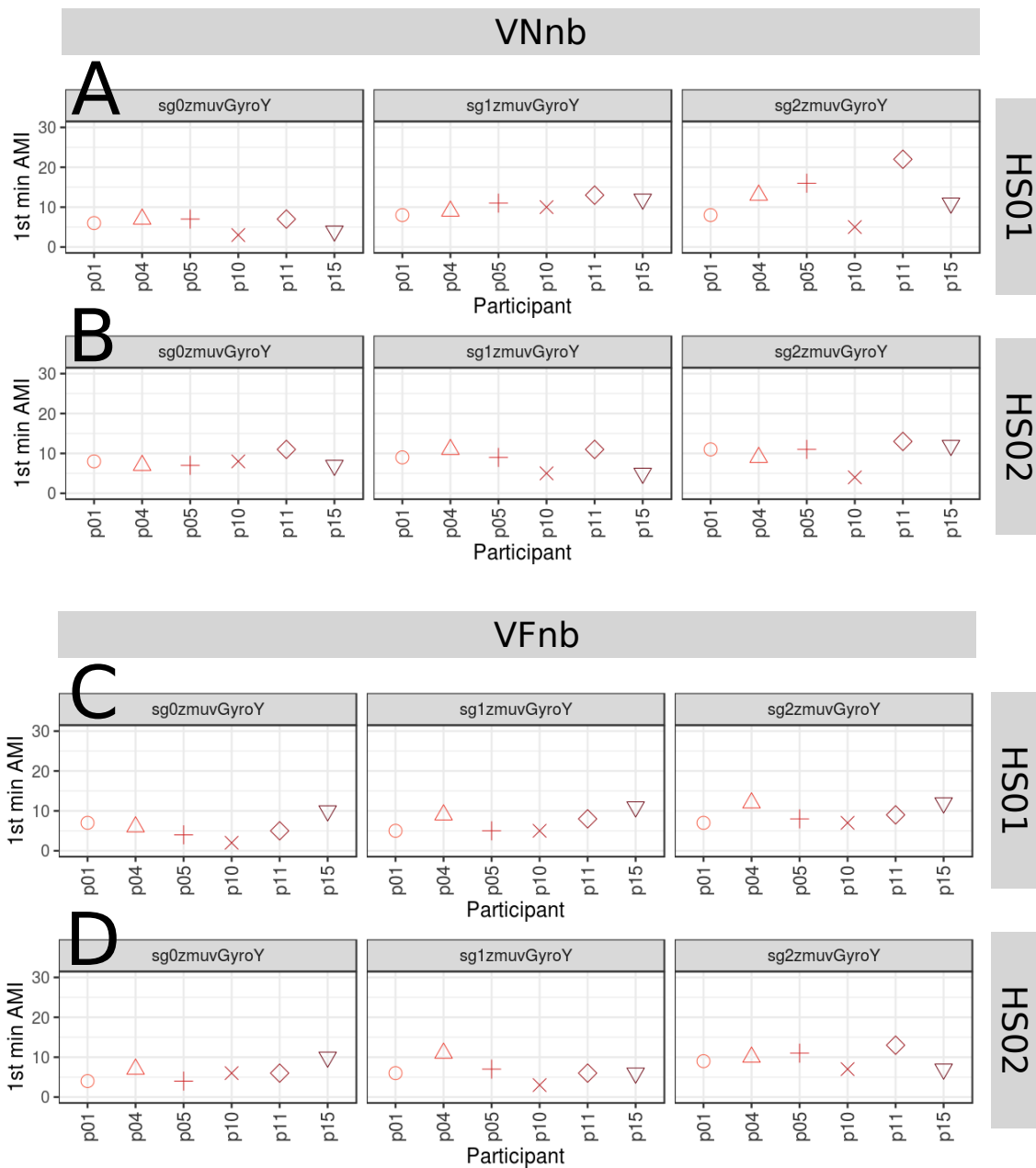


Fig. E.13 **First minimum AMI values for vertical arm movements (no beat).** (A, B) Vertical Normal with no beat (VNB), and (C, D) Vertical Faster with no beat (VFNB) movements. (A, C) Sensor attached to the participant (HS01), and (B, D) sensor attached to the participant (HS02). First minimum AMI values are for six participants (p01, p04, p05, p10, p11, p15) with three smoothed signals (sg0zmuvGyroZ, sg1zmuvGyroZ and sg2zmuvGyroZ) and window length of 10-sec (500 samples). R code to reproduce the figure is available at [GitHub](#).

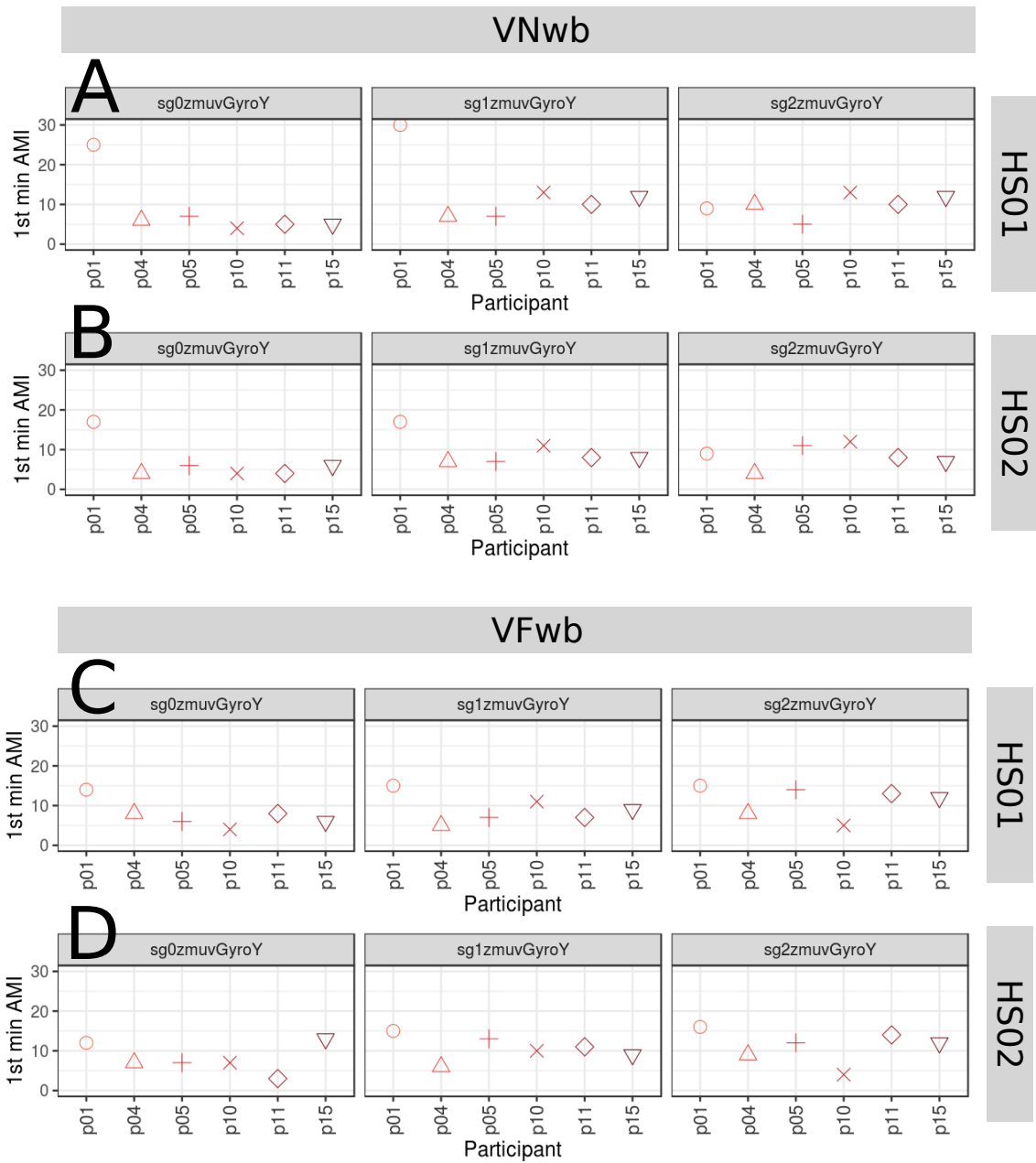


Fig. E.14 **First minimum AMI values for vertical arm movements (with beat)**. (A, B) Vertical Normal with beat (VNwb), and (C, D) Vertical Faster with beat (VFwb) movements. (A, C) Sensor attached to the participant (HS01), and (B, D) sensor attached to the participant (HS02). First minimum AMI values are for six participants (p01, p04, p05, p10, p11, p15) with three smoothed signals (sg0zmuvGyroZ, sg1zmuvGyroZ and sg2zmuvGyroZ) and window length of 10-sec (500 samples). R code to reproduce the figure is available at [\[4\]](#).

### E.3 RSSs

The following Figs. E.17, E.18, E.15, E.16, E.21, E.22, E.19, E.20 illustrate reconstructed state spaces of participant  $p04$  with a window length size of 500 samples. We refer the reader to download the data and code at Xochicale (2019) for the remained window size lengths and other participants.

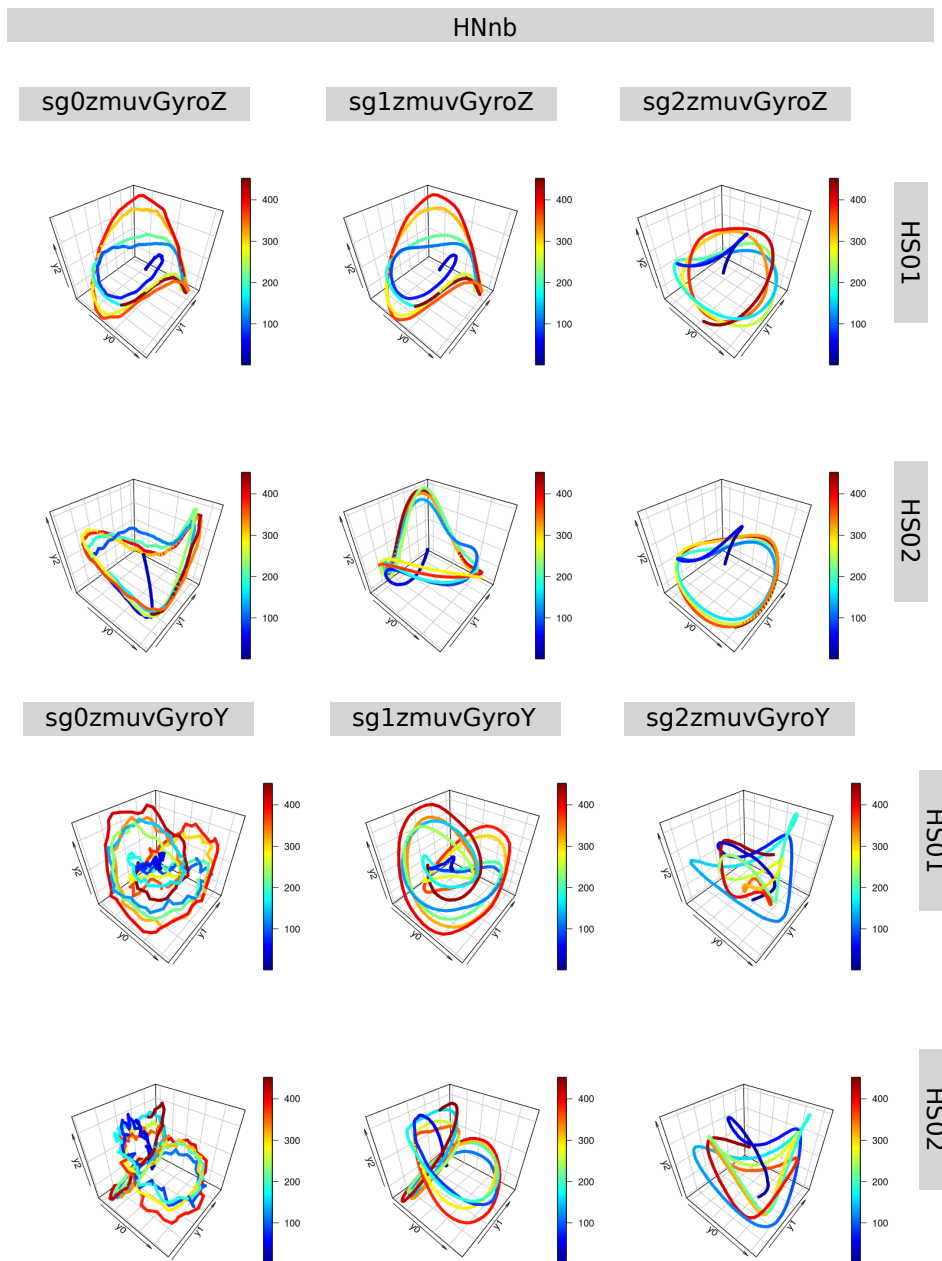


Fig. E.15 **RSSs for horizontal normal arm movements (no beat)**. Reconstructed state spaces of participant  $p04$  with time series for raw-normalised (sg0), normalised-smoothed 1 (sg1) and normalised-smoothed 2 (sg2), with sensors attached to the participant (HS01, HS02). Reconstructed state spaces were computed with embedding parameters  $\bar{m}_0 = 6$ ,  $\bar{\tau}_0 = 10$ . R code to reproduce the figure is available at [\[42\]](#).

## Additional Results for HII experiment

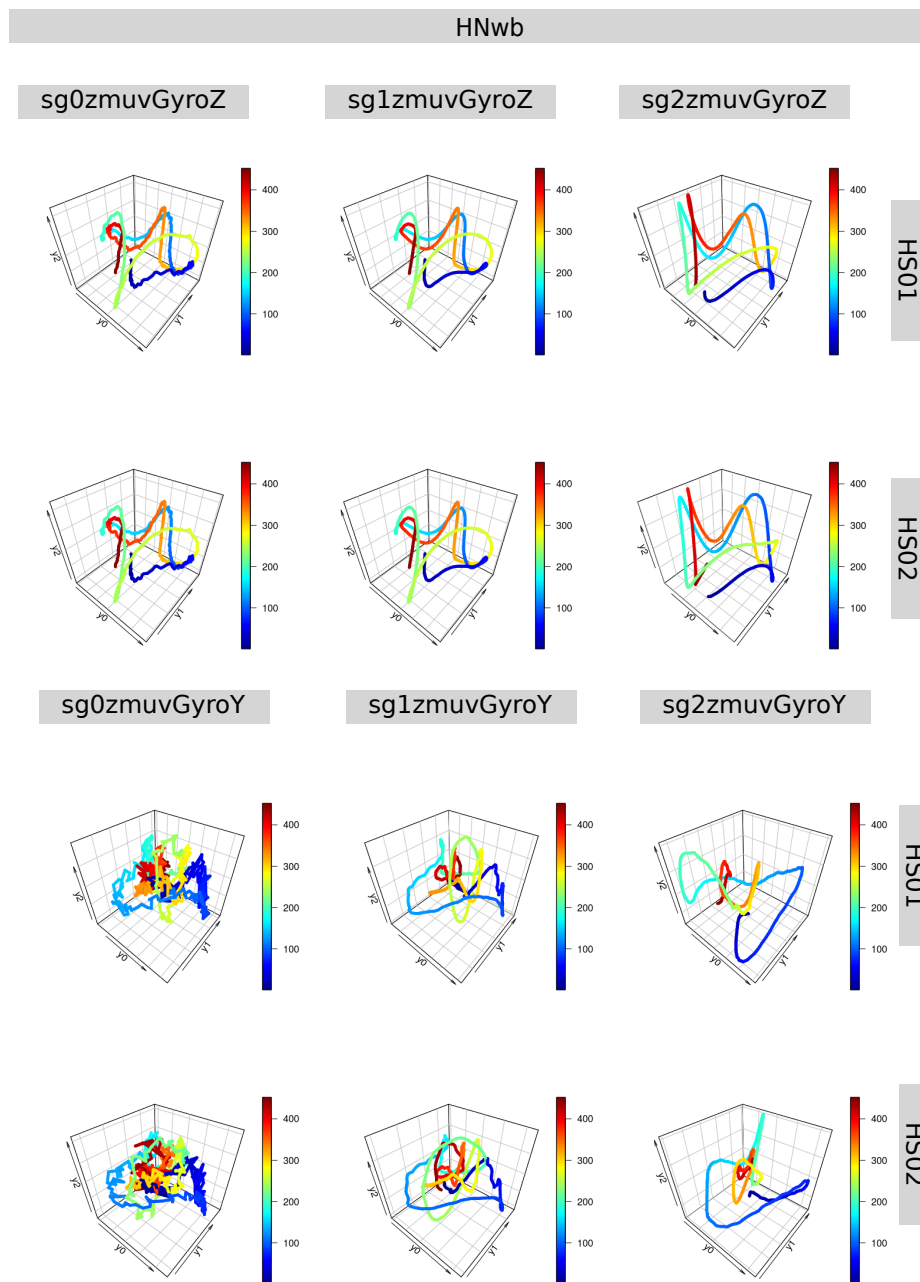


Fig. E.16 **RSSs for horizontal normal arm movements (with beat)**. Reconstructed state spaces of participant  $p04$  with time series for raw-normalised (sg0), normalised-smoothed 1 (sg1) and normalised-smoothed 2 (sg2), with sensors attached to the participant (HS01, HS02). Reconstructed state spaces were computed with embedding parameters  $\overline{m}_0 = 6$ ,  $\overline{\tau}_0 = 10$ . R code to reproduce the figure is available at [\[4\]](#).

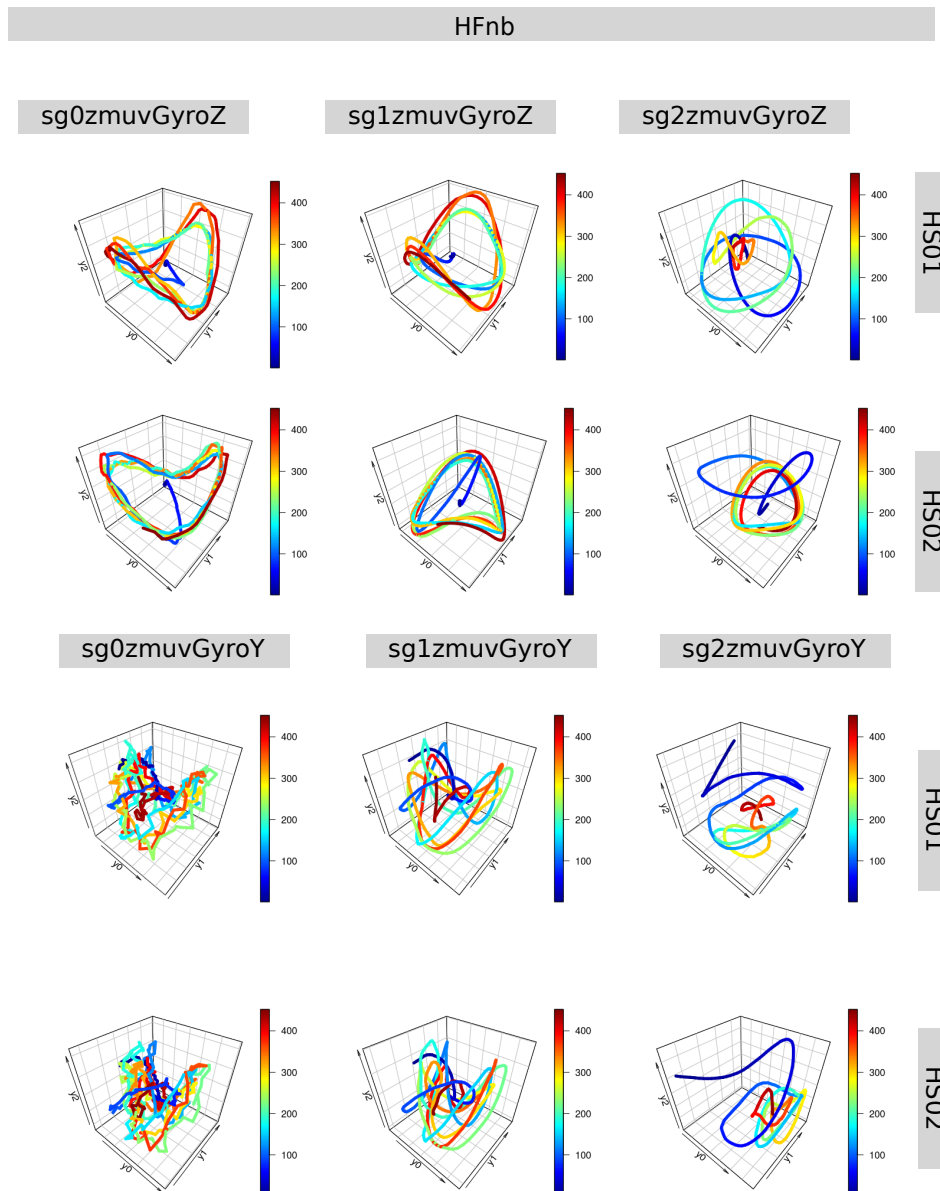


Fig. E.17 **RSSs for horizontal faster arm movements (no beat)**. Reconstructed state spaces of participant *p04* with time series for raw-normalised (sg0), normalised-smoothed 1 (sg1) and normalised-smoothed 2 (sg2), with sensors attached to the participant (HS01, HS02). Reconstructed state spaces were computed with embedding parameters  $\bar{m}_0 = 6$ ,  $\bar{\tau}_0 = 10$ . R code to reproduce the figure is available at [\[42\]](#).



## Additional Results for HII experiment

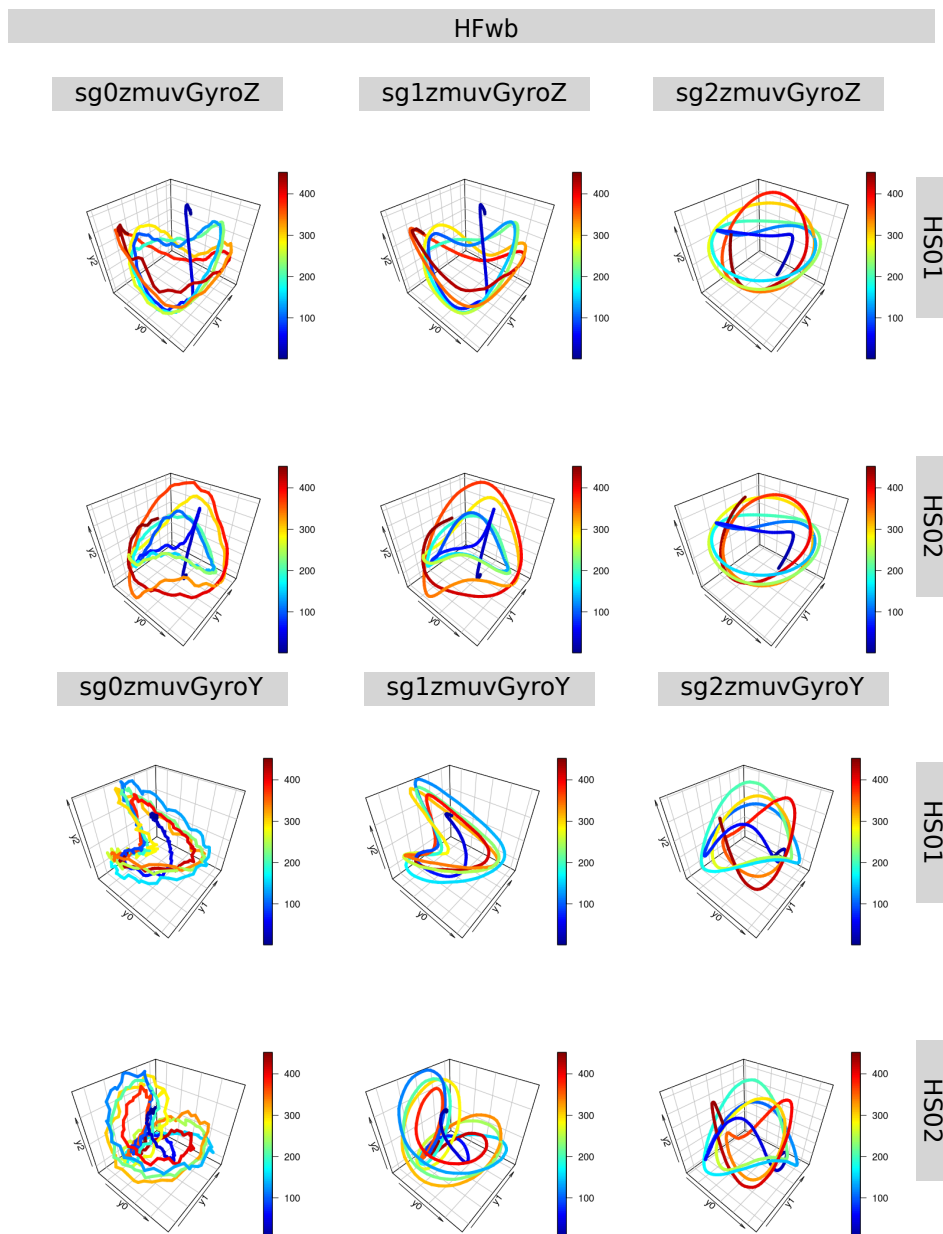


Fig. E.18 **RSSs for horizontal faster arm movements (with beat)**. Reconstructed state spaces of participant  $p04$  with time series for raw-normalised (sg0), normalised-smoothed 1 (sg1) and normalised-smoothed 2 (sg2), with sensors attached to the participant (HS01, HS02). Reconstructed state spaces were computed with embedding parameters  $\overline{m}_0 = 6$ ,  $\overline{\tau}_0 = 10$ . R code to reproduce the figure is available at [\[4\]](#).

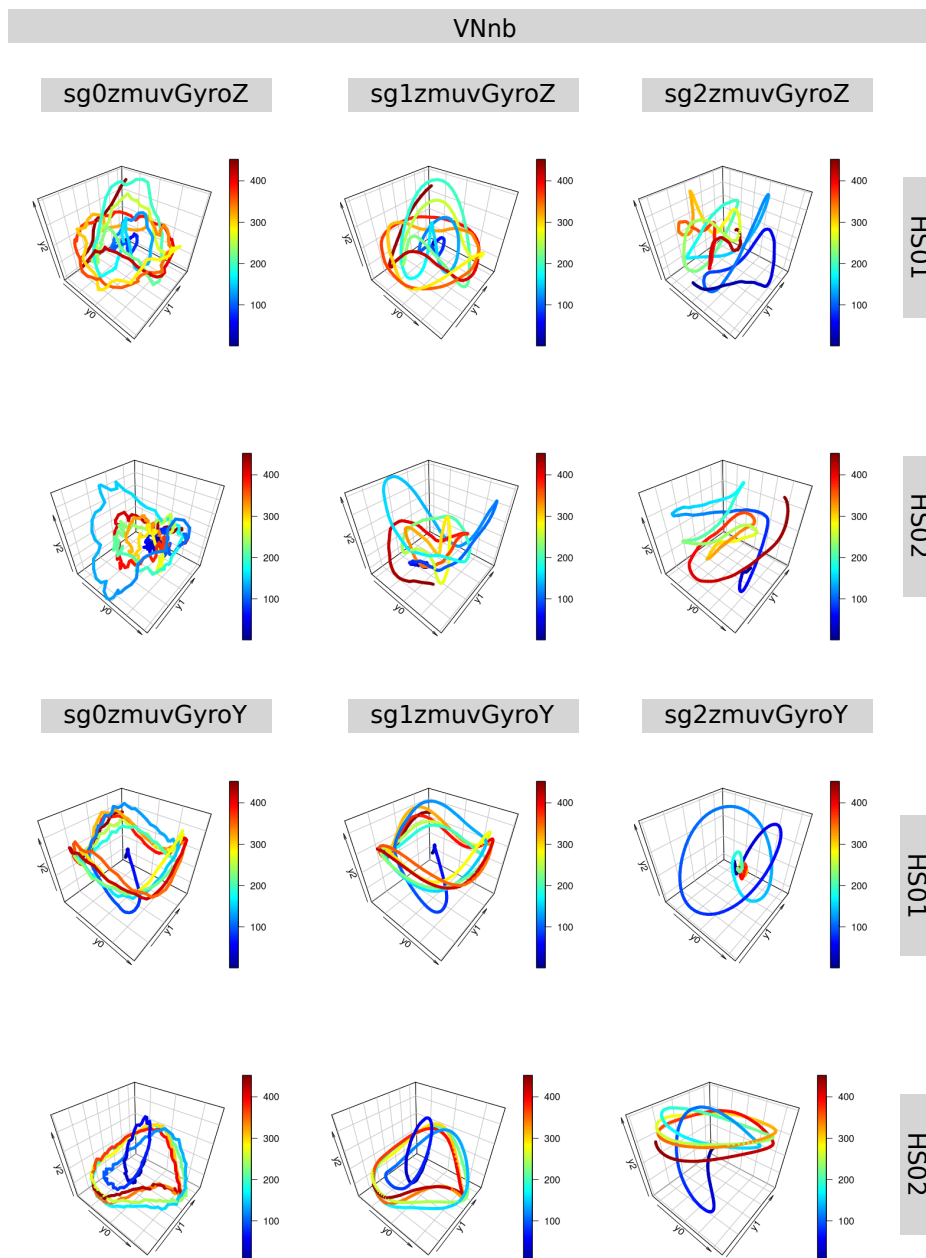


Fig. E.19 **RSSs for vertical normal arm movements (no beat)**. Reconstructed state spaces of participant  $p04$  with time series for raw-normalised (sg0), normalised-smoothed 1 (sg1) and normalised-smoothed 2 (sg2), with sensors attached to the participant (HS01, HS02). Reconstructed state spaces were computed with embedding parameters  $\bar{m}_0 = 6$ ,  $\bar{\tau}_0 = 10$ . R code to reproduce the figure is available at [\[4\]](#).

## Additional Results for HII experiment

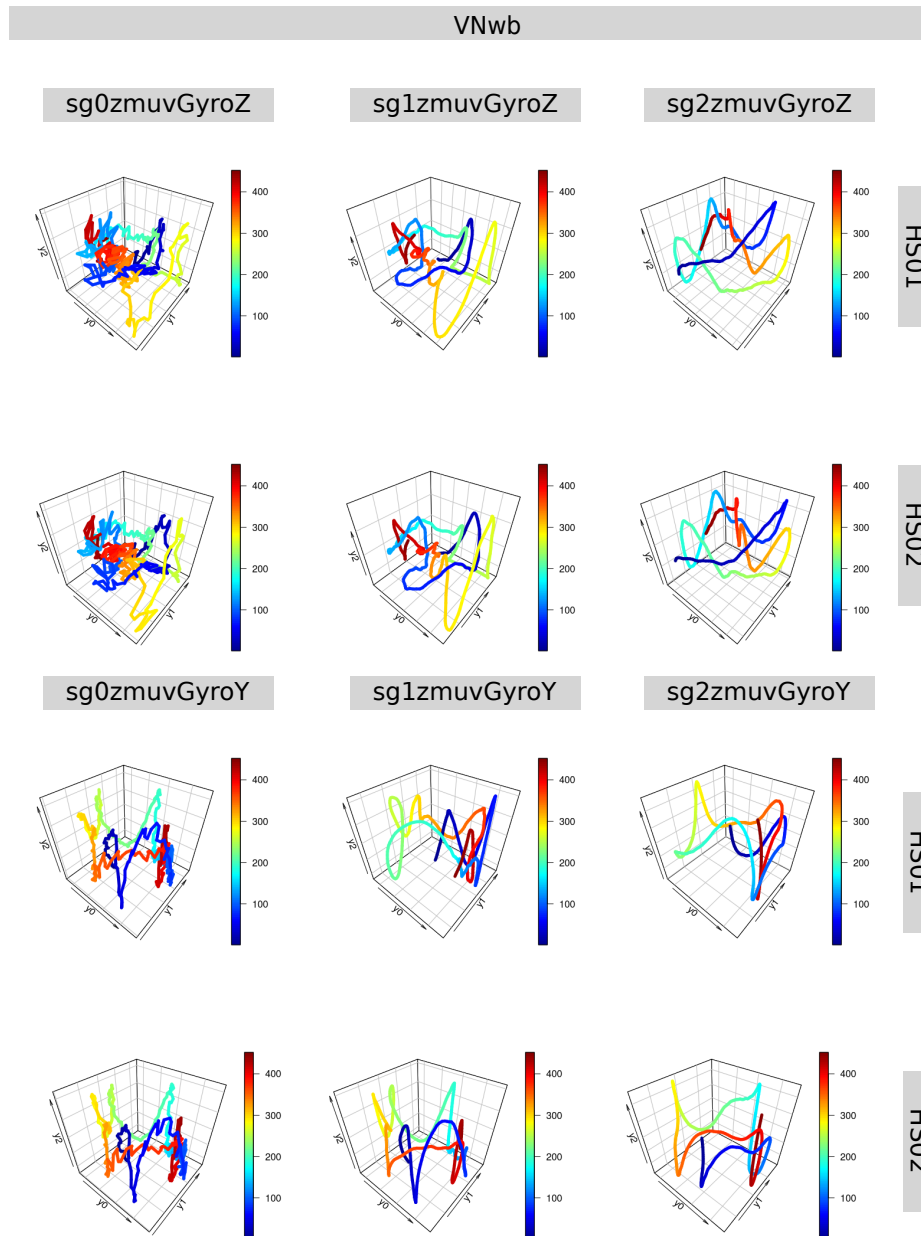


Fig. E.20 **RSSs for vertical normal arm movements (with beat)**. Reconstructed state spaces of participant  $p04$  with time series for raw-normalised (sg0), normalised-smoothed 1 (sg1) and normalised-smoothed 2 (sg2), with sensors attached to the participant (HS01, HS02). Reconstructed state spaces were computed with embedding parameters  $\bar{m}_0 = 6$ ,  $\bar{\tau}_0 = 10$ . R code to reproduce the figure is available at [GitHub](#).

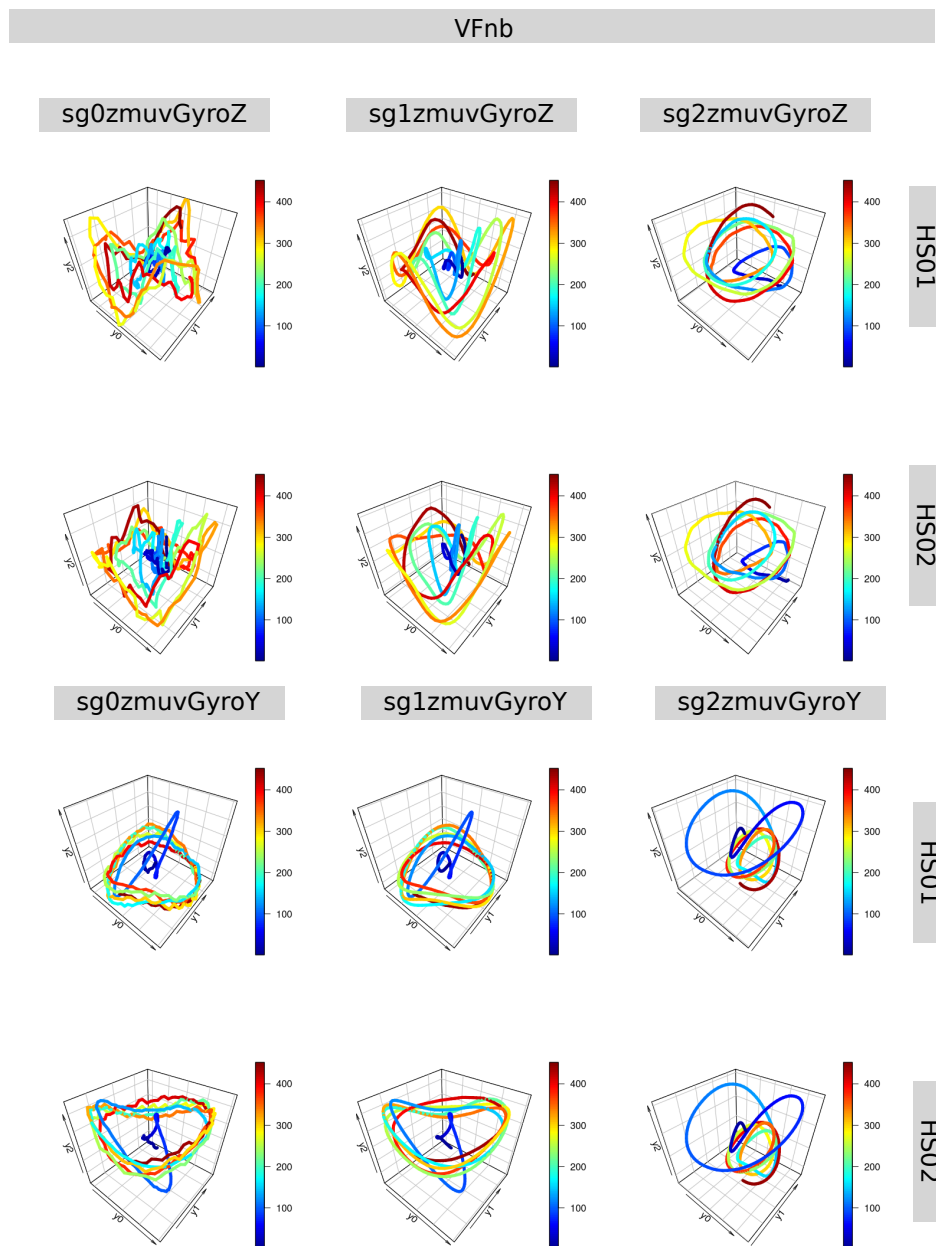


Fig. E.21 **RSSs for vertical faster arm movements (no beat)**. Reconstructed state spaces of participant *p04* with time series for raw-normalised (sg0), normalised-smoothed 1 (sg1) and normalised-smoothed 2 (sg2), with sensors attached to the participant (HS01, HS02). Reconstructed state spaces were computed with embedding parameters  $\bar{m}_0 = 6$ ,  $\bar{\tau}_0 = 10$ . R code to reproduce the figure is available at [\[42\]](#).

## Additional Results for HII experiment

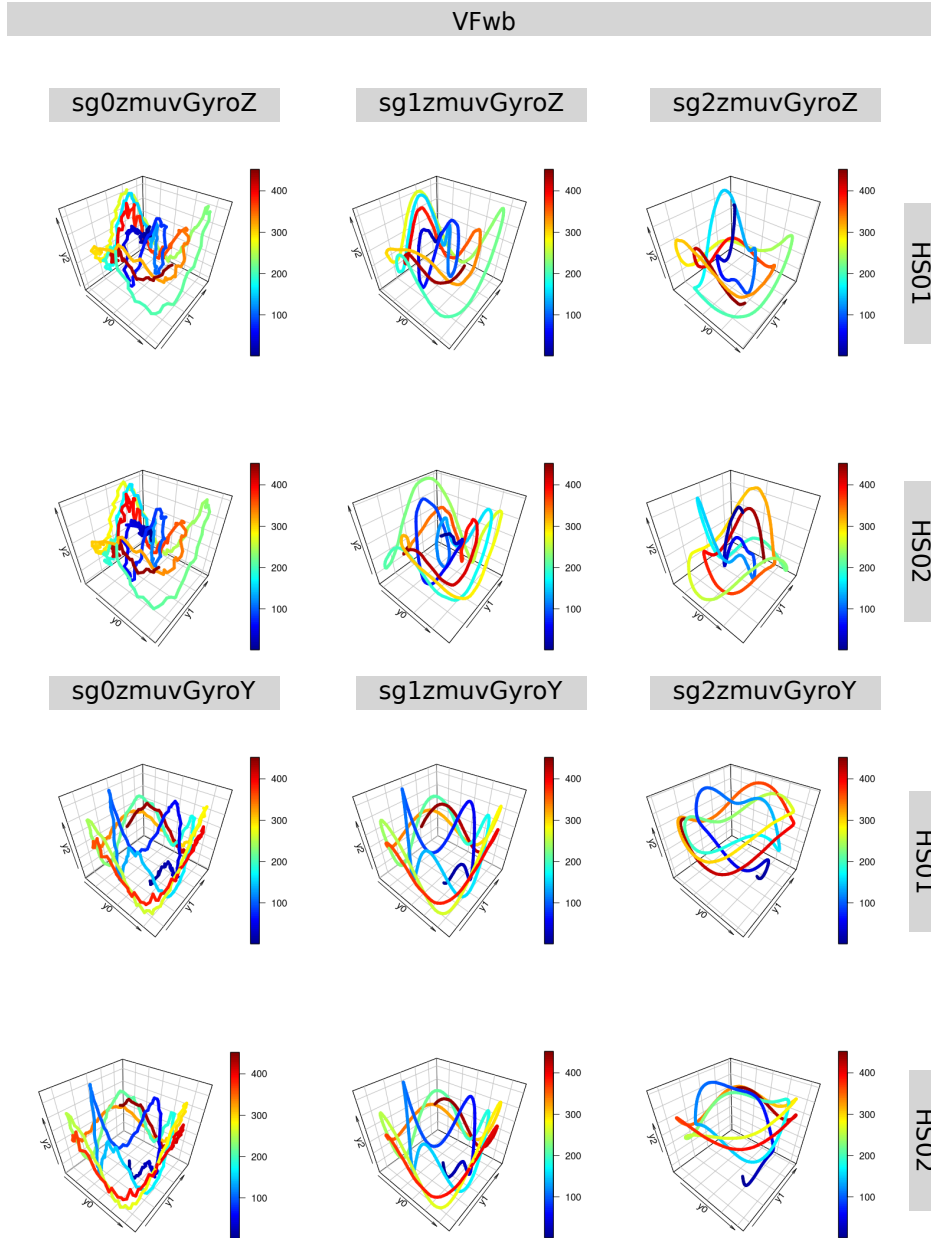


Fig. E.22 **RSSs for vertical faster arm movements (with beat)**. Reconstructed state spaces of participant  $p04$  with time series for raw-normalised (sg0), normalised-smoothed 1 (sg1) and normalised-smoothed 2 (sg2), with sensors attached to the participant (HS01, HS02). Reconstructed state spaces were computed with embedding parameters  $\overline{m}_0 = 6$ ,  $\overline{\tau}_0 = 10$ . R code to reproduce the figure is available at [GitHub](#).

## E.4 RPs

The following Figs. E.24, E.23, E.26, E.25 illustrate reconstructed state spaces of participant *p04* with a window length size of 500 samples. We refer the reader to download the data and code at Xochicale (2019) for the remained window size lengths and other participants.

## Additional Results for HII experiment

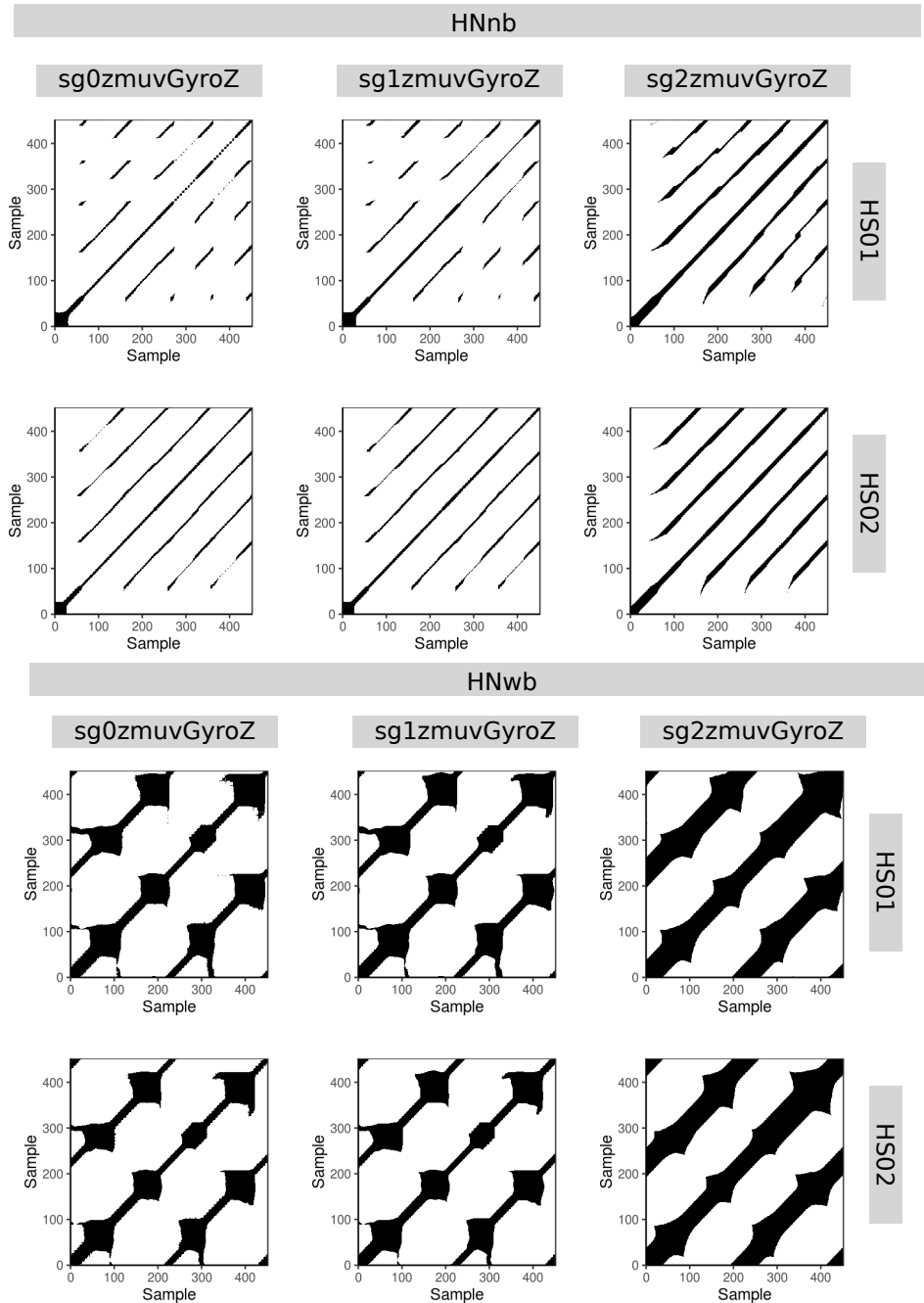


Fig. E.23 **RPs for horizontal normal arm movements.** Recurrence plots of participant  $p04$  for horizontal normal movements with no beat (HNNb) and horizontal normal movements with beat (HFWb). Time series for raw-normalised (sg0zmuvGyroZ), normalised-smoothed 1 (sg1zmuvGyroZ) and normalised-smoothed 2 (sg2zmuvGyroZ) with sensors attached to the participant (HS01, HS02). Recurrence plots were computed with embedding parameters  $\bar{m}_0 = 6$ ,  $\bar{\tau}_0 = 10$  and recurrence threshold  $\epsilon = 1$ . R code to reproduce the figure is available at [\[42\]](#).

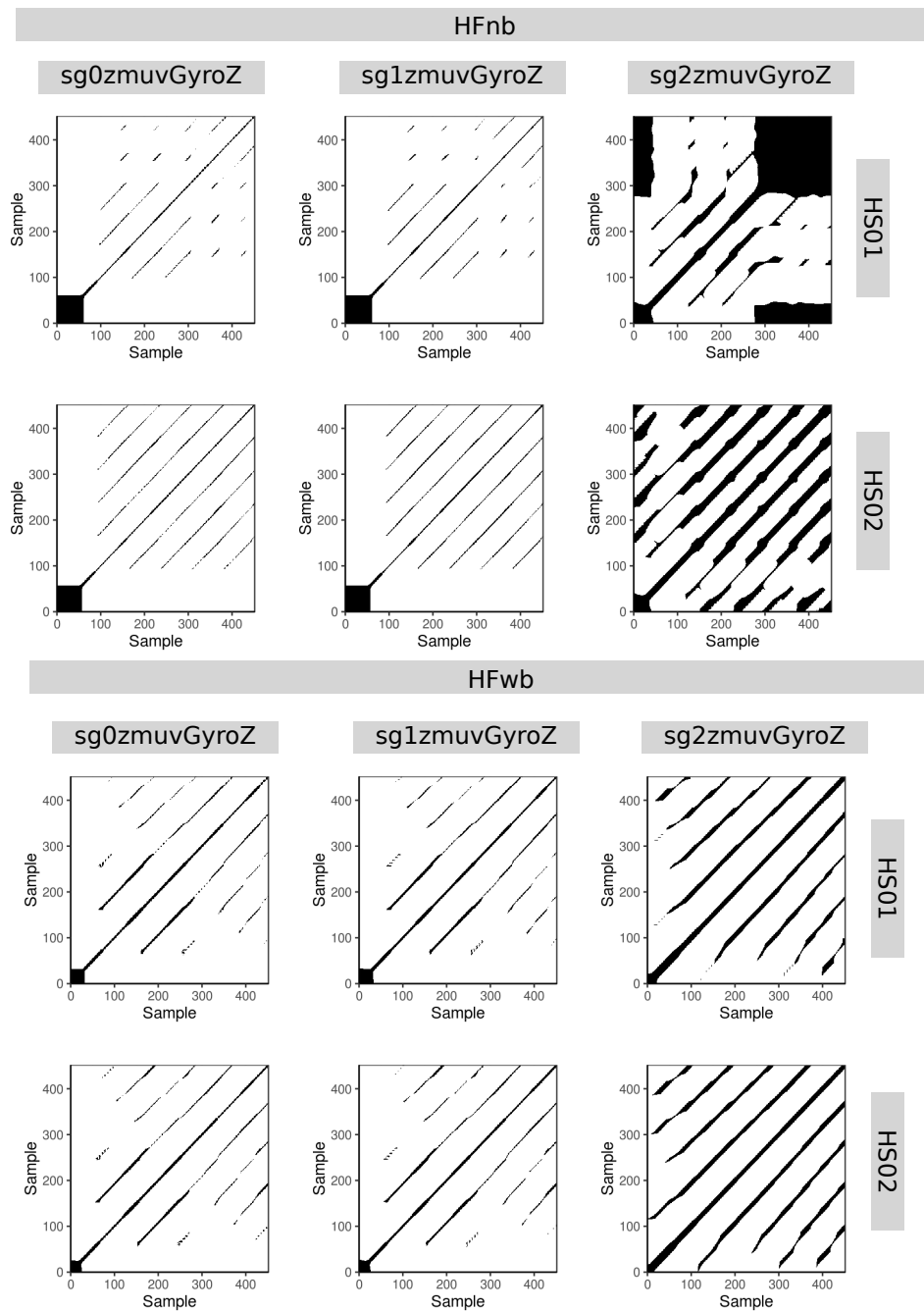


Fig. E.24 **RPs for horizontal faster arm movements.** Recurrence plots of participant  $p04$  for horizontal faster movements with no beat (HNnb) and horizontal faster movements with beat (HFwb). Time series for raw-normalised (sg0zmuvgyroZ), normalised-smoothed 1 (sg1zmuvgyroZ) and normalised-smoothed 2 (sg2zmuvgyroZ) with sensors attached to the participant (HS01, HS02). Recurrence plots were computed with embedding parameters  $\overline{m}_0 = 6$ ,  $\overline{\tau}_0 = 10$  and recurrence threshold  $\epsilon = 1$ . R code to reproduce the figure is available at [\[4\]](#).



## Additional Results for HII experiment

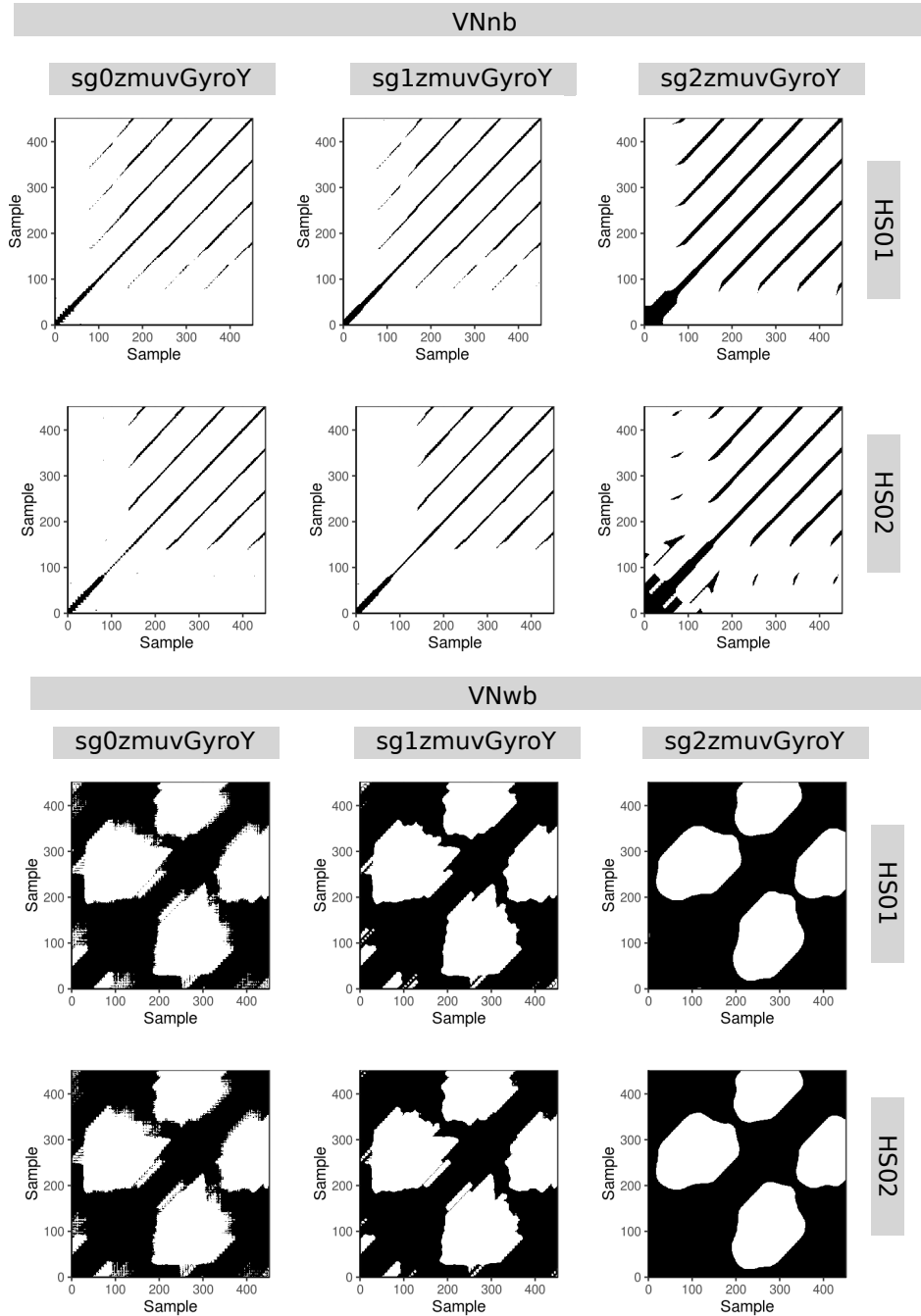


Fig. E.25 RPs for vertical normal arm movements. Recurrence plots of participant  $p04$  for horizontal normal movements with no beat (VNnb) and horizontal normal movements with beat (VFwb). Time series for raw-normalised (sg0zmuvgyroY), normalised-smoothed 1 (sg1zmuvgyroY) and normalised-smoothed 2 (sg2zmuvgyroY) with sensors attached to the participant (HS01, HS02). Recurrence plots were computed with embedding parameters  $\bar{m}_0 = 6$ ,  $\bar{\tau}_0 = 10$  and recurrence threshold  $\epsilon = 1$ . R code to reproduce the figure is available at [\[42\]](#).

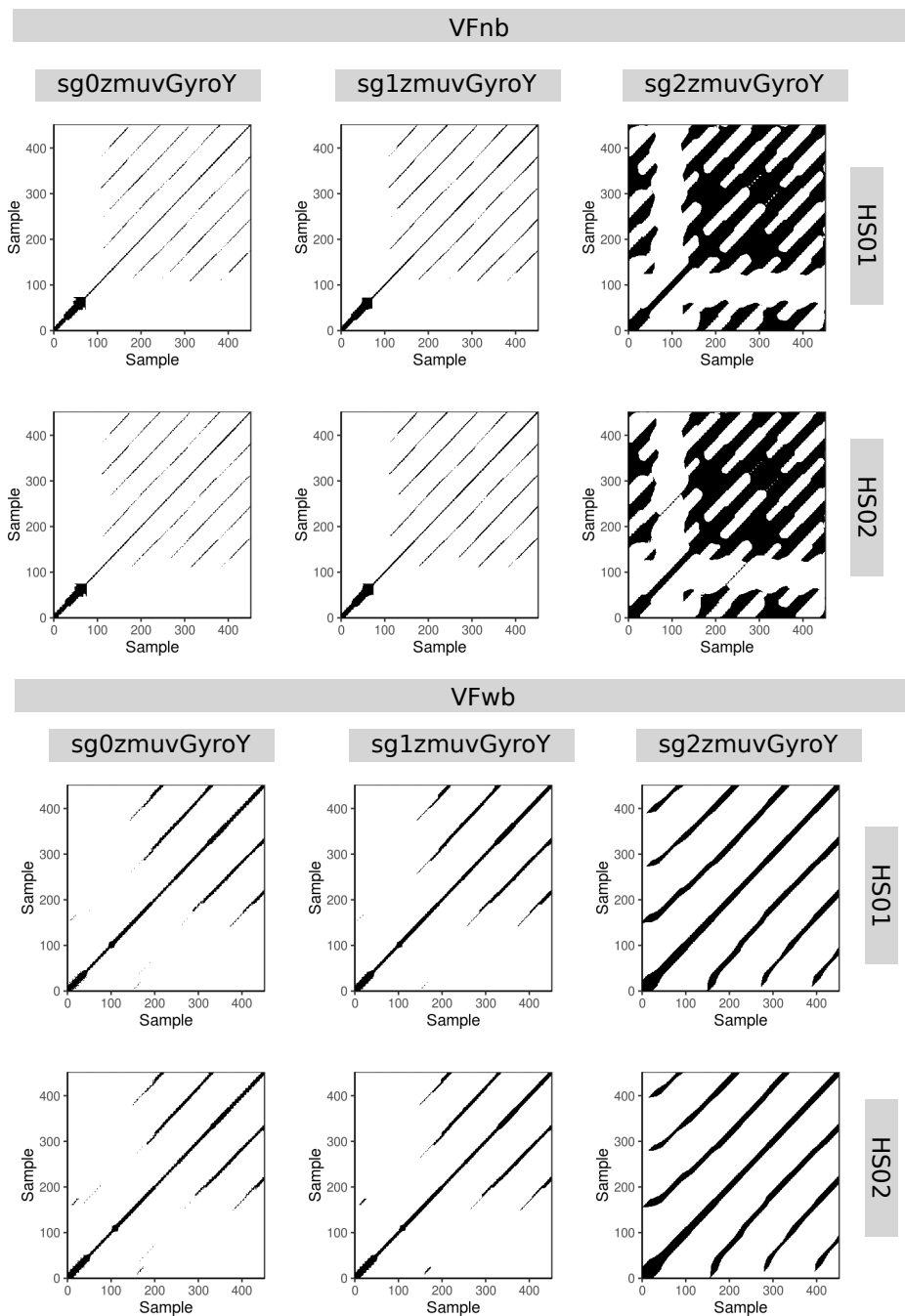


Fig. E.26 **RPs for vertical faster arm movements.** Recurrence plots of participant *p04* for horizontal faster movements with no beat (VFnb) and horizontal faster movements with beat (VFwb). Time series for raw-normalised (sg0zmvGyroY), normalised-smoothed 1 (sg1zmvGyroY) and normalised-smoothed 2 (sg2zmvGyroY) with sensors attached to the participant (HS01, HS02). Recurrence plots were computed with embedding parameters  $\overline{m}_0 = 6$ ,  $\overline{\tau}_0 = 10$  and recurrence threshold  $\epsilon = 1$ . R code to reproduce the figure is available at [\[4\]](#).

### E.5 RQAs

#### E.5.1 REC values

Figs E.27 and E.28 show REC values, representing the % of black dots in the RPs, for vertical and horizontal arm movements.

It can be noted in Fig E.27 that REC values present little differences when comparing sensor HS01 and HS02. Similarly, considering the smoothness of the time series, REC values for participants appear to be similar in each of the activities (HNnb, HNwb, HFnb, HFwb) for sg0zmuVgyroZ and sg1zmuVgyroZ, while REC values for sg2zmuVgyroZ appear to fluctuate a bit more. With regards to the type of activity, horizontal arm movements with beat (HNwb) appear to fluctuate more than other activities (HNnb, HFnb, HFwb). Also RET values appear to fluctuate more and be greater for faster arm movements whereas RET values for normal arm movements appear to be constant (Fig E.27).

Figs E.28 show RET values for vertical arm movements. It can be noted that RET values appear to be similar for sensors HS01 and HS02 and the smoothness effect in REC values is more evident for sg2zmuVgyroY than REC values for sg0zmuVgyroY and sg1zmuVgyroY. RET values appear to fluctuate more for vertical normal arm movements with beat (VNwb) than other activities (VNnb, VFnb, VFwb) and RET values for VNnb, VFnb and VFwb appear to be constant and show little fluctuation between participants.

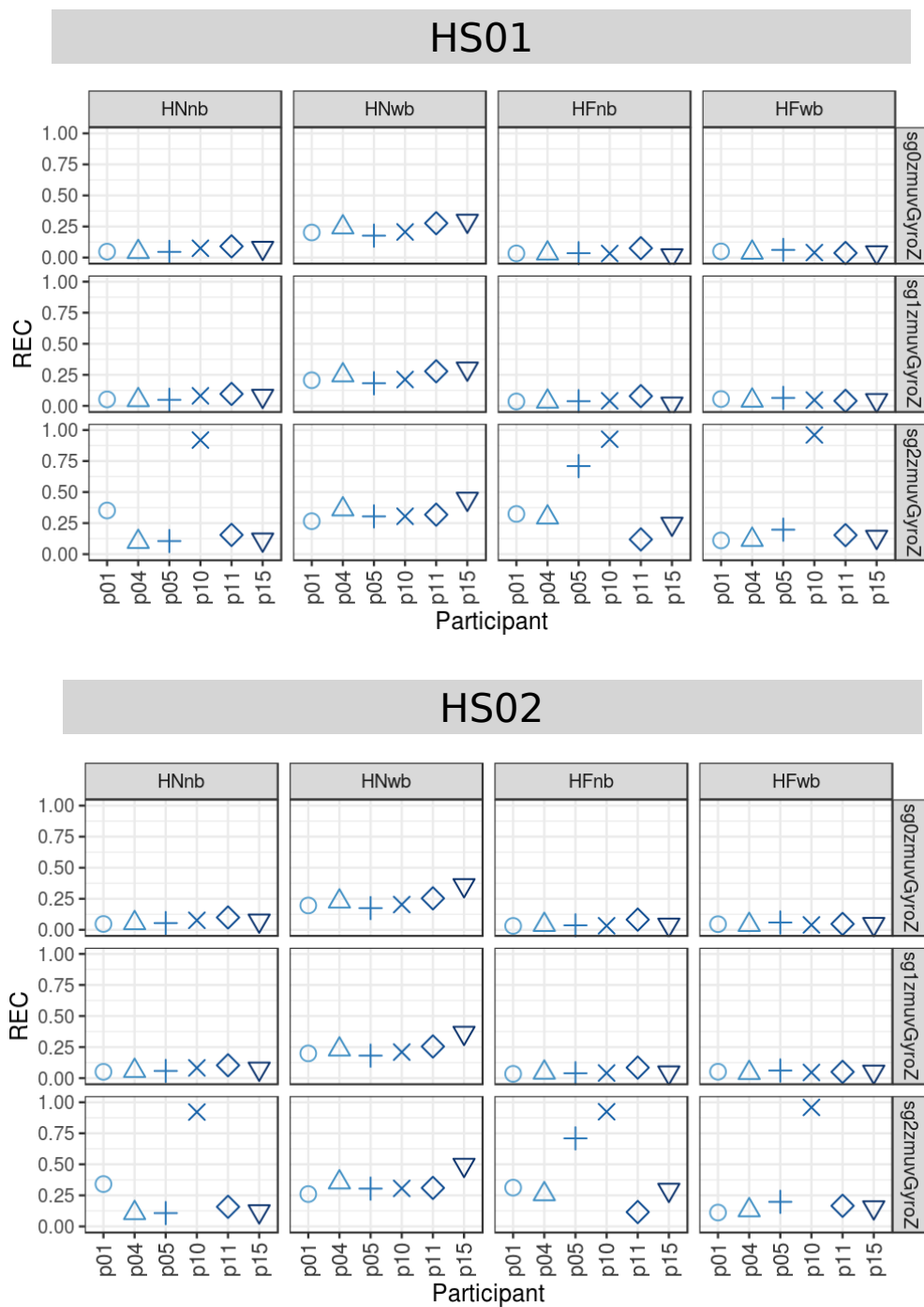


Fig. E.27 **REC values for horizontal arm movements.** REC values (representing % of black dots in the RPs) for 6 participants performing horizontal arm movements (HNNb, HNwb, HFnb, HFwb) for sensors HS01, HS02 and three smoothed-normalised axis of GyroZ (sg0zmvGyroZ, sg1zmvGyroZ and sg2zmvGyroZ). REC values were computed with embedding parameters  $\overline{m}_0 = 6$ ,  $\overline{\tau}_0 = 10$  and recurrence threshold  $\epsilon = 1$ . R code to reproduce the figure is available at [\[47\]](#).

## Additional Results for HII experiment

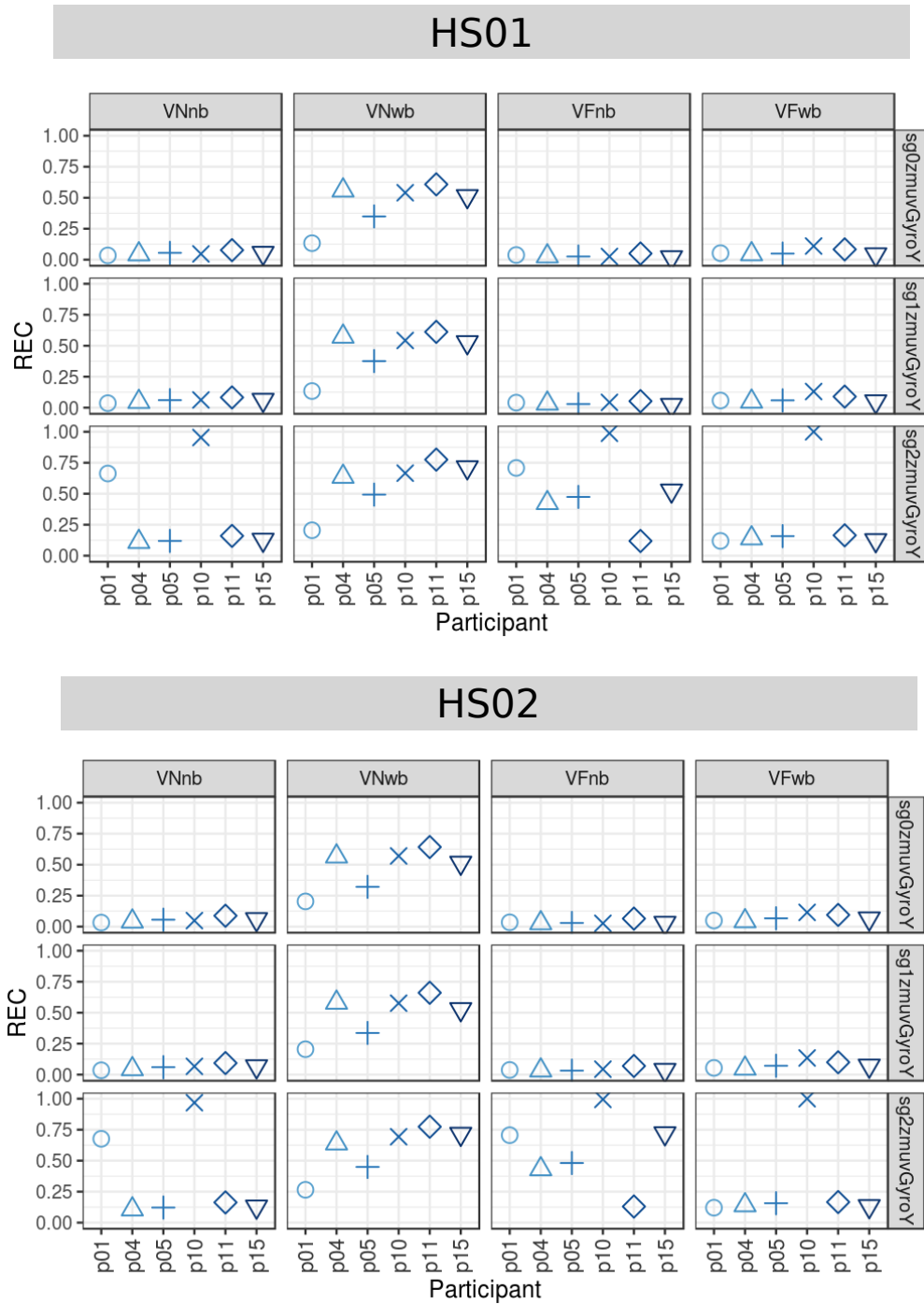


Fig. E.28 **REC values for vertical arm movements.** REC values (representing % of black dots in the RPs) for 6 participants performing vertical arm movements (VNnb, VNwb, VFnb, VFwb) for sensors HS01, HS02 and three smoothed-normalised axis of GyroZ (sg0zmuvgyroZ, sg1zmuvgyroZ and sg2zmuvgyroZ). REC values were computed with embedding parameters  $\overline{m}_0 = 6$ ,  $\overline{\tau}_0 = 10$  and recurrence threshold  $\epsilon = 1$ . R code to reproduce the figure is available at [\[45\]](#).

### E.5.2 DET values

DET values appear to be constant for any source of time series (Figs E.29 and E.30). For both horizontal and vertical arm movements, the increase of smoothness of time series appear to affect the smoothness of DET values by making them to appear more similar as the smoothness increase. Additionally, it can be noted more fluctuations of DET values for faster activities (HFnb, HFwb) than normal activities (HNnb, HNwb), specifically for sg0zmuvGyroY (Figs E.29, E.30).

## Additional Results for HII experiment

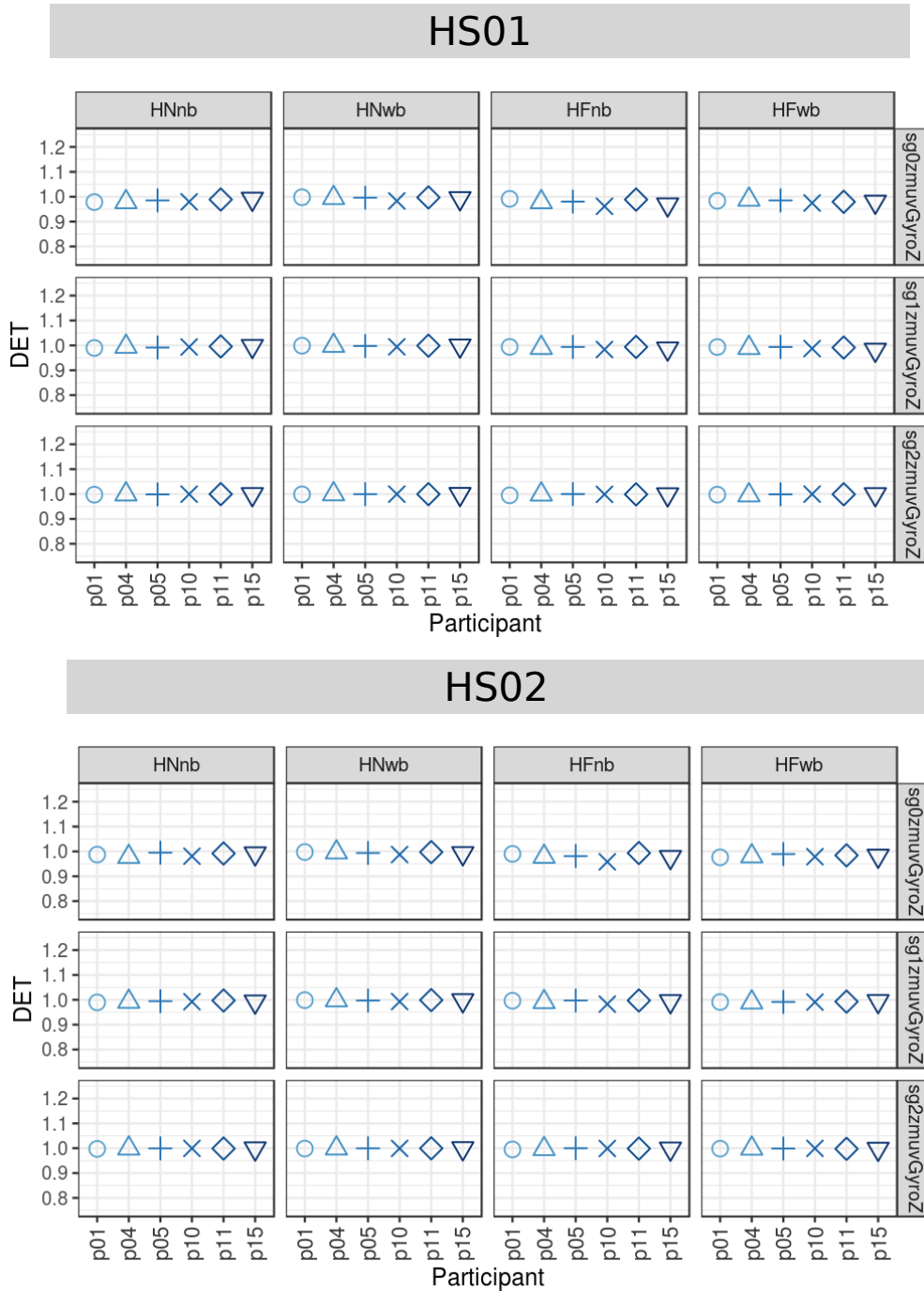


Fig. E.29 **DET values for horizontal arm movements.** DET values (representing predictability and organisation of the RPs) for 6 participants performing horizontal arm movements (HNNb, HNwb, HFnb, HFwb) for sensors HS01, HS02 and three smoothed-normalised axis of GyroZ (sg0zmuVgyroZ, sg1zmuVgyroZ and sg2zmuVgyroZ). DET values were computed with embedding parameters  $\overline{m}_0 = 6$ ,  $\overline{\tau}_0 = 10$  and recurrence threshold  $\epsilon = 1$ . R code to reproduce the figure is available at [\[4\]](#).

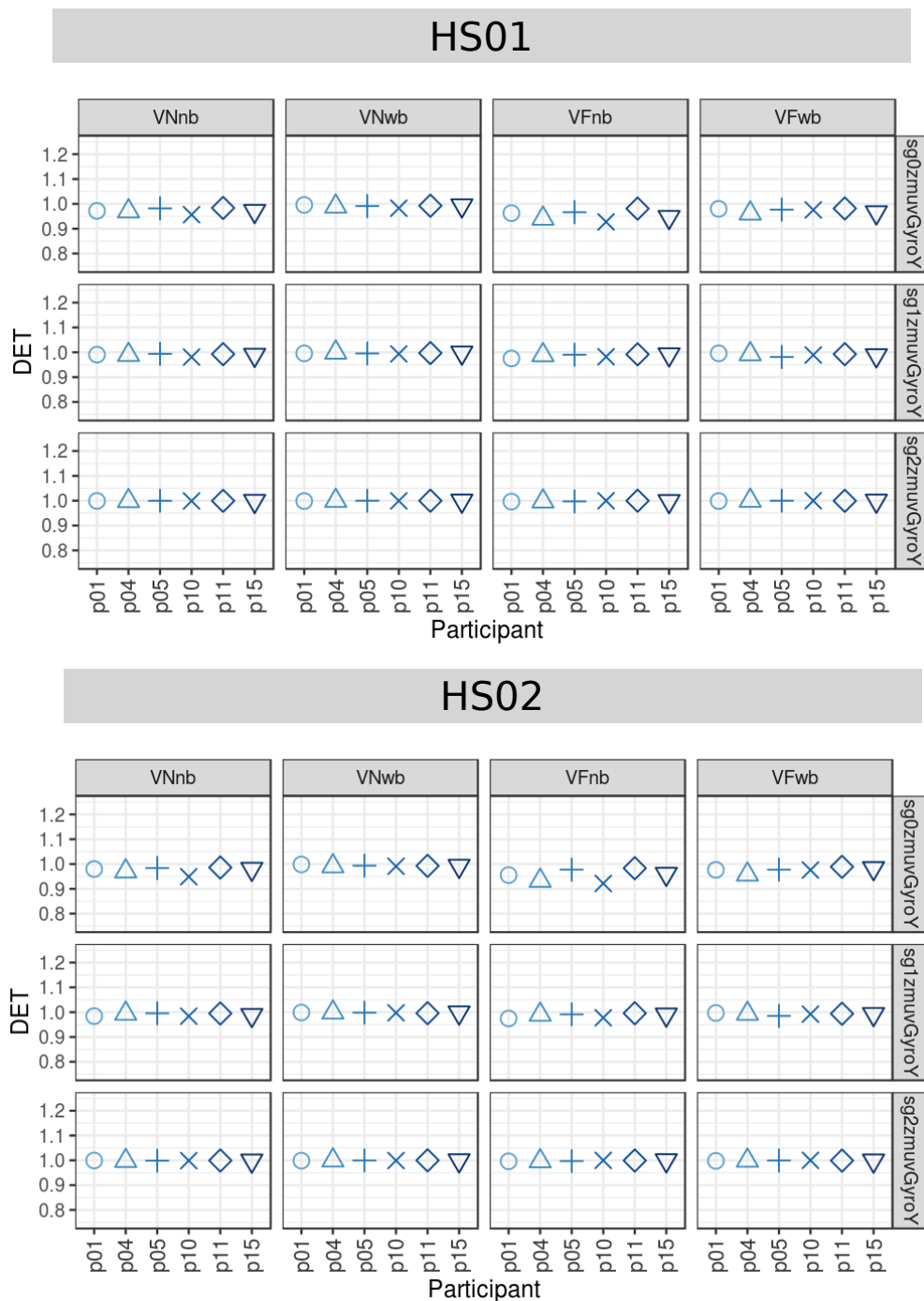


Fig. E.30 **DET values for vertical arm movements.** DET values (representing predictability and organisation of the RPs) for 6 participants performing vertical arm movements (VNnb, VNwb, VFnb, VFwb) for sensors HS01, HS02 and three smoothed-normalised axis of GyroY (sg0zmvGyroY, sg1zmvGyroY and sg2zmvGyroY). DET values were computed with embedding parameters  $\overline{m}_0 = 6$ ,  $\overline{\tau}_0 = 10$  and recurrence threshold  $\epsilon = 1$ . R code to reproduce the figure is available at [\[48\]](#).



### E.5.3 RATIO values

RATIO values for horizontal and vertical arm movements are shown in Figs E.31 and E.32.

The fluctuation of RATIO values for horizontal faster arm movements appear to be more notable than RATIO values for horizontal normal arm movements. RATIO values appear to be constant for activity HNwb than other activities (HNnb, HFnb, HFwb). Regarding the smoothness of time series, RATIO values appear to have similar values for sg0zmuVgyroZ and sg1zmuVgyroZ while RATIOS values are more uniform for sg2zmuVgyroZ. With regards to type of sensor, RET values appear to be similar for HS01 and HS02 with the exception of *p15* in HFnb activity (Figs E.31).

Figs E.32 show RATIO values for vertical arm movements. The fluctuation of RATIO values appears to be constant for the activity VNwb whereas other RATIO values for other activities (VNnb, VFnb, VFwb) appear to fluctuate more. The smoothness of the time series affects only the RATIO values for sg2zmuVgyroY as these appear to be constant, while RET values for sg0zmuVgyroY and sg1zmuVgyroZ appear to have the similar RATIO values. Additionally, RATIO values for type of sensors HS01 and HS02 appear to show similar values as well, with the exception of *p15* in the VFnb activity.

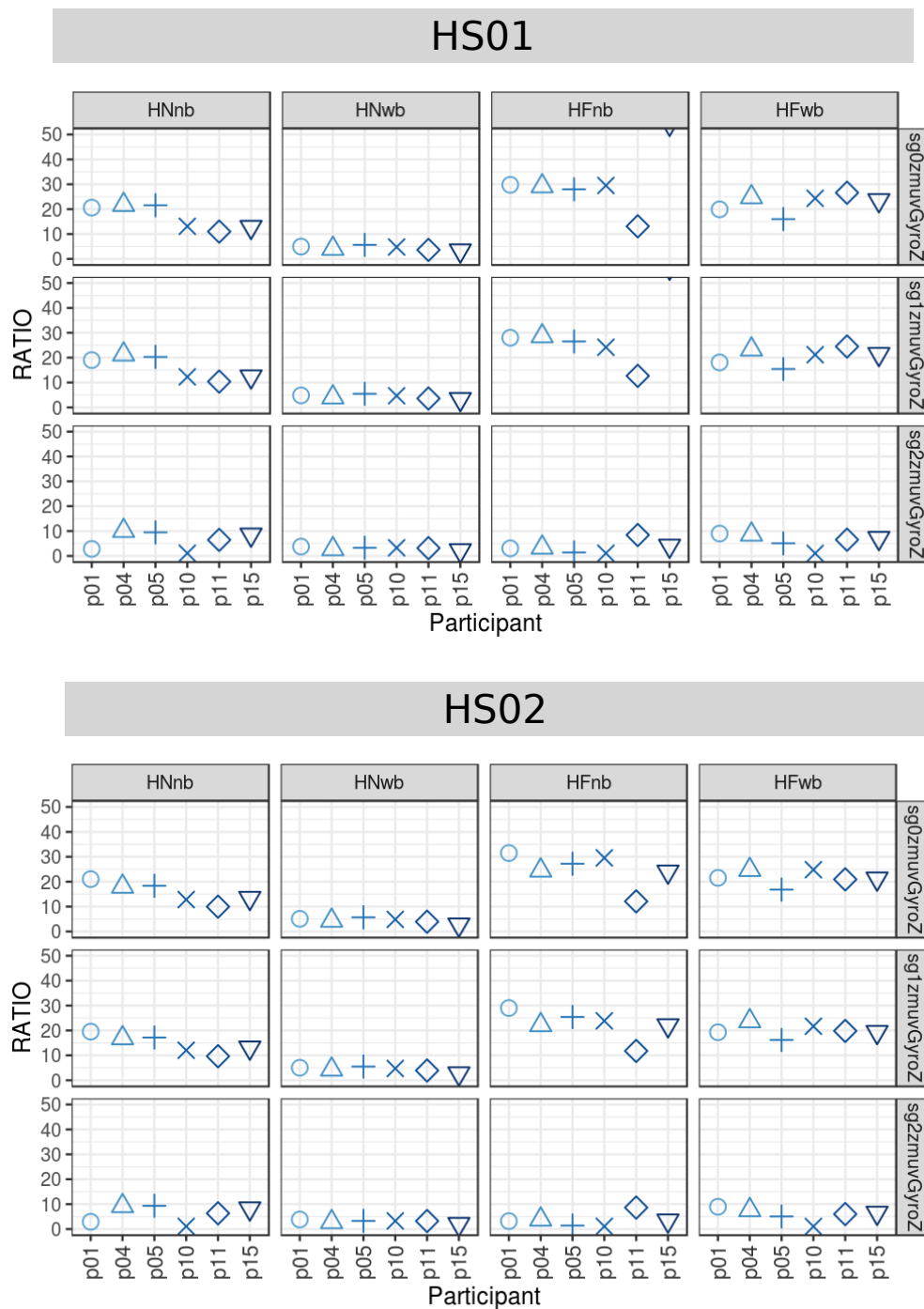


Fig. E.31 **RATIO** values for horizontal arm movements. RATIO values, representing dynamic transitions, for 6 participants performing horizontal arm movements (HNNb, HNwb, HFnb, HFwb) with sensors HS01, HS02 and three smoothed-normalised axis of GyroZ (sg0zmuVgyroZ, sg1zmuVgyroZ and sg2zmuVgyroZ). RATIO values were computed with embedding parameters  $\overline{m_0} = 6$ ,  $\overline{\tau_0} = 10$  and recurrence threshold  $\epsilon = 1$ . R code to reproduce the figure is available at [\[4\]](#).

## Additional Results for HII experiment

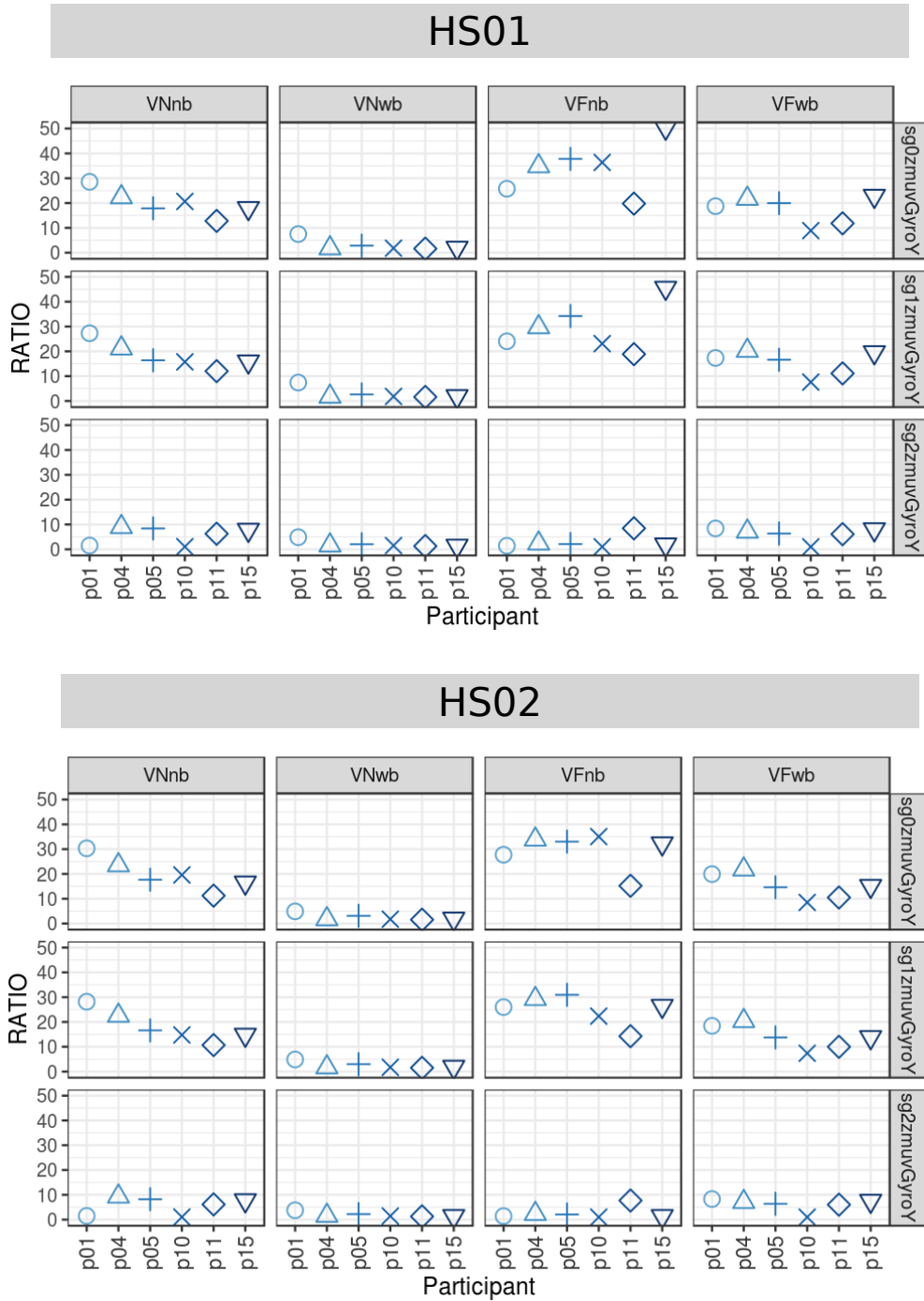


Fig. E.32 **RATIO** values for vertical arm movements. RATIO values, representing dynamic transitions, for 6 participants performing vertical arm movements (VNnb, VNwb, VFnb, VFwb) with sensors HS01, HS02 and three smoothed-normalised axis of GyroY (sg0znmuvGyroY, sg1znmuvGyroY and sg2znmuvGyroY). RATIO values were computed with embedding parameters  $\overline{m}_0 = 6$ ,  $\overline{\tau}_0 = 10$  and recurrence threshold  $\epsilon = 1$ . R code to reproduce the figure is available at [\[45\]](#).

#### E.5.4 ENTR values

ENTR values for horizontal and vertical arm movements are shown in Figs E.33 and E.34.

Figs E.33 show ENTR values for horizontal arm movements. ENTR values appear to be similar for `sg0zmovGyroZ` and `sg1zmovGyroZ` and oscillate between 2 to 4, while ENTR values for `sg2zmovGyroZ` appear to show similar fluctuations but with higher ENTR values oscillating between 3.5 to 5 with the exception of `p10` with activities `VNnb` and `VFwb` for `sg2zmovGyroY` which ENTR values are slightly out of range. ENTR values appear to be similar for sensor HS01 and HS02.

Figs E.34 show ENTR values for vertical arm movements. ENTR values for `sg0zmovGyroY` and `sg1zmovGyroY` appear to show the same values and oscillate between 2 to 4, while ENTR values appear to oscillate between 3.5 to 5 with the exception of `p10` with activities `VNnb` and `VFwb` for `sg2zmovGyroY` which ENTR values are out of range. ENTR values for sensor HS01 and HS02 appear to show the same values.

## Additional Results for HII experiment

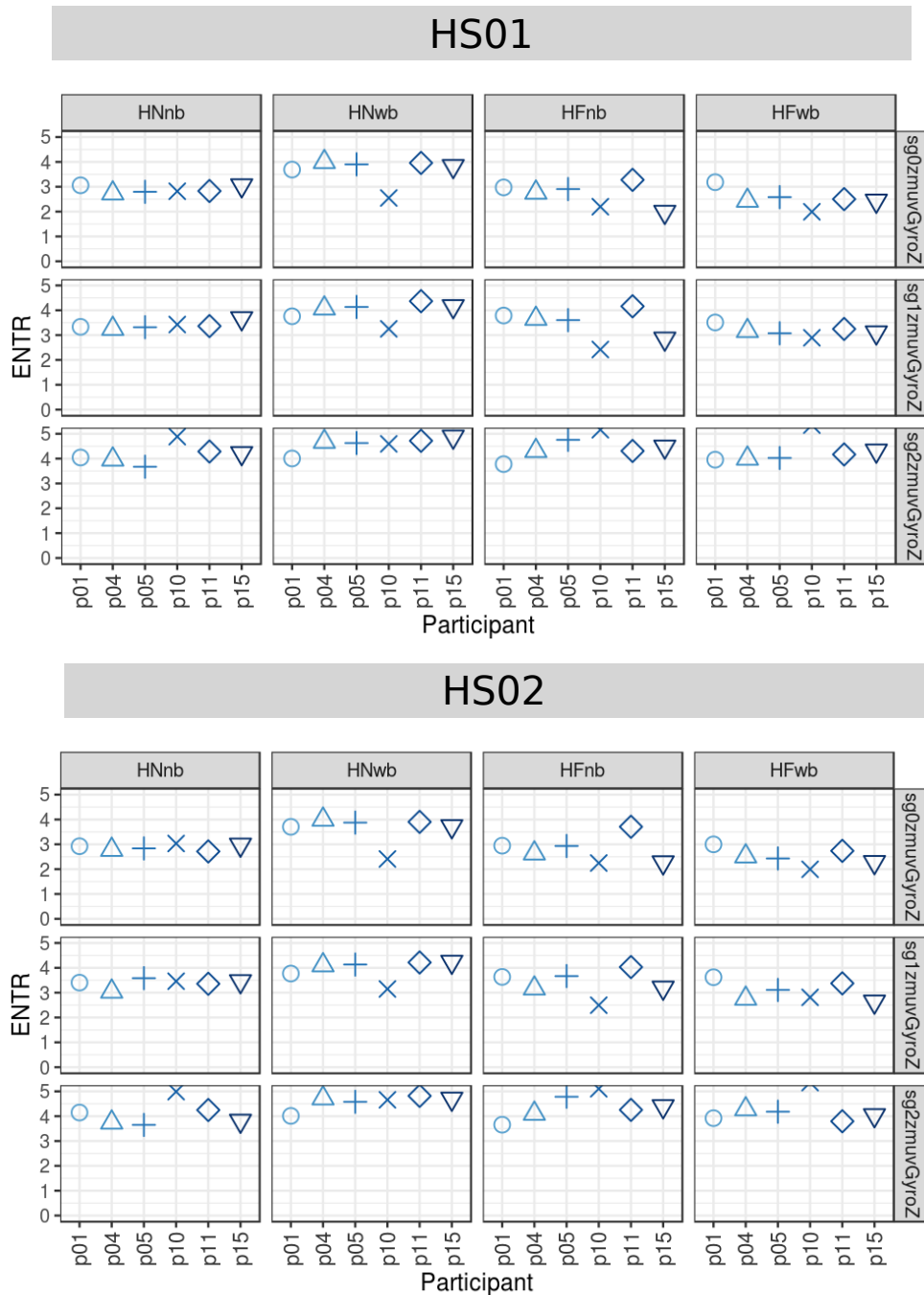


Fig. E.33 **ENTR values for horizontal arm movements.** ENTR values (representing the complexity of the deterministic structure in time series) for 6 participants performing horizontal arm movements (HNNb, HNwb, HFnb, HFwb) for sensors HS01, HS02 and three smoothed-normalised axis of GyroZ (sg0zmmuvGyroZ, sg1zmmuvGyroZ and sg2zmmuvGyroZ). ENTR values were computed with embedding parameters  $\overline{m_0} = 6$ ,  $\overline{\tau_0} = 10$  and recurrence threshold  $\epsilon = 1$ . R code to reproduce the figure is available at [\[1\]](#).

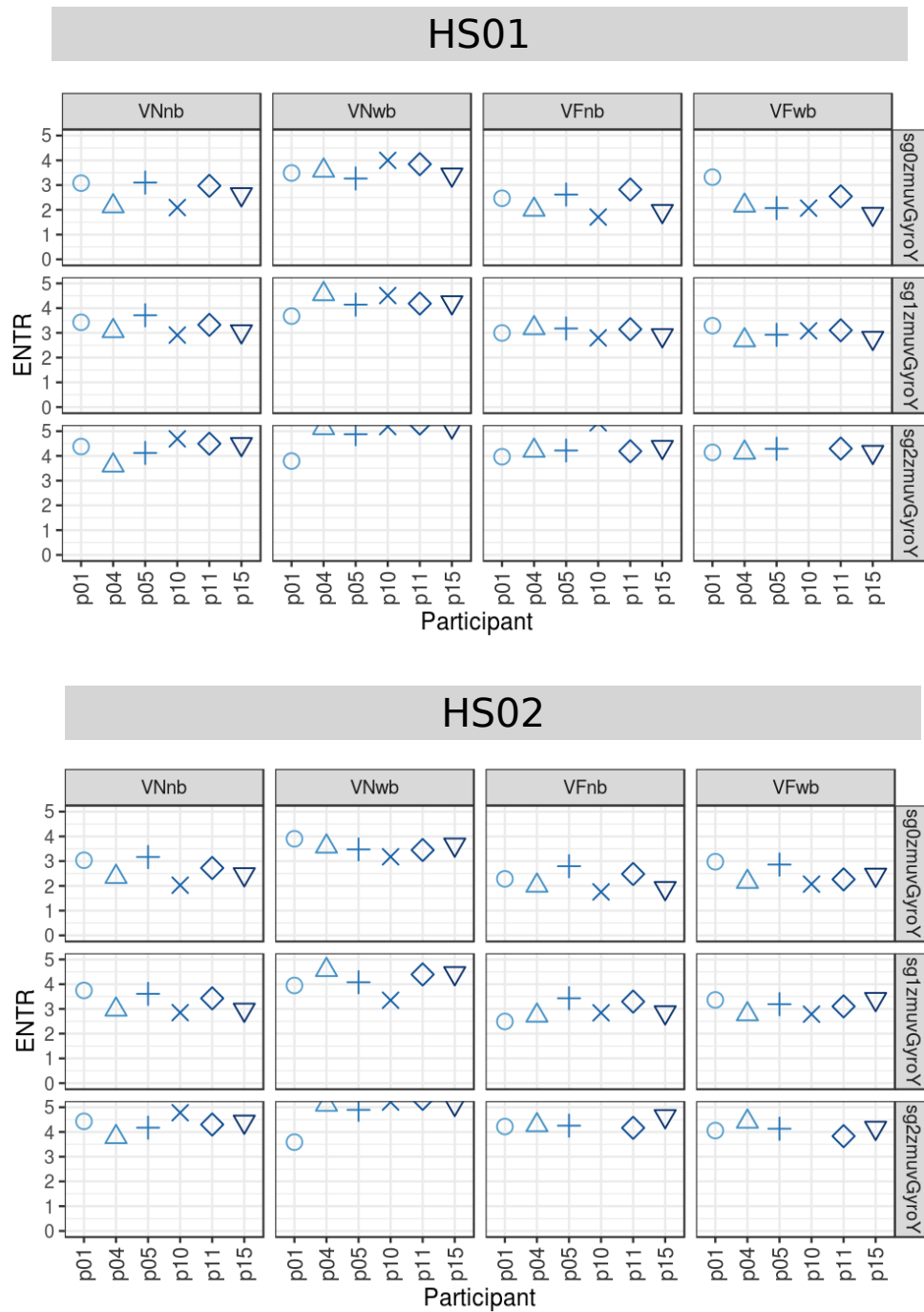


Fig. E.34 **ENTR values for vertical arm movements.** ENTR values (representing the complexity of the deterministic structure in time series) for 6 participants performing vertical arm movements (VNnb, VNwb, VFnb, VFwb) for sensors HS01, HS02 and three smoothed-normalised axis of GyroY (sg0zmuVgyroY, sg1zmuVgyroY and sg2zmuVgyroY). ENTR values were computed with embedding parameters  $\overline{m_0} = 6$ ,  $\overline{\tau_0} = 10$  and recurrence threshold  $\epsilon = 1$ . R code to reproduce the figure is available at [\[1\]](#).



# Appendix F

## Additional results for HHI experiment

### F.1 Time Series

Time series for twenty participants with a window length size of 500 samples of horizontal arm movements (Figs. F.1, F.2, F.3) and vertical arm movements (Figs. F.4, F.5, F.6). For the remained window lengths, the reader is welcome to download the data and code at Xochicale (2019). See Appendix A for details on how code and data is organised and how results can be replicated.



## Additional results for HHI experiment

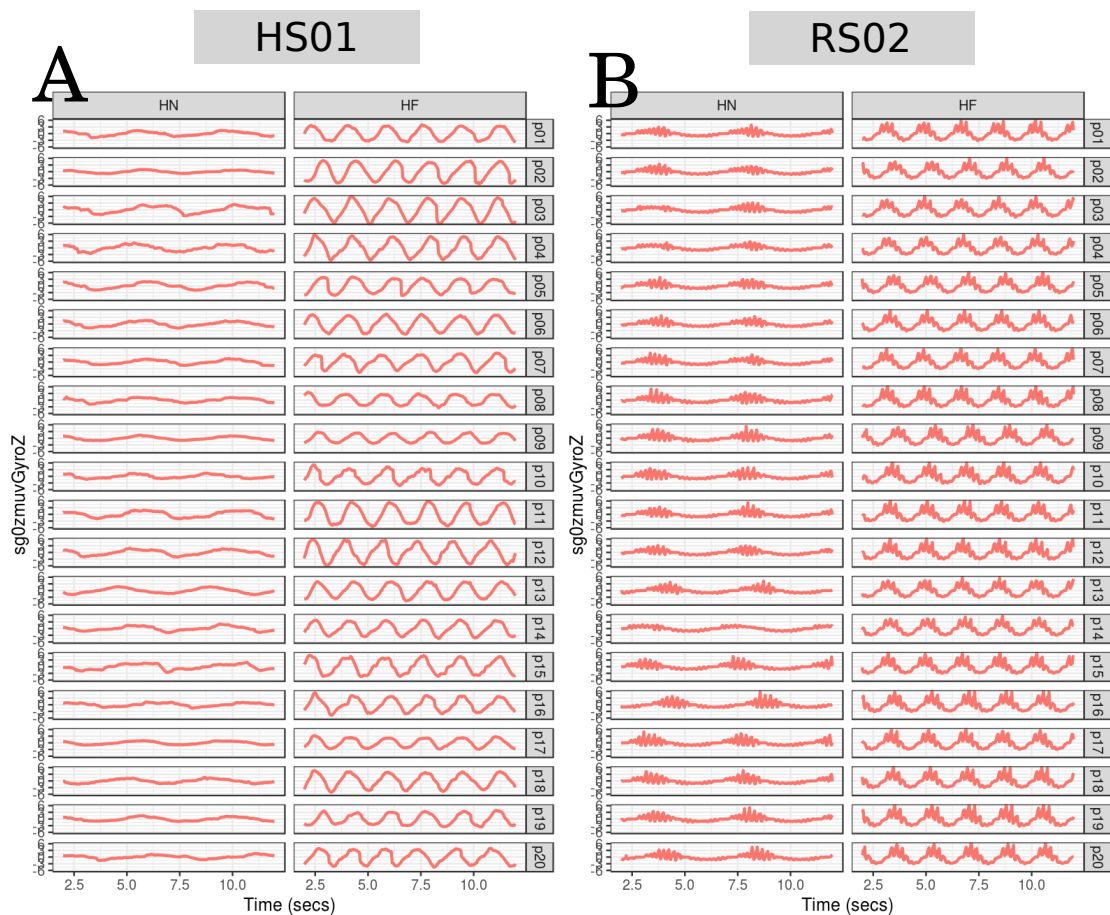


Fig. F.1 **Time series for horizontal arm movements (sg0)** Time series for `sg0zmvGyroZ` for twenty participants ( $p01$  to  $p20$ ) for horizontal movements in normal (HN) and horizontal faster (HF) velocity with sensors attached to the participant wrist (HS01) and to the humanoid wrist (RS02). R code to reproduce the figure is available at [\[4\]](#).

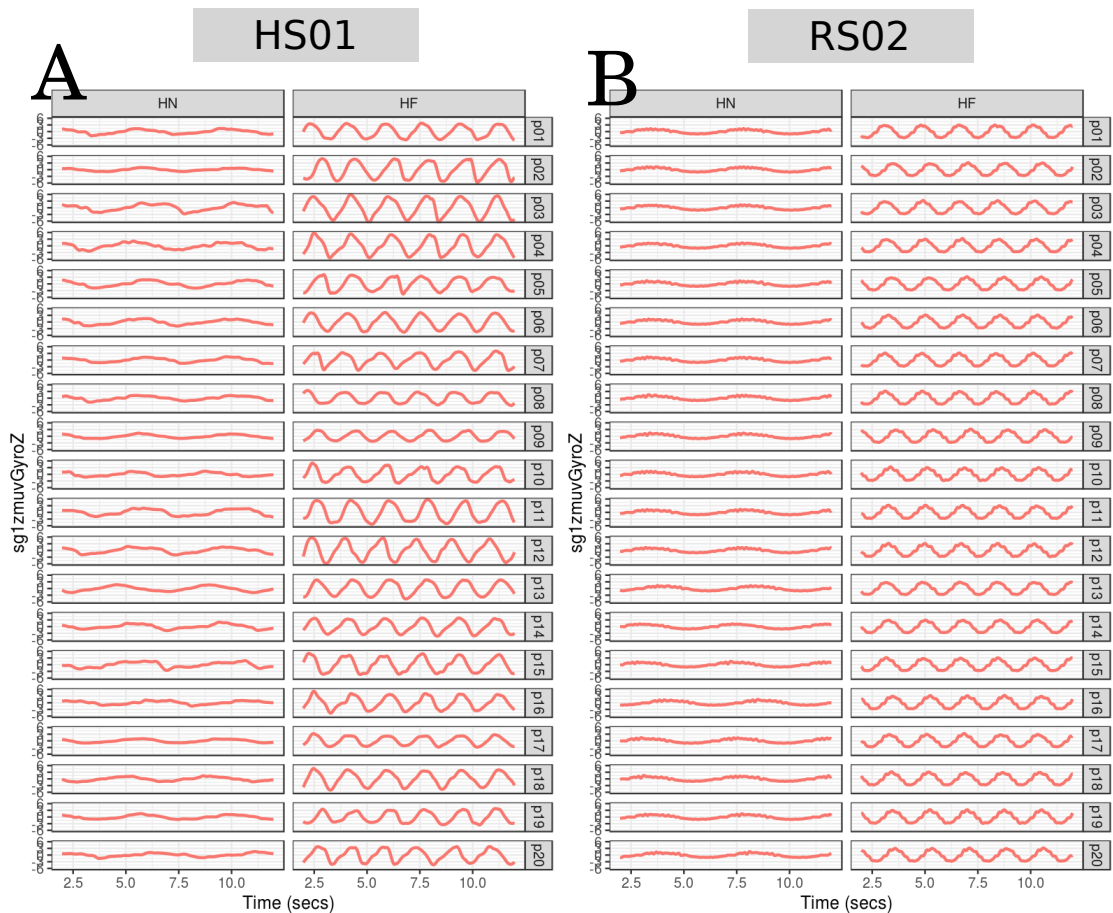


Fig. F.2 **Time series for horizontal arm movements (sg1)** Time series for `sg0zmuvgyroZ` for twenty participants ( $p01$  to  $p20$ ) for horizontal movements in normal (HN) and horizontal faster (HF) velocity with sensors attached to the participant wrist (HS01) and to the humanoid wrist (RS02). R code to reproduce the figure is available at [\[45\]](#).

## Additional results for HHI experiment

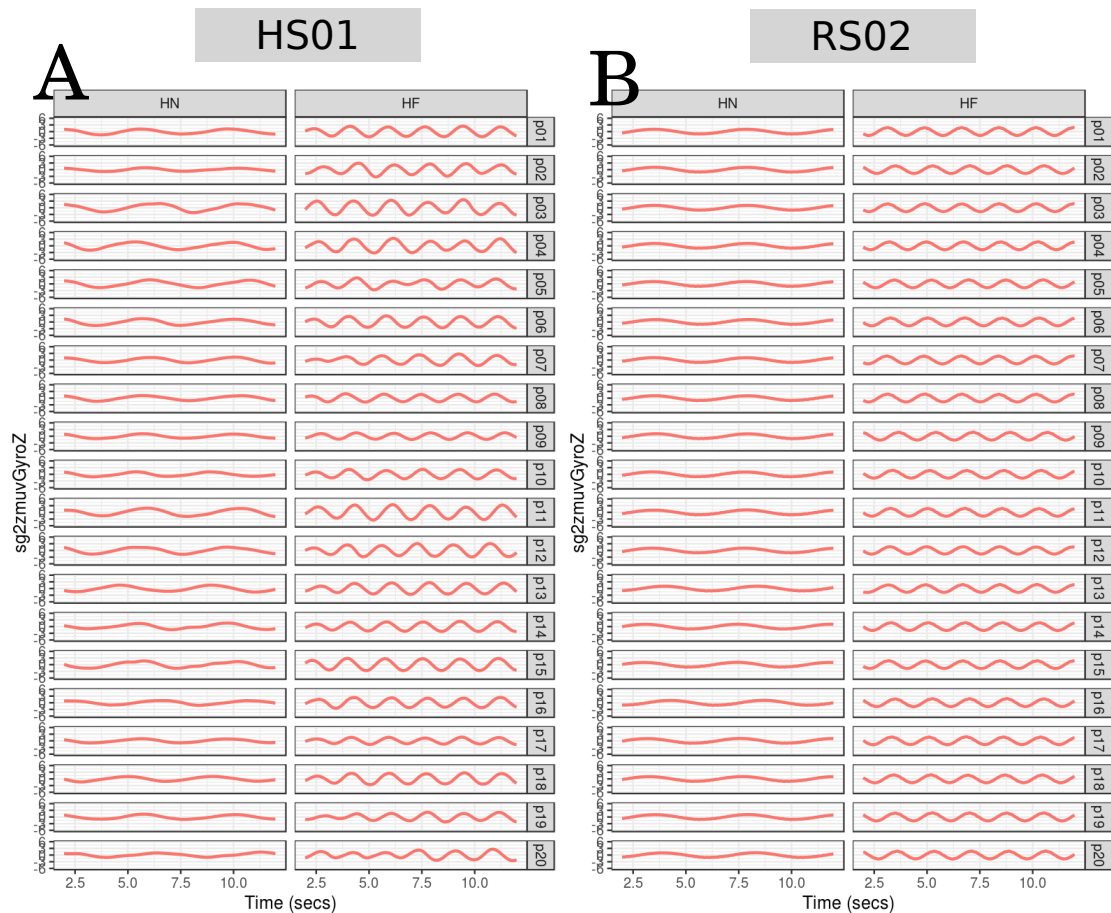


Fig. F.3 **Time series for horizontal arm movements (sg2)** Time series for  $sg0zmvGyroZ$  for twenty participants ( $p01$  to  $p20$ ) for horizontal movements in normal (HN) and horizontal faster (HF) velocity with sensors attached to the participant wrist (HS01) and to the humanoid wrist (RS02). R code to reproduce the figure is available at [\[1\]](#).

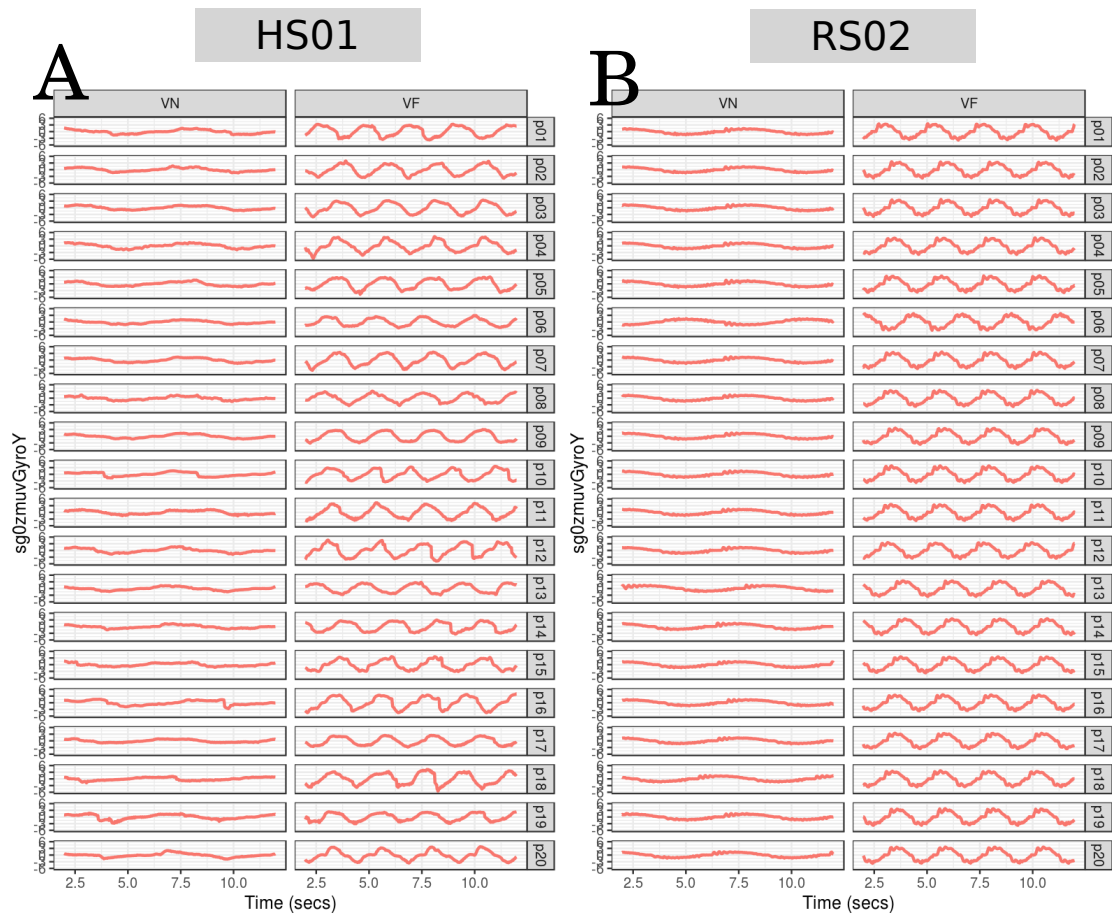


Fig. F.4 **Time series for vertical arm movements (sg0)** Time series for `sg0zmvGyroY` for twenty participants ( $p01$  to  $p20$ ) for vertical movements in normal (HN) and horizontal faster (HF) velocity with sensors attached to the participant wrist (HS01) and to the humanoid wrist (RS02). R code to reproduce the figure is available at [\[4\]](#).

## Additional results for HHI experiment

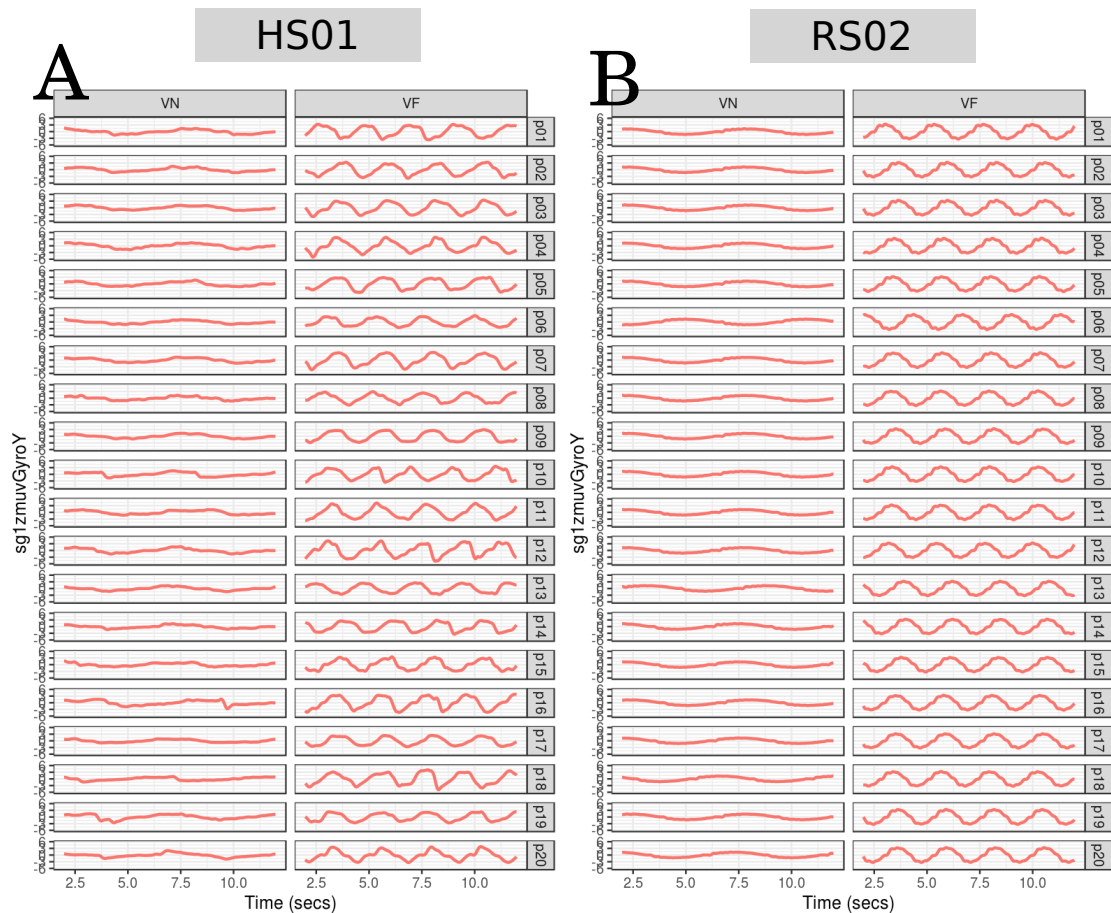


Fig. F.5 **Time series for vertical arm movements (sg1)** Time series for sg0zmuvGyroY for twenty participants ( $p01$  to  $p20$ ) for horizontal movements in normal (HN) and horizontal faster (HF) velocity with sensors attached to the participant wrist (HS01) and to the humanoid wrist (RS02). R code to reproduce the figure is available at [\[1\]](#).

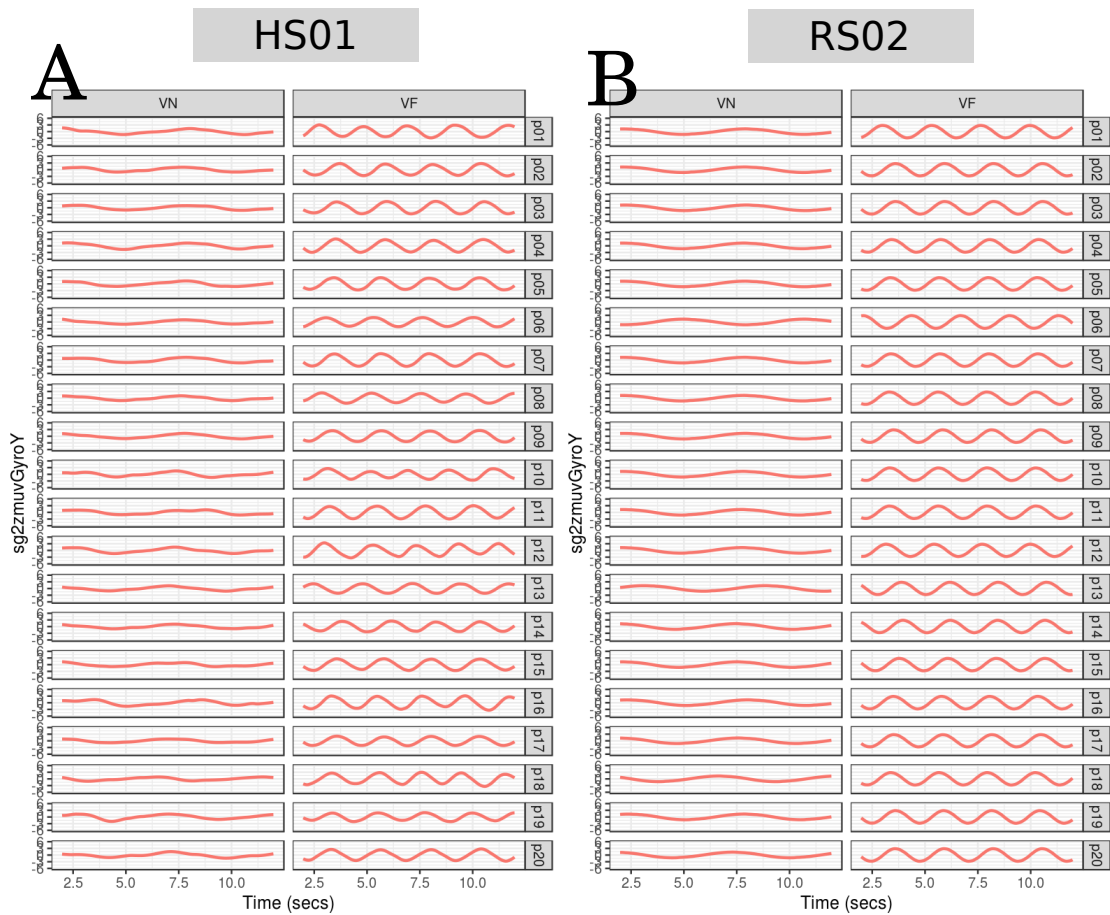


Fig. F.6 **Time series for vertical arm movements (sg2)** Time series for  $sg0zmmvGyroY$  for twenty participants ( $p01$  to  $p20$ ) for vertical movements in normal (HN) and horizontal faster (HF) velocity with sensors attached to the participant wrist (HS01) and to the humanoid wrist (RS02). R code to reproduce the figure is available at [\[link\]](#).

## F.2 Embedding parameters

### F.2.1 Minimum dimension embedding values

Minimum embedding dimensions for horizontal and vertical arm movements are presented in Figs. F.7 and F.8, respectively. For remained results with window size lengths of time series data, we refer the reader to download the data and code at Xochicale (2019).

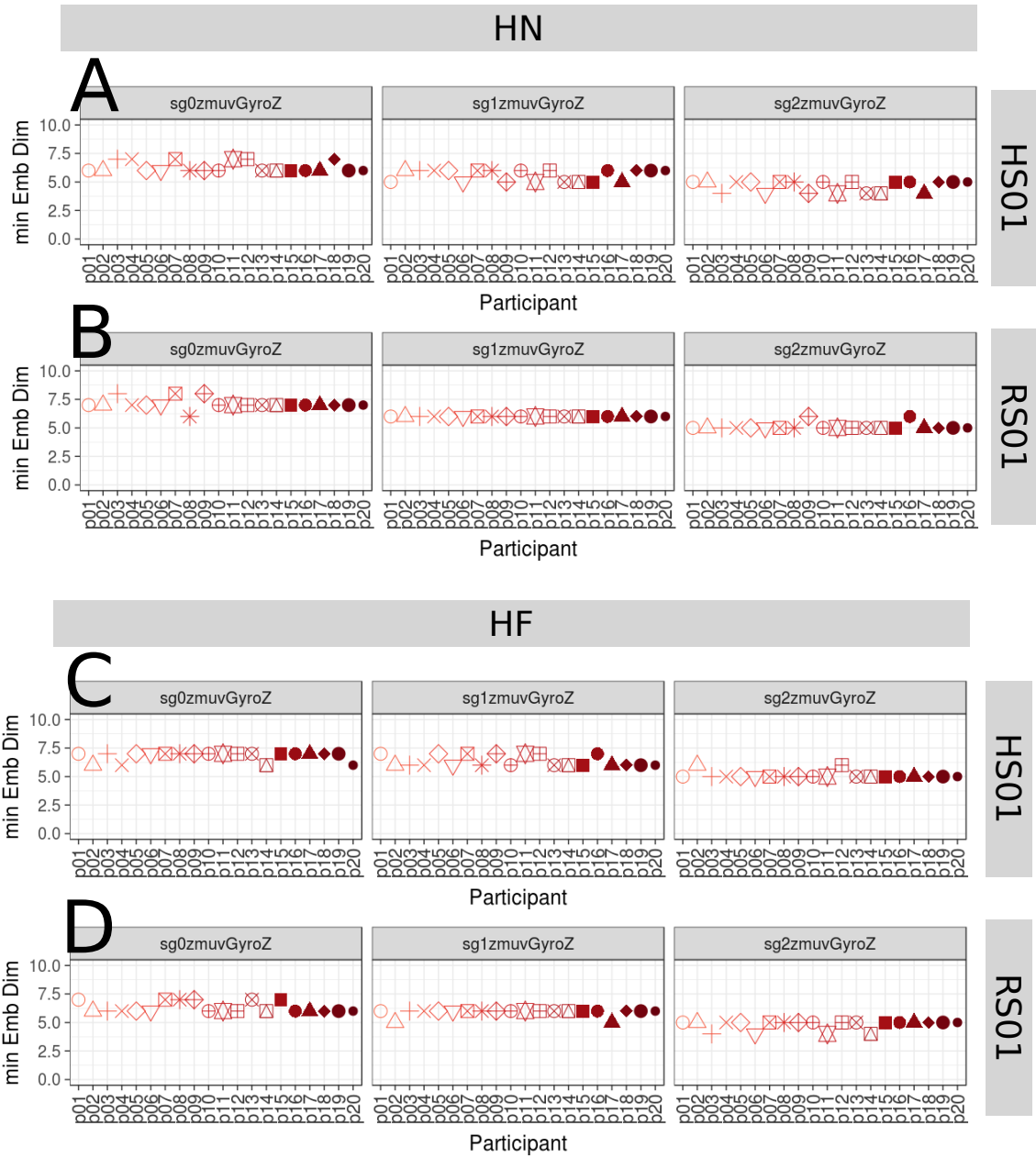


Fig. F.7 **Minimum embedding dimensions for horizontal arm movements.** (A, B) Horizontal Normal (HN), (C, D) Horizontal Faster (HF) movements, (A, C) sensor attached to participants (HS01), and (B, D) sensor attached to robot (RS01). Minimum embedding dimensions are for twenty participants (p01 to p20) with three smoothed signals (sg0zmuvGyroZ, sg1zmuvGyroZ and sg2zmuvGyroZ) and window length of 10-sec (500 samples). R code to reproduce the figure is available at [\[42\]](#).



## Additional results for HHI experiment

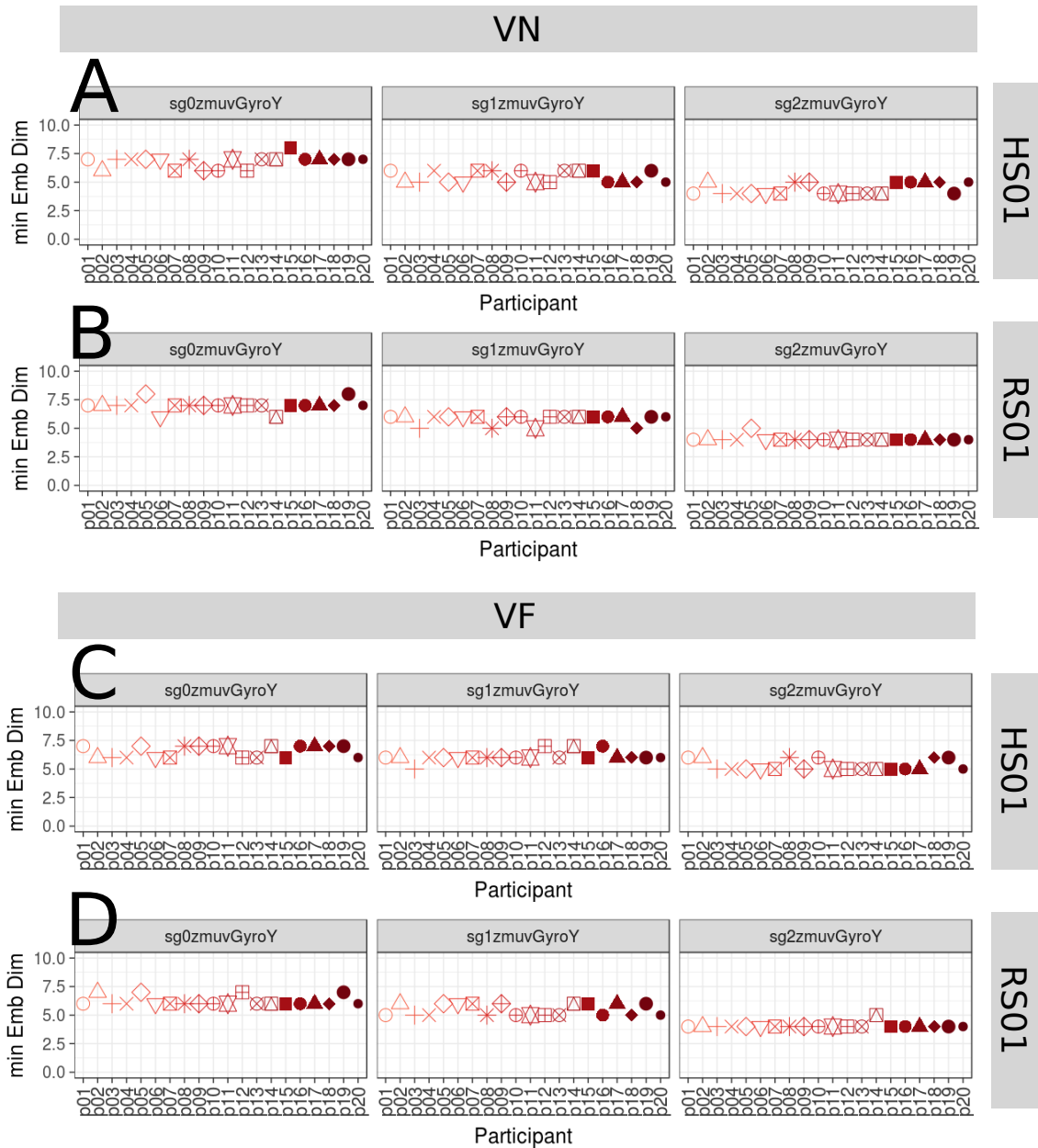


Fig. F.8 **Minimum embedding dimensions for vertical arm movements.** (A, B) Vertical Normal (VN), (C, D) Vertical Faster (VF) movements, (A, C) sensor attached to participants (HS01), and (B, D) sensor attached to robot (RS01). Minimum embedding dimensions are for twenty participants (p01 to p20) with three smoothed signals (sg0zmvGyroY, sg1zmvGyroY and sg2zmvGyroY) and window length of 10-sec (500 samples). R code to reproduce the figure is available at [\[4\]](#).

### F.2.2 Minimum delay embedding values

First minimum AMI values for horizontal and vertical arm movements are presented in Figs. F.9 and F.10, respectively. For remained results with window size lengths of time series data, we refer the reader to download the data and code at Xochicale (2019).

## Additional results for HHI experiment

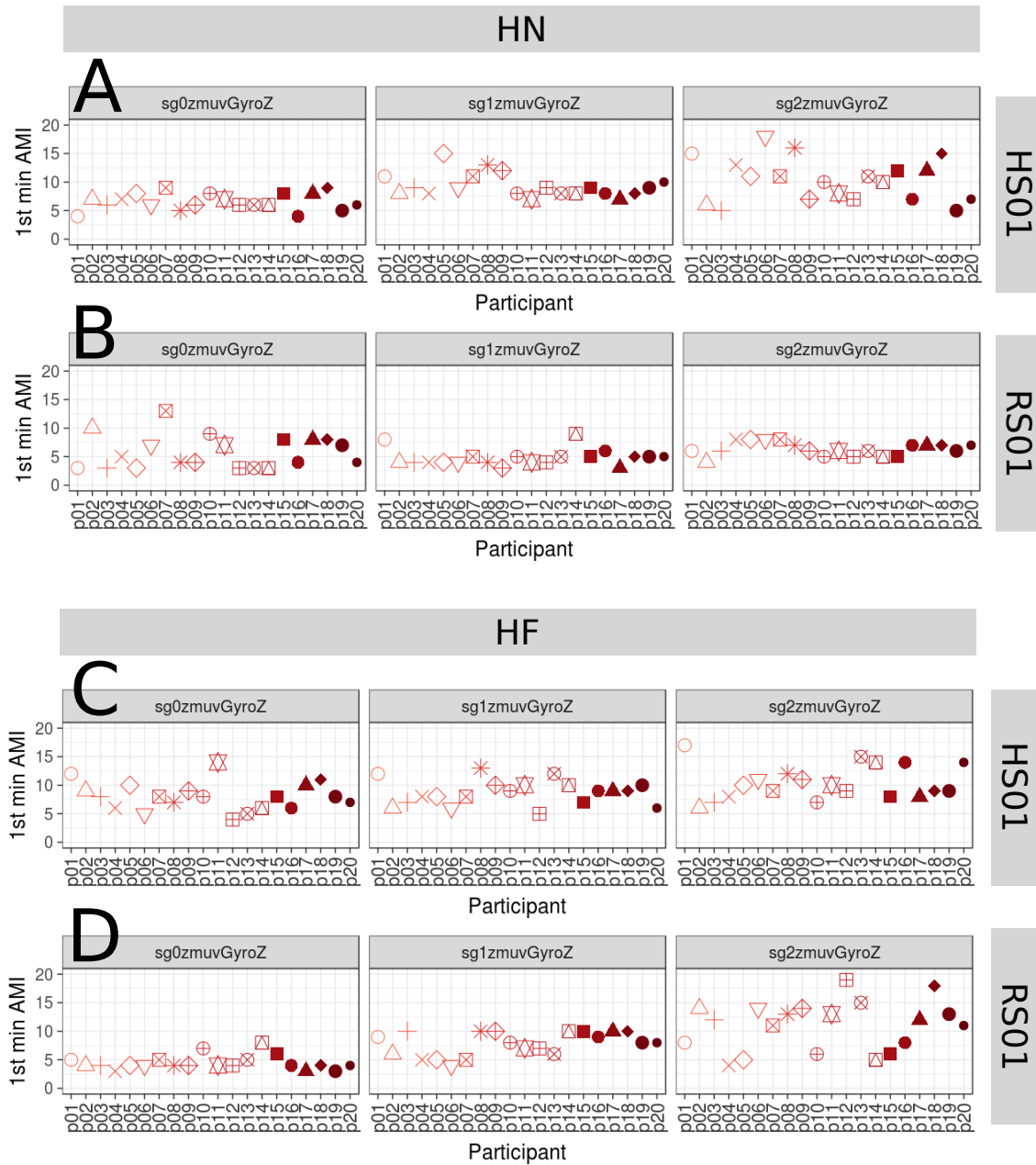


Fig. F.9 **First minimum AMI values for horizontal arm movements.** (A, B) Horizontal Normal (HN), (C, D) Horizontal Faster (HF) movements, (A, C) sensor attached to participants (HS01), and (B, D) sensor attached to robot (RS01). First minimum AMI values are for twenty participants (p01 to p020) with three smoothed signals (sg0zmuvGyroZ, sg1zmuvGyroZ and sg2zmuvGyroZ) and window length of 10-sec (500 samples). R code to reproduce the figure is available at [\[4\]](#).

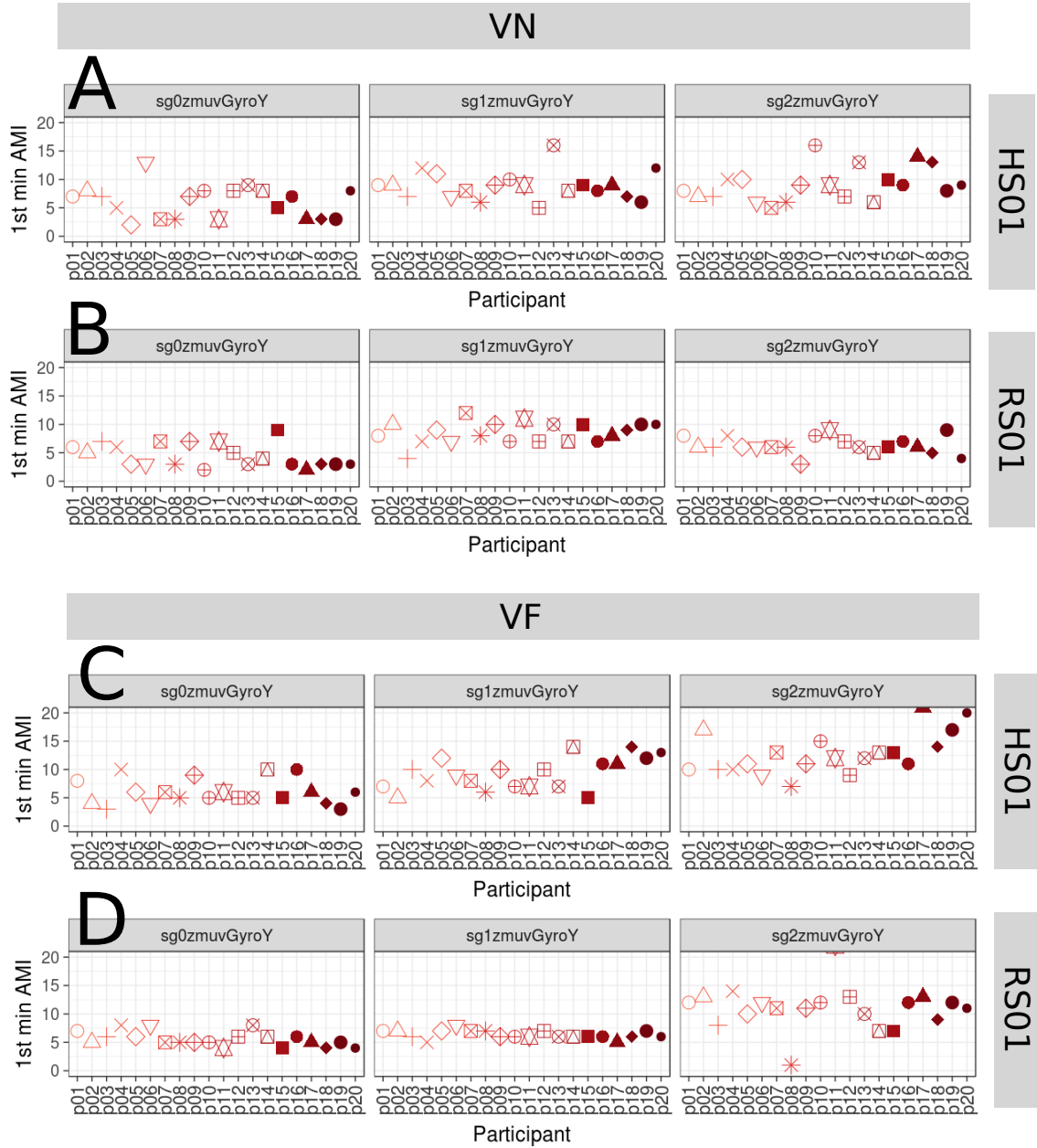


Fig. F.10 **First minimum AMI values for vertical arm movements.** (A, B) Vertical Normal (VN), (C, D) Vertical Faster (VF) movements, (A, C) sensor attached to participants (HS01), and (B, D) sensor attached to robot (RS01). First minimum AMI values are for twenty participants (p01 to p20) with three smoothed signals (sg0zmvGyroZ, sg1zmvGyroZ and sg2zmvGyroZ) and window length of 10-sec (500 samples). R code to reproduce the figure is available at [\[4\]](#).

### F.3 RSSs

Reconstructed state spaces of participant  $p01$ ,  $p02$  and  $p03$  for horizontal arm movements (Figs. F.11 and F.12) and vertical arm movements (Figs. F.13 and F.14). For remained results with window size lengths of time series data, we refer the reader to download the data and code at Xochicale (2019).

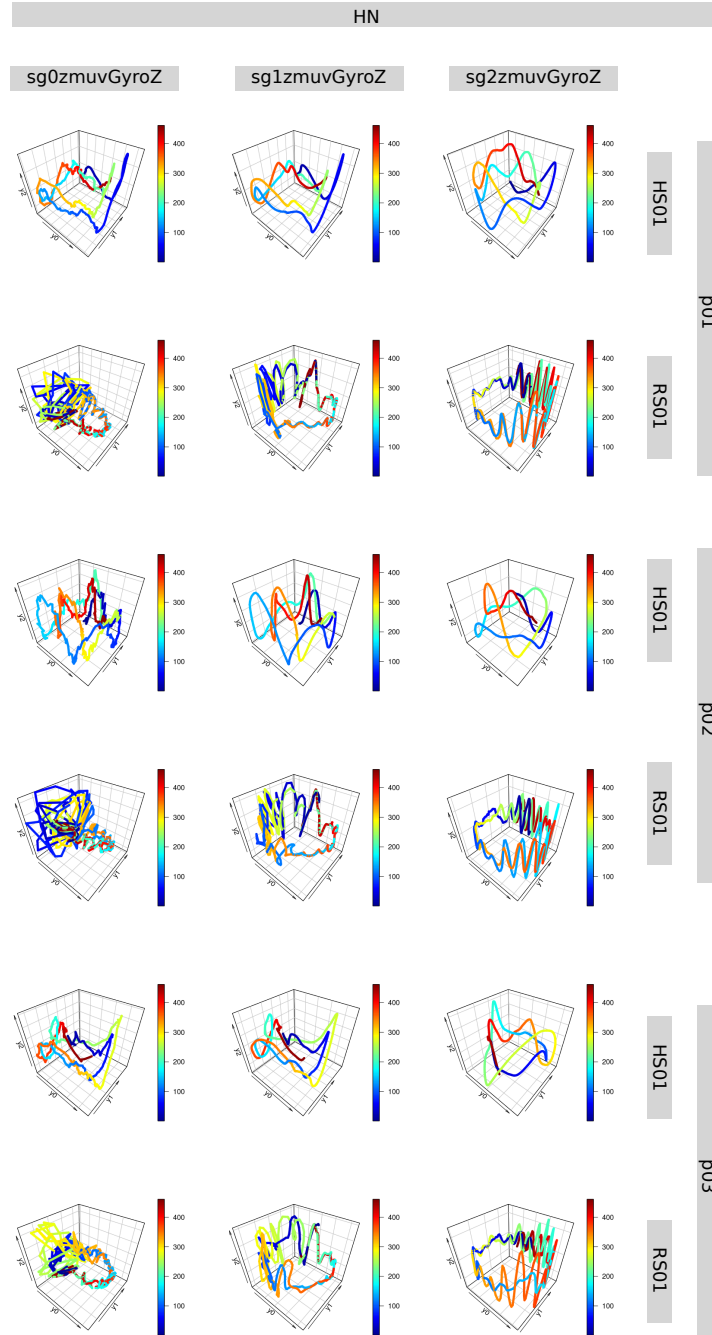


Fig. F.11 **RSSs for horizontal normal arm movements.** Reconstructed state spaces of participant  $p01$ ,  $p02$  and  $p03$  for horizontal movements with raw-normalised (sg0zmvGyroZ), normalised-smoothed 1 (sg1zmvGyroZ) and normalised-smoothed 2 (sg2zmvGyroZ) time series of the sensors attached to the participant (HS01) and other sensor attached to the robot (RS01). Reconstructed state spaces were computed with embedding parameters  $\bar{m}_0 = 6$ ,  $\bar{\tau}_0 = 8$ . R code to reproduce the figure is available at [\[4\]](#).

## Additional results for HHI experiment

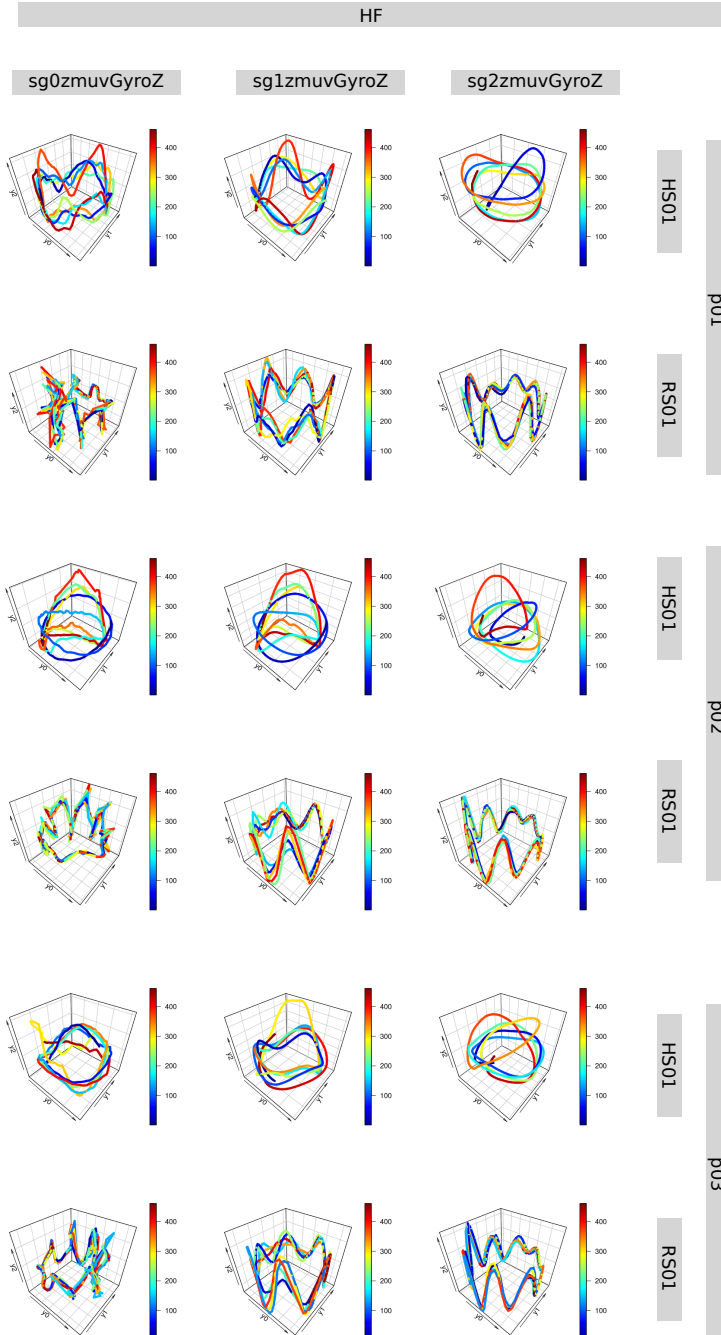


Fig. F.12 **RSSs for horizontal faster arm movements.** Reconstructed state spaces of participant  $p01$ ,  $p02$  and  $p03$  for horizontal faster movements with raw-normalised (sg0zmvGyroZ), normalised-smoothed 1 (sg1zmvGyroZ) and normalised-smoothed 2 (sg2zmvGyroZ) time series of the sensors attached to the participant (HS01) and other sensor attached to the robot (RS01). Reconstructed state spaces were computed with embedding parameters  $\bar{m}_0 = 6$ ,  $\bar{\tau}_0 = 8$ . R code to reproduce the figure is available at [\[1\]](#).

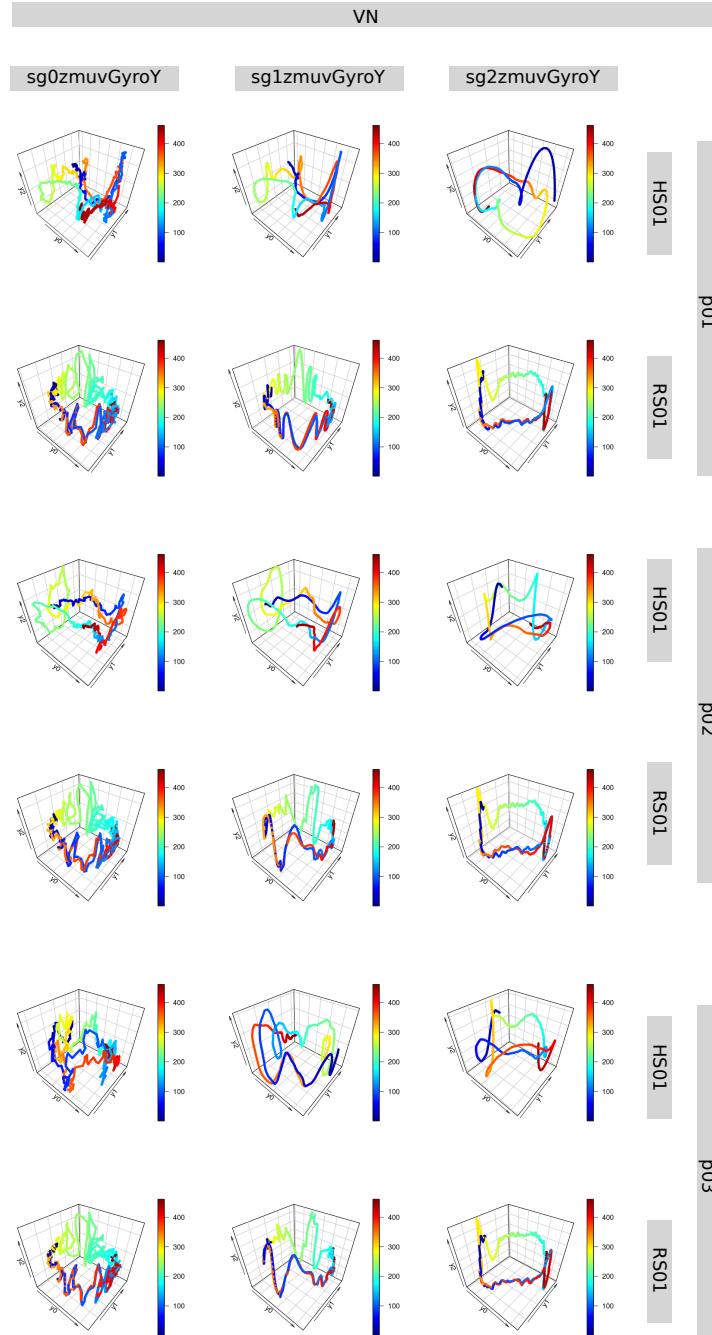


Fig. F.13 **RSSs for vertical normal arm movements.** Reconstructed state spaces of participant  $p01$ ,  $p02$  and  $p03$  for horizontal movements with raw-normalised (sg0zmuvGyroY), normalised-smoothed 1 (sg1zmuvGyroY) and normalised-smoothed 2 (sg2zmuvGyroY) time series of the sensors attached to the participant (HS01) and other sensor attached to the robot (RS01). Reconstructed state spaces were computed with embedding parameters  $\bar{m}_0 = 6$ ,  $\bar{\tau}_0 = 8$ . R code to reproduce the figure is available at [\[4\]](#).



## Additional results for HHI experiment

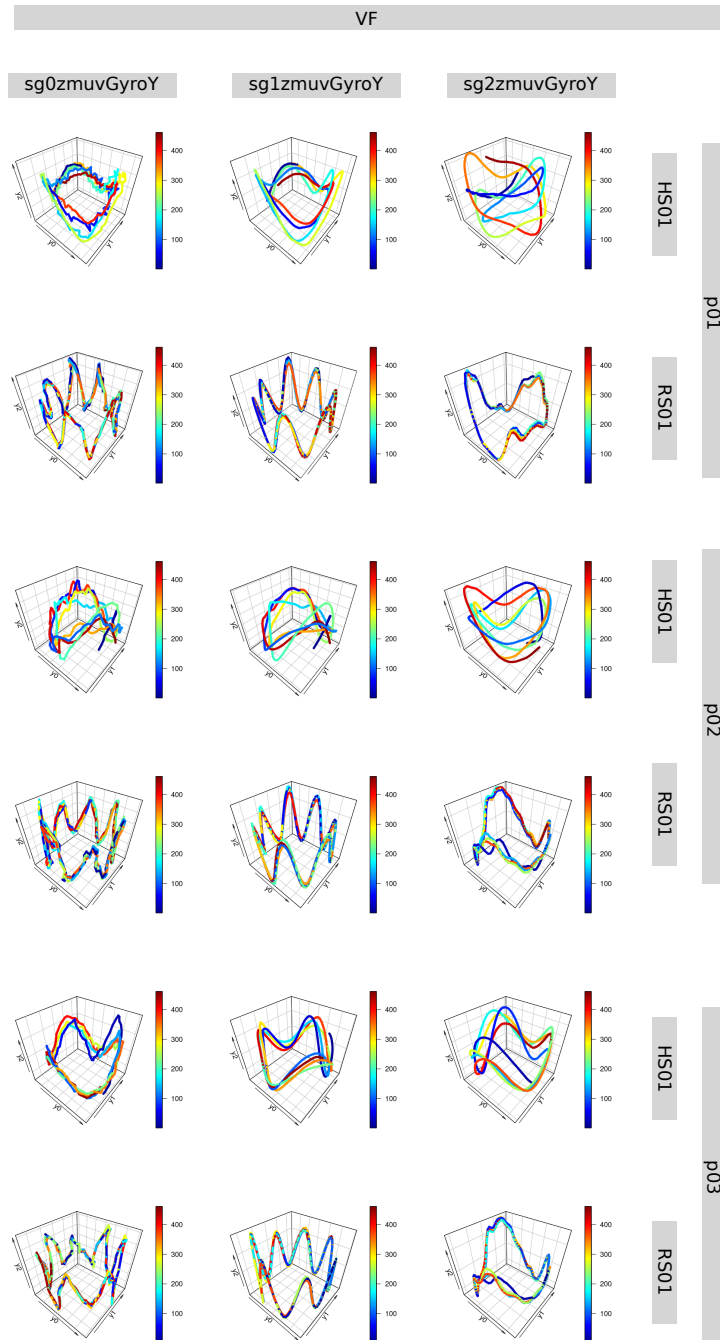


Fig. F.14 **RSSs for vertical faster arm movements.** Reconstructed state spaces of participant  $p01$ ,  $p02$  and  $p03$  for horizontal faster movements with raw-normalised (sg0zmvGyroY), normalised-smoothed 1 (sg1zmvGyroY) and normalised-smoothed 2 (sg2zmvGyroY) time series of the sensors attached to the participant (HS01) and other sensor attached to the robot (RS01). Reconstructed state spaces were computed with embedding parameters  $\bar{m}_0 = 6$ ,  $\bar{\tau}_0 = 8$ . R code to reproduce the figure is available at [\[1\]](#).

## F.4 RPs

Recurrence Plots participant  $p01$ ,  $p02$  and  $p03$  for horizontal arm movements (Figs. F.15, F.16) and vertical arm movements (Figs. F.17, F.18). For remained results with window size lengths of time series data, we refer the reader to download the data and code at Xochicale (2019).

## Additional results for HHI experiment

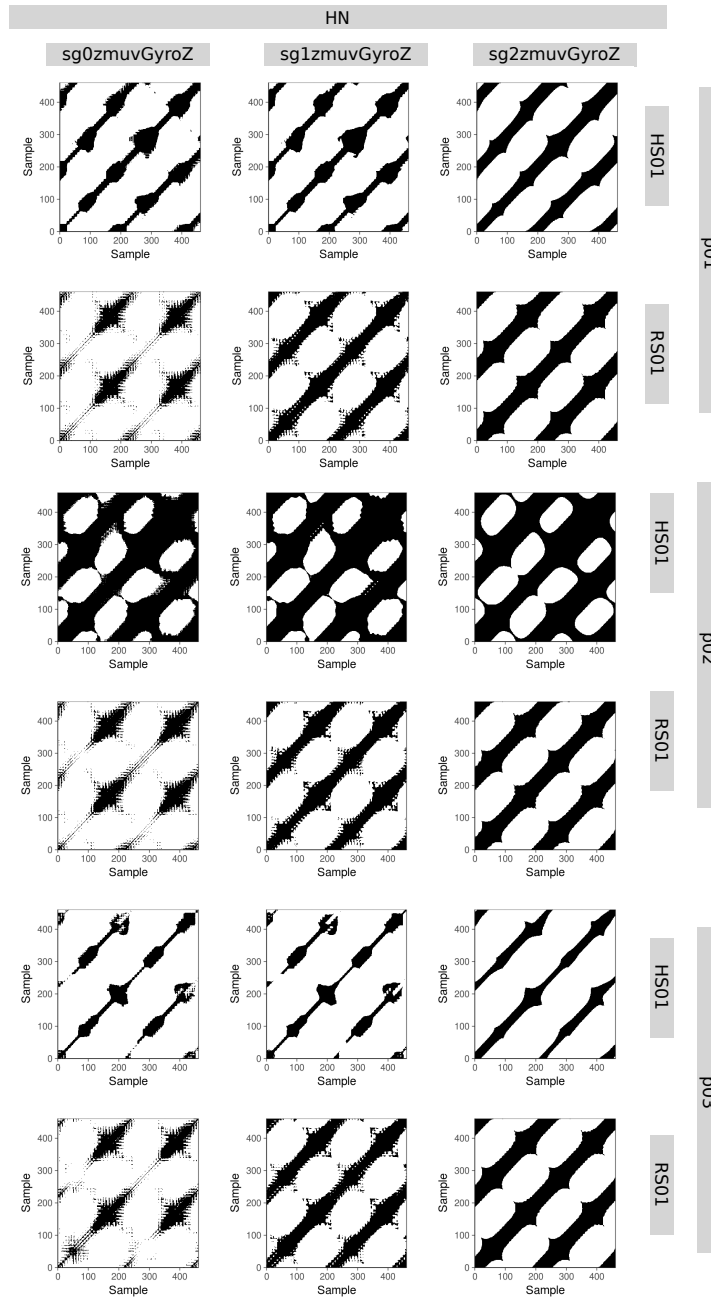


Fig. F.15 **RPs for horizontal normal arm movements.** Recurrence plots of participant  $p01$ ,  $p02$ ,  $p03$  for horizontal normal movements with time series of raw-normalised (sg0zmuvGyroZ), normalised-smoothed 1 (sg1zmuvGyroZ) and normalised-smoothed 2 (sg2zmuvGyroZ), and sensors attached to the participant (HS01) and to the robot (RS01). Recurrence plots were computed with embedding parameters  $\overline{m}_0 = 6$ ,  $\overline{\tau}_0 = 8$  and recurrence threshold  $\epsilon = 1$ . R code to reproduce the figure is available at [\[17\]](#).

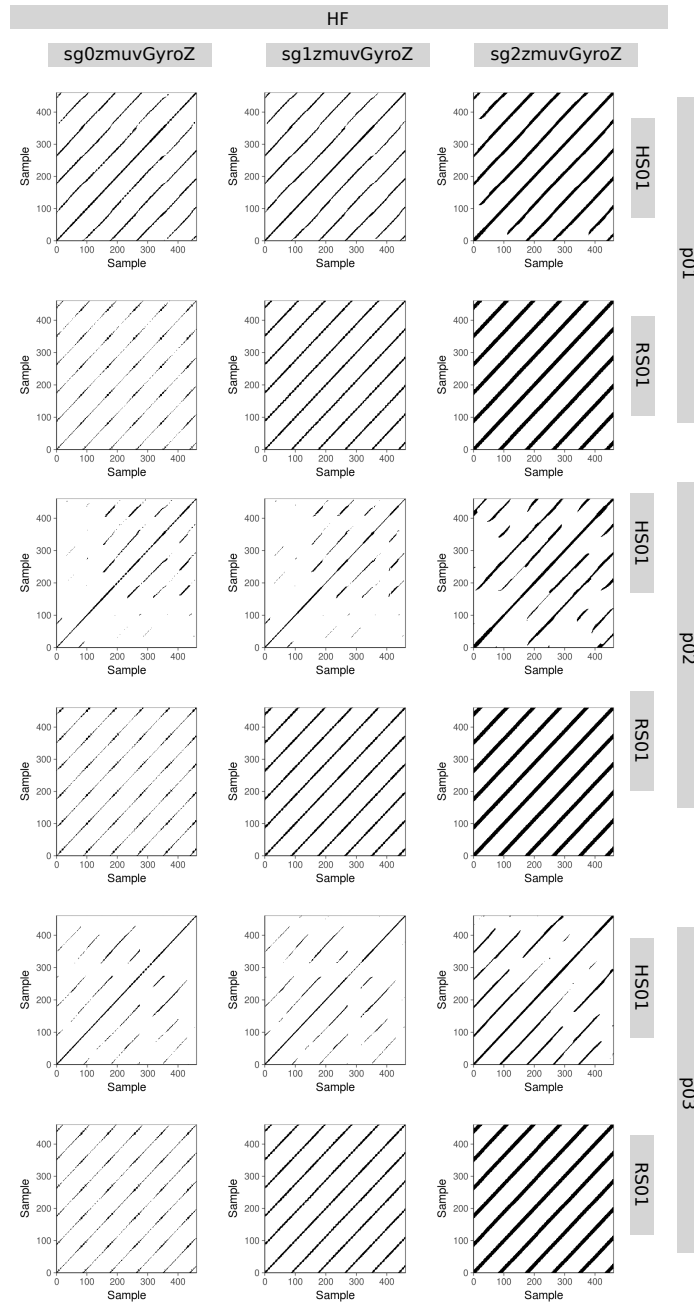


Fig. F.16 **RPs for horizontal faster arm movements.** Recurrence plots of participant  $p01$ ,  $p02$ ,  $p03$  for horizontal faster movements with time series of raw-normalised (sg0zmuvGyroZ), normalised-smoothed 1 (sg1zmuvGyroZ) and normalised-smoothed 2 (sg2zmuvGyroZ), and sensors attached to the participant (HS01) and to the robot (RS01). Recurrence plots were computed with embedding parameters  $\overline{m}_0 = 6$ ,  $\overline{\tau}_0 = 8$  and recurrence threshold  $\epsilon = 1$ . R code to reproduce the figure is available at [\[4\]](#).

## Additional results for HHI experiment

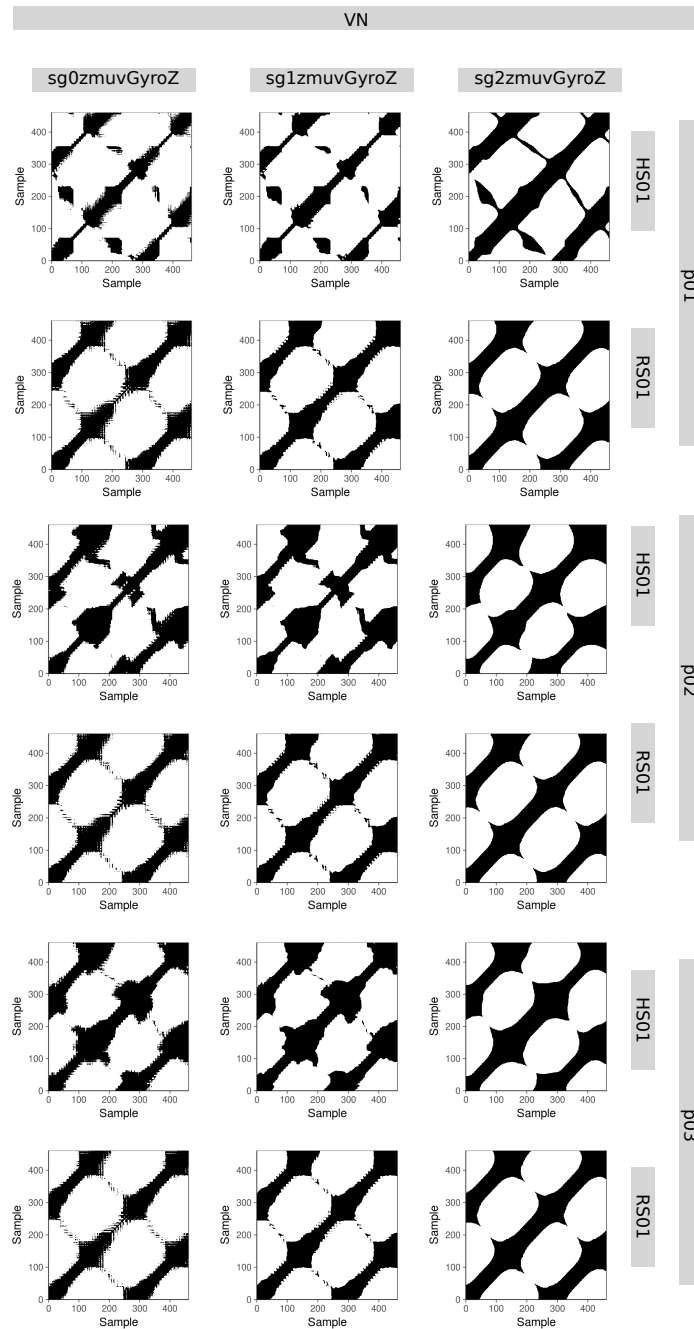


Fig. F.17 RPs for vertical normal arm movements. Recurrence plots of participant  $p01$ ,  $p02$ ,  $p03$  for vertical normal movements with time series of raw-normalised ( $sg0zmuvGyroY$ ), normalised-smoothed 1 ( $sg1zmuvGyroY$ ) and normalised-smoothed 2 ( $sg2zmuvGyroY$ ), and sensors attached to the participant (HS01) and to the robot (RS01). Recurrence plots were computed with embedding parameters  $\overline{m_0} = 6$ ,  $\overline{\tau_0} = 8$  and recurrence threshold  $\epsilon = 1$ . R code to reproduce the figure is available at [\[4\]](#).

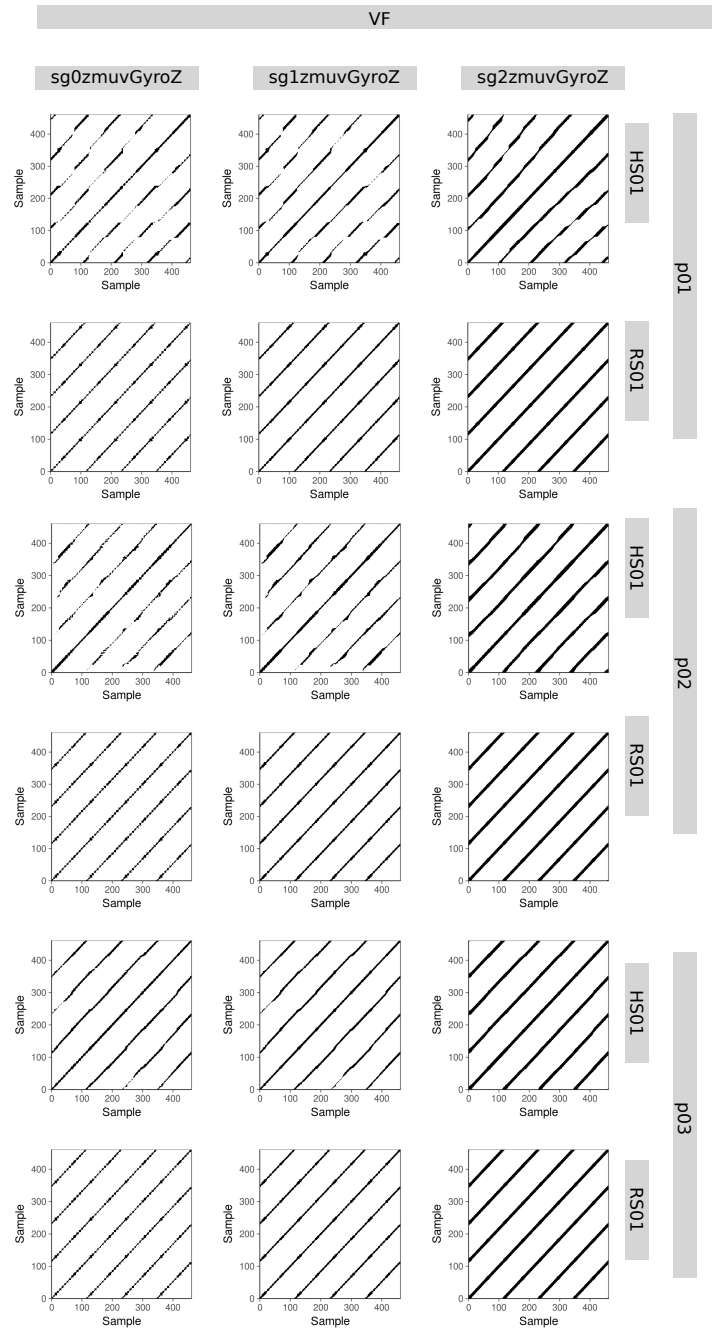


Fig. F.18 **RPs for vertical faster arm movements.** Recurrence plots of participant  $p01$ ,  $p02$ ,  $p03$  for vertical faster movements with time series of raw-normalised (sg0zmuvGyroY), normalised-smoothed 1 (sg1zmuvGyroY) and normalised-smoothed 2 (sg2zmuvGyroY), and sensors attached to the participant (HS01) and to the robot (RS01). Recurrence plots were computed with embedding parameters  $\overline{m_0} = 6$ ,  $\overline{\tau_0} = 8$  and recurrence threshold  $\epsilon = 1$ . R code to reproduce the figure is available at [\[4\]](#).

## Additional results for HHI experiment

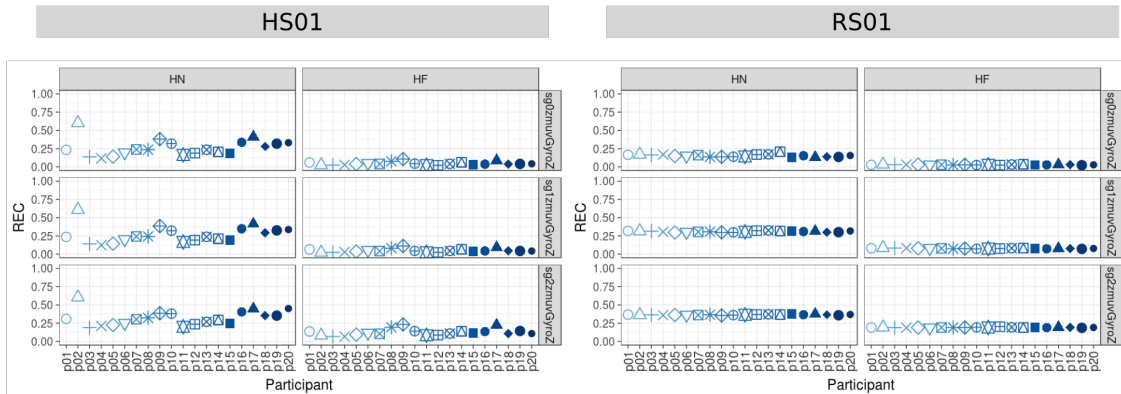


Fig. F.19 **REC values for horizontal arm movements.** REC values (representing % of black dots in the RPs) for 20 participants performing HN and HF movements with sensors HS01, RS01 and three smoothed-normalised axis of GyroZ (sg0zmuvgyroZ, sg1zmuvgyroZ and sg2zmuvgyroZ). REC values were computed with embedding parameters  $\overline{m}_0 = 6$ ,  $\overline{\tau}_0 = 8$  and recurrence threshold  $\epsilon = 1$ . R code to reproduce the figure is available at [\[4\]](#).

## F.5 RQAs

### F.5.1 REC values

REC values, representing the % of black dots in the RPs, are shown in Figs. F.19 and F.20.

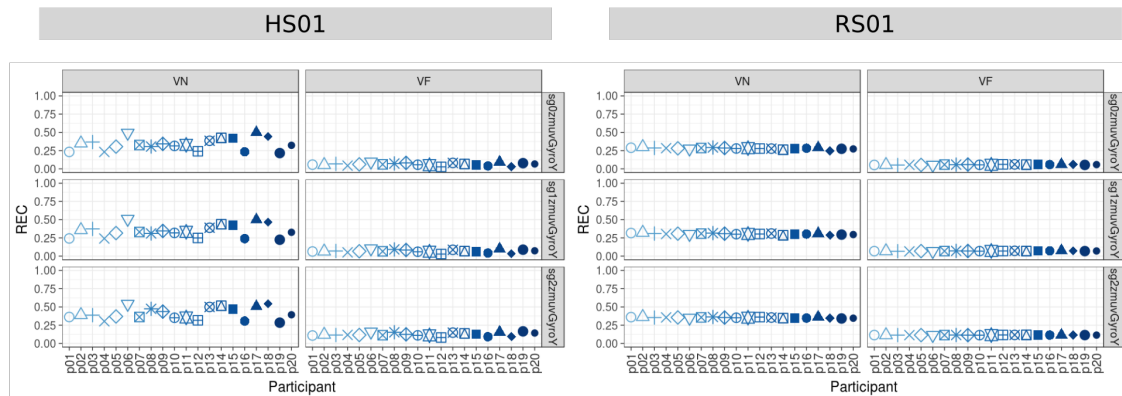


Fig. F.20 **REC values for vertical arm movements.** REC values (representing % of black dots in the RPs) for 20 participants performing VN and VF movements with sensors HS01, RS01 and three smoothed-normalised axis of GyroY ( $sg0zmvGyroY$ ,  $sg1zmvGyroY$  and  $sg2zmvGyroY$ ). REC values were computed with embedding parameters  $\overline{m}_0 = 6$ ,  $\overline{\tau}_0 = 8$  and recurrence threshold  $\epsilon = 1$ . R code to reproduce the figure is available at [\[45\]](#).

## F.5.2 DET values

DET values, representing predictability and organisation of the RPs. are shown in Figs. F.21 and F.22.



## Additional results for HHI experiment

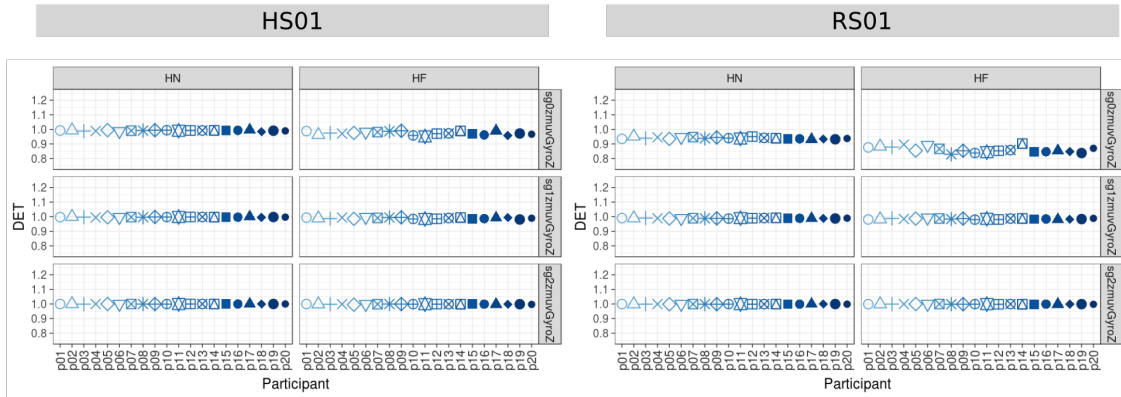


Fig. F.21 **DET values for horizontal arm movements.** DET values (representing predictability and organisation of the RPs) for 20 participants performing HN and HF movements with sensors HS01, RS01 and three smoothed-normalised axis of GyroZ (sg0zmvGyroZ, sg1zmvGyroZ and sg2zmvGyroZ). DET values were computed with embedding parameters  $\overline{m}_0 = 6$ ,  $\overline{\tau}_0 = 8$  and recurrence threshold  $\epsilon = 1$ . R code to reproduce the figure is available at [\[4\]](#).

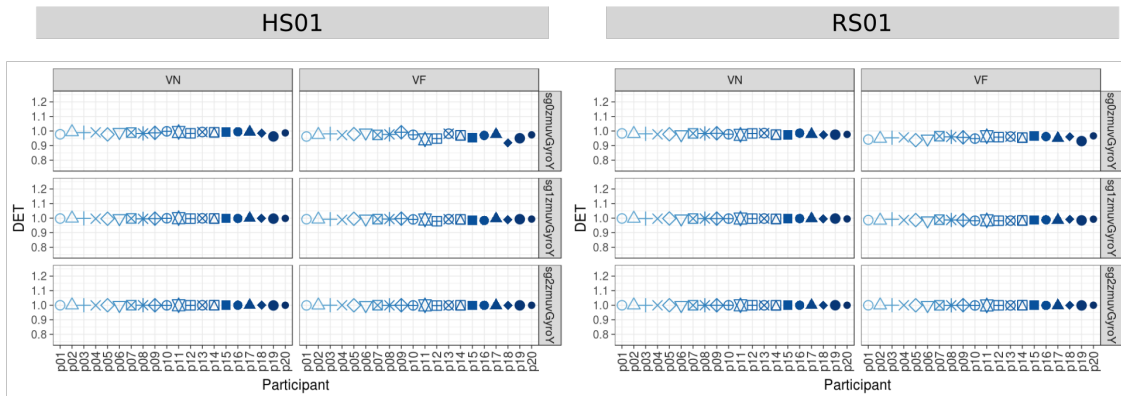


Fig. F.22 **DET values for vertical arm movements.** DET values (representing predictability and organisation of the RPs) for 20 participants performing VN and VF movements with sensors HS01, RS01 and three smoothed-normalised axis of GyroY (sg0zmvGyroY, sg1zmvGyroY and sg2zmvGyroY). DET values were computed with embedding parameters  $\overline{m}_0 = 6$ ,  $\overline{\tau}_0 = 8$  and recurrence threshold  $\epsilon = 1$ . R code to reproduce the figure is available at [\[4\]](#).

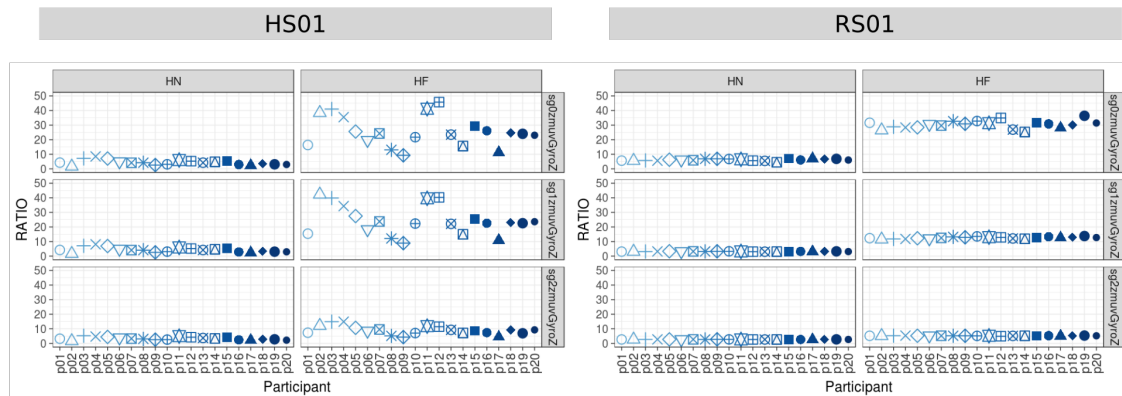


Fig. F.23 **RATIO** values for horizontal arm movements. RATIO (representing dynamic transitions) for 20 participants performing HN and HF movements with sensors HS01, RS01 and three smoothed-normalised axis of GyroZ ( $sg0zmuvgyroZ$ ,  $sg1zmuvgyroZ$  and  $sg2zmuvgyroZ$ ). RATIO values were computed with embedding parameters  $\overline{m}_0 = 6$ ,  $\overline{\tau}_0 = 8$  and recurrence threshold  $\epsilon = 1$ . R code to reproduce the figure is available at [\[45\]](#).

### F.5.3 RATIO values

RATIO values, representing dynamic transitions, are shown in Figs. F.23 and F.24.

## Additional results for HHI experiment

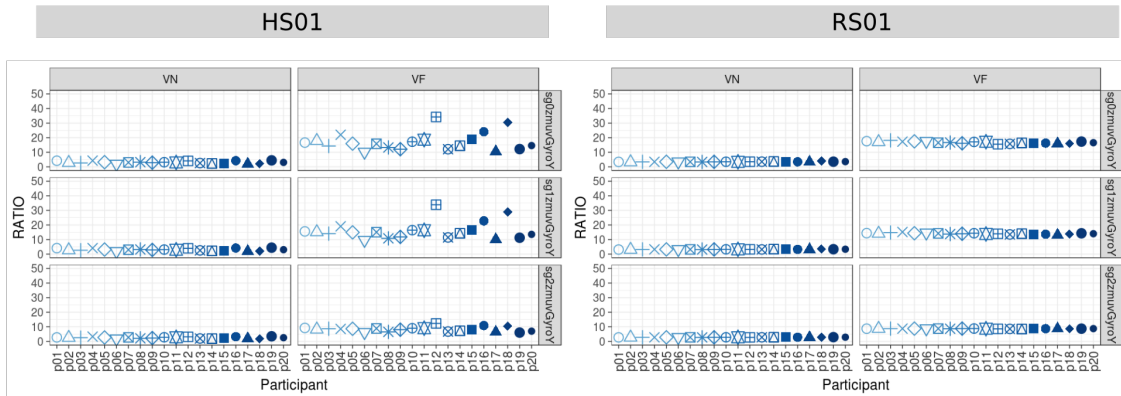


Fig. F.24 **RATIO** values for vertical arm movements. RATIO (representing dynamic transitions) for 20 participants performing VN and VF movements with sensors HS01, RS01 and three smoothed-normalised axis of GyroY ( $sg0zmvGyroY$ ,  $sg1zmvGyroY$  and  $sg2zmvGyroY$ ). RATIO values were computed with embedding parameters  $\overline{m}_0 = 6$ ,  $\overline{\tau}_0 = 8$  and recurrence threshold  $\epsilon = 1$ . R code to reproduce the figure is available at [\[45\]](#).

### F.5.4 ENTR values

ENTR values, representing the complexity of the structure in time series, are shown in Figs. F.25 and F.26.

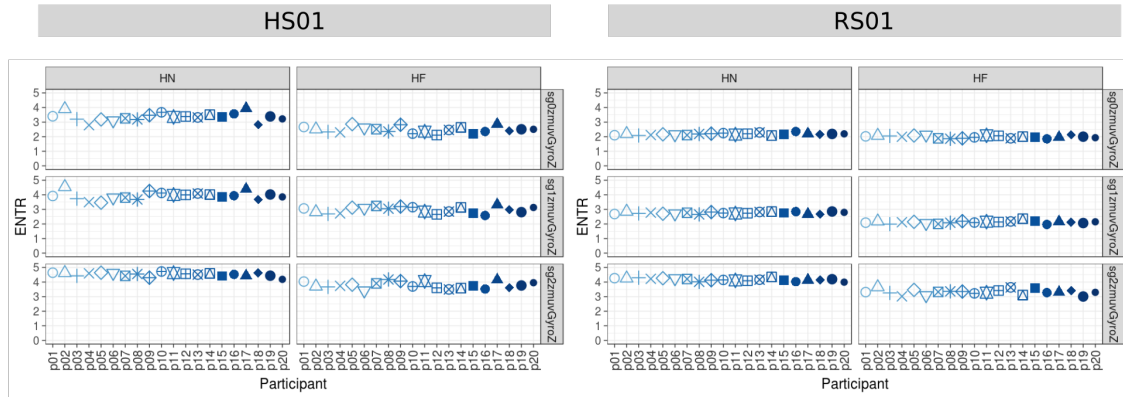


Fig. F.25 **ENTR values for horizontal arm movements.** ENTR values (representing the complexity of the deterministic structure in time series) for 20 participants performing HN and HF movements with sensors HS01, RS01 and three smoothed-normalised axis of GyroZ (sg0zmvGyroZ, sg1zmvGyroZ and sg2zmvGyroZ). ENTR values were computed with embedding parameters  $\overline{m_0} = 6$ ,  $\overline{\tau_0} = 8$  and recurrence threshold  $\epsilon = 1$ . R code to reproduce the figure is available at [\[4\]](#).

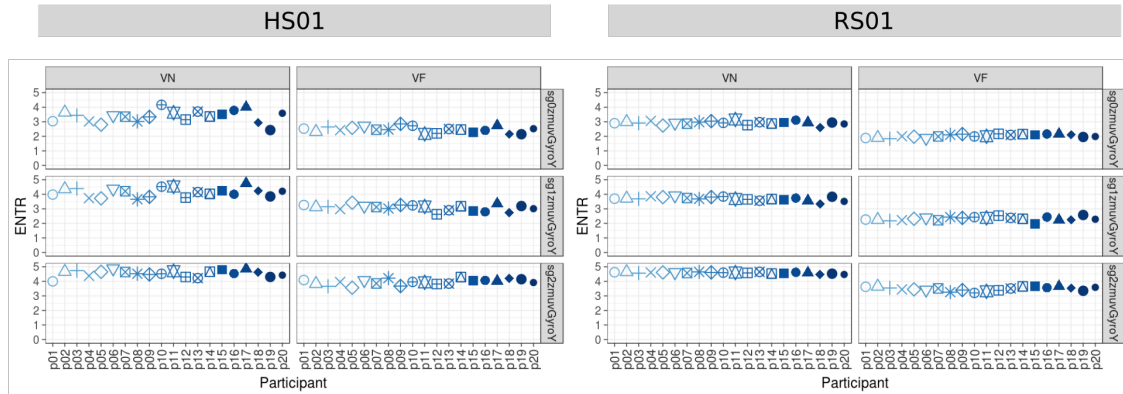


Fig. F.26 **ENTR values for vertical arm movements.** ENTR values (representing the complexity of the deterministic structure in time series) for 20 participants performing VN and VF movements with sensors HS01, RS01 and three smoothed-normalised axis of GyroY (sg0zmvGyroY, sg1zmvGyroY and sg2zmvGyroY). ENTR values were computed with embedding parameters  $\overline{m_0} = 6$ ,  $\overline{\tau_0} = 8$  and recurrence threshold  $\epsilon = 1$ . R code to reproduce the figure is available at [\[4\]](#).



# References

- Aguirre, L. A. and Letellier, C. (2009). Modeling nonlinear dynamics and chaos: A review. *Mathematical Problems in Engineering*, 11(12):1–22.
- Amato, I. (1992). Chaos breaks out at nih, but order may come of it. *Science*, 256(5065):1763–1764.
- Anguita, D., Ghio, A., Oneto, L., Parra, X., and Reyes-Ortiz, J. L. (2013). A public domain dataset for human activity recognition using smartphones. In *21th European Symposium on Artificial Neural Networks, Computational Intelligence and Machine Learning, ESANN 2013*.
- Azami, H. and Escudero, J. (2016). Amplitude-aware permutation entropy: Illustration in spike detection and signal segmentation. *Computer Methods and Programs in Biomedicine*, 128:40 – 51.
- Bandt, C. and Pompe, B. (2002). Permutation entropy: A natural complexity measure for time series. *Phys. Rev. Lett.*, 88:174102.
- Bartlett, R., Wheat, J., and Robins, M. (2007). Is movement variability important for sports biomechanists? *Sports Biomechanics*, 6(2):224–243. PMID: 17892098.
- Benzeghiba, M., Mori, R. D., Deroo, O., Dupont, S., Erbes, T., Jouvet, D., Fissore, L., Laface, P., Mertins, A., Ris, C., Rose, R., Tyagi, V., and Wellekens, C. (2007). Automatic speech recognition and speech variability: A review. *Speech Communication*, 49(10):763 – 786. Intrinsic Speech Variations.
- Bernstein, N. (1967). *The co-ordination and regulation of movements*. Pergamon-Press.
- Bonnet, V., Ramdani, S., Azevedo-Coste, C., Fraise, P., Mazzà, C., and Cappozzo, A. (2014). Integration of human walking gyroscopic data using empirical mode decomposition. *Sensors*, 14(1):370–381.
- Bradley, E. and Kantz, H. (2015). Nonlinear time-series analysis revisited. *Chaos: An Interdisciplinary Journal of Nonlinear Science*, 25(9):097610.
- Bruijn, S. M., van Dieën, J. H., Meijer, O. G., and Beek, P. J. (2009). Is slow walking more stable? *Journal of Biomechanics*, 42(10):1506 – 1512.
- Bryce, R. and Sprague, K. (2012). Revisiting detrended fluctuation analysis. *Scientific reports*, 2:315.

## References

---

- Caballero, C., Barbado, D., and Moreno, F. (2013). El procesado del desplazamiento del centro de presiones para el estudio de la relación complejidad/rendimiento observada en el control postural en bipedestación. *Revista Andaluza de Medicina del Deporte*, 6(3):101 – 107.
- Caballero, C., Barbado, D., and Moreno, F. J. (2014). Non-linear tools and methodological concerns measuring human movement variability: An overview. *European Journal of Human Movement*, 32:31–81.
- Cao, L. (1997). Practical method for determining the minimum embedding dimension of a scalar time series. *Physica D: Nonlinear Phenomena*, 110:43–50.
- Carroll, J. P. and Freedman, W. (1993). Nonstationary properties of postural sway. *Journal of biomechanics*, 26(4):409–416.
- Casdagli, M., Eubank, S., Farmer, J., and Gibson, J. (1991). State space reconstruction in the presence of noise. *Physica D: Nonlinear Phenomena*, 51(1):52 – 98.
- Cavanaugh, J. T., Kochi, N., and Stergiou, N. (2010). Nonlinear analysis of ambulatory activity patterns in community-dwelling older adults. *The Journals of Gerontology: Series A*, 65A(2):197–203.
- Chen, W., Wang, Z., Xie, H., and Yu, W. (2007). Characterization of surface emg signal based on fuzzy entropy. *IEEE Transactions on Neural Systems and Rehabilitation Engineering*, 15(2):266–272.
- Chen, W., Zhuang, J., Yu, W., and Wang, Z. (2009). Measuring complexity using fuzzyen, apen, and sampen. *Medical Engineering and Physics*, 31(1):61 – 68.
- Chiari, L., Rocchi, L., and Cappello, A. (2002). Stabilometric parameters are affected by anthropometry and foot placement. *Clinical Biomechanics*, 17(9):666 – 677.
- Coffey, N., Harrison, A., Donoghue, O., and Hayes, K. (2011). Common functional principal components analysis: A new approach to analyzing human movement data. *Human Movement Science*, 30(6):1144 – 1166.
- Comotti, D., Galizzi, M., and Vitali, A. (2014). nememsi: One step forward in wireless attitude and heading reference systems. In *2014 International Symposium on Inertial Sensors and Systems (ISISS)*, pages 1–4.
- Corso, G., Prado, T. L., Lima, G. Z. d. S., and Lopes, S. R. (2017). A novel entropy recurrence quantification analysis. *ArXiv e-prints*.
- Costa, M., Goldberger, A. L., and Peng, C.-K. (2002). Multiscale entropy analysis of complex physiologic time series. *Phys. Rev. Lett.*, 89:068102.
- Costa, M., Priplata, A. A., Lipsitz, L. A., Wu, Z., Huang, N. E., Goldberger, A. L., and Peng, C.-K. (2007). Noise and poise: Enhancement of postural complexity in the elderly with a stochastic-resonance-based therapy. *EPL (Europhysics Letters)*, 77(6):68008.

- Daubechies, I., Lu, J., and Wu, H.-T. (2011). Synchrosqueezed wavelet transforms: An empirical mode decomposition-like tool. *Applied and Computational Harmonic Analysis*, 30(2):243 – 261.
- Davids, K., Glazier, P., Araújo, D., and Bartlett, R. (2003). Movement systems as dynamical systems. *Sports Medicine*, 33(4):245–260.
- de Vries, J., Visser, G., and Prechtl, H. (1982). The emergence of fetal behaviour. i. qualitative aspects. *Early Human Development*, 7(4):301 – 322.
- Delignères, D., Deschamps, T., Legros, A., and Caillou, N. (2003). A methodological note on nonlinear time series analysis: Is the open-and closed-loop model of collins and de luca (1993) a statistical artifact? *Journal of Motor Behavior*, 35(1):86–96. PMID: 12724102.
- Dhingra, R. R., Jacono, F. J., Fishman, M., Loparo, K. A., Rybak, I. A., and Dick, T. E. (2011). Vagal-dependent nonlinear variability in the respiratory pattern of anesthetized, spontaneously breathing rats. *Journal of Applied Physiology*, 111(1):272–284. PMID: 21527661.
- Dingwell, J. B. and Cusumano, J. P. (2000). Nonlinear time series analysis of normal and pathological human walking. *Chaos: An Interdisciplinary Journal of Nonlinear Science*, 10(4):848–863.
- Dingwell, J. B. and Kang, H. G. (2007). Differences between local and orbital dynamic stability during human walking. *Journal of biomechanical engineering*, 129(4):586—593.
- Donker, S. F., Roerdink, M., Greven, A. J., and Beek, P. J. (2007). Regularity of center-of-pressure trajectories depends on the amount of attention invested in postural control. *Experimental Brain Research*, 181(1):1–11.
- Duarte, M. and Sternad, D. (2008). Complexity of human postural control in young and older adults during prolonged standing. *Experimental Brain Research*, 191(3):265–276.
- Eager, D., Pendrill, A.-M., and Reistad, N. (2016). Beyond velocity and acceleration: jerk, snap and higher derivatives. *European Journal of Physics*, 37(6):065008.
- Eckmann, J.-P., Kamphorst, S. O., and Ruelle, D. (1987). Recurrence plots of dynamical systems. *EPL (Europhysics Letters)*, 4(9):973.
- Emrani, S., Gentimis, T., and Krim, H. (2014). Persistent homology of delay embeddings and its application to wheeze detection. *IEEE Signal Processing Letters*, 21(4):459–463.
- Ferdenzi, C., Roberts, S. C., Schirmer, A., Delplanque, S., Cekic, S., Porcherot, C., Cayeux, I., Sander, D., and Grandjean, D. (2013). Variability of affective responses to odors: Culture, gender, and olfactory knowledge. *Chemical Senses*, 38(2):175–186.



## References

---

- Flandrin, P., Gonçalves, P., and Rilling, G. (2004). Detrending and denoising with empirical mode decompositions. In *2004 12th European Signal Processing Conference*, pages 1581–1584.
- Flash, T. and Hogan, N. (1985). The coordination of arm movements: an experimentally confirmed mathematical model. *Journal of Neuroscience*, 5(7):1688–1703.
- Frank, J., Mannor, S., and Precup, D. (2010). Activity and gait recognition with time-delay embeddings. *AAAI Conference on Artificial Intelligence*, pages 407–408.
- Fraser, A. M. and Swinney, H. L. (1986). Independent coordinates for strange attractors from mutual information. *Phys. Rev. A*, 33:1134–1140.
- Garcia, C. A. and Sawitzki, G. (2016). *nonlinearTseries: Nonlinear Time Series Analysis*. R package version 0.2.4 — For new features, see the ‘Changelog’ file (in the package source).
- Garcia, S. P. and Almeida, J. S. (2005). Nearest neighbor embedding with different time delays. *Phys. Rev. E*, 71:037204.
- Garland, J., Bradley, E., and Meiss, J. D. (2016). Exploring the topology of dynamical reconstructions. *Physica D: Nonlinear Phenomena*, 334:49 – 59. Topology in Dynamics, Differential Equations, and Data.
- Gates, D. H. and Dingwell, J. B. (2007). Peripheral neuropathy does not alter the fractal dynamics of stride intervals of gait. *Journal of Applied Physiology*, 102(3):965–971. PMID: 17110519.
- Gates, D. H. and Dingwell, J. B. (2008). The effects of neuromuscular fatigue on task performance during repetitive goal-directed movements. *Experimental Brain Research*, 187(4):573–585.
- Gibson, J. F., Farmer, J. D., Casdagli, M., and Eubank, S. (1992). An analytic approach to practical state space reconstruction. *Physica D: Nonlinear Phenomena*, 57(1):1 – 30.
- Goldberger, A. (1996). Non-linear dynamics for clinicians: chaos theory, fractals, and complexity at the bedside. *The Lancet*, 347(9011):1312 – 1314.
- Goldberger, A. L., Peng, C.-K., and Lipsitz, L. A. (2002). What is physiologic complexity and how does it change with aging and disease? *Neurobiology of Aging*, 23(1):23 – 26.
- Goldberger, A. L., Rigney, D. R., and West, B. J. (1990). Chaos and fractals in human physiology. *Scientific American*, 262(2):42–49.
- Görer, B., Salah, A. A., and Akın, H. L. (2013). A robotic fitness coach for the elderly. In Augusto, J. C., Wichert, R., Collier, R., Keyson, D., Salah, A. A., and Tan, A.-H., editors, *Ambient Intelligence*, pages 124–139, Cham. Springer International Publishing.

- Gouaillier, D., Hugel, V., Blazevic, P., Kilner, C., Monceaux, J., Lafourcade, P., Marnier, B., Serre, J., and Maisonnier, B. (2009). Mechatronic design of nao humanoid. In *Proceedings of the 2009 IEEE International Conference on Robotics and Automation, ICRA'09*, pages 2124–2129, Piscataway, NJ, USA. IEEE Press.
- Guastello, S. J. and Gregson, R. A. M. (2011). *Nonlinear Dynamical Systems Analysis for the Behavioral Science Using Real Data*. CRC Press.
- Guneysu, A., Arnrich, B., and Ersoy, C. (2015). Children’s rehabilitation with humanoid robots and wearable inertial measurement units. In *Proceedings of the 9th International Conference on Pervasive Computing Technologies for Healthcare, PervasiveHealth '15*, pages 249–252, ICST, Brussels, Belgium, Belgium. ICST (Institute for Computer Sciences, Social-Informatics and Telecommunications Engineering).
- Guneysu, A., Siyli, R. D., and Salah, A. A. (2014). Auto-evaluation of motion imitation in a child-robot imitation game for upper arm rehabilitation. In *The 23rd IEEE International Symposium on Robot and Human Interactive Communication*, pages 199–204.
- Gómez-García, J. A., Godino-Llorente, J. I., and Castellanos-Dominguez, G. (2014). Non uniform embedding based on relevance analysis with reduced computational complexity: Application to the detection of pathologies from biosignal recordings. *Neurocomputing*, 132(Supplement C):148 – 158. Innovations in Nature Inspired Optimization and Learning Methods Machines learning for Non-Linear Processing.
- Harbourne, R. T. and Stergiou, N. (2009). Movement variability and the use of nonlinear tools: Principles to guide physical therapist practice. *Physical Therapy*, 89(3):267–282.
- Hatze, H. (1986). Motion variability—its definition, quantification, and origin. *Journal of Motor Behavior*, 18(1):5–16. PMID: 15136282.
- Hausdorff, J. M. (2009). Gait dynamics in parkinson’s disease: Common and distinct behavior among stride length, gait variability, and fractal-like scaling. *Chaos: An Interdisciplinary Journal of Nonlinear Science*, 19(2):026113.
- Hausdorff, J. M., Peng, C. K., Ladin, Z., Wei, J. Y., and Goldberger, A. L. (1995). Is walking a random walk? evidence for long-range correlations in stride interval of human gait. *Journal of Applied Physiology*, 78(1):349–358. PMID: 7713836.
- Herzfeld, D. J. and Shadmehr, R. (2014). Motor variability is not noise, but grist for the learning mill. *nature neuroscience*, 17(2):149.
- Huang, N. E., Shen, Z., Long, S. R., Wu, M. C., Shih, H. H., Zheng, Q., Yen, N.-C., Tung, C. C., and Liu, H. H. (1998). The empirical mode decomposition and the hilbert spectrum for nonlinear and non-stationary time series analysis. *Proceedings of the Royal Society of London A: Mathematical, Physical and Engineering Sciences*, 454(1971):903–995.
- Huffaker, R., Bittelli, M., and Rosa, R. (2017). *Nonlinear Time Series Analysis with R*. Oxford University Press.

## References

---

- Ioffe, S. and Szegedy, C. (2015). Batch normalization: Accelerating deep network training by reducing internal covariate shift. *CoRR*, abs/1502.03167.
- Iwanski, J. S. and Bradley, E. (1998). Recurrence plots of experimental data: To embed or not to embed? *Chaos: An Interdisciplinary Journal of Nonlinear Science*, 8(4):861–871.
- Kabiraj, L., Saurabh, A., Wahi, P., and Sujith, R. I. (2012). Route to chaos for combustion instability in ducted laminar premixed flames. *Chaos: An Interdisciplinary Journal of Nonlinear Science*, 22(2):023129.
- Kanai, R. and Rees, G. (2011). The structural basis of inter-individual differences in human behaviour and cognition. *Nature Reviews Neuroscience*, 12(4):231.
- Kantz, H. and Schreiber, T. (2003). *Nonlinear Time Series Analysis*. Cambridge University Press, New York, NY, USA.
- Kennel, M. B., Brown, R., and Abarbanel, H. D. I. (1992). Determining embedding dimension for phase-space reconstruction using a geometrical construction. *Phys. Rev. A*, 45:3403–3411.
- Kitagawa, G. and Gersch, W. (1984). A smoothness priors–state space modeling of time series with trend and seasonality. *Journal of the American Statistical Association*, 79(386):378–389.
- Klonowski, W. (2002). Chaotic dynamics applied to signal complexity in phase space and in time domain. *Chaos, Solitons and Fractals*, 14(9):1379 – 1387.
- Klonowski, W. (2007). From conformons to human brains: an informal overview of nonlinear dynamics and its applications in biomedicine. *Nonlinear Biomedical Physics*, 1(1):5.
- Klonowski, W. (2009). Everything you wanted to ask about eeg but were afraid to get the right answer. *Nonlinear Biomedical Physics*, 3(1):2.
- Krakovská, A., Mezeiová, K., and I, H. B. (2015). Use of False Nearest Neighbours for Selecting Variables and Embedding Parameters for State Space Reconstruction. *Journal of Complex Systems*, 2015.
- Krüger, M., Eggert, T., and Straube, A. (2013). Age-related differences in the stabilization of important task variables in reaching movements. *Motor Control*, 17(3):313–320.
- Kurz, M. J. and Hou, J. G. (2010). Levodopa influences the regularity of the ankle joint kinematics in individuals with parkinson’s disease. *Journal of Computational Neuroscience*, 28(1):131–136.
- Kurz, M. J., Markopoulou, K., and Stergiou, N. (2010). Attractor divergence as a metric for assessing walking balance. *Nonlinear dynamics, psychology, and life sciences*, 14(2):151—164.

- Lake, D. E. and Moorman, J. R. (2011). Accurate estimation of entropy in very short physiological time series: the problem of atrial fibrillation detection in implanted ventricular devices. *American Journal of Physiology-Heart and Circulatory Physiology*, 300(1):H319–H325. PMID: 21037227.
- Letellier, C. (2006). Estimating the shannon entropy: Recurrence plots versus symbolic dynamics. *Phys. Rev. Lett.*, 96:254102.
- Liao, F., Wang, J., and He, P. (2008). Multi-resolution entropy analysis of gait symmetry in neurological degenerative diseases and amyotrophic lateral sclerosis. *Medical Engineering and Physics*, 30(3):299 – 310.
- MacDonald, S. W., Nyberg, L., and Bäckman, L. (2006). Intra-individual variability in behavior: links to brain structure, neurotransmission and neuronal activity. *Trends in Neurosciences*, 29(8):474 – 480.
- Madeleine, P. and Madsen, T. (2009). Changes in the amount and structure of motor variability during a deboning process are associated with work experience and neck–shoulder discomfort. *Applied Ergonomics*, 40(5):887 – 894.
- Madeleine, P., Mathiassen, S. E., and Arendt-Nielsen, L. (2008). Changes in the degree of motor variability associated with experimental and chronic neck–shoulder pain during a standardised repetitive arm movement. *Experimental Brain Research*, 185(4):689–698.
- Mandic, D. P., u. Rehman, N., Wu, Z., and Huang, N. E. (2013). Empirical mode decomposition-based time-frequency analysis of multivariate signals: The power of adaptive data analysis. *IEEE Signal Processing Magazine*, 30(6):74–86.
- Marwan, N. (2008). A historical review of recurrence plots. *The European Physical Journal Special Topics*, 164(1):3–12.
- Marwan, N. (2011). How to Avoid Potential Pitfalls in Recurrence Plot Based Data Analysis. *International Journal of Bifurcation and Chaos*, 21:1003.
- Marwan, N., Romano, M. C., Thiel, M., and Kurths, J. (2007). Recurrence plots for the analysis of complex systems. *Physics Reports*, 438(5):237 – 329.
- Marwan, N. and Webber, C. L. (2015). Mathematical and computational foundations of recurrence quantifications. In Webber, C. L. and Marwan, N., editors, *Recurrence Quantification Analysis: Theory and Best Practices*, chapter 1, pages 3–43. Springer, Cham, 1 edition.
- Mathiassen, S. E. (2006). Diversity and variation in biomechanical exposure: What is it, and why would we like to know? *Applied Ergonomics*, 37(4):419 – 427. Special Issue: Meeting Diversity in Ergonomics.
- Mert, A. and Akan, A. (2018). Emotion recognition from eeg signals by using multivariate empirical mode decomposition. *Pattern Analysis and Applications*, 21(1):81–89.
- Miller, D. J., Stergiou, N., and Kurz, M. J. (2006). An improved surrogate method for detecting the presence of chaos in gait. *Journal of Biomechanics*, 39(15):2873 – 2876.

## References

---

- Mori, H. and Kuniyoshi, Y. (2012). Is the developmental order of fetal behaviors self-organized in an uterine environment? In *2012 IEEE International Conference on Development and Learning and Epigenetic Robotics (ICDL)*, pages 1–2.
- Müller, H. and Sternad, D. (2004). Decomposition of variability in the execution of goal-oriented tasks: three components of skill improvement. *Journal of Experimental Psychology: Human Perception and Performance*, 30(1):212.
- Newell, K. and Corcos, D. (1993). *Variability and Motor Control*. Human Kinetics Publishers.
- Newell, K. M. and Slifkin, A. B. (1998). The nature of movement variability. In Piek, J. P., editor, *Motor behavior and human skill : a multidisciplinary approach*, chapter 7, pages 143–160. Champaign, IL : Human Kinetics.
- Packard, N. H., Crutchfield, J. P., Farmer, J. D., and Shaw, R. S. (1980). Geometry from a time series. *Phys. Rev. Lett.*, 45:712–716.
- Pecora, L. M., Moniz, L., Nichols, J., and Carroll, T. L. (2007). A unified approach to attractor reconstruction. *Chaos: An Interdisciplinary Journal of Nonlinear Science*, 17(1):013110.
- Pellecchia, G. L. and Shockley, K. (2015). Application of recurrence quantification analysis: Influence of cognitive activity on postural fluctuations. In Riley, M., Van Orden, G., and (U.S.), N. S. F., editors, *Tutorials in Contemporary Nonlinear Methods for the Behavioral Sciences*, chapter 3, pages 95–141. National Science Foundation.
- Peng, C., Havlin, S., Stanley, H. E., and Goldberger, A. L. (1995). Quantification of scaling exponents and crossover phenomena in nonstationary heartbeat time series. *Chaos: An Interdisciplinary Journal of Nonlinear Science*, 5(1):82–87.
- Peng, H., Zhou, C., Hu, H., Chao, F., and Li, J. (2015). Robotic dance in social robotics – a taxonomy. *IEEE Transactions on Human-Machine Systems*, 45(3):281–293.
- Pincus, S. (1995). Approximate entropy (apen) as a complexity measure. *Chaos: An Interdisciplinary Journal of Nonlinear Science*, 5(1):110–117.
- Pincus, S. M. (1991). Approximate entropy as a measure of system complexity. *Proceedings of the National Academy of Sciences of the United States of America*, 88(6):2297–2301.
- Preatoni, E. (2007). *Innovative methods for the analysis of sports movements and for the longitudinal monitoring of individual motor skills*. PhD thesis, Politecnico di Milano.
- Preatoni, E., Ferrario, M., Donà, G., Hamill, J., and Rodano, R. (2010). Motor variability in sports: A non-linear analysis of race walking. *Journal of Sports Sciences*, 28(12):1327–1336. PMID: 20853204.

- Preatoni, E., Hamill, J., Harrison, A. J., Hayes, K., Emmerik, R. E. V., Wilson, C., and Rodano, R. (2013). Movement variability and skills monitoring in sports. *Sports Biomechanics*, 12(2):69–92. PMID: 23898682.
- Press, W. H., Teukolsky, S. A., Vetterling, W. T., and Flannery, B. P. (1992). *Numerical Recipes in C (2Nd Ed.): The Art of Scientific Computing*. Cambridge University Press, New York, NY, USA.
- Quetzalcoatl (2018). Quetzalcoatl—Wikipedia, the free encyclopedia. <https://en.wikipedia.org/wiki/Quetzalcoatl> [Online; accessed 06-June-2018].
- Quintana-Duque, J. and Saupe, D. (2013). *Evidence of Chaos in Indoor Pedaling Motion using Non-linear Methods*. Number July in Performance Analysis of Sport. Routledge.
- Quintana-Duque, J. C. (2012). Non-linear dynamic invariants based on embedding reconstruction of systems for pedaling motion. In Byshko, R., editor, *Sportinformatik 2012 : 9. vom 12.- 14. Sept. 2012 in Konstanz : Beiträge*, pages 28–38. Universität.
- Quintana-Duque, J. C. (2016). *Non-linear methods for the quantification of cyclic motion*. PhD dissertation, University of Konstanz, Konstanz, Germany.
- Rajendra Acharya, U., Paul Joseph, K., Kannathal, N., Lim, C. M., and Suri, J. S. (2006). Heart rate variability: a review. *Medical and Biological Engineering and Computing*, 44(12):1031–1051.
- Rangarajan, G. and Ding, M. (2000). Integrated approach to the assessment of long range correlation in time series data. *Phys. Rev. E*, 61:4991–5001.
- Rehman, N. and Mandic, D. P. (2010). Multivariate empirical mode decomposition. *Proceedings of the Royal Society of London A: Mathematical, Physical and Engineering Sciences*, 466(2117):1291–1302.
- Rhea, C. K., Silver, T. A., Hong, S. L., Ryu, J. H., Studenka, B. E., Hughes, C. M. L., and Haddad, J. M. (2011). Noise and complexity in human postural control: Interpreting the different estimations of entropy. *PLOS ONE*, 6(3):1–9.
- Richman, J. S. and Moorman, J. R. (2000). Physiological time-series analysis using approximate entropy and sample entropy. *American Journal of Physiology-Heart and Circulatory Physiology*, 278(6):H2039–H2049. PMID: 10843903.
- Riley, M., Balasubramaniam, R., and Turvey, M. (1999). Recurrence quantification analysis of postural fluctuations. *Gait and Posture*, 9(1):65 – 78.
- Rosenstein, M. T., Collins, J. J., and Luca, C. J. D. (1993). A practical method for calculating largest lyapunov exponents from small data sets. *Physica D: Nonlinear Phenomena*, 65(1):117 – 134.
- Rosenstein, M. T., Collins, J. J., and Luca, C. J. D. (1994). Reconstruction expansion as a geometry-based framework for choosing proper delay times. *Physica D: Nonlinear Phenomena*, 73(1):82 – 98.

## References

---

- Samà, A., Ruiz, F. J., Agell, N., Pérez-López, C., Català, A., and Cabestany, J. (2013). Gait identification by means of box approximation geometry of reconstructed attractors in latent space. *Neurocomputing*, 121:79–88.
- Sandlund, J., Røijezon, U., Björklund, M., and Djupsjöbacka, M. (2008). Acuity of goal-directed arm movements to visible targets in chronic neck pain. *Journal of Rehabilitation Medicine*, 40(5):366–374.
- Sandlund, J., Srinivasan, D., Heiden, M., and Mathiassen, S. E. (2017). Differences in motor variability among individuals performing a standardized short-cycle manual task. *Human Movement Science*, 51:17 – 26.
- Savitzky, A. and Golay, M. J. E. (1964). Smoothing and differentiation of data by simplified least squares procedures. *Analytical Chemistry*, 36:1627–1639.
- Schafer, R. W. (2011). On the frequency-domain properties of savitzky-golay filters. In *2011 Digital Signal Processing and Signal Processing Education Meeting (DSP/SPE)*, pages 54–59.
- Schreiber, T. and Schmitz, A. (2000). Surrogate time series. *Physica D: Nonlinear Phenomena*, 142(3):346 – 382.
- Schumacher, A. (2004). Linear and nonlinear approaches to the analysis of r-r interval variability. *Biological Research For Nursing*, 5(3):211–221. PMID: 14737922.
- Seifert, L., Leblanc, H., Herault, R., Komar, J., Button, C., and Chollet, D. (2011). Inter-individual variability in the upper–lower limb breaststroke coordination. *Human Movement Science*, 30(3):550 – 565.
- Shoaib, M., Bosch, S., Incel, O. D., Scholten, H., and Havinga, P. J. M. (2016). Complex human activity recognition using smartphone and wrist-worn motion sensors. *Sensors*, 16(4).
- signal R developers (2014). *signal: Signal processing*.
- Small, M. and Tse, C. (2002). Applying the method of surrogate data to cyclic time series. *Physica D: Nonlinear Phenomena*, 164(3):187 – 201.
- Sosnoff, J. J., Valantine, A. D., and Newell, K. M. (2006). Independence between the amount and structure of variability at low force levels. *Neuroscience Letters*, 392(3):165 – 169.
- Sosnoff, J. J. and Voudrie, S. J. (2009). Practice and age-related loss of adaptability in sensorimotor performance. *Journal of Motor Behavior*, 41(2):137–146. PMID: 19201684.
- Srinivasan, D. and Mathiassen, S. E. (2012). Motor variability in occupational health and performance. *Clinical Biomechanics*, 27(10):979 – 993.
- Stam, C., Pijn, J., and Pritchard, W. (1998). Reliable detection of nonlinearity in experimental time series with strong periodic components. *Physica D: Nonlinear Phenomena*, 112(3):361 – 380.

- Stergiou, N. (2016). *Nonlinear Analysis for Human Movement Variability*. CRC Press.
- Stergiou, N. and Decker, L. M. (2011). Human movement variability, nonlinear dynamics, and pathology: Is there a connection? *Human Movement Science*, 30(5):869 – 888. EWOMS 2009: The European Workshop on Movement Science.
- Stergiou, N., Harbourne, R., and Cavanaugh, J. (2006). Optimal movement variability: a new theoretical perspective for neurologic physical therapy. *Journal of neurologic physical therapy : JNPT*, 30(3):120–129.
- Stergiou, N., Kent, J. A., and McGrath, D. (2016). Human movement variability and aging. *Kinesiology Review*, 5(1):15–22.
- Stins, J., Michielsen, M., Roerdink, M., and Beek, P. (2009). Sway regularity reflects attentional involvement in postural control: Effects of expertise, vision and cognition. *Gait and Posture*, 30(1):106 – 109.
- Svendsen, J. H. and Madeleine, P. (2010). Amount and structure of force variability during short, ramp and sustained contractions in males and females. *Human Movement Science*, 29(1):35 – 47.
- Takens, F. (1981). Detecting strange attractors in turbulence. *Dynamical Systems and Turbulence, Warwick 1980: Proceedings of a Symposium Held at the University of Warwick 1979/80*, pages 366–381.
- Tononi, G., Edelman, G. M., and Sporns, O. (1998). Complexity and coherency: integrating information in the brain. *Trends in Cognitive Sciences*, 2(12):474 – 484.
- Trulla, L., Giuliani, A., Zbilut, J., and Webber, C. (1996). Recurrence quantification analysis of the logistic equation with transients. *Physics Letters A*, 223(4):255 – 260.
- Tsuchida, S., Terada, T., and Tsukamoto, M. (2013). A system for practicing formations in dance performance supported by self-propelled screen. In *Proceedings of the 4th Augmented Human International Conference, AH '13*, pages 178–185, New York, NY, USA. ACM.
- Uzal, L. C., Grinblat, G. L., and Verdes, P. F. (2011). Optimal reconstruction of dynamical systems: A noise amplification approach. *Phys. Rev. E*, 84:016223.
- Uzal, L. C. and Verdes, P. F. (2010). Optimal Irregular Delay Embeddings. In *Dynamics Days South America 2010*. National Institute for Space Research.
- Vaillancourt, D. E. and Newell, K. M. (2002). Changing complexity in human behavior and physiology through aging and disease. *Neurobiology of Aging*, 23(1):1 – 11.
- Vaillancourt, D. E. and Newell, K. M. (2003). Aging and the time and frequency structure of force output variability. *Journal of Applied Physiology*, 94(3):903–912. PMID: 12571125.
- Vaillancourt, D. E., Slifkin, A. B., and Newell, K. M. (2001). Regularity of force tremor in parkinson’s disease. *Clinical Neurophysiology*, 112(9):1594 – 1603.



## References

---

- Vaillancourt, D. E., Sosnoff, J. J., and Newell, K. M. (2004). Age-related changes in complexity depend on task dynamics. *Journal of Applied Physiology*, 97(1):454–455. PMID: 15220326.
- Vakharia, V., Gupta, V., and Kankar, P. (2015). A multiscale permutation entropy based approach to select wavelet for fault diagnosis of ball bearings. *Journal of Vibration and Control*, 21(16):3123–3131.
- van Dieën, J. H., Koppes, L. L., and Twisk, J. W. (2010). Postural sway parameters in seated balancing; their reliability and relationship with balancing performance. *Gait and Posture*, 31(1):42 – 46.
- Wagner, H., Pfusterschmied, J., Klous, M., von Duvillard, S. P., and Müller, E. (2012). Movement variability and skill level of various throwing techniques. *Human Movement Science*, 31(1):78 – 90.
- Webber, C. L. (2018). *Introduction to Recurrence Quantification Analysis. RQA Version 15.1 README.PDF*. <http://cwebber.sites.luc.edu/>.
- Webber, C. L. and Zbilut, J. P. (1994). Dynamical assessment of physiological systems and states using recurrence plot strategies. *Journal of Applied Physiology*, 76(2):965–973. PMID: 8175612.
- Webber, C. L. and Zbilut, J. P. (2005). Recurrence quantification analysis of nonlinear dynamical systems. In Riley, M. A. and Orden, G. C. V., editors, *Tutorials in contemporary nonlinear methods for behavioral science*, chapter 2, pages 26–94. National Science Foundation.
- Wijnants, M. L., Bosman, A. M., Hasselman, F., Cox, R. F., and Van Orden, G. C. (2009). 1/f scaling in movement time changes with practice in precision aiming. *Nonlinear Dynamics, Psychology, and Life Sciences*, 13(1):79–98. cited By 88.
- Wolf, A., Swift, J. B., Swinney, H. L., and Vastano, J. A. (1985). Determining lyapunov exponents from a time series. *Physica D: Nonlinear Phenomena*, 16(3):285 – 317.
- Wu, H. G., Miyamoto, Y. R., Castro, L. N. G., Ölveczky, B. P., and Smith, M. A. (2014). Temporal structure of motor variability is dynamically regulated and predicts motor learning ability. *Nature neuroscience*, 17(2):312.
- Wu, M.-C. and Hu, C.-K. (2006). Empirical mode decomposition and synchrogram approach to cardiorespiratory synchronization. *Phys. Rev. E*, 73:051917.
- Wu, Z. and Huang, N. E. (2004). A study of the characteristics of white noise using the empirical mode decomposition method. *Proceedings of the Royal Society of London A: Mathematical, Physical and Engineering Sciences*, 460(2046):1597–1611.
- Wu, Z. and Huang, N. E. (2009). Ensemble empirical mode decomposition: A noise-assisted data analysis method. *Advances in Adaptive Data Analysis*, 01(01):1–41.
- Xochicale, M. (2019). *Github repository for code and data of this PhD thesis*. <https://github.com/mxochicale/phd-thesis>.

- Yang, C. and Wu, C. Q. (2011). A robust method on estimation of lyapunov exponents from a noisy time series. *Nonlinear Dynamics*, 64(3):279–292.
- Yao, C.-Z. and Lin, Q.-W. (2017). Recurrence plots analysis of the cny exchange markets based on phase space reconstruction. *The North American Journal of Economics and Finance*, 42:584 – 596.
- Zbilut, J. P. and Webber, C. L. (1992). Embeddings and delays as derived from quantification of recurrence plots. *Physics Letters A*, 171(3):199 – 203.
- Zunino, L., Zanin, M., Tabak, B. M., Pérez, D. G., and Rosso, O. A. (2009). Forbidden patterns, permutation entropy and stock market inefficiency. *Physica A: Statistical Mechanics and its Applications*, 388(14):2854 – 2864.

